THE DYNAMIC CHARACTERISATION AND MODELLING OF LEAD-ACID BATTERIES FOR ELECTRIC VEHICLE APPLICATIONS

Clive Morgan, B.Sc.

A dissertation submitted to the Council for National Academic Awards for the degree of Doctor of Philosophy

The Polytechnic of Wales,
Department of Electrical and Electronic Engineering.

April 1985

in Collaboration with

Lucas Chloride Electric Vehicles

DECLARATION

This dissertation has not been, nor is being currently submitted for the award of any other degree or similar qualification.

C. Morgan

Clive Morgan.

CONTENTS PAGE

CONTENTS PAGE

CONTENTS PAGE

CONTENTS

MEMORANDUM

This thesis incorporates the results of a three year investigation into the performance of lead-acid batteries as used in electric vehicle drive systems, with particular reference to the development of a mathematical model of the batteries for use as a state indicator. The work was carried out in the laboratories of The Polytechnic of Wales from August 1980 to October 1984, under the supervision of Dr. M.G. Jayne and with the industrial collaboration of Lucas/Chloride Electric Vehicles of Manchester.

All the work and ideas are original unless otherwise acknowledged in the text or by reference. The contribution that the author claims to have made in the context of the investigations are:

(1) The selective use of pulsed currents can considerably improve the discharge performance of the batteries when compared to using continuous discharge currents. Previous investigations into this subject area had been contradictory.

(2) The use of complex current (pulsed or asymmetric current) techniques do not significantly improve the charging performance of the batteries when compared to using more conventional charging techniques. In fact in some instances a comparative reduction in charging performance was observed when using the complex current techniques. The results of previous investigations using the asymmetric current technique had shown there to be significant improvements in the charging performance of the batteries. The use of pulsed charging currents by the author was at the time considered to be novel, however, a previous investigation was later discovered, although the investigation only covered part of the subject area covered by the author.

(3)(i) The development of novel mathematical models (terminal voltage and state-of-charge) of the battery based on experimental results obtained from (1) and (2) above. The models account for all the performance affecting factors normally encountered by batteries which are used in electric vehicles.

(ii) The development of novel models for use with pulsed discharge currents as found in the "chopper" control of electric vehicles for use under operating conditions specified in (i).

As a result of (3), a system for dynamic testing of the models was developed using the PET microcomputer, which involved the real-time sampling of battery discharge parameters.

To-date the investigations have supported the publication of three articles:

(1) Jayne, M.G., Morgan, C. : The Effects of Complex Current Wave-Forms on the Behaviour of Lead Acid Batteries, EVC Symposium IV, Baltimore, Maryland. October 21-23, 1981.

(2) Jayne, M.G., Morgan, C. : An Investigation Into Fast Charging Techniques For Lead Acid Batteries. Drive Electric, 25-28 October 1982, Amsterdam, Netherlands.

(3) A patent application incorporating the novel features contained in this thesis has been made with the co-operation of the National Research and Development Corporation (NRDC).

SYMBOLS AND ABBREVIATIONS

V = (1) Voltage

(2) Volts

i,I = Current; A = Ampere

r = Resistance; Ω = ohm

t = time; s = second; h = hour

f = frequency; Hz = Hertz

u = micro (10^{-6}); m = milli (10^{-3}); k = kilo (10^{3}); M = mega (10^{6})

C = (1) Capacity (Ampere-Hour)

(2) Capacitance

F = Farad

T = Temperature; °C = degree centigrade

a.c.; A.C. = Alternating Current

d.c.; D.C. = Direct Current

Δ = increment

Wh = Watt-Hour

Ah = Ampere-Hour

l = litre

C_5 = Nominal 5-hour discharge rate capacity

M = Mark/Space Ratio

EV = Electric Vehicle

r.m.s. = root-mean-square

e.m.f. = electromotive force

h.p. = horse-power

$\sim$ = Approximation

kg = Kilogram

$\sum_{1}^{}$ = the sum of the terms indicated

L = (1) Depth-of-Discharge

(2) Inductance

H = Henry

SUBSCRIPTS

av = average or mean value

pk = peak value

mn = minimum value

rms = r.m.s. value

CHEMICAL FORMULAE

Pb = Lead

PbO = Lead Oxide

PbO_2 = Lead Dioxide

$PbSO_4$ = Lead Sulphate

H_2SO_4 = Sulphuric Acid

ABSTRACT

In an effort to increase the available capacity of a lead-acid battery, the effects of pulsed discharge currents as opposed to the effects of continuous discharge currents on the battery were investigated, for a wide range of frequency, mark/space ratio and peak current of the discharge waveform. It was found that for certain conditions of pulsed discharge, the use of pulsed currents can provide a considerable increase in available capacity when compared to that obtained from using conventional continuous currents.

In order to increase the efficiency and reduce the time of the lead-acid battery charge, the effects of using pulsed charging currents with and without depolarisation discharge pulses interspersed throughout the charging period as opposed to using conventional continuous current charging was investigated. For the tests performed, it was found that pulsed current charging without depolarisation pulses offers no advantages over conventional continuous current charging for three-stage and single-stage charging techniques. The use of pulsed currents with depolarisation pulses was found to be less effective than using conventional continuous current or straight pulsed current charging.

A model for the cell terminal voltage and state-of-charge of the battery is derived from the results of an extensive series of tests performed by the author. In this writing for the first time a model accurately accounts for the dependence of recuperation, regeneration and wide variations in the discharge rate on the temperature of the electrolyte and the effects of these factors on the terminal voltage and state-of-charge. Additionally, for the first time a comprehensive model for use with pulsed discharge currents is derived. The models were tested under dynamic conditions of battery operation and were found to be able to predict battery state to a high degree of accuracy, and were also found to be more accurate than existing models.

1. INTRODUCTION

1.1 The History of Battery Powered Electric Vehicles

The first step towards an effective electric vehicle (EV) battery was taken by Volta in about 1800 when he produced a potential from stacks of different metals separated by cloth moistened with an ionic solution. Later, in 1860 Planté produced an elementary lead-acid system; developments of which provided the basis for a commercially usable lead-acid battery.

EVs came into existence at about the same time as the first internal combustion engined vehicles (ICEVs); the first to be constructed in this country was by Stanley in 1888, and in the United States by Kimball. In these early years the EV was popular and sold well compared with the noisy and inconvenient early ICEVs. During these promising days the EV fleet in the United States grew to over 20,000. The taxis in New York, Boston, and Berlin, were mainly electric, and an electric car held the world speed record in 1899 at 105 km/h. In 1910 there were some 6000 electric cars and 4000 commercial EVs registered [1] in London.

Further developments to ICEVs however, meant that by the beginning of the First World War EVs had lost their dominance. By the end of the First World War the improvements to the performance of the ICEVs, the high specific energy of petroleum fuels and the use of mass production techniques to reduce cost, had removed any doubt about their superiority as road vehicles. The use of electric propulsion became confined to rather specific types of transport. The most successful of these used wayside power-trains, trams, and trolley-buses; and slowly the tram and the trolley-bus became superseded by the diesel engined bus. The last trams ran in London in 1952 and the last trolley-buses in 1962.

The 20th Century has therefore seen a steady increase in society's dependence upon the ICEV to the point where lifestyle is dominated by its universal availability and use. This trend has been towards private rather than public transport for the past 30 years, due to increasing affluence and the convenience and flexibility afforded by the private motor car.

1.2 Renewed Interest in Battery Powered Electric Vehicles

During the past decade or so, environmental and energy considerations have gained worldwide importance. One facet of these considerations is the application of EVs to urban road transportation and, in particular, the relative merits of these vehicles and ICEVs.

Exhaust fumes generated by motor vehicles are in the foreground in discussions on the need to protect the cleanliness of the air. The amount of atmospheric pollution is increasing with both the increase in population and the number of motor cars. By products of the ICEV exhaust are unsaturated hydrocarbons and carbon dioxide gas. The conspicuous obnoxiousness of these fumes is caused by the fact that they are produced at the same level as pedestrians and affect them directly, particularly at locations of traffic jams where a high concentration of the fumes would develop. Furthermore, these ICEV emissions react with certain constituents of the air to form fog and smog.

In the industrial sector, the sulphur dioxide produced as a result of burning fossil fuels is emitted high into the atmosphere, where it can be easily converted [2] into sulphur trioxide and sulphuric acid by atmospheric reactions, and rained down onto the earth and seas, thereby adding to the environmental pollution.

In addition to these major ecological hazards, it is possible

that there may be other environmental implications, perhaps of a biochemical nature, that have not yet been isolated.

The energy considerations basically relate to the conservation of primary energy sources such as petroleum and coal. The EEC* used approximately [3] 975 million toe+ of primary energy in 1977; of this, 540 million tonnes (55%) was oil, of which 25% (135 million tonnes) was used in the transport sector, which may be categorised as follows: road $\sim$83%, air $\sim$ 10%, rail $\sim$ 4%, and ship $\sim$ 3%. Evidently, these figures vary somewhat from country to country; for instance, the U.K. with its indigenous coal for electricity generation and natural gas for heating, consumes a higher percentage of its oil in the transport sector (33%). In view of the dwindling resources of petroleum, and the increasing cost in extracting such resources, the conservation of petroleum - particularly in the transport sector - is desirable, for then petroleum may be conserved for other premium uses such as aircraft fuels, lubricants and petrochemicals. Another incentive for the substitution of petroleum in the transport sector would be to diversify the energy base of transport, thereby reducing Europe's vulnerability to uncertain supplies from overseas. These are important national and EEC objectives which constitute a justification for EV development. It is expected [3] that in the next two decades there will be a major decline in oil consumption for space heating, and by the year 2000 the contribution of transport to oil consumption will be more than 50%. At this point the remaining major opportunity for oil substitution will be in transport, and a large scale introduction of EVs will, for this point of view, be more urgent. Even the modest market penetrations of EVs envisaged [3] will make a worthwhile contribution to oil

* European Economic Community

\+ tonnes of oil equivalent

substitution due to the fact that they will mostly be used in urban driving where ICEVs are especially inefficient.

It could be argued that coal may be used as the base primary fuel. However, the conversion of coal to transport fuel is only 50-60% efficient [4] and, based on coal as a primary fuel, the comparison of overall efficiencies is favourable with regard to EVs. With regenerative braking - well suited for EV systems - the efficiency of EVs is further increased, and overall it seems likely that starting from coal as a primary energy the EV could have an efficiency which is significantly greater than the ICEV for urban/suburban driving. Evidently, in the long term there is an energy conservation case for EVs.

A further desirable feature associated with EV operation, particularly in urban areas, is the reduction in noise when compared to the ICEV. This results from the elimination of the accelerating clutch, gears, and mechanical differential, and the fact that an electric motor requires no idling phase. However, it should be noted that only with a purely electrically driven vehicle can the above mentioned advantages of electric traction systems be fully attained.

1.3 Limiting Factors and Operational Problems of Electric Vehicles

The major difficulty in the realisation of EV transportation lies mainly with the battery power source. The present contenders as EV batteries are [5]:

1. Lead-Acid
2. Nickel-Zinc
3. Nickel-Iron

When determining the suitability of a battery for EV applications, four basic factors must be considered:

1. Energy density
2. Power density
3. Cycle life
4. Cost

A comparison of these factors for the above three types of battery is given in Table 1, where it may be seen that the nickel-based batteries have a considerably higher energy density than the lead-acid battery, and the nickel-iron battery has, in addition, a very high cycle life. However, the cost of a nickel-based battery is four times greater than the cost of a lead-acid battery, and it is mainly this factor which prohibits the use of nickel-based batteries in EV applications.

Other types of battery which are under investigation are the sodium-sulphur, lithium-chlorine, zinc-air, zinc-chlorine, nickel-cadmium, and silver-zinc, for example. Although all these batteries have a higher energy density than the lead-acid, their near term candidature as EV batteries is prohibited by [6-8]: a requirement for high operating temperatures for the sodium-sulphur (300-400°C) and lithium-chlorine (400°C) batteries; a low cycle life for the zinc-air and zinc-chlorine batteries; and a high manufacturing cost for the nickel-cadmium and silver-zinc batteries.

From the foregoing it may be seen that the lead-acid battery holds a dominant position for general EV applications, and is expected to continue to do so for the near future.

The fundamental problem with using lead-acid batteries as a power source in EVs is their low energy density, which is particularly noticeable when compared with the energy density of the liquid fuel used to operate ICEVs. For example: the energy stored in 7 tons

BATTERY	ENERGY DENSITY Wh/kg	POWER DENSITY W/kg	CYCLE LIFE	RELATIVE COST FACTOR*
LEAD-ACID	40	115	800	1
NICKEL/ZINC	64	110	200	4
NICKEL/IRON	54	110	1500	4

TABLE 1

*RELATIVE TO THE LEAD-ACID BATTERY

(about 7200 kg) of lead is only equivalent to the energy stored in 5 gallons (about 18 kg) of petrol [9].

The low energy density of the battery imposes corresponding limitations on the operating range and performance of the vehicle. Furthermore, between battery charges, the vehicle's performance deteriorates throughout its period of operation, due to the decreasing power density of the battery. However, payloads must not be limited, and must be maintained particularly as in the case of public bus line services where passengers left behind during the rush hours would not appreciate that the buses may have to operate with only part loads, due to such a deterioration in the performance of the vehicle.

As a consequence of the limited storage capacity of the battery, frequent (at least daily) recharging of the battery is necessary. However, using existing charging techniques, the efficient recharging of a lead-acid traction battery takes approximately 8-12 hours, whereas, the petrol tank of an ICEV can be filled within minutes.

1.4 Possible Solutions to the Problems Associated with the Use of Lead-acid Batteries in EVs

1.4.1 Improving the Available Discharge Capacity

Although the energy density of current commercial lead-acid traction batteries is approximately 40 Wh/kg, the theoretical energy density of such batteries is approximately 170 Wh/kg [10]. Evidently, efforts must be made to improve the realisable energy density.

About half the weight of a lead-acid battery consists of inert materials, such as: supports (grid metal), separators, connectors, terminals, and cell containers; water in the electrolyte may also be considered in this category. The remainder of the battery weight consists of active materials, such as: PbO_2, Pb and H_2SO_4. However,

these active materials are inefficiently used and less than half their amount actually take part in the cell reactions during discharge at the high rates required in EV applications [10].

Many on-the-road EVs are fitted with solid-state switches (transistor or thyristor) for stepless speed control. These electronic devices are turned-on and off at a fairly high frequency (up to 1,000 Hz) and have the effect of chopping the constant voltage of the battery into a series of rectangular voltage pulses at the armature terminals of the motor. The average armature voltage is varied by changing the mark/space ratio of these pulses, that is, by either maintaining constant pulse repetition frequency and allowing the pulsewidth to vary, or by maintaining a constant pulse-width and varying the frequency, or by some combination of these two techniques. This method of regulating the energy delivered to the motor is known as 'chopper control'. There is some controversy over the performance obtained from lead-acid batteries by using continuous pulsed discharge currents, when compared to that obtained by using continuous constant currents: Jayne [11] obtained a marked improvement in capacity from lead-acid batteries subjected to high speed pulsed discharge, whereas other investigators have observed no discernable increase [12, 13] or even a decrease [14] in the available capacity of the battery at discharge rates normally encountered in EV use*. The increase in capacity of lead-acid batteries which are subjected to such intermittent discharge has been attributed to a capacity 'recuperation' or 'recovery' phenomenon which occurs either during the pulse discharge itself [15], or during the rest periods between the discharge pulses [16]. This phenomenon is associated with improved utilisation of the active plate material by

*A review of previous pulsed discharge investigations is given in Section 4.2

increased penetration of acid into the pores of the plates.

In view of the conflict of opinion about the effects of pulsed discharge currents on the available capacity of a lead-acid battery, further investigations were thought to be appropriate.

1.4.2 Reducing the Recharge Time

One method of increasing the daily range of an EV and its utilisation is to rapidly recharge the battery at a suitably equipped on-the-road service station in a similar manner to the refuelling of ICEVs. However, due to certain charging effects, a rapid recharge of the battery cannot be realised by using conventional charging techniques. During the charging process, the battery experiences a temperature increase and an evolution of gas. An excess of either or both of these effects reduces the cycle life of the battery. The fundamental problem with conventional charging techniques is that in limiting the gassing and heating effects of the charge process so as to obtain a relatively high charge efficiency, fully charging the battery involves a time period of several hours.

Evidently, if EV transportation is to be realised, the recharge time of a lead-acid battery must be reduced considerably. In an effort to explore ways of maintaining, or preferably improving the charge efficiency while reducing the time taken to fully charge the battery, extensive investigations were made into two alternate methods of charging: (1) Pulsed current charging; and (2) Asymmetric current charging.

(1) Pulsed current charging

The decision to investigate the effects of pulsed charging currents on the charging performance of a lead-acid battery was based

upon the possibility of the no-load periods of the pulsed waveform having a 'relaxation' effect on the battery, which would allow the gases produced by the charge to disassociate themselves from the surfaces of the battery plates, thereby increasing the charge acceptance of the battery, and hence reducing the time taken to fully charge the battery.

A wide range of pulsed current charging techniques were investigated and the results were compared to those obtained from an equivalent constant current charge. The investigations involved charging up to, and beyond the gassing level of the battery so as to comprehensively determine the relative merits of the pulsed and continuous current charging techniques. Throughout the investigation, the charging performance of the battery was measured in terms of four parameters: (1) the increase in temperature of the electrolyte; (2) the volume of gas evolved; (3) the charge efficiency; and (4) the time taken to charge the battery.

A first literature search for previous pulsed charging investigations gave no indication of existing work. However, after the investigations of the author had been completed, work on part of this subject area was discovered to exist [17]. Nevertheless, due to the more detailed nature of the author's investigation, the author believes that the results obtained by him form the basis for a more comprehensive assessment of the virtues in using pulsed charging techniques.

(2) Asymmetric current charging

Asymmetric current charging involves the interspersing of negative or discharge current pulses throughout the charging process. It is possible that the discharge pulses reverse the chemical process

of charging, causing the gas bubbles on the surfaces of the battery plates to be forcibly removed. As stated previously, the removal of the gas bubbles from the surfaces of the plates should lead to a reduction in the time taken to fully charge the battery.

Using this charging technique, extravagant claims* have been made of a reduction in charging time, and in the gassing and heating effects of the charge, for lead-acid and nickel-cadmium batteries [18-20]. If such claims are valid, the asymmetric charging technique is revolutionary and of great significance for the realisation of EV transportation. The author therefore devoted considerable effort in investigating the validity of these claims.

1.4.3 Battery State-of-Charge Indicator and Model

An accurate state-of-charge indicator would help to increase the life of the battery by protecting it against excessive discharge. Since the cost of the batteries forms a considerable part of the total cost of the vehicle [21], an increase in the life of the batteries would result in a more cost effective vehicle; this would make the prospect of EV transportation more attractive, particularly where EV fleets are employed.

An accurate battery state indicator would also help to make optimum use of the available discharge capacity of the battery. Additionally, the battery charging facilities could become more cost effective, for rather than recharging or exchanging batteries at fixed times in the driving cycle, such procedures could be performed as and when required, and unnecessary charging, which can be detrimental to battery life, could be prevented. The EV could also be used more effectively, particularly in the industrial sector, where re-allocation

* A review of previous investigations is given in Section 5.3

of vehicles between heavy and light duties would be possible to avoid total battery discharge before the end of the working shift.

The development of an accurate mathematical model of the battery would greatly assist in the computer aided design of EVs. Computer simulation of EV systems has in the past years received increasing interest [22], because simulation entails less cost and time than is involved in constructing and testing prototypes, and also enables the most suitable EV system for a particular duty cycle and load profile to be obtained. The absence of an accurate model of the battery has been recognised [23] as the major weakness in modern EV simulation programs.

The main problem with commercial battery state indicators* is the failure to account for dynamic changes in battery operating characteristics, which are primarily caused by fluctuations in the discharge rate and electrolyte temperature of the battery. Although recently developed battery models/state indictors+ have contributed towards solving the problems associated with using commercial indicators, the problems of accounting for the changes in the performance of the battery as experienced in EV applications still remain, particularly regarding the fluctuations in electrolyte temperature. Also, all battery state indicators developed to-date, only attempt to monitor the performance of a battery which is subjected to continuous current discharge, and no consideration has been given to the case of pulsed discharge. For EVs which employ a 'chopper' for speed control, this is a considerable deficiency in existing models.

* A description of commercial indicators is given in Section 2.5

+ A review of existing battery model/state indicators in given in Section 6.2

To overcome the deficiencies of existing techniques of determining the performance of lead-acid batteries, the author developed a lead-acid battery model/state indicator that is applicable to a battery experiencing practical discharge conditions found in the EV application.

2. THE FUNCTION OF LEAD-ACID BATTERIES IN ELECTRIC VEHICLES

2.1 Types of Electric Vehicle

EVs may be broadly divided into two groups: (1) the straight or conventional EV; and (2) the hybrid electric vehicle (HEV). Conventional EVs employ only secondary storage batteries for their power source, whereas HEVs have an alternative energy source or storage system in addition to the secondary storage batteries.

A growing number of specialist EVs for industrial, leisure, and other purposes have been developed. For example, apart from the familiar milk float, the fork lift truck, golf buggy, hospital trolley and pedestrian controlled van have become established applications of conventional EVs. Other conventional EVs such as buses, cars, and light trucks have also been developed, and are being used to a greater extent in various parts of the world. In this country alone, 62 light truck EVs are in daily service, and EV cars are available which have a combined speed and operating range of 50 km/h and 50 km respectively [24].

However, due to the range and performance limitations imposed by the energy source on EVs, considerable effort has been directed towards developing the HEV.

2.1.1 The Hybrid Electric Vehicle

Various energy sources and power plants can be arranged into a system for a HEV. Although there are a great number of possible arrangements with different operating philosophies and component sizes, generally the power sources may be linked together either as a Series or as a Parallel Hybrid arrangement. In the series hybrid, prime movers and/or power sources are combined electrically (or hydraulically) before application to the final drive, and the energy

conversions are consecutive for the power flow [25]. In the parallel hybrid each power source has a direct mechanical coupling to the driven wheels. These configurations are illustrated in Fig. 1.

The complexity of hybrid drive trains compared with a conventional electric transmission can be readily appreciated from the systems depicted in Fig. 1. A comparison of the systems explains the preference with some manufacturers for series hybrids because these avoid the need for a continuously variable transmission (CVT). The series hybrid is, however, inherently less efficient than the parallel hybrid because of the increased number of energy transformations between the storage elements and the drive wheels.

The hybrid vehicle application will determine the mode of operation adopted and this may dictate the type of system used. For example: part of the duty cycle may involve low speed urban operation for the majority of the work schedule with intermittent higher speed trips; alternatively, the vehicle may spend a larger proportion of its time in rural environments with which it needs to be compatible and have longer range capability; additionally, the requirement may be to reduce the consumption of hydrocarbon fuel and operate with improved fuel economy.

Although a variety of HEV systems exist, the most common (due to the relative simplicity of its operating mode) is the Heat Engine-Battery System.

2.1.1.1 The Heat Engine-Battery System

(1) The Series Form

The Heat Engine output is converted into electrical energy [26] by a d.c. generator or alternator-rectifier. This electrical power is then converted to mechanical power by the traction motor. The traction

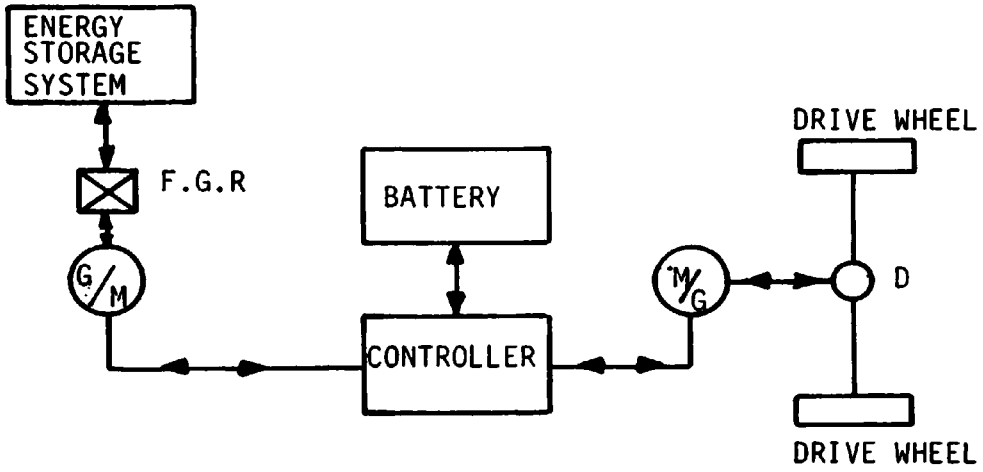

FIG. 1.1 A SERIES HYBRID CONFIGURATION

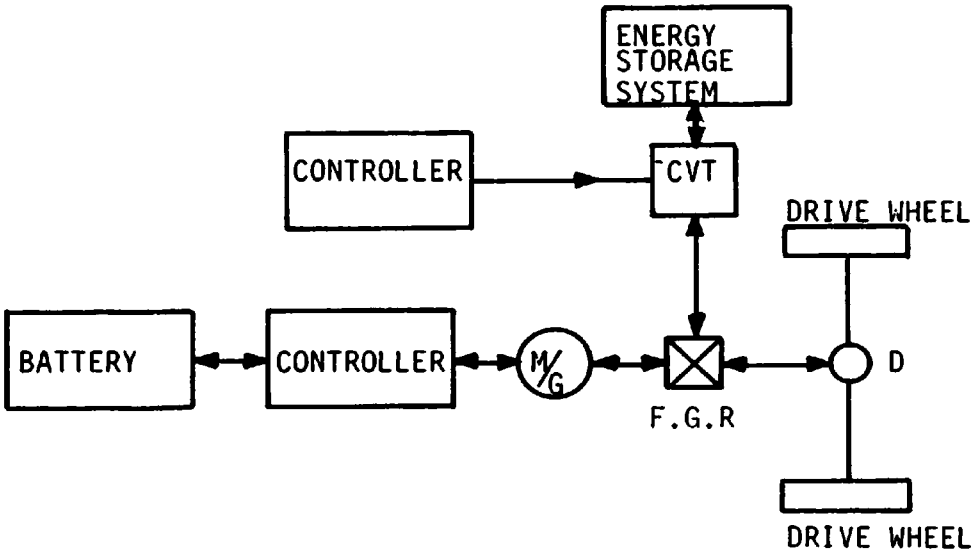

FIG.1.2 A PARALLEL HYBRID CONFIGURATION

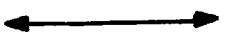

DENOTES ENERGY EXCHANGE

M	MOTOR
G	GENERATOR
F.G.R	FIXED GEAR RATIO
D	DIFFERENTIAL
CVT	CONTINUOUSLY VARIABLE TRANSMISSION

FIG.1 HYBRID VEHICLE CONFIGURATIONS

components are sized as for a conventional EV and the speed is set by the motor controller. When the power demand of the traction system differs from the engine/generator rating, the battery is used either to provide the extra power demand or absorb the excess generator output. The engine operates at a constant speed and load for optimum fuel economy, and the engine/generator output is set to the average vehicle loading under cruise conditions. The traction motor may also be used as a generator to recover some of the vehicle's braking energy. The major criticism with this vehicle configuration is that the traction motor has to be rated for full power, so that the engine rating has to be somewhat greater than the mean power requirement of the vehicle.

(2) The Parallel Form [27]

A portion of the heat engine output is delivered directly to the wheels via a mechanical transmission, and an electric traction motor acts in parallel so that engine and motor torques are additive. The surplus energy output passes through the generator to the battery when the traction power requirements are less than the engine rating. When the power requirements are greater than the engine output, only the extra power requirements pass through the electric transmission.

A variety of configurations have been proposed and tested. The simplest of these is to mount a single motor/generator on the same shaft. The bulk and weight of the systems can be minimised since the components in the system can be rated for their individual duties; however, to some extent this depends upon the operation required of the vehicle. For example, the vehicle may be required to operate as a conventional EV and would, therefore, need a battery and a traction motor to satisfy this duty.

2.1.1.2 Other Hybrid Vehicle Systems

Other recognised hybrid vehicle systems are: the flywheel-battery, the fuel cell-battery, the battery-battery, the triple, and the trolley-battery and trolley-diesel.

The flywheel-battery system [28] uses a flywheel as a means of storing the short term energy requirements of the vehicle. The flywheel has the advantage of virtually unlimited cycle life. Present technology flywheels have an energy density of 3-12 Wh/kg, which is less than the energy density of a lead-acid traction battery; however, the power density of the flywheel is in principle limited only by the hub, shaft, and gearbox strength. The battery need only supply the average power, thereby improving the vehicle range and battery life since the battery is never required to provide heavy discharge. The system configurations allow either a series or parallel arrangement to be adopted.

The fuel cell-battery system [29] arose because of the inability of fuel cells to provide the necessary peak power required by the vehicle. The battery characteristics required are similar to those of the heat engine-battery system, that is, it acts as a load-leveller. The fuel cell is the prime energy source.

In the battery-battery system [30] an established traction type battery is used as a load-leveller or 'power' battery for the other 'energy' battery.

In the triple system [31] a flywheel storage element is added to the heat engine-battery system in an attempt to combine the virtues of the latter and the flywheel-battery system.

The trolley-battery and trolley-diesel system [32] is in a different category to the above systems in that the two operating modes function independently of each other. This is the concept of the duo-bus, in which the bus may be operated either as a trolley-bus

picking up current on overhead trolley lines that feed the traction motor, or in diesel mode. In the latter case, the diesel engine is connected to an auxiliary electric motor which is used as a generator providing current to the traction motor. In the former case, a control system simultaneously regulates the traction motor and the battery charging requirements. The main disadvantages of the trolley-bus are [33]: (1) inflexibility, due to a dependence on overhead wires; (2) a tendency to dewire; and (3) the problems associated with overhead line maintenance.

2.1.2 Operational Systems

Cars, buses, and small trucks employing the aforementioned hybrid systems have been developed. However, apart from certain Japanese trucks, buses are the only hybrid vehicles that have been operated in fleet proportions. Typically such buses have a combined speed and range of 45 mph and 47 miles respectively [23].

The HEV and the conventional EV systems use the same basic components [23]. Fundamental to both systems is the drive train. In the parallel hybrid the drive train can be the same as for a conventional EV, with the transmission modified so as to accept a parallel input from the alternative energy source. In the series hybrid the drive train is identical to that of a conventional EV.

2.2 The Basic Electric Vehicle Drive System and its Interaction with the Battery

To maximise the range of a vehicle operated by electric storage devices it is particularly important to use the stored energy efficiently. Therefore, the traction system as well as the control and steering of the vehicle should involve only a minimum of energy

losses. This is an area for the application of high-performance electronic devices.

2.2.1 Electric Vehicle Drives

A block diagram of a basic EV drive system is illustrated in Fig. 2. The main consideration of the drive system is whether it should be d.c. or a.c.

2.2.1.1 The Direct Current Drive System

The preferred motor for use in EV applications has historically been the d.c. series machine which exhibits a characteristic tending to a constant h.p. output. This is because of its inherent feedback characteristic which strengthens the field excitation in sympathy with the armature current and, as a consequence, the machine tends to slow down when encountering increased torque requirements. Fig. 3.1 illustrates a typical characteristic of such a machine from which it can be clearly seen that speed reduction with increased load is experienced, and also that the torque characteristic which is proportional to the square of the armature current initially, becomes linear as the machine tends to saturate. A further advantage with this type of machine is associated with the strengthening of field current with increase in armature current, thus permitting operation under high armature current conditions, which would normally tend to produce large armature reaction effects, causing poor commutation.

The use of separately excited d.c. machines has, until the development of electronic control, been associated with many difficulties, the principal one being that since these are essentially constant speed machines, the power output requirements would increase considerably when encountering gradients or other loading conditions.

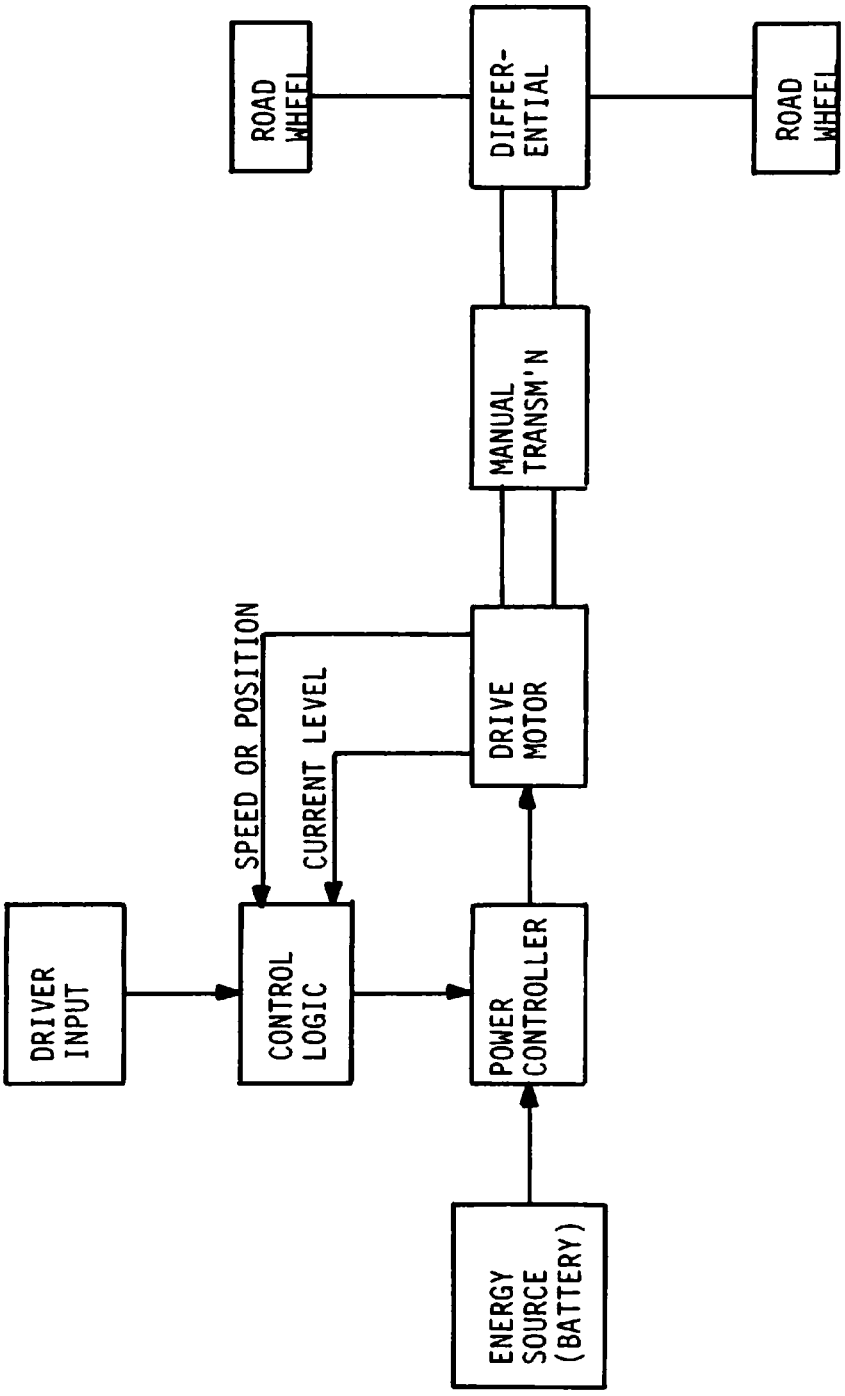

FIG. 2 BLOCK DIAGRAM OF A BASIC ELECTRIC VEHICLE DRIVE SYSTEM

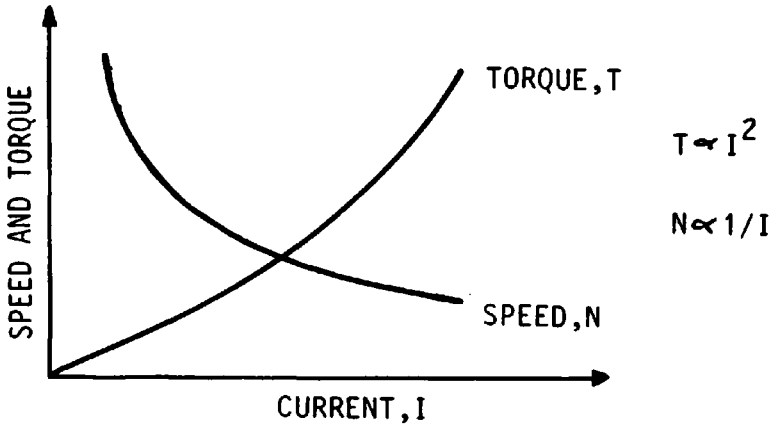

FIG. 3.1 SERIES MOTOR CHARACTERISTICS

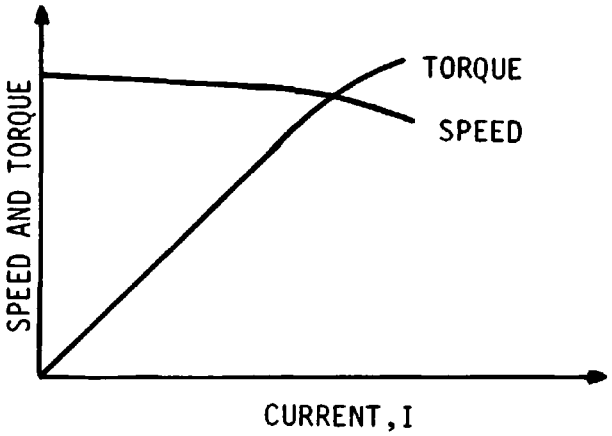

FIG. 3.2 SEPARATELY EXCITED MOTOR CHARACTERISTICS

FIG. 3 D.C. MOTOR CHARACTERISTICS

Fig. 3.2 illustrates a typical characteristic of such a machine which is essentially the same as a shunt motor characteristic. From this characteristic it can be seen that the curve of speed against armature current is roughly constant, dropping-off rapidly towards the high armature current end due to armature reaction effects. A similar situation exists as regards the torque characteristic whose initial rate of rise is virtually linear, but subsequently tapers-off.

The operation of the d.c. series motor, in sympathy with all types of d.c. motors, is essentially governed by the equation:

$$V_b = E + I_a \cdot R_a \qquad (1)$$

where V_b = the supply voltage; I_a = the armature current; and R_a = the armature resistance and field resistance in the case of a series machine. The factor E is normally denoted as the back-emf of the machine and is the counter voltage produced by the armature conductors rotating in the magnetic field of the stator.

When using these motors, two basic factors that relate to the starting of the motor must be considered: (1) some means of starting the motor from rest must be provided, since under these conditions E is zero and therefore V_b is equal to $I_a \cdot R_a$; and (2) the starting current would be very high since to achieve a high operating efficiency, R_a is generally made as small as possible. Apart from these considerations, traction vehicles require speed control, and where batteries are used as the prime source of energy, the source voltage is essentially constant and some means must be provided to effectively reduce this voltage when it appears across the motor terminals to enable a varying speed output to be obtained.

The effective voltage presented to the motor terminals is regulated by means of 'chopper' control. The availability of thyristor and transistor choppers has caused a swing away from the series to the

separately excited machine, since both armature and field currents can be controlled at will. Thyristors capable of carrying the currents involved in EV operation were developed before similarly rated transistors and so most existing d.c. drive systems employ thyristor choppers.

The characteristic of a thyristor, which is well known, is that the device can very readily be switched into conduction but cannot be easily turned-off when supplied from a d.c. source. Various methods of turn-off have been developed over the years, all of which rely on the basic principle that a capacitor is charged to the correct polarity to provide a reverse voltage across the main conducting device when commutation is required, and it is the means by which this capacitor is charged that are the main differences between the various chopper circuits. One such chopper is illustrated in Fig. 81 of Appendix 1.2, and is known as the Jones Chopper. T1 is the main current conducting thyristor, and capacitor C turns-off T1 by means of the auxiliary thyristor T2. This chopper circuit was used by the author in his investigations into the effects of pulsed discharge currents on the behaviour of lead-acid batteries, and a detailed description of the operation of the circuit is given in the above Appendix.

2.2.1.2 The Alternating Current Drive System

Although the d.c. system is highly developed and available, there is an incentive to move to a.c. transmission. The main reasons for this are: (1) the d.c. machine does not lend itself to mass production techniques owing to the wound armature and commutator; (2) the induction motor is normally cheaper, and could respond to automative type production; (3) the induction motor is lighter and can attain higher rotational speeds; (4) the induction motor has a

construction which is simple and rugged, and requires only minimal maintenance; and (5) there are no starting problems as with the d.c. motor.

Fundamentally, the induction motor is a constant frequency, constant speed machine, but when supplied with a variable frequency or variable voltage, or with both simultaneously, it can produce a wide variation of speed, as illustrated in Fig. 4. Supply voltage variation on its own, requires a relatively simple controller but produces heavy losses and low efficiency, particularly at the lower speeds, making the arrangement most unsuitable for road vehicle drives. An alternative control system, using variable frequency and variable voltage from a more sophisticated electronic controller, gives an appreciably higher efficiency, but the inherent speed-torque characteristics are fundamentally opposite to those normally required for the vehicle. For example, at the lower speeds, which are attained at the lower supply frequencies, the starting torque is a minimum, whereas the vehicle may require maximum torque under these conditions, as normally provided by a series connected d.c. motor. Consequently, although the torque at low frequency may be increased by various means, the induction motor cannot normally be used to its best advantage on vehicle drives. However, this disadvantage is more than compensated for by the advantages in using the motor and, as a consequence, a.c. drive systems are gaining greater acceptance. Solid state inverters for the conversion of d.c. to variable frequency a.c. are widely available using either thyristors or transistors, depending upon the required magnitude of output voltage and current. The basic three-phase bridge inverter is made up of six load-carrying semiconductor power switches, with a feedback diode connected in inverse parallel across each switch to allow for reaction power flows, as shown in Fig. 5. Battery

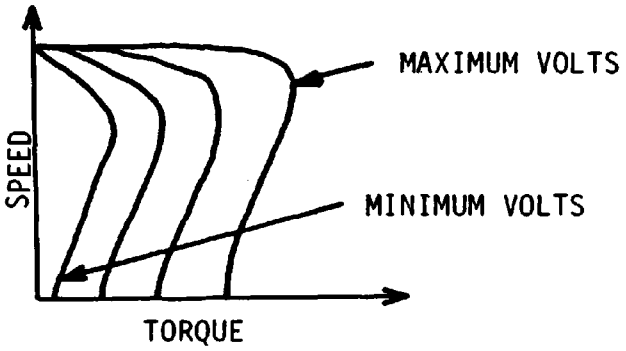

FIG. 4.1 A.C. INDUCTION MOTOR CHARACTERISTIC WITH VARIABLE VOLTAGE CONTROL

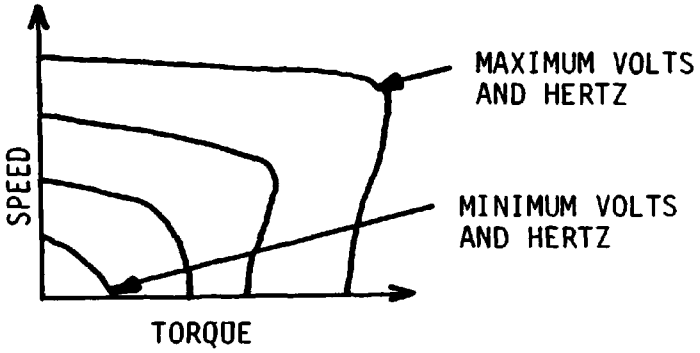

FIG. 4.2 A.C. INDUCTION MOTOR CHARACTERISTIC WITH VARIABLE VOLTAGE AND VARIABLE FREQUENCY CONTROL

FIG. 4 A.C. MOTOR CHARACTERISTICS

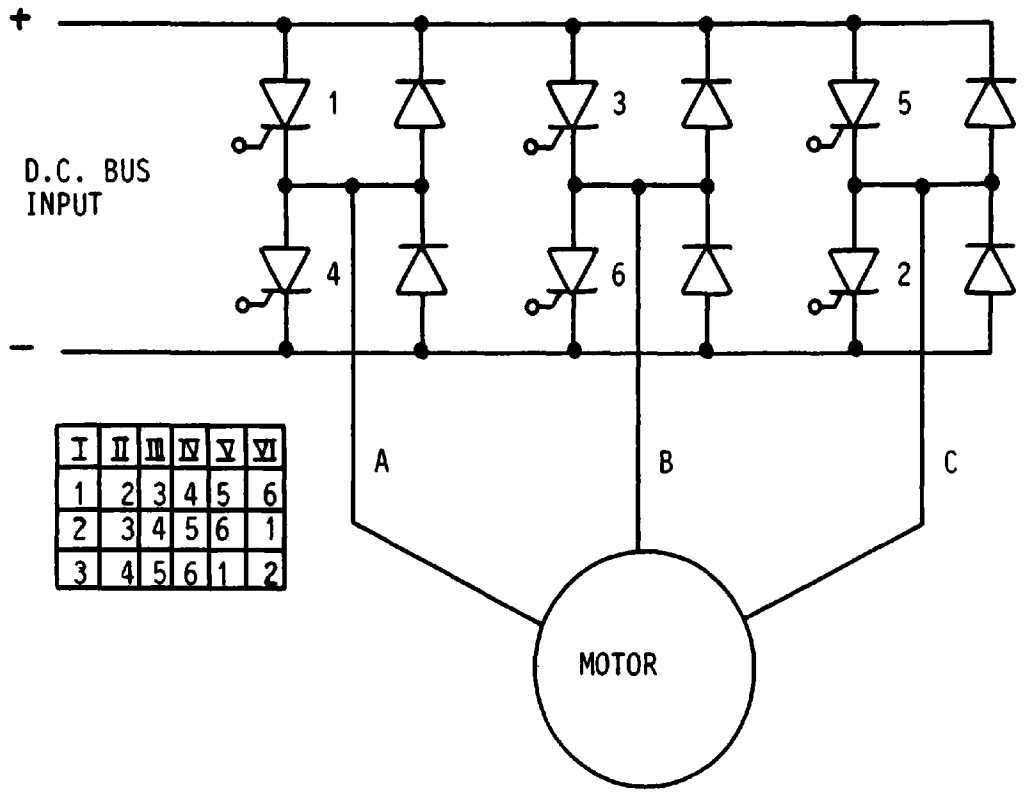

I	II	III	IV	V	VI
1	2	3	4	5	6
2	3	4	5	6	1
3	4	5	6	1	2

FIG. 5 BASIC THREE PHASE INVERTER WITH MOTOR
(SHOWING THYRISTOR FIRING SEQUENCE)

inverter systems suitable for EV drives may be classified by the method used to vary the inverter output voltage and also by the commutation circuit used to force-off the conducting SCR's while they are carrying the load current [34]. The former classification yields two distinct systems suitable for use in vehicle drives: (1) the Direct Current Chopper-Inverter System; and (2) the Pulse-Width Modulated (PWM) Inverter System. Making full use of integrated circuitry and suitable microprocessors, modern inverters mainly employ PWM techniques for producing alternating currents. A detailed evaluation of the relative advantages and disadvantages of the above two inverter systems is described elsewhere [35].

2.2.1.3 A Comparison of A.C. and D.C. Drive Systems

When making comparisons as to whether the drive system should be a.c. or d.c. it is necessary for the traction motor and controller to be considered together [36]: the d.c. machine is generally more costly than the a.c. machine but the reverse is currently true of the controllers; the efficiency of an induction motor is higher than the efficiency of a d.c. motor, but an inverter (thyristor or transistor) is less efficient than a chopper; an inverter (thyristor or transistor) is heavier than a chopper, however, when considering the motor/controller system as a whole, the d.c. system is lighter than the a.c. thyristor inverter system but heavier than the a.c. transistor inverter system. By considering all these factors it has been suggested that the a.c. transistor inverter system is the most promising.

In an effort to improve drive systems, other traction drives are under investigation: variable speed reluctance motors, and permanent magnet disc machines. The variable speed reluctance motor

[37] has the advantages of other a.c. motors. The controller requires less components than a PWM inverter for an induction motor. The permanent magnet disc machine [38] has the potential for high efficiency and high speed operation. Unfortunately, these machines are expensive, and the high cost of permanent magnet material is likely to continue.

2.2.2 Practical Control Systems

In addition to providing speed control, it is necessary to provide other facilities for a practical EV control system:

(1) Facilities to enable the direction of rotation of the motor to be changed.

(2) A foot control system, which enables the driver to provide the necessary signals to the control circuit, to affect speed control (Fig. 2).

(3) A pulse generator control circuit which fires the components in the power control circuit at the correct sequence, and also at the rates dictated by the input from the foot control, and any other feedbacks that may be employed (Fig. 2).

(4) A current limit circuit. It is not economically feasible to design the power circuit to be capable of dealing with stalled current. Generally, the power circuit is designed to deal with a prefixed percentage value of the stalled current and a current limit circuit is employed which constantly monitors the current flowing in the power circuit, and ensures that the preset value cannot be exceeded.

(5) A safety circuit to ensure against EV malfunction.

(6) A braking system. The preferred method of vehicle braking would be to return the kinetic energy of the vehicle to the supply (the

battery) - a process known as regenerative braking. Under such conditions the traction motor operates as a generator. Regenerative braking has three distinct advantages:

(i) the recovery of braking energy would be advantageous because of the limited energy output of the battery,

(ii) the utilisation of the motor to replace in-part the normal mechanical brakes would reduce the amount of wear-and-tear on the braking system components, and

(iii) braking facilities would be available in the event of mechanical brake failure.

Efficient control of EVs with correct response to driver demands, almost certainly requires a microcomputer to supervise the system. The use of microprocessors for engine management in ICEVs is a well researched area and manufacturers are producing experimental models world wide. The transactions of the Society of Automotive Engineers (SAE) are a good indication of the amount of work in this field [39]. The necessary electronics can operate satisfactorily on a vehicle and promises substantial benefits in fuel economy. Similarly, microprocessor control of conventional EVs is developing [40], and will no doubt feature particularly in a.c. drive systems. Recent examples of HEVs have also included microcomputer control of the systems [41]. For such controllers to be successful, a correct operating strategy for the vehicle has to be developed, which will be dependent on the type of vehicle used and the load and duty cycle to which it is subjected.

2.3 Electric Vehicle Duty Cycles and Load Profiles

The limitations in EV operating range and performance, and the different operating characteristics of the various EV systems, requires that the EV be designed to suit a particular duty cycle and load

profile. The need to determine the suitability of an EV system for a particular duty cycle has resulted in the development of the SAE J227a standard experimental test procedure [42], which defines a test cycle as shown in Fig. 6, where:

V = Vehicle cruise speed

t_a = acceleration time

t_{cr} = cruise time at a specified speed

t_{co} = coast time

t_b = braking time to zero speed

t_i = idle time at zero speed

T = total cycle time

The purpose of SAE J227a is to determine the maximum range travelled and energy consumed by a test vehicle when operated on a level surface in a defined and repeatable driving cycle. The test procedure is divided into four different testing schedules, and the values of the parameters of these schedules are given in Table 2. The schedules are intended for use in testing a vehicle as follows:

Schedule A: characterised by a peak speed of 16 km/h and is intended for use in testing a vehicle designed for use on a fixed route with high frequency stop and go operation (for example, residential postal delivery van, milk truck, etc.).

Schedule B: characterised by a cruise speed of 32 km/h and is intended for use in testing a vehicle designed for use on a fixed route with medium frequency stop and go operation (for example, bakery van, shuttle bus, etc.)

Schedule C: characterised by a cruise speed of 48 km/h and is intended for use in testing a vehicle designed to be

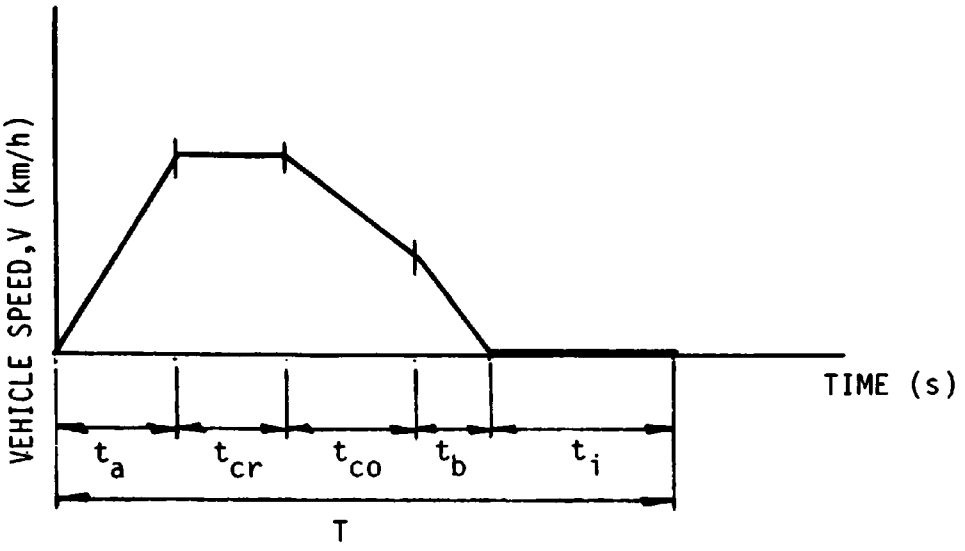

FIG. 6 VEHICLE TEST CYCLE (SAE J227a)

SCHEDULE	A	B	C	D
V	16±1.5	32±1.5	48±1.5	72±1.5
t_a	4±1	19±1	18±2	28±2
t_{cr}	0	19±1	20±1	50±2
t_{co}	2±1	4±1	8±1	10±1
t_b	3±1	5±1	9±1	9±1
t_i	30±2	25±2	25±2	25±2
T	39±2	72±2	80±2	122±2

Note: All times shown are in seconds and speeds in km/h

TABLE 2 TEST SCHEDULE FOR REPEATABLE DRIVING PATTERN

used over a variable route with medium frequency stop and go operation (for example, parcel post delivery van, retail store delivery truck, etc.).

Schedule D: characterised by a cruise speed of 72 km/h and is intended for use in testing a vehicle designed to be used over a variable route in stop and go driving, typical of suburban areas (for example, commuter car, etc.).

The most common vehicle type in production today, satisfies the characteristic of Schedule C [43]. An example of how the battery load current varies under Schedule C operating conditions is shown in Fig. 7. Evidently, the current drawn from the battery under practical operating conditions will be of a less regular pattern, and this is illustrated by the load profile of Fig. 8 which is based upon data obtained for an electric mini-truck on a delivery round in Japan [44]. As can be seen from Fig. 8, the variation of battery load current for a conventional EV can be considerable, ranging from zero to a few hundred amperes; and in an EV where regenerative braking is employed, the battery will also be subjected to charging currents of varying magnitude. The lead-acid batteries that are used in EVs will, therefore, need to be durable and have a suitably high ampere-hour capacity so as to deal with such variations in discharge and charge rates. The choice of battery and the duty cycle to which the battery is subjected will effect the technique used to recharge the battery.

2.4 Lead-Acid Battery Charging Techniques

2.4.1 Charging Considerations

For most of the charging period of a lead-acid battery, the charging current converts the active material into lead dioxide (PbO_2)

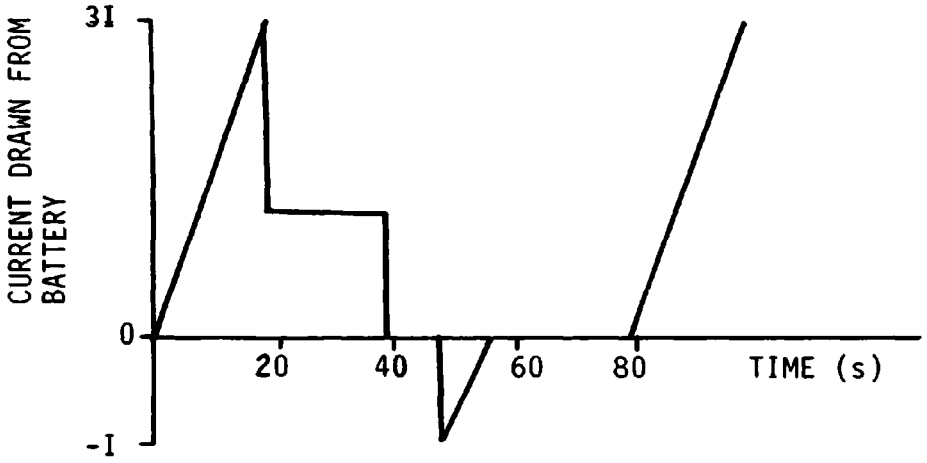

FIG. 7 CURRENT TEST SCHEDULE FOR ELECTRIC VEHICLE BATTERIES (J227aC)

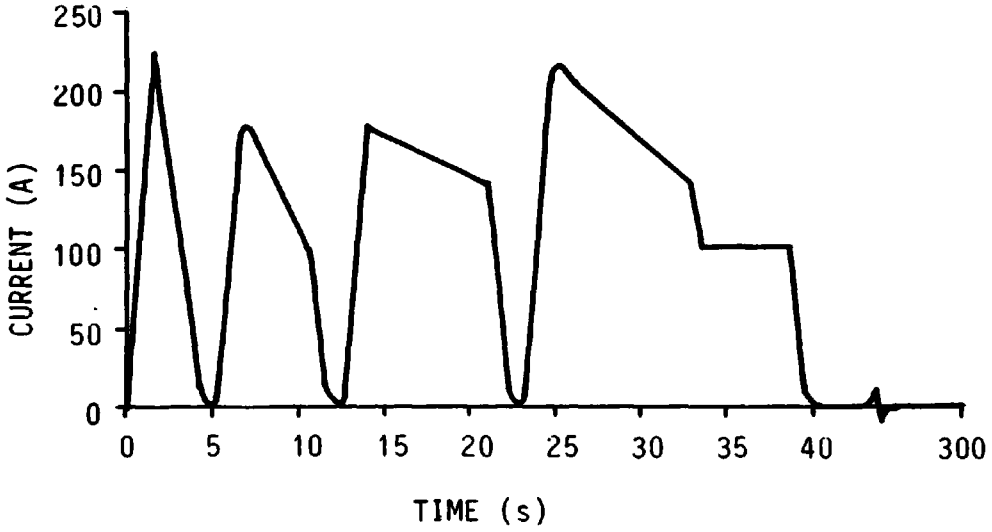

FIG. 8 LOAD PROFILE BASED ON VEHICLE USE [44]

on the positive plates and spongy lead (Pb) on the negative plates. However, after the cell has received about 75-80% of its full charge, the charging current acts less efficiently on the remaining particles of lead sulphate, and the excess current decomposes the water in the electrolyte, releasing this as oxygen at the positive plates and hydrogen at the negatives. There is a considerable rise in cell voltage as the rate of gassing increases, until the battery is nearly fully charged. The extrusion of gas bubbles from the plates tends to dislodge particles of PbO_2 and push electrolyte out of the plate pores, so the plates may be weakened and the charging process may be slowed down due to electrolyte starvation in the region of the plates, if gassing is allowed to continue at a rapid rate. In addition, the increased energy dissipated in the cell from electrochemical polarisation may cause an appreciable rise in electrolyte temperature, which will have a detrimental effect on the cell plates and separators [45]. Thus, unnecessary gassing must be avoided if a battery is to attain its maximum life.

In an effort to restrict gassing rates to a tolerable level, conventional charging techniques as used in the present industrial application of EVs, are designed to operate on a long term basis, that is, to recharge the battery in a matter of 8-12 hours.

2.4.2 Conventional Charging Techniques

2.4.2.1 The "Ampere-Hour Law"

This law states that a battery, at any state-of-charge, can accept a current up to an ampere value equal to the ampere-hours to be put into the battery without it experiencing excessive heating or gassing. For example, if the battery has been discharged to the extent of 100 ampere-hours, any rate up to 100 A may be used; when the charge

has been continued until 10 ampere-hours have been put in, leaving 90 ampere-hours still out, the rate must be reduced below 90 A etc.; that is, the rate is continually reduced or tapered to keep within the value defined by the "Ampere-Hour Law". When the rate is finally reduced to the prescribed 'finishing' rate for the battery, the charge may be completed at that rate without further reduction. The law may be expressed by equation (2), which results from the condition that the

$$di = -i.dt \qquad (2)$$

charging rate i is continually reduced by the amount of charge in ampere-hours replaced in the interval of time dt.

The integration of this expression gives the exponential relationship:

$$i = A.e^{-t} \qquad (3)$$

where: A = the number of ampere-hours out of the battery at the commencement of the charge (t = 0)

e = the base of natural logarithms

t = the time in hours

The law is shown graphically in Fig. 9.

The charging technique has three basic disadvantages:

(1) the charging rates during the initial period of the charge need not be so moderate,

(2) the technique calls for constant control to maintain a carefully predetermined schedule of charging rates for given intervals of time; the process is further complicated by the dependence of the capacity upon temperature and cell 'memory'; and

(3) the system requires a charger with a comparatively high output which is used at full capacity for a short time only, at the commencement of the charge.

2.4.2.2 Constant Voltage Charging

In this method of charging, a voltage of 2.30 - 2.40 V/cell is applied without any ballast in the circuit. The charging current is given by:

$$i = \frac{V - E}{r_c} \qquad (4)$$

where: V = the voltage applied to the battery, Volts

E = the back-emf of the battery, Volts

r_c = the internal resistance of the battery, ohms.

During the charging period, r_c decreases with increase in the electrolyte temperature and battery state-of-charge, while E increases.

Fig. 9 shows that a large current passes into the battery initially. As the battery voltage increases, the charging current falls quickly, and near the completion of the charge, reaches a value which is less than the specified finishing rate. When set to the correct voltage, the characteristic is very similar to that obtained by the "Ampere-Hour Law".

The charging technique has three basic disadvantages:

(1) the system requires a charger with a high output which is used at full capacity for only a short time, at the commencement of the charge,

(2) the applied voltage must be maintained virtually constant, the correct value of which will depend upon the temperature of the battery, and

(3) the technique is unstable if comparatively high voltages are used, since small variations of voltage or temperature cause considerable variations in the charging rate. Because of these disadvantages, this method is mainly used for systems where batteries are not discharged by more than about 25% of their rated 5-hour capacity.

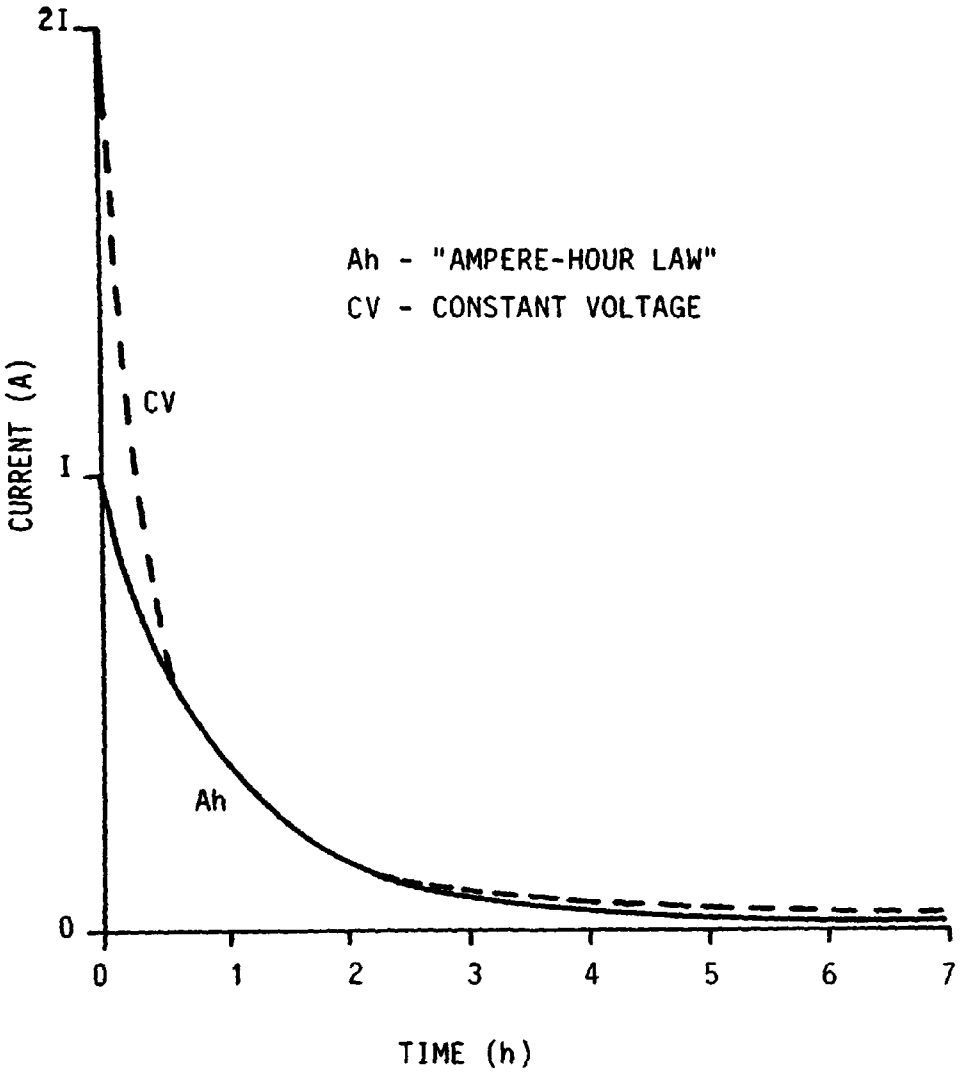

FIG. 9 THE "AMPERE-HOUR LAW" AND CONSTANT VOLTAGE CHARGING TECHNIQUES

To overcome these disadvantages, a modified constant voltage technique has been developed and is widely used for charging batteries in motive power applications. In this technique, the charging voltage is maintained substantially constant (at about 2.8 V/cell) at a value higher than that required for straight constant voltage charging, and a ballast is included in the charging circuit. The time required for a complete charge is longer than that obtained by using the straight constant voltage technique but no manual control is required. The charging rate automatically reduces as the charge progresses (Fig. 10). A typical charge time is about 10 hours [46].

2.4.2.3 Two-Step Charging

When charging is necessary in about 8 hours, a 'two-step' charging routine is used. Each step may have either a tapered (Fig. 11) or a constant current characteristic.

In the tapered method, the charging current of the first step is initially higher than that of the modified constant voltage method, causing the cell gassing level to be reached earlier. In the second stage the taper is similar to that of the modified constant voltage characteristic, and the current at 2.5 V/cell is approximately 1/12th of the battery capacity. When gassing starts, the characteristics of the two charging techniques are basically the same. In the constant current method, the charging current for each stage is maintained constant.

2.4.2.4 Spegel Charging

In 1972 Chloride introduced the Spegel method of charging. A typical recharge characteristic is shown in Fig. 12. The charge proceeds until the battery voltage exceeds 2.3 V/cell, after which, the

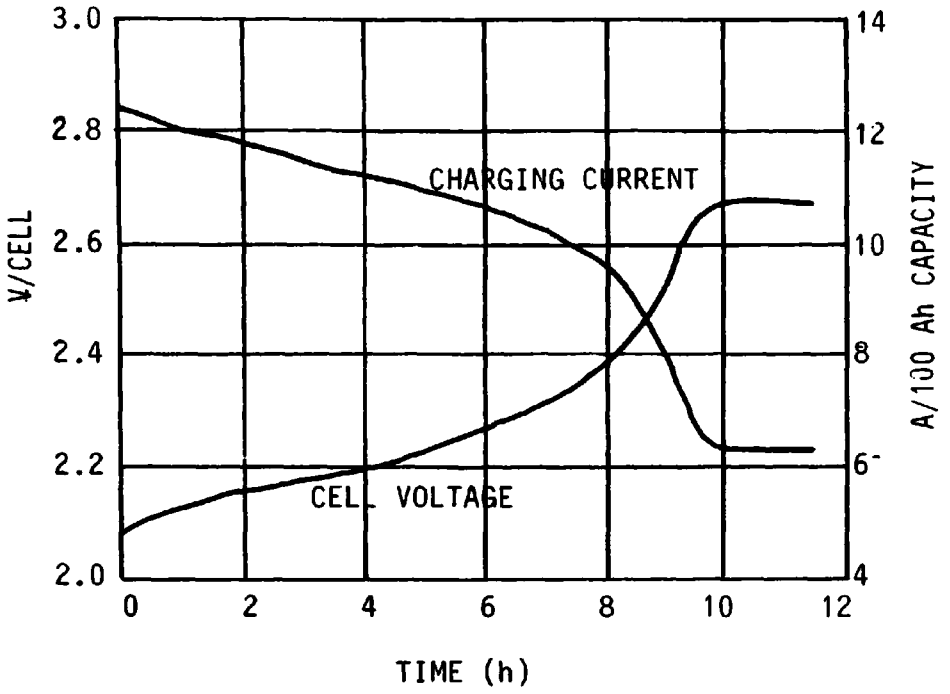

FIG. 10 MODIFIED CONSTANT-VOLTAGE CHARGING CHARACTERISTICS

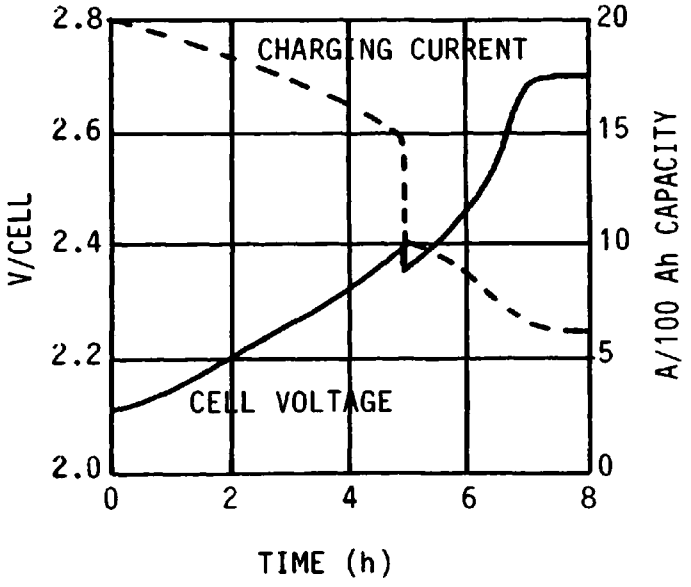

FIG. 11 TWO-STEP TAPER CHARGING CHARACTERISTICS

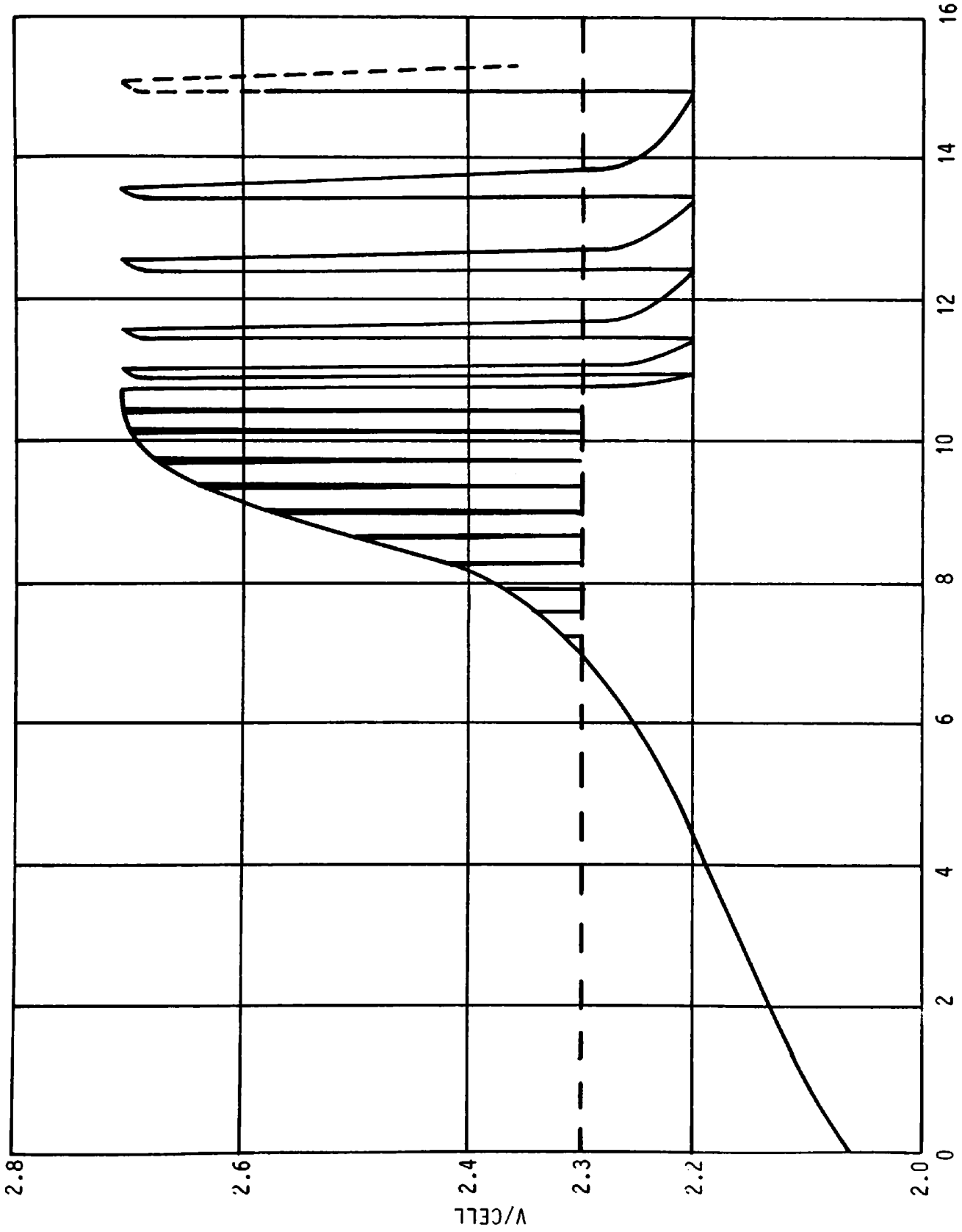

FIG. 12 TYPICAL RECHARGE CHARACTERISTIC UNDER "SPEGEL" CONTROL

charge is given in pulses, each having a duration of 15 minutes. When each pulse of charge is switched-off, an electric clock measures the time taken for the battery voltage to fall back to 2.3 V/cell, at which the next pulse is initiated. This sequence of operations continues until the open-circuit periods, or decay times, are equal. The main charge is now completed, and the battery is charged and ready for service. If not required, the battery receives about 2 minutes charge each time the battery terminal voltage falls to 2.2 V/cell. The frequency of these pulses is determined by the time taken for the battery voltage to fall to 2.2 V/cell. These 'equalising' pulses provide just enough charge to replace battery internal losses and keep it fully charged.

The Spegel charging method is preferred to the previously described methods, since it reduces the gassing and heating effects. By comparing Figs. 10 and 12, it may be seen that the Spegel and modified constant voltage characteristics are essentially the same, and it should also be noted that no significant reduction in the charge time is accrued by using the Spegel method.

2.4.2.5 Gas Controlled Charging

A number of gas monitoring techniques have been used to establish charge regulation, but the most familiar of these was introduced in the mid 1960's and is known by its trade name 'Cyclocat'. This system utilises the properties of a thermistor - a small semiconductor device, of which the resistance changes sharply for comparatively small changes in temperature around the critical temperature for which the device has been designed - with a negative temperature coefficient. The resistance of the thermistor remains fairly constant until, when gassing commences, the thermistor is cooled

by the gases on their way to the atmosphere. The thermistor forms part of a bridge circuit used to control the signal current of a transductor, thus varying the impedance and voltage drop of the transductor to control the voltage applied to, and the charging current of, the battery. Because of the relatively higher thermal conductivity of hydrogen compared to oxygen, it is this gas constituent which becomes the controlling influence. The cell temperature which affects the correct charging rate, is monitored by a second thermistor which influences the transductor output parameters. A typical 'Cyclocat' charging characteristic is shown in Fig. 13.

2.4.3 Limitations of Conventional Charging Techniques

All the above charging techniques are unsuitable if EV transportation is to be realised, since efficient recharging of the batteries, which entails limiting gas evolution and heat generation, involves a time period of several hours. The more recently developed Spegel and Cyclocat techniques do not significantly reduce the charging time when compared to the less complicated conventional techniques, but do, however, improve the charging efficiency by monitoring the battery condition using voltage and gas sensing techniques respectively. It is also important to note that the conventional charging techniques do not take advantage of the high charge acceptance of the battery during the initial period of the charge. In view of the limitations of existing charging techniques, the author thought it to be of considerable importance to investigate the effects of pulsed and asymmetric current charging techniques on the charging performance of lead-acid traction batteries, and to determine, when compared to a conventional charging technique, whether or not they reduce the heat generation, gas evolution, and charge time.

2.5 Electric Vehicle Instrumentation for Monitoring the Battery State

The most basic method of measuring the battery state would be by means of an integrating-type ampere-hour meter. However, the available capacity and voltage of the battery is greatly influenced by the discharge rate and electrolyte temperature and so this method would be grossly inaccurate.

Another method, which is mainly used by present commercial instrumentation, is to utilise the electrical characteristics of the battery. The method may be illustrated by Fig. 14, where it may be seen that if both the discharge rate and terminal voltage are known, the state-of-charge of the battery may be determined. The common types of indicators, which are mainly based on direct voltage sensing techniques, attempt to estimate the discharge rate by indirect means based on some assumed relationships, and the random scatter of on-load battery voltages due to rapidly fluctuating electric vehicle power demands are then interpreted in terms of the discharge capacity.

The degree of accuracy of the state-of-charge indicators will depend upon the assumptions made about the relationship between voltage and state-of-charge. As with the ampere-hour method of state indication, instrumentation based on the voltage sensing techniques incur substantial errors because the battery state is dependent upon, amongst other factors, temperature. This for example therefore eliminates the possibility of using any generalised voltage versus state-of-charge curve for accurate state-of-charge monitoring.

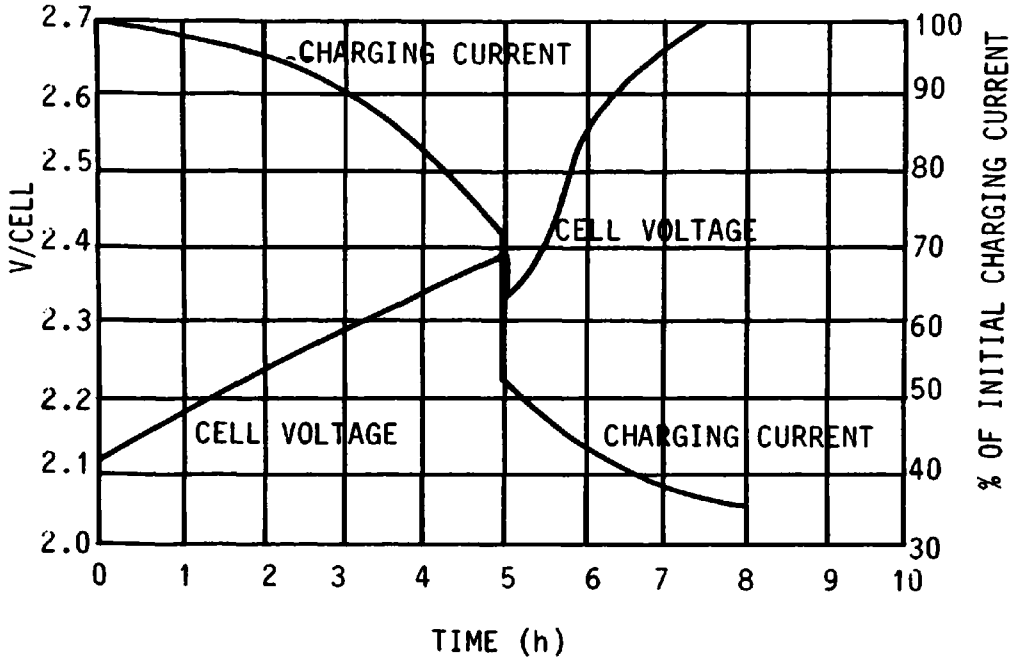

FIG. 13 THE "CYCLOCAT" CHARACTERISTIC

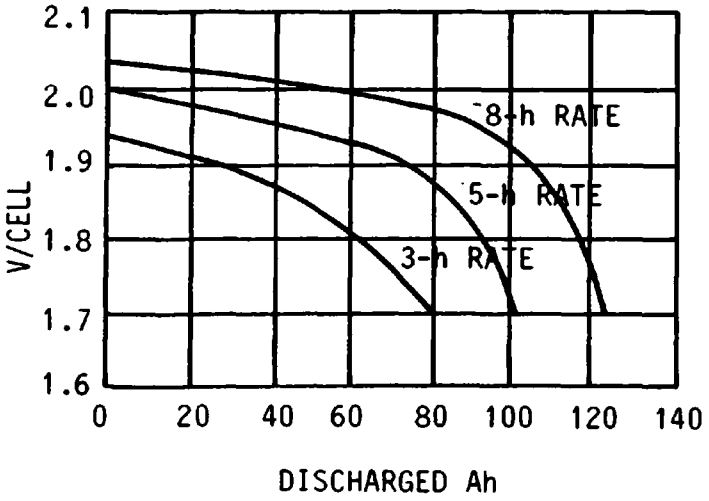

FIG. 14 BATTERY TERMINAL VOLTAGE VERSUS DEPTH-OF-DISCHARGE

3. THE LEAD-ACID TRACTION BATTERY

3.1 Introduction

According to the type of duty they have to satisfy, batteries may be broadly divided into two classes: (1) stationary batteries; and (2) portable batteries. Stationary batteries are those which are located in a fixed place during their life. Examples of such applications are: power stations, telephone exchanges, and emergency lighting systems. Portable batteries are those which are operated in various locations or transported in the course of operation either by hand or in the vehicle of which they form a component part. Examples of such applications are: automobiles (cars and motor vehicles), aircrafts, and industrial vehicles (e.g. trucks and EVs).

The basic components and materials used in the construction of these two classes of lead-acid battery are mainly the same, their fundamental difference lies in the thickness, shape, and size of the cell plates.

Batteries used in EVs are mainly of the traction type which are designed to provide high currents for comparatively long periods of time with a good cycle life.

3.2 Traction Battery Types and Constructional Features

According to the design of the cell plates, lead-acid batteries may be divided into two groups: (1) tubular plate batteries; and (2) flat-plate batteries. The tubular type battery (Fig. 15) takes its name from the positive plate which is of tubular construction. In these plates the active material is formed around conducting lead spines which run the length of the enclosing tube. The negative plates of the tubular type battery are of the flat pasted design; which is used for both the positive and negative plates in the flat-plate battery.

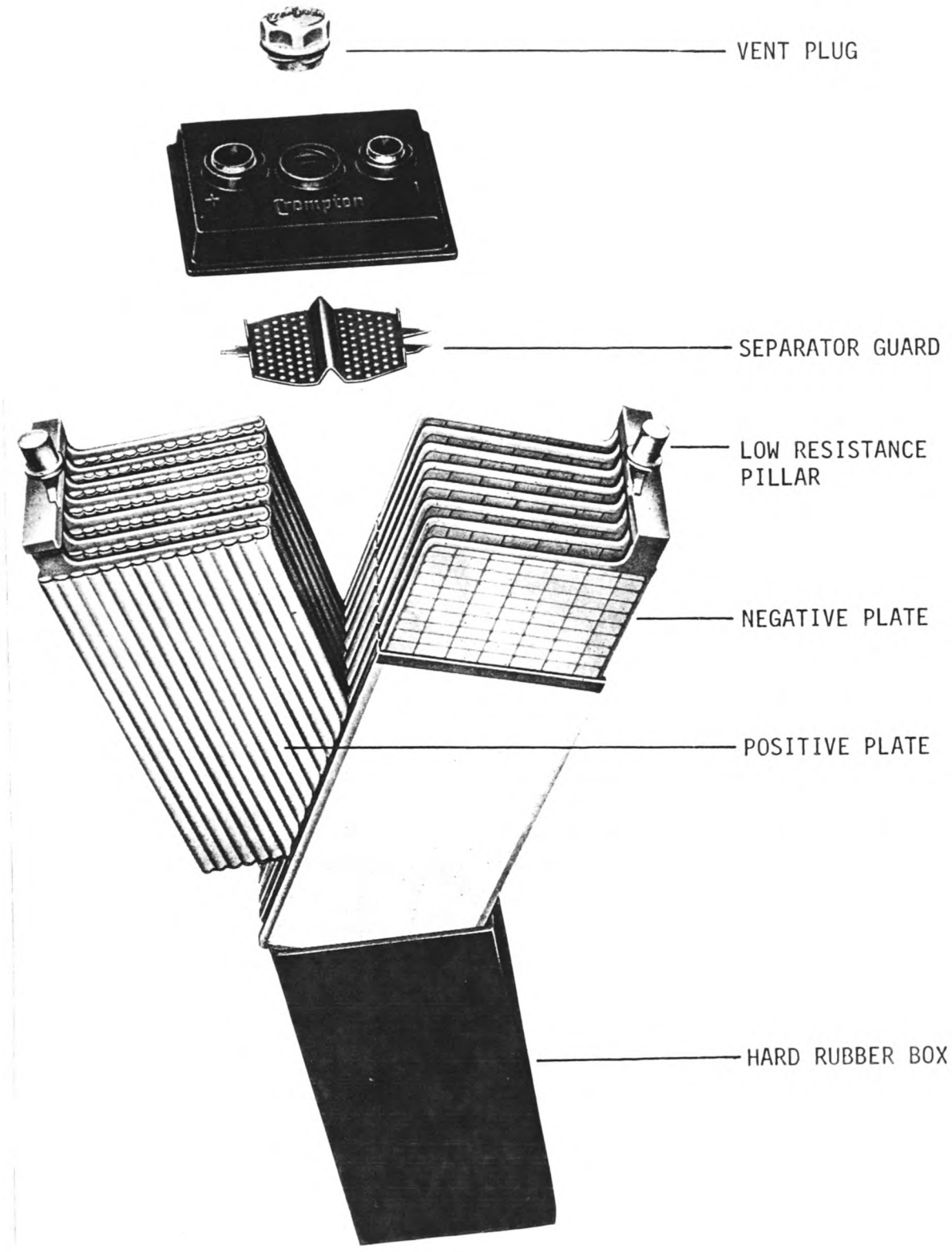

FIG. 15 THE TUBULAR ARMOURED CELL

The type of lead-acid battery used will depend upon the application. Demands for high discharge currents from relatively small plate volume are met by batteries with a large number of thin pasted plates. These provide maximum surface electrolyte interface and are of low internal resistance. Where the battery is to be continually cycled, i.e. charged and discharged at widely varying current rates, these requirements are met by batteries particularly designed to retain the active plate material - tubular type batteries. This feature, together with the fact that tubular type batteries provide a higher capacity per unit volume when compared with flat-plate batteries [47], makes them particularly suitable for EV applications.

The main components of a lead-acid traction battery are:

(1) the positive and negative electrodes (the plates),

(2) the separators, and

(3) the electrolyte.

3.2.1 The Plates

A cell plate basically consists of a grid structure which is impregnated with active material.

(1) The grid

The grid serves as a support for the active material of the plates and as a conductor for the electric current. The grid is also intended to maintain a uniform current distribution throughout the mass of the active material. If the current distribution is not uniform, the changes in volume of the plates during charge and discharge will be uneven, resulting in a tendency for the active material to buckle or crumble.

The grid is made mainly of antimonial-lead alloy, consisting of pure lead to which has been added 6-12% of antimony. Frequently, small

quantities of other metals such as tin, copper, silver, or arsenic are added to give greater corrosion resistance to the electrolytic action. The addition of antimony to the pure lead produces a sharper and stronger casting than that produced by lead alone, and also gives it greater resistance to the electrolytic action and chemical changes which take place in the active material which the grid supports [6].

(2) The active material

The method used for forming the active plate material determines the plate designation, which may be of the Pasted or Planté types.

(i) The Pasted plate

The paste material used in making these plates is usually a mixture of some or all of: Pb, PbO_2 (orthorhombic and tetragonal), and Pb_3O_4. This mixture is combined with water and sulphuric acid and produces complex chemical reactions. The product is a combination of: Pb, PbO, Pb_3O_4, $PbSO_4$, $PbO.PbSO_4$, $3PbO.PbSO_4.nH_2O$, and $4PbO.PbSO_4$, where n is an integer number; and is applied to the grids either by hand or by machine. The concentrations of each of these products is dependent on many variables such as the ratio of acid concentration to water, the rate of mixing, the uniformity of mixing, and the temperature. The plates are then dried and 'formed' electrochemically in a tank containing dilute sulphuric acid, which results in oxidation of the paste material to PbO_2 at the positive plate and to Pb at the negative plate. After 'formation' the plates are removed from the acid tank and dried. Since the plate properties are dependent on the 'mixing' and 'forming' conditions, the developing process must be accurately controlled and clearly defined.

For a tubular plate, the dry lead oxide is shaken into the tubes threaded over the grid spines. The open end of the tube is then sealed by a polythene bar.

(ii) The Planté plate

The basic difference between Planté and Pasted plates is that the active materials of the former are obtained from the body of the plate itself, whereas in the latter, they are formed from oxides or other pastes applied to the plates either by hand or by machine.

The active materials of the Planté plates are obtained by oxidising the surface of the lead plate or reducing the material to spongy lead. The process occurs when two plates of lead are dipped into a solution of sulphuric acid and a charging current is passed between them. A thin layer of PbO_2 is then formed on the prospective positive plate, and the oxide of lead covering the surfaces of the negative plate is reduced to a very thin layer of spongy lead. If the charging current is stopped, the PbO_2 on the surface of the positive plate forms a large number of tiny primary cells in co-operation with the lead underneath. The local chemical reactions produced form $PbSO_4$ on the surface of the underlying lead, and after a few minutes the plate losses its charge. Meanwhile, the spongy lead layer on the surface of the negative plate has practically no potential difference with the lead surface beneath, and no local chemical reactions take place. If charging is now resumed, a larger amount of PbO_2 is formed on the surface of the positive plate as a consequence of the conversion of the $PbSO_4$ formed by the previous local chemical discharge reaction. By repeating the above process the amount of PbO_2 increases. However, to obtain an increase in the amount of spongy lead on the surfaces of the negative plate, the current must be reversed

periodically so that use may be made of the process that occurs at the positive plate.

3.2.2 The Separators

To make a compact battery of reduced volume, plates of opposite polarity must be arranged very close to each other without experiencing electrical contact. In the early stages of battery design this requirement created a major problem since 'scaling' of the active material and the formation of 'trees' (substances which gradually thicken on the surface of the negative plate) would eventually make electrical contact between plates of opposite polarity, resulting in internal discharge. Separators are, therefore, necessary to avoid short circuits and to impart mechanical strength to the cell structure. Separators must have a number of special properties, the main ones of which are:

(1) chemical stability against sulphuric acid and oxidation action of the positive mass,

(2) structural stability when wetted with sulphuric acid,

(3) a small influence on the elctrolyte resistance, and

(4) low specific density, sufficient mechanical strength, and low manufacturing costs.

No separator can fulfill all these requirements simultaneously, but depending on the application of the battery the best suited requirements are selected. Presently, separators made of micro-porous polyvinyl chloride (P.V.C.) or terylene are used almost universally, since both compounds are light, very highly porous, and extremely strong.

3.2.3 The Electrolyte

The electrolyte is a solution of pure sulphuric acid in pure water. The purity of the acid and the concentration of the acid solution is precisely defined [48].

The specific gravity of the electrolyte is a measurement of the concentration of the acid solution. The specific gravity varies with the state-of-charge of the battery; the usual range of specific gravity for a lead-acid traction battery is 1.280 (fully charged) to 1.120 - 1.150 (fully discharged) at the 5-hour discharge rate.

3.3 Theory of Operation

A number of theories have been proposed to account for the reactions taking place in a lead-acid battery. Of these theories, the so-called 'double-sulphate' theory which was first proposed by Gladstone and Tribe in 1882 [49] is the more generally accepted.

The double-sulphate theory is most conveniently stated by the equation for the reaction:

$$PbO_2 + 2H_2SO_4 + Pb \rightleftharpoons 2PbSO_4 + 2H_2O \qquad (5)$$

From left to right this equation represents discharge, and from right to left, charge. The significance of the term 'double-sulphate' lies in the fact that lead sulphate is formed at both the positive and negative plates during the process of discharge.

3.3.1 Cell on Discharge

The component reactions [11] of equation (5) for a cell on discharge, are shown diagramatically in Fig. 16. At the negative plate, the solution pressure of lead causes lead ions to pass into the solution; and these are in the divalent state. Coincident with the departure of each of the positive lead ions from the surface of the

plate, sulphate ions move to the negative plate and part with their negative charge. The excess of electrons on the negative plate is relieved by a flow of electrons into the external conductor that connects the negative and positive terminals. The lead ions react with the sulphate ions to form lead sulphate, which is virtually insoluble in the electrolyte so that it immediately precipitates out of solution and is deposited on the plate. The passage of electrons from the negative plate through the external conductor, allows more sulphate ions from the electrolyte to combine with the lead ions to form more $PbSO_4$. At the positive plate, the highly oxidised PbO_2 is deficient in negative charge so that it readily accepts electrons from the external conductor. Hydrogen ions now move from the electrolyte towards the positive plate and combine with oxygen to form water, which leaves some lead ions free to combine with the sulphuric acid to form $PbSO_4$ and more water. As the discharge continues, more $PbSO_4$ and water is produced.

3.3.2 Cell on Charge

The component reactions [11] of equation (5) for a cell on charge, are shown diagramatically in Fig. 17. The $PbSO_4$ at both plates passes into solution and ionises; the water is also ionised as quickly as the equilibrium conditions will permit. The charging source that is connected across the cell terminals, supplies an excess of electrons to the negative plate and creates a shortage of electrons at the positive plate. The hydrogen ions are attracted to the negative plate where they combine with the $PbSO_4$ to form lead and sulphuric acid. The lead ions at the positive plate are forced by the charging current to release two electrons, converting the lead ions from the divalent to the tetravalent state. Each of these ions unite with two oxygen ions

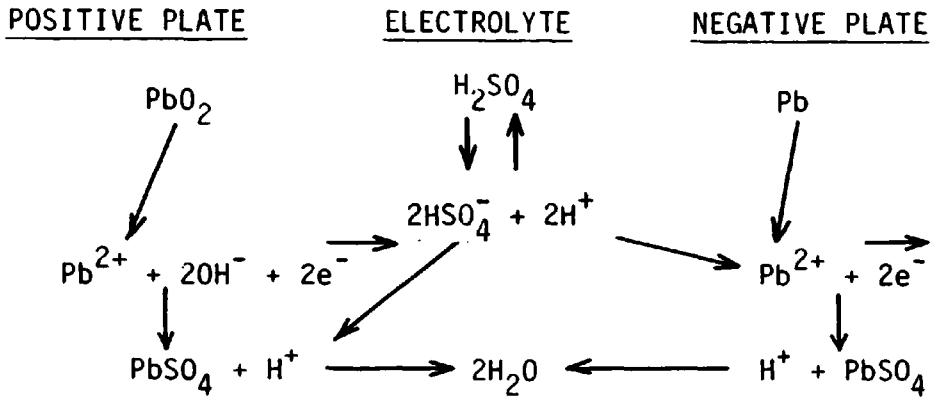

FIG. 16 DISCHARGE REACTIONS

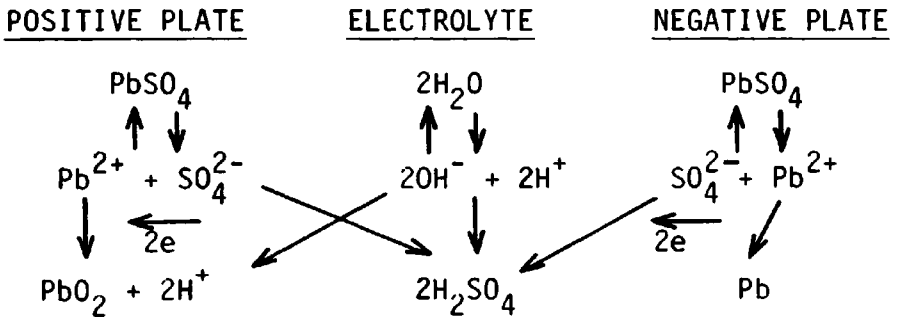

FIG. 17 CHARGE REACTIONS

to form PbO_2, which is deposited on the plate. The sulphate ions at the positive plate combine with the hydrogen of the water to form sulphuric acid.

As the charge proceeds, acid which is released from the plates passes into the electrolyte and its specific gravity increases.

3.4 Factors which Influence the Performance of the Battery

3.4.1 Introduction

For given discharge conditions, the performance of the battery is usually determined in terms of two parameters: (1) total available capacity; and (2) terminal voltage.

The available capacity can be expressed either in terms of ampere-hours or watt-hours. The ampere-hour capacity, C, is given by:

$$C = I_d \cdot t \qquad (6)$$

where: I_d = the discharge rate, A.

t = the discharge time, hours.

The watt-hour capacity is a measurement of the batteries ability to do work, and is the product of the ampere-hour capacity and the average value of the battery voltage throughout the discharge period. The ampere-hour method of measuring capacity is the most commonly used of the two.

Electrochemical reactions take place in the cell in accordance with Faraday's Laws [50] and the ampere-hour capacity is a measure of these reactions. According to Faraday's Law, the capacity of an arbitrary chemical source (including lead-acid batteries) producing electrical current, is determined solely by the quantity of active materials participating in the current-forming processes. Thus, in order to obtain one ampere-hour of electrical current from the battery, it is necessary to convert 3.86 g. of porous lead and 4.45 g. of lead

dioxide into lead sulphate.

The principal factors that affect the performance of the cell are: the rate of discharge, the temperature, the previous history of the plates, the quantity and concentration of the electrolyte, the porosity of the plates, the design of the plates, and the amount of active material. The first three factors will be discussed in succeeding pages, since the user has some control over these. The remaining factors are mainly related to the constructional and design characteristics of the cell, and are adequately discussed in other publications [6,48].

3.4.2 The Influence of Discharge Rate

In reality, the capacity of a cell is considerably less than the capacity calculated theoretically in accordance with Faraday's Law. The main reason for this is the restriction on the velocity diffusion of the electrolyte into the pores of the cell plates; the higher the discharge rate, the more pronounced the restriction [51]. Therefore, with low current rates the active mass participates to a greater extent in the chemical reactions than is possible at high discharge rates; the result is well known: the capacity and terminal voltage of the cell decreases as the discharge rate increases.

The processes occuring in the active mass during a discharge of the cell can be imagined as follows: by connecting the cell for discharging, the active mass begins to absorb the acid from the solution, thereby forming lead sulphate. During this process, the solution of the active mass loses the electrolyte, and there occurs a difference in the concentration of the electrolyte, whose diffusion is dependent upon it. The difference in concentration of the electrolyte between the internal and external part of the plate continues until a

steady state is attained. When the loss of acid is compensated by an equalising of concentration by means of a diffusion, at such a state the quantity of acid which has penetrated inside the plate in a unit of time should be equal to the quantity of acid consumed in the formation of lead sulphate. The resulting characteristic of the variation of the acid concentration between the internal and external part of the plate during discharge is derived by the author in Appendix 3, where the characteristic is shown to have an exponentially rising form (see equation (87))

The diffusion process is strongly dependent upon the diffusion coefficient; this may be readily appreciated from Fick's First Law of Diffusion [52]. Therefore, it may be deduced that all factors affecting the coefficient of diffusion must also affect the performance of the cell. Vinal [48] suggested that the coefficient is a constant, unique for a particular substance. However, other [51] investigations have shown that the coefficient is dependent upon a number of factors, the more significant of these were stated by Davtyan to be: the cross sectional area of the plate pores; and the temperature, concentration, and electo-conductivity of the electrolyte. Davtyan observed that these factors were themselves dependent upon the discharge rate, and that at high discharge rates the cross sectional area of the pores, and the concentration and temperature of the electrolyte were the most significant factors affecting the coefficient of diffusion, whereas at low discharges rates the most significant factor was the electro-conductivity of the electrolyte.

Numerous attempts have been made to develop equations which relate the available capacity to the discharge rate. Schroeder [53] in 1891 was the first person to achieve success. However, the equation only applied to a limited range of discharge times of approximately 3.5 - 8.5 hours, and was thought not to be applicable to low discharge

rates. Due to this, Leibenow [54] developed an equation which could be applied to such rates, and also developed an equation which could be applied to the more practical case of a continually varying load current. In 1897, Peukert [55] published the equation:

$$I_d^n . t = K \qquad (7)$$

where: I_d = the discharge rate, A

t = the total discharge time, hours.

n and K = constants for the battery.

The equation has proved to be very representative of the behaviour of a discharging lead-acid cell, although, it has been noted [48] that under certain discharge conditions - particularly at very high or very low discharge rates - the experimental results deviate slightly from the calculated values, which has been attributed [48] to ohmic resistance of the cells and to a fixed or incorrect choice of termination of discharge voltages. Although more recent attempts [56] have been made to develop suitable equations, the equation developed by Peukert has gained the greater acceptance, since, unlike Peukert's equation, all the other equaions are either not truly representative for the various types of battery or they are difficult to implement.

3.4.3 The Influence of Temperature

The performance of a cell is considerably affected by the temperature of the electrolyte. Changes in temperature produce corresponding changes in performance: a decrease in temperature produces a decrease in available capacity and terminal voltage, whereas an increase in temperature produces an increase in available capacity and terminal voltage. The effect is only temporary and normal performance is restored with a return to normal temperature.

The dependence of the cell performance on temperature, is mainly due to the dependence of the electrolyte resistivity and viscosity on the temperature; the resistivity and viscosity are related to the diffusion processes within the electrolyte. Davtyan [51], in his investigations on the coefficient of diffusion, stated that the coefficient is strongly dependent upon the temperature (see Section 3.4.2). In his equation for the coefficient of diffusion, the temperature was not only a multiple, but a factor of the other magnitudes contained in it, namely, the electro-conductivity of the electrolyte and the mobility of the ions. Therefore, when the temperature falls, the coefficient of diffusion in this instance would decrease not proportionately but in a greater degree. This is probably the reason for the sharp decrease in the performance of the cell, when the temperature drops.

Attempts have been made to develop equations which relate the available capacity to the temperature [56] or to determine the temperature coefficient of capacity [54]. However, because of the variations in make and type of traction battery, none of these equations have found general acceptance.

3.4.4 The Influence of Previous History

When the plates in the battery are new, there is an increase in the performance during the first few cycles of charge and discharge up to a maximum value, beyond which the capacity becomes relatively constant and then gradually decreases. During the later cycles in the life history of the plates, the decrease in performance of the negative plates is caused primarily by a decrease in the porosity of the active material or shrinkage of the plate itself; the loss of performance of the positive plates is caused by corrosion of the grids and loosening

of the active material [48]. In addition to these effects, however, there is a third effect arising from the wearing of the separators. As the separators become thinner - particularly the ribbed portions - the space available for the electrolyte next to the positive plate becomes inadequate, and the performance of the cell may be impaired by insufficient acid for the action of the positive plate.

The performance of the cell is affected by the discharges immediately preceding the discharge. This effect was first observed by Jumau [57], and is sometimes referred to as cell 'memory'. Jumau found that the capacity delivered at any given rate depends on the previous discharge; the capacity is lower if the discharge has been preceded by a discharge at a higher rate, and it is higher if preceded by a discharge at a lower rate. In this context, it may also be assumed that the performance of the cell is also affected by the charges immediately preceding the discharge.

The performance of the cell is also affected by the method of discharge. For example, if the cell is discharged at any rate down to a particular voltage level, and then left on open-circuit for a short time, a recovery in cell voltage is observed, and the cell may then be further discharged at the same rate and to the same voltage level. It, therefore, appears as though the cell contains a 'recuperative' capacity. This effect was first observed by Leibenow [54] in 1897. The observation infers that if the cell is discharged intermittently, then greater capacity can be obtained than when using uninterrupted continuous discharge currents, provided the discharge rates and all other capacity affecting conditions are identical. This inference is the underlying theory in using pulsed discharging techniques to increase the available capacity of a cell.

4. THE EFFECTS OF PULSED DISCHARGE CURRENTS ON THE AVAILABLE CAPACITY OF LEAD-ACID TRACTION BATTERIES

4.1 Introduction

When compared to continuous current discharge it is possible that pulsed current discharge can produce an increase in the available capacity of a lead-acid traction cell. This increase could be explained in terms of electrolyte diffusion. During discharge, chemical reactions occur at the surfaces of the cell plates. It follows that at the proximity of the plates the concentration of the reacting electrolyte is weaker than at some distance away from the plates. Therefore, if the cell is left on open-circuit for some period of time then the more concentrated electrolyte in the cell would diffuse towards the plates and into the pores of the plates. It should then be possible to discharge the cell again to realise a 'recuperative' capacity.

4.2 A Review of Previous Investigations

A number of investigations have been performed to determine whether a recuperative effect occurs with lead-acid traction batteries under pulsed discharge conditions of operation, but the results obtained have been contradictory:

From the results of tests performed on a lead-acid traction cell having a 5-hour discharge rate capacity of 219 ampere-hours, it has been stated [11] that when compared to continuous current discharging, equivalent high-speed pulsed current discharging produces an increase in the available capacity. In fact, for the particular tests performed, an increase in available capacity of up to 68% was achieved, and the investigation further demonstrated that pulsed discharging virtually always produces an increase in available capacity

when compared to the continuous current discharging mode.

However, it is also stated [12, 13] that high-speed pulsed discharge currents produce no discernable increase in the available capacity of the cell when compared to using continuous discharge currents. Furthermore, from tests performed on a lead-acid traction cell having a 5-hour discharge rate capacity of 125 ampere-hours, it is said [14] that pulsed discharging actually reduces the available capacity when compared to equivalent constant current discharging.

In view of these conflicting opinions concerning the effects of pulsed discharge currents on the available capacity of lead-acid traction cells, further investigations were performed by the author.

4.3 Test Apparatus

To ensure that any results obtained were not unique to a particular type of lead-acid traction battery, tests were performed on both a tubular armoured and a flat-plate battery. The tubular armoured battery consisted of three nominal 2-volt cells connected in series, with each cell having a nominal 5-hour rate discharge capacity of 110 ampere-hours at 30°C. The cell dimensions were: overall height - 352 mm, length - 156 mm, width - 62 mm. The cells were manufactured by Chloride Industrial Batteries Limited, and have the commercial designation IMF 7A. The flat- plate battery consisted of three nominal 2-volt cells in monoblock form, with each cell having a nominal 5-hour rate discharge capacity of 150 ampere-hours at 30°C. The battery dimensions were: overall height - 220 mm, length - 158 mm, width - 276 mm. The battery was manufactured by Lucas Industrial Batteries Limited.

The pulsed discharge test facility for the tubular armoured cells was a bi-polar power transistor chopper, whose description is

given in Appendix 1.1. The power associated with discharge was dissipated as heat in the heat-sink of the chopper circuit which was aided by forced cooling.

The pulsed discharge test facility for the flat-plate battery consisted of a thyristor chopper circuit which was of the 'resonant commutated' type and was originally developed by the General Electric Company of America [58]. The chopper circuit together with its theory of operation is described in Appendix 1.2. The 36-volt battery pack (see Fig. 81 of Appendix 1.2) was composed of 15 'booster cells' of approximately 150 ampere-hour capacity, connected in series with the three cells under test. The high capacity booster cells were necessary to hold the terminal voltage of the battery pack relatively constant throughout the discharge period, so as to allow the commutating capacitor to acquire sufficient charge to commutate the current - carrying thyristor. The load was provided by wire-wound resistors.

Typical cell current and cell voltage waveforms obtained from the present investigations when using the transistor and resonant commutated thyristor choppers are shown in Fig. 18. Using the charging facility shown in Fig. 19 the cells were charged by means of a two-stage constant current routine.

4.4 Capacity Measurement Techniques Associated with Pulsed Discharging

The ideal pulsed waveforms of cell voltage and cell current are illustrated in Fig. 20. It may be seen that there are two values of current and three values of voltage associated with pulsed discharge. The available capacity of the cell is dependent upon which value of current is taken as the discharge rate and which value of voltage is taken as the termination of discharge voltage. The choice of these

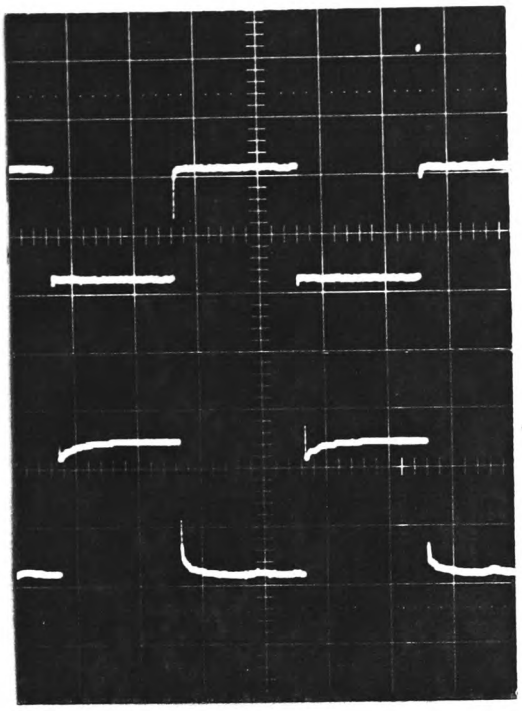

CURRENT WAVEFORM

FIG. 18(a) TRANSISTOR CHOPPER WAVEFORMS

VOLTAGE WAVEFORM

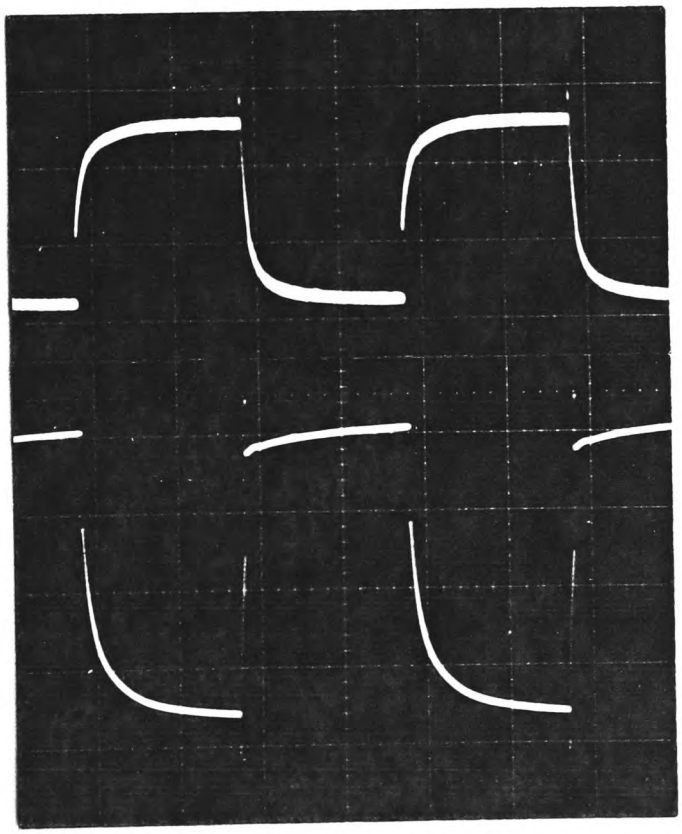

CURRENT WAVEFORM

FIG. 18(b) THYRISTOR CHOPPER WAVEFORMS

VOLTAGE WAVEFORM

FIG. 18 TYPICAL CURRENT AND VOLTAGE WAVEFORMS OF THE CELL FOR THE TRANSISTOR CHOPPER AND THYRISTOR CHOPPER

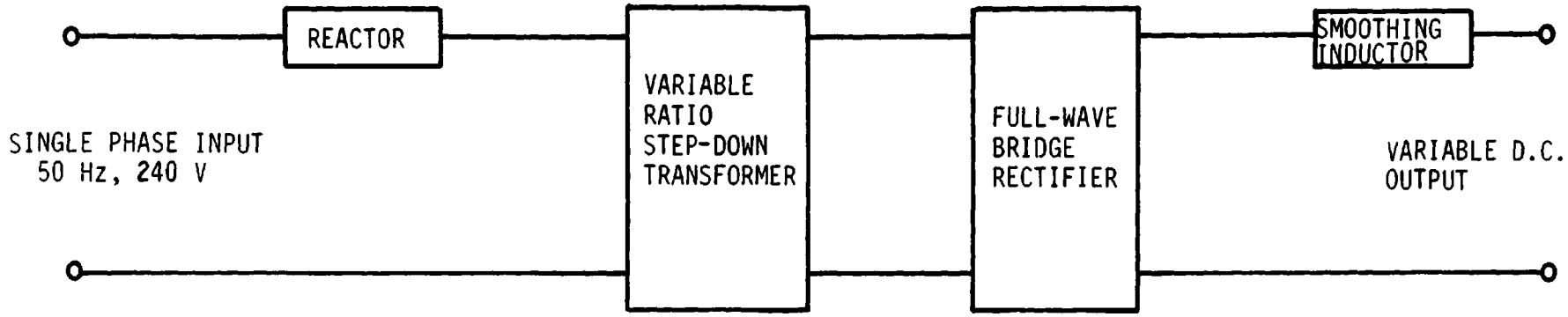

FIG. 19 THE CHARGING FACILITY

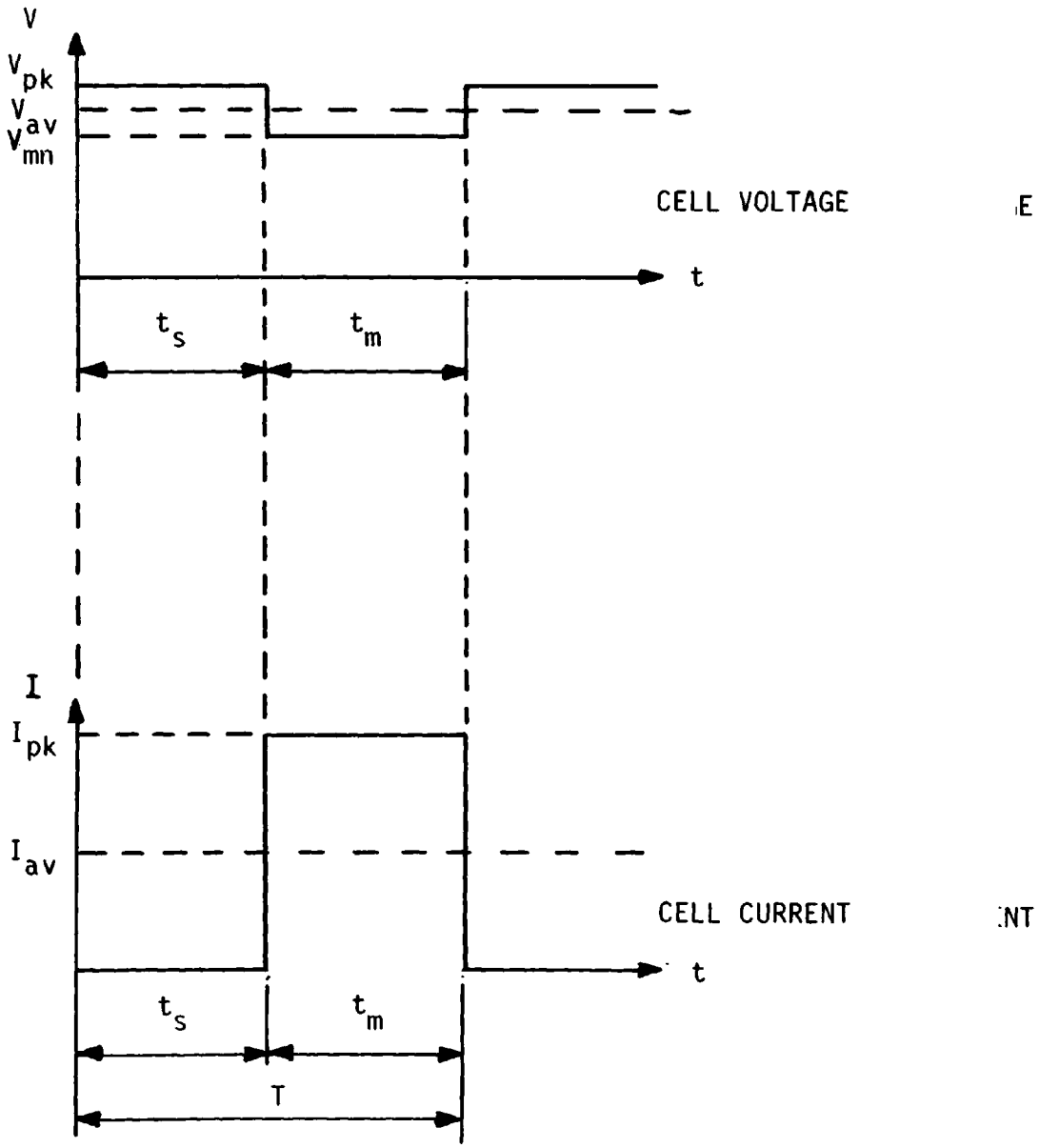

FIG. 20 IDEAL VOLTAGE AND CURRENT WAVEFORMS FOR PULSED DISCHARGE

values has a very significant affect on the value of available capacity. It should also be noted that the cell voltage waveform experiences considerable change between the load and no-load states, mainly because of the internal resistance and recovery time of the cell. Therefore, when a comparison is to be made between the values of capacity associated with continuous and pulsed discharge, the value of the continuous discharge current should be made equal to the peak value of the pulsed current, since it is this value of current which the chemical reaction process produces. Similarly, to make a true account of the internal impedance voltage drop of the cell, the minimum value of the voltage should be taken as the termination of discharge voltage. The true value of cell capacity is then determined from the formula:

$$C = I_{pk} \sum_{1}^{1} t_m \qquad (8)$$

where: I_{pk} = the peak value of the current, A

t_m = the mark-time of the waveform, hour.

Since the performance of a chopper controlled EV is mainly dependent upon the mean values of battery voltage and current, useful characteristics can be obtained by taking the mean value of current as the discharge rate and the mean value of voltage (V_{av}) as the termination of discharge voltage. The capacity of the cell is then determined from the formula:

$$C = I_{av} \cdot t_d \qquad (9)$$

where: I_{av} = the mean value of current, A

t_d = discharge time, hour.

However, it is important to note that such characteristics are not representative of the current producing chemical reactions.

From the ideal waveforms of Fig. 20, the following well known relationships can be derived:

$$I_{av} = \frac{M \cdot I_{pk}}{1 + M} \tag{10}$$

$$I_{rms} = I_{pk} \sqrt{f \cdot t_m} \tag{11}$$

$$V_{av} = \frac{V_{pk} + V_{mn} \cdot M}{M + 1} \tag{12}$$

$$f = \frac{1}{t_m + t_s} = \frac{1}{T_d} \tag{13}$$

where: $M = t_m/t_s$ = the mark/space ratio

I_{rms} = the root-mean-square value of the current, A

V_{pk} = the peak value of the voltage, V

t_s = the space-time of the wavefore, seconds.

f = the frequency of the waveform, Hz

T_d = the periodic time of the waveform, seconds.

The peak and minimum values of cell voltage were measured by means of a calibrated C.R.O. connected directly across the cell terminals, whereas the peak value of current was measured using a non-inductive shunt. The frequency and mark/space ratio of the pulsed discharge waveform were also measured by means of a calibrated C.R.O. The mean values of cell voltage and current were measured by means of a precision moving coil voltmeter and moving coil ammeter respectively. The specific gravity of the electrolyte was measured by an hydrometer, and temperature corrected to 15°C by means of a scale correcting thermometer.

The cell internal resistance under pulsed discharge conditions was determined by empirical means. Although the resistance is said to consist of numerous component resistances [59], as far as the present investigations are concerned the effective internal resistance of the cell, r, with reference to Fig. 20, is given by:

$$r = \frac{V_{pk} - V_{mn}}{I_{pk}} \ \Omega \qquad (14)$$

It may be seen from Fig. 18 that during the rise-time of the current pulse, a significant transient drop in cell voltage occurs; a typical transient waveform obtained from the present investigations is shown in Fig. 21. This phenomenon was first reported by Mandil [60] in 1976, but no thorough investigation was performed by him. Since that time no further results have been reported. The author decided to investigate the characteristics of this transient, with the intention of evaluating its significance in battery state determination. The characteristics measured were the duration and the depth of the transient, as defined in Fig. 22. When using semiconductor devices, the transient will be affected by the switching characteristics of the device. To make a true account of the transient voltage, a number of continuous current discharge tests were performed using a carbon stack for the battery load. At intervals throughout the discharge period, the load current was switched on-and-off manually using a mechanical switch, and the duration and depth of the transient was recorded.

4.5 Design of Experimentation

Before producing a constant ampere-hour output it is necessary for a new cell to experience a number of charge/discharge cycles. For the tubular armoured and flat-plate cells used in the experimentation, a constant output was attained after 10 and 17 charge/discharge cycles respectively.

The experimentation was designed so that all but one of the known factors which influence the behaviour of a lead-acid cell were suppressed or held constant:

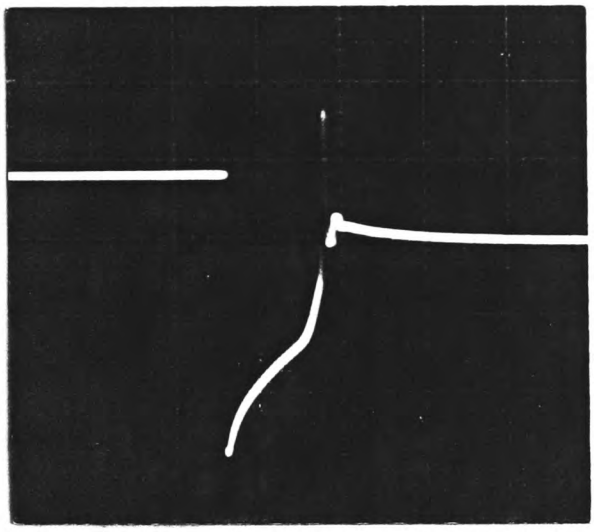

CELL VOLTAGE WAVEFORM

FIG. 21 TRANSIENT DROP IN CELL VOLTAGE UNDER PULSED DISCHARGE CONDITIONS

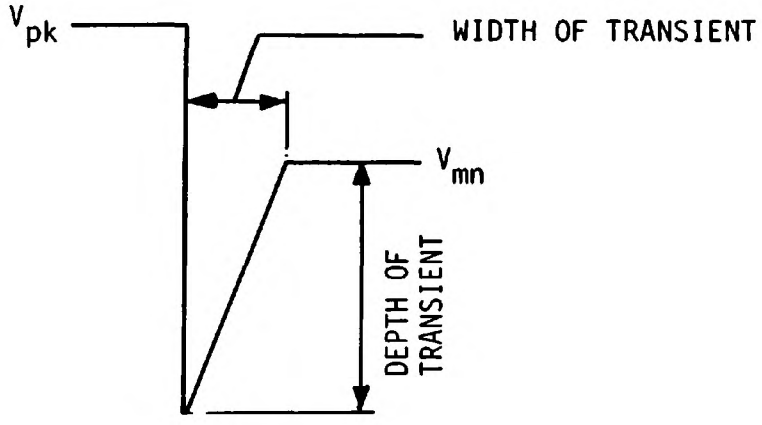

FIG. 22 THE DURATION AND DEPTH OF THE VOLTAGE TRANSIENT

To counteract the effects of 'memory' a reference charge/discharge cycle was interposed between each specific discharge test. For the tubular armoured cells a reference discharge rate of $C_5/5$ A was used, whereas for the flat-plate cells the reference rate was $C_5/4$ A. The reference charge was performed using a two-stage charging routine, with the initial and final charging rates chosen so as to comply with those recommended by the battery manufacturers. For the tubular armoured cells the initial and final charging rates were 13 A and 4.5 A respectively, whereas for the flat-plate cells the respective rates were 17.5 A and 8 A. The fully charged condition was established when no changes were observed between three consecutive readings of specific gravity and terminal voltage taken at 1-hour intervals.

The ambient temperature of the cells was maintained within 1°C of 30°C by immersing the cells in a temperature controlled tank.

The small temperature rise of the cell electrolyte during discharge was recorded and the average discharge temperature of the electrolyte calculated. The capacity was then corrected to 30°C as detailed in B.S. 2550 (1971).

Each discharge test was terminated when the terminal voltage of the test cell reached a predetermined value. The value of terminal voltage chosen, 1.7 V, was taken from B.S. 2550 (1971). Prior to the commencement of all discharge tests, the test cells were allowed to rest on open-circuit for 1 - 3 hours after being charged to allow the bulk of the occluded gases to escape, thus permitting the cells to reach an equilibrium state. This procedure prevents erroneous values of terminal voltage and capacity from being realised.

4.6 The Tests Performed

The tubular armoured and flat-plate cells were subjected to the following specific continuous discharge currents:

$$I_d = 25, 50, 75, 100 \text{ and } 150 \text{ A}$$

The pulsed discharge tests performed on the respective cells are detailed in Tables 3 and 4.

4.7 Results

The results of the tests performed on the tubular armoured and flat-plate cells are presented in Figs. 23 - 30 and Figs. 31 - 34 respectively.

4.8 Comments on Results

4.8.1 Comments on Figs. 23 - 34

From Fig. 23 it may be seen that when V_{mn} is taken as the termination of discharge voltage and the peak current, I_{pk}, as the discharge rate, the increase in available capacity when compared to continuous current discharging is dependent on the value of the peak current. For the range of currents considered, the increase in available capacity ranges from 27% to 0% for discharge rates between 50 A and 140 A respectively. However, it is interesting to note from Fig. 24 that when V_{av} is taken as the termination of discharge voltage and I_{av} as the discharge rate, pulsed discharge provides a negligible increase in available capacity.

From Fig. 25 it is apparent that increasing the mark/space ratio from 1/4 to 4/1 results in a decrease in available capacity of approximately 33%, and increasing the frequency of operation from 50 Hz to 1000 Hz brings about a loss in capacity of approximately 4.5% for all values of mark/space ratio.

	I_{pk} (A)													
	40	100												140
M	1/1	1/4				1/1				4/1				1/1
f (Hz)	50	50	100	500	1000	50	100	500	1000	50	100	500	1000	50

TABLE 3 TESTS PERFORMED ON THE TUBULAR ARMOURED CELLS

	I_{pk} (A)				
	30	75			150
M	4/1	1/4	1/1	4/1	4/1
f (Hz)	50	50			50

TABLE 4 TESTS PERFORMED ON THE FLAT-PLATE CELLS

The variation of the effective internal resistance of a cell with time of discharge, for various values of mark/space ratio when the peak current and frequency are maintained constant at 100 A and 50 Hz respectively, is illustrated in Fig. 26. It may be seen that for a mark/space ratio of 4/1 there is an apparent increase in resistance of 0.33×10^{-3} ohms throughout the period of discharge, whereas for a mark/space ratio of 1/4 there is an increase in internal resistance of approximately 1.66×10^{-3} ohms.

The effect of the magnitude of the peak current on the effective value of cell resistance when the mark/space ratio and frequency are maintained constant at 1/1 and 50 Hz respectively is illustrated in Fig. 27. It is apparent that the variation of cell resistance with time is dependent on the peak value of current. For a peak current of 40 A, the resistance increases from 1.34×10^{-3} ohms to 3.50×10^{-3} ohms, whereas for a current of 140 A the resistance increases from 1.73×10^{-3} ohms to 2.13×10^{-3} ohms.

The influence of frequency on the effective internal resistance of the cell is illustrated in Fig. 28 where the peak current and mark/space ratio are held constant at 100 A and 1/1 respectively. It may be seen that throughout the discharge period the variation in resistance for the 500 Hz frequency of operation is only slightly greater than that for 100 Hz, whereas for 1000 Hz the variation is very much greater.

The variation in the magnitude of the voltage dip throughout the discharge period of the cell for a range of continuous discharge rates is illustrated in Fig. 29. It is apparent that for a rate of 25 A, the magnitude of the voltage dip decreases from 0.051 V at the commencement of discharge to 0.015 V at the end of discharge. When the rate of discharge is increased to 75 A and then to 150 A, the magnitude

of the voltage dip throughout the period of discharge increases.

The variation in the duration of the voltage dip throughout the discharge period for various values of continuous discharge rate is illustrated in Fig. 30, where it is evident that the duration of the voltage transient increases with the time of discharge. It is equally evident that there is a considerable decrease in the duration of the voltage dip for an increase in discharge rate. In fact, at the termination of discharge, the duration of the transient decreases by approximately 0.20 milliseconds when the rate is increased from 25 A to 150 A.

It is interesting to note the similarity between the transient voltage characteristic of Fig. 21 and the 'coup de fouet' characteristic of the cell. The coup de fouet characteristic illustrated in Fig. 35 was obtained from the present investigations on the tubular armoured cell. Under constant current discharge conditions it may be seen that initially, the cell experiences a high rate of voltage drop which, after reaching a minimum value begins to rise, and continues to do so up to a certain voltage level, when it again begins to drop. To explain this effect, Berndt and Voss [61] proposed that the initial, almost linear voltage drop, is partly ohmic but the greater part is due to charge transfer. At point A the electrolyte is saturated with bivalent lead ions, but formation of $PbSO_4$ nuclei has not yet started, and will not do so until a higher saturation level occurs. Once this point is reached, $PbSO_4$ nuclei and crystal growth rate are lower than the formation rate of lead ions which is proportional to the discharge rate. At point C, for example, the crystal growth rate is higher than the rate of formation of the lead ions, and consequently, the saturation level decreases, which is indicated by an increase in cell voltage which finally reaches a

steady-state peak value (point D). Although the transient voltage characteristic has not been previously analysed, the present writer believes that the above chemical behaviour associated with the coup de fouet characteristic may be similarly applied to the transient voltage characteristic. The increasing duration of the voltage transient with depth-of-discharge (Fig. 30) for example, may therefore be primarily due to the relative decrease of crystal growth rate with the rate of formation of lead ions with increasing depth-of-discharge.

For the flat-plate cell, Fig. 31 shows that when V_{mn} is taken as the termination of discharge voltage, and the peak current as the discharge rate, the increase in available capacity when compared to continuous current discharging, is dependent on the value of the peak current. For the range of pulsed discharge currents considered, the maximum increase in available capacity when compared to continuous current discharging is approximately 3%, for a frequency of 50 Hz and mark/space ratio of 4/1.

From Fig. 32, it may be seen that increasing the mark/space ratio from 1/4 to 4/1 results in a decrease in available capacity of 16% for the flat-plate cell, at a frequency and peak current of 50 Hz and 75 A respectively.

Fig. 33 illustrates the effect of the magnitude of the peak current on the effective value of the cell resistance of the flat-plate cell. For a peak current of 30 A the resistance increased from 0.96×10^{-3} ohms to 1.66×10^{-3} ohms, whereas for 75 A the resistance increased from 1.03×10^{-3} ohms to 1.25×10^{-3} ohms. The frequency and mark/space ratio were held constant at 50 Hz and 4/1 respectively.

The variation of the effective internal resistance of the flat-plate cell with time of discharge, for various values of mark/space ratio at a constant peak current and frequency of 75 A and

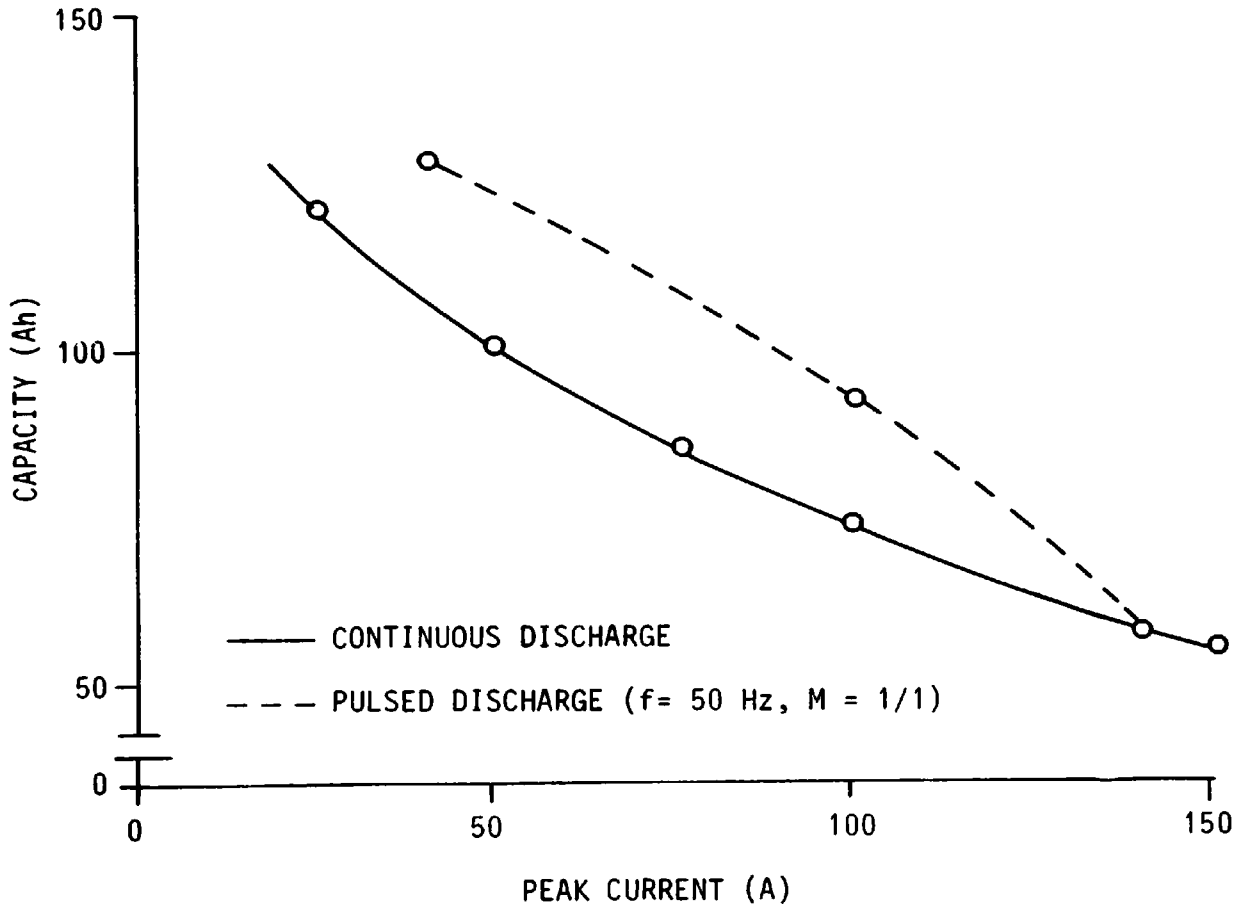

FIG. 23 VARIATION OF CAPACITY WITH DISCHARGE CURRENT FOR CONTINUOUS AND PULSED DISCHARGE

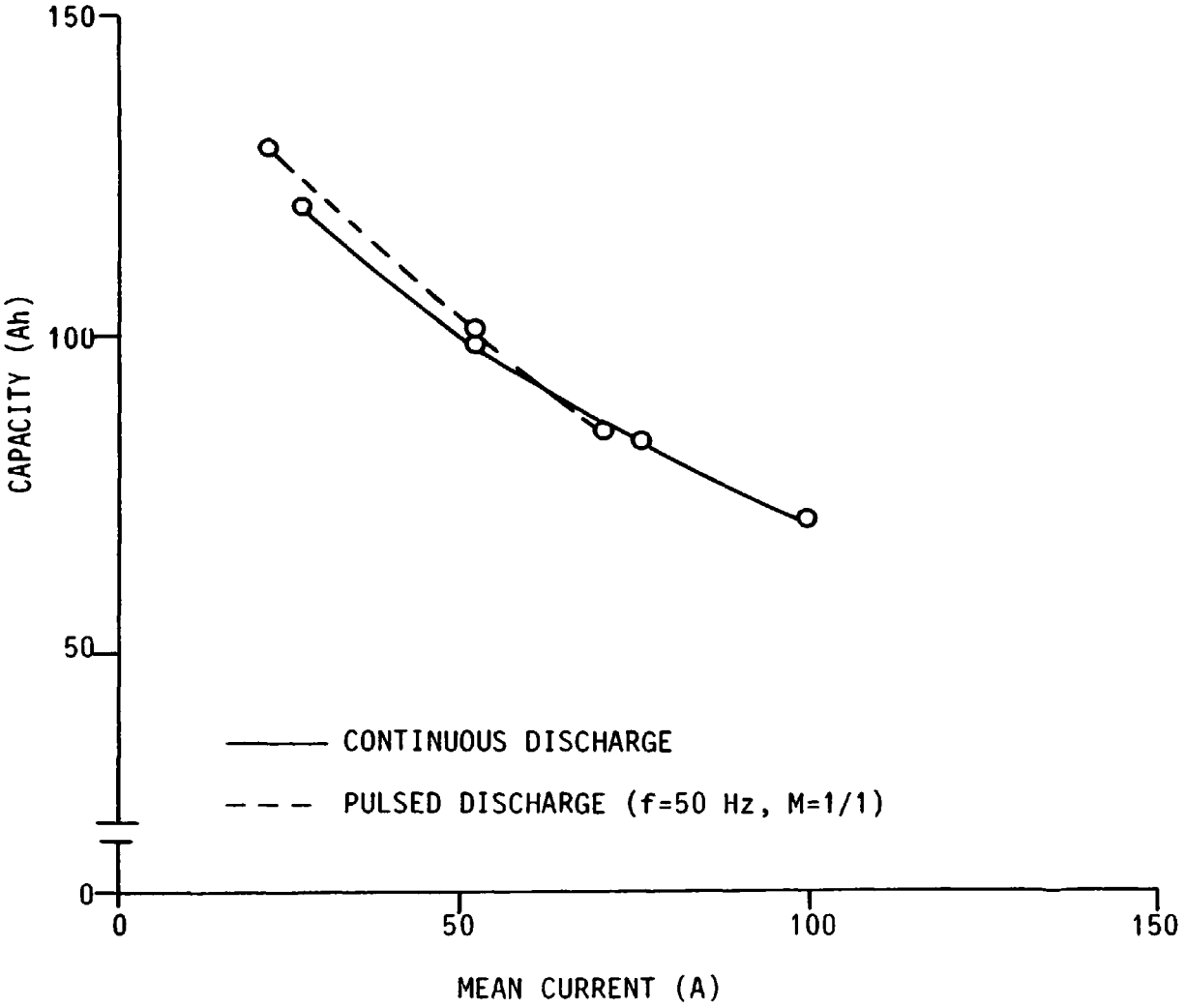

FIG. 24 VARIATION OF CAPACITY WITH DISCHARGE CURRENT FOR CONTINUOUS AND PULSED DISCHARGE

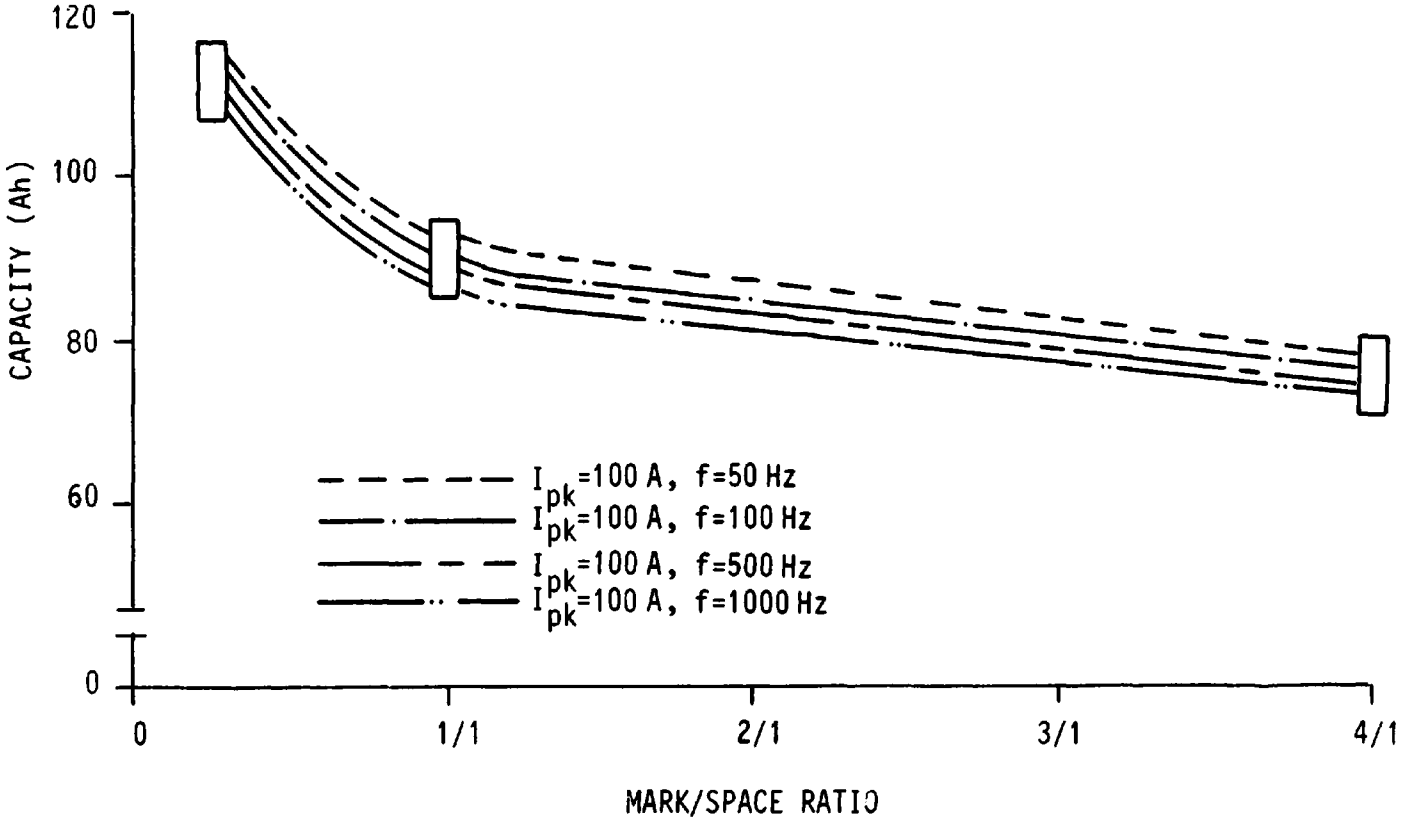

FIG. 25 VARIATION OF CAPACITY WITH MARK/SPACE RATIO FOR DIFFERENT VALUES OF FREQUENCY

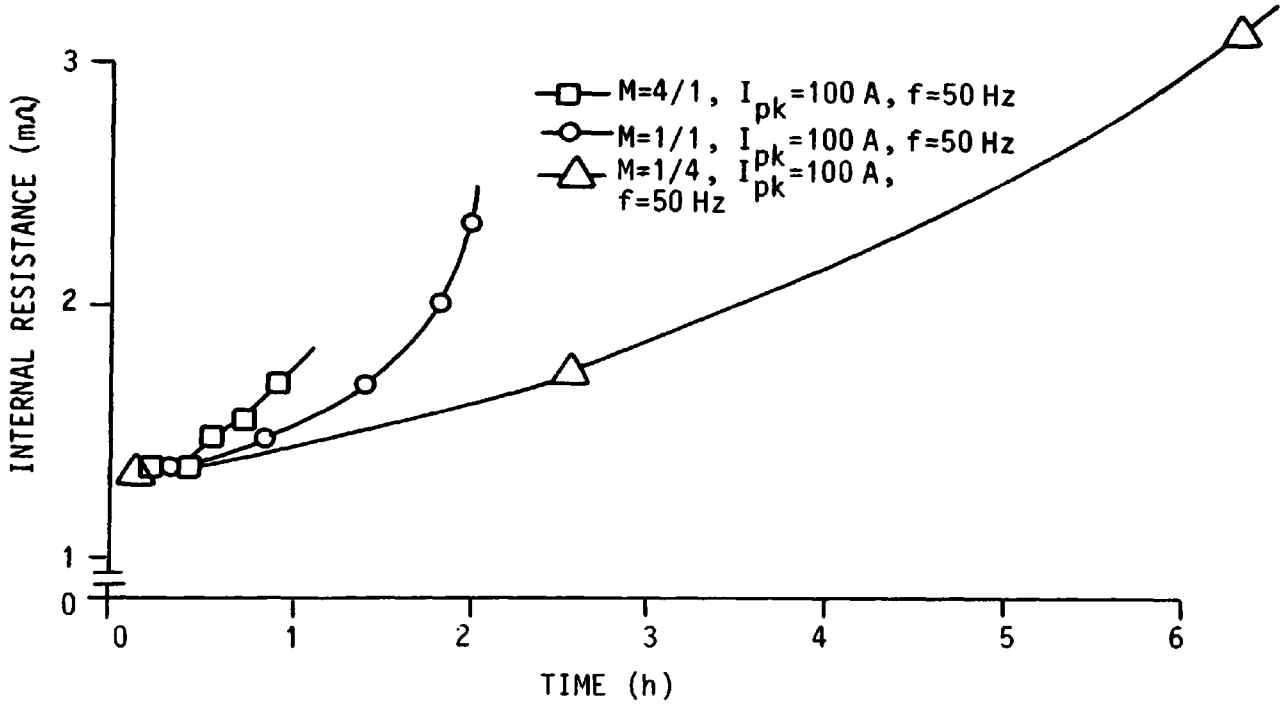

FIG. 26 VARIATION OF INTERNAL RESISTANCE OF THE CELL WITH TIME OF DISCHARGE FOR VARIOUS VALUES OF MARK/SPACE RATIO

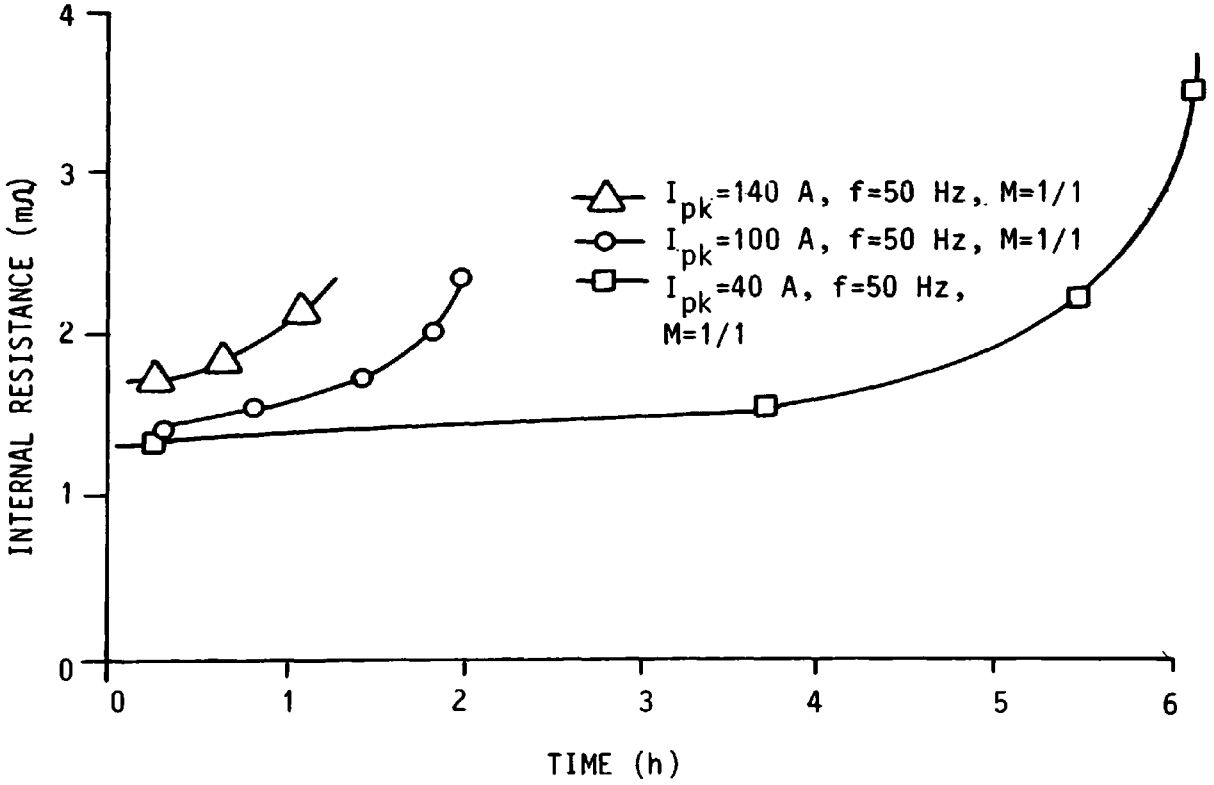

FIG. 27 VARIATION OF THE INTERNAL RESISTANCE OF THE CELL WITH TIME OF DISCHARGE FOR VARIOUS VALUES OF PEAK CURRENT

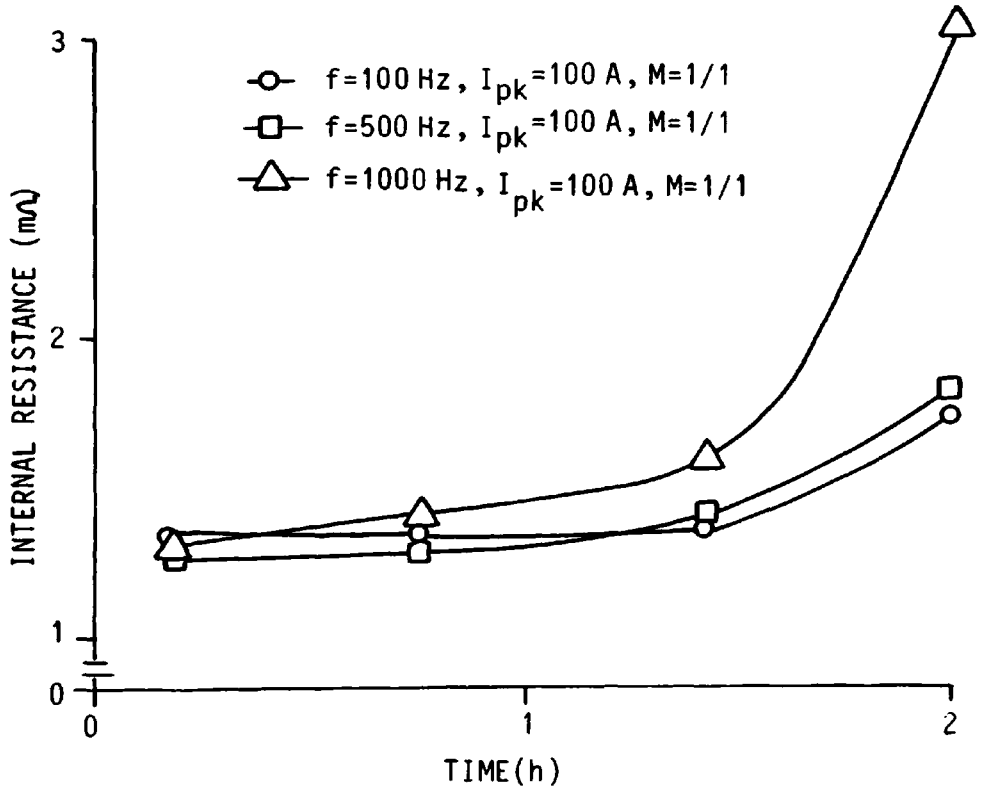

FIG. 28 VARIATION OF INTERNAL RESISTANCE OF THE CELL WITH TIME OF DISCHARGE FOR VARIOUS VALUES OF FREQUENCY

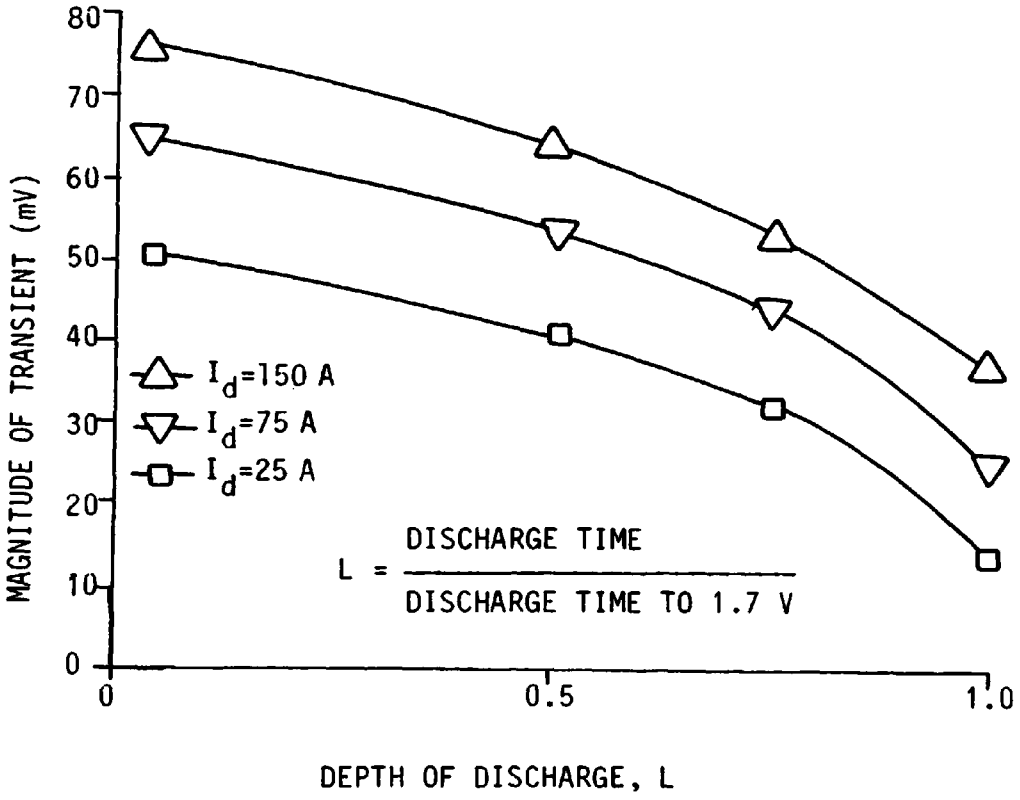

FIG. 29 VARIATION OF MAGNITUDE OF VOLTAGE TRANSIENT WITH DEPTH OF DISCHARGE FOR VARIOUS VALUES OF CONTINUOUS DISCHARGE CURRENT

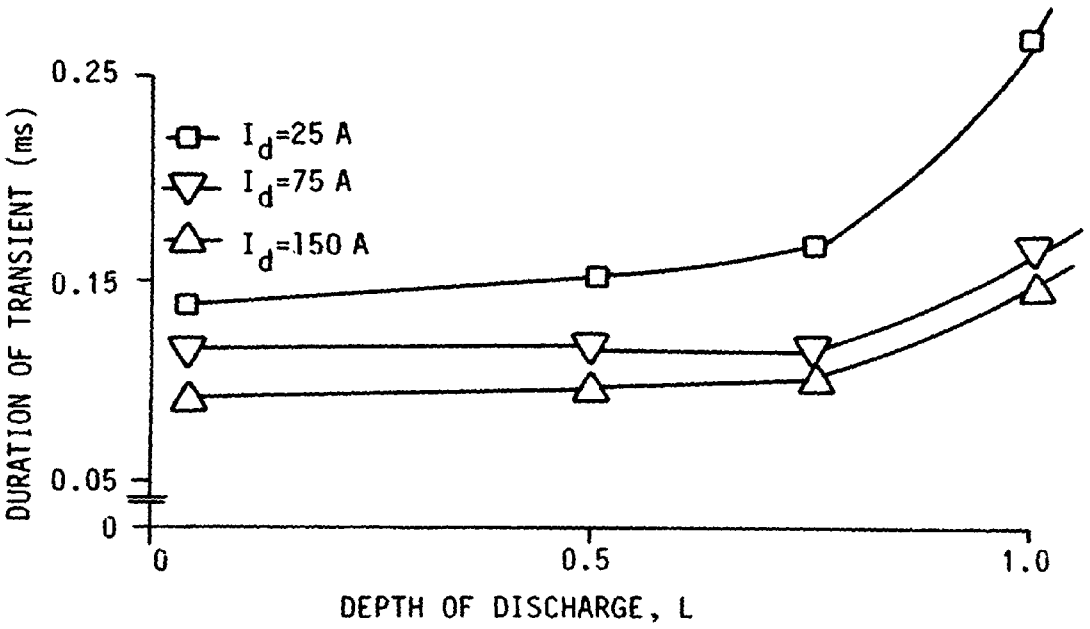

FIG. 30 VARIATION OF DURATION OF VOLTAGE TRANSIENT WITH DEPTH OF DISCHARGE FOR VARIOUS VALUES OF CONTINUOUS DISCHARGE CURRENT

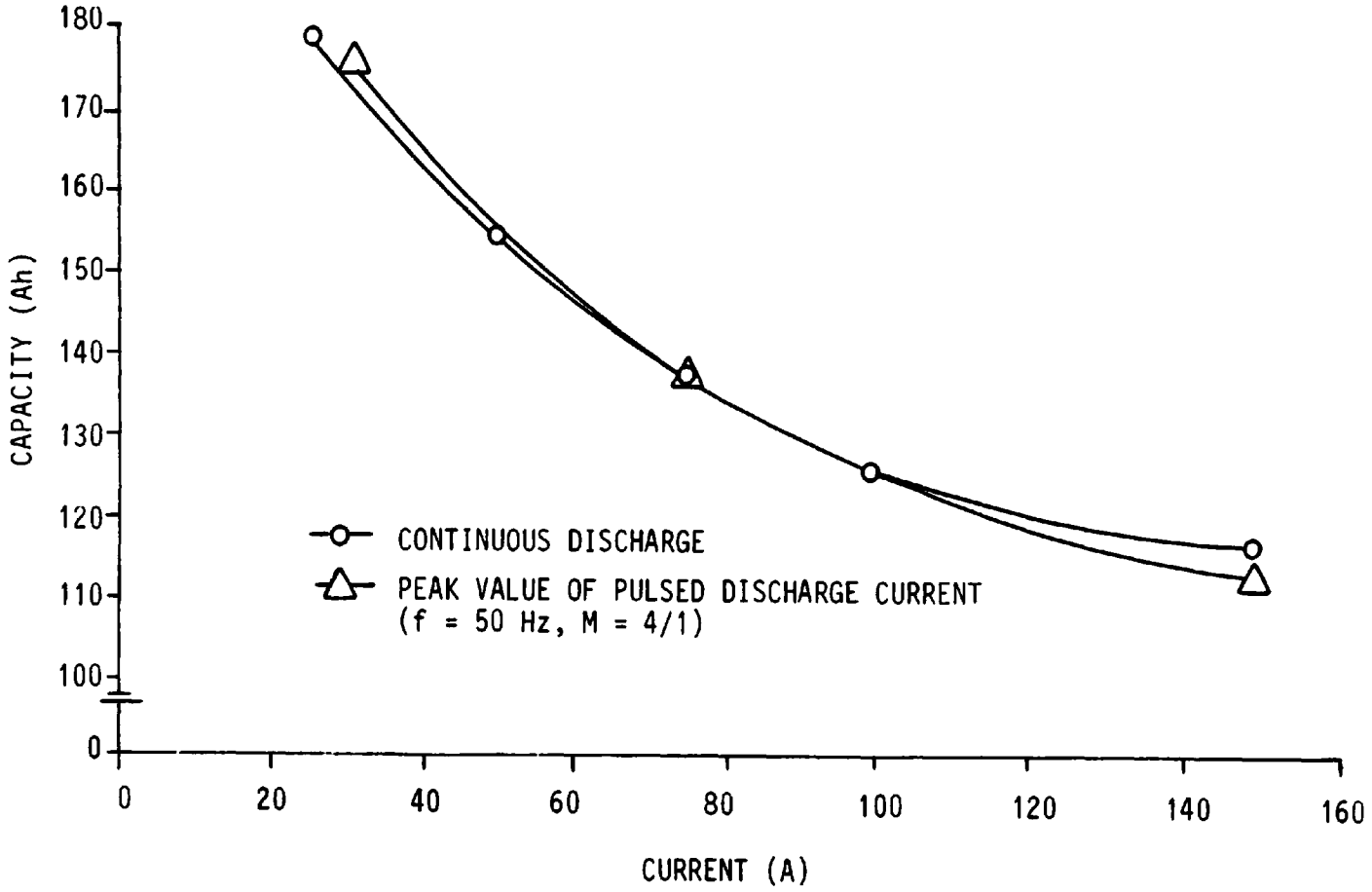

FIG. 31 VARIATION OF CAPACITY WITH DISCHARGE CURRENT FOR CONTINUOUS AND PULSED DISCHARGE

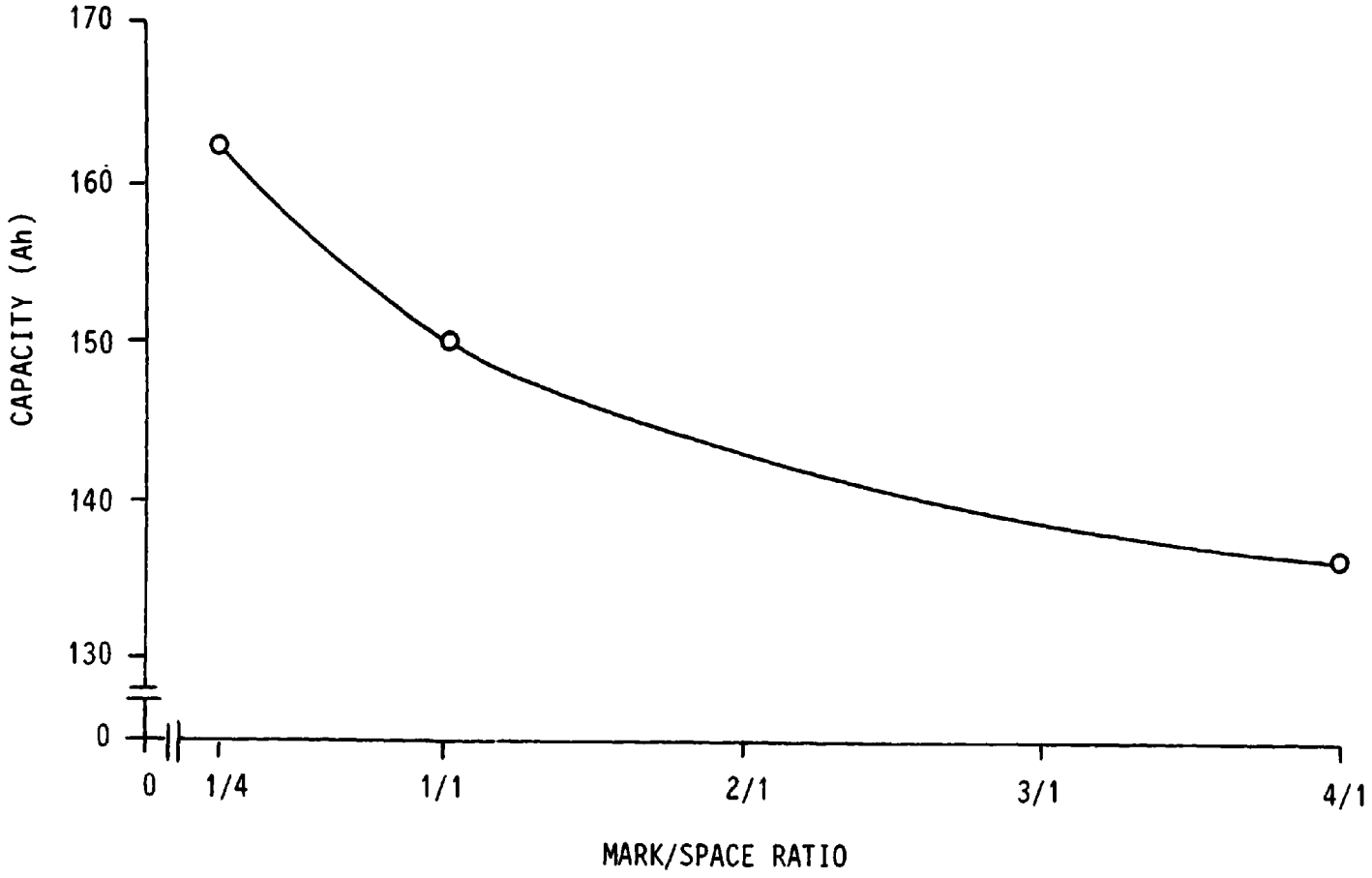

FIG. 32 VARIATION OF CAPACITY WITH MARK/SPACE RATIO (f=50 Hz, I_{pk}=75 A)

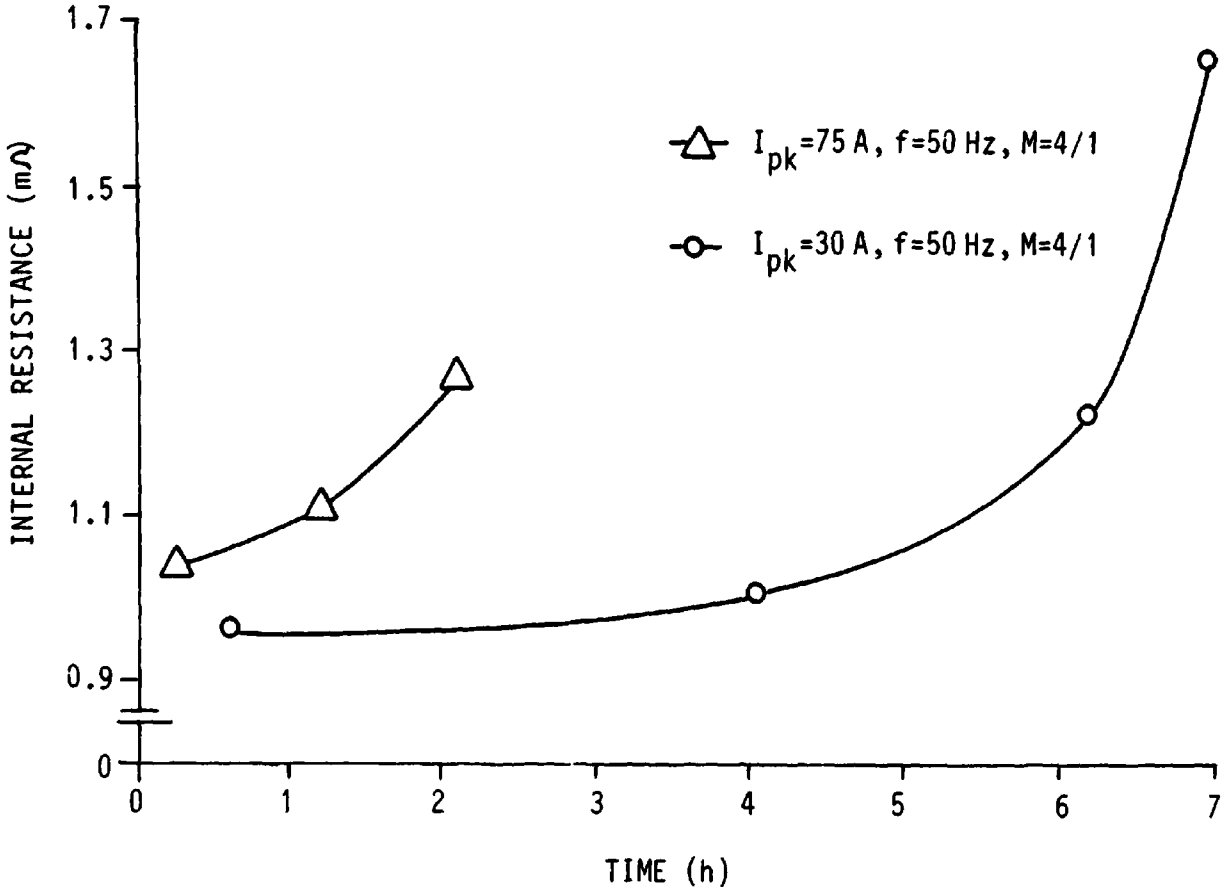

FIG. 33 VARIATION OF INTERNAL RESISTANCE OF THE CELL WITH TIME OF DISCHARGE FOR VARIOUS VALUES OF PEAK CURRENT

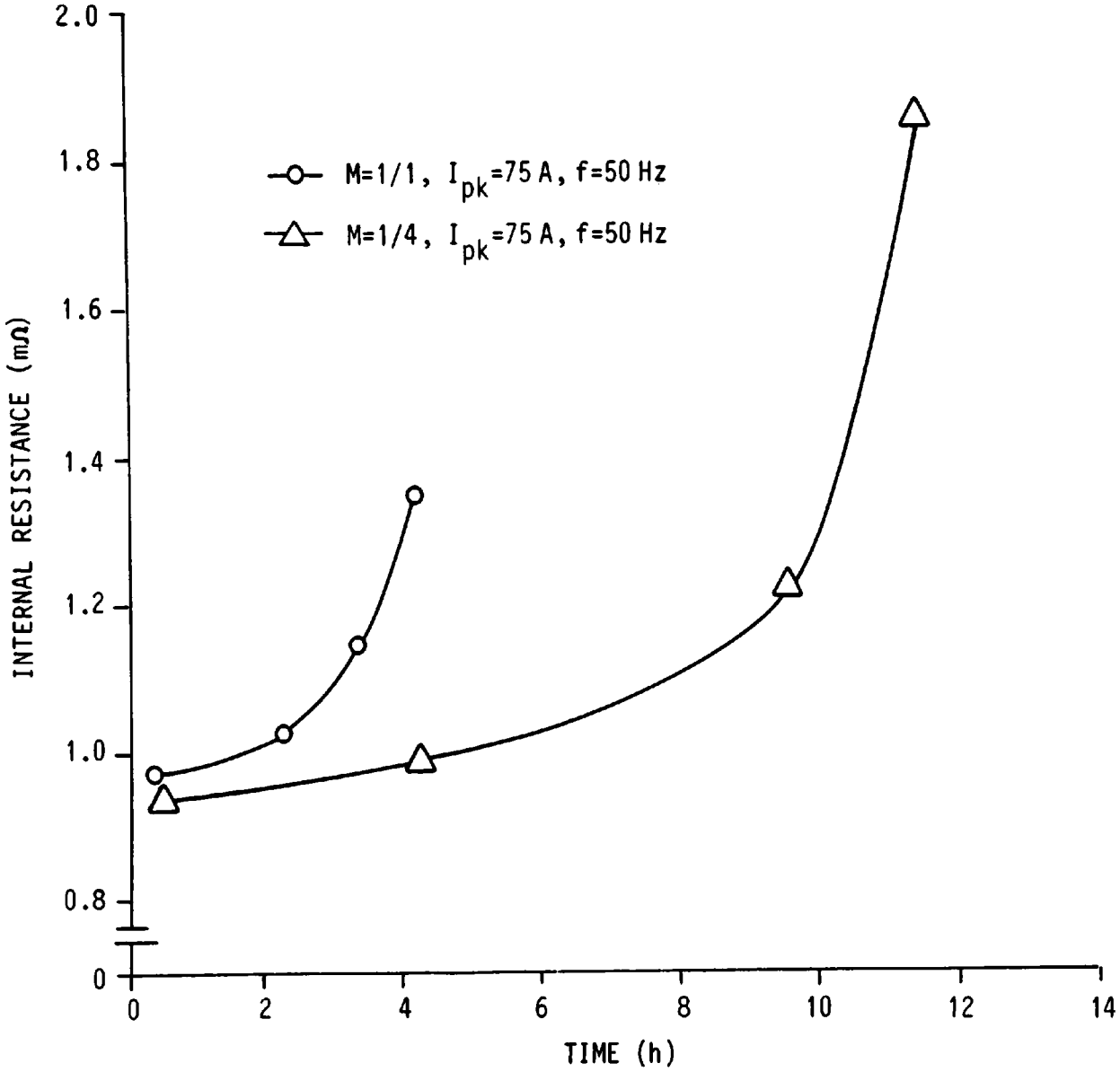

FIG. 34 VARIATION OF INTERNAL RESISTANCE OF THE CELL WITH TIME OF DISCHARGE FOR VARIOUS VALUES OF MARK/SPACE RATIO

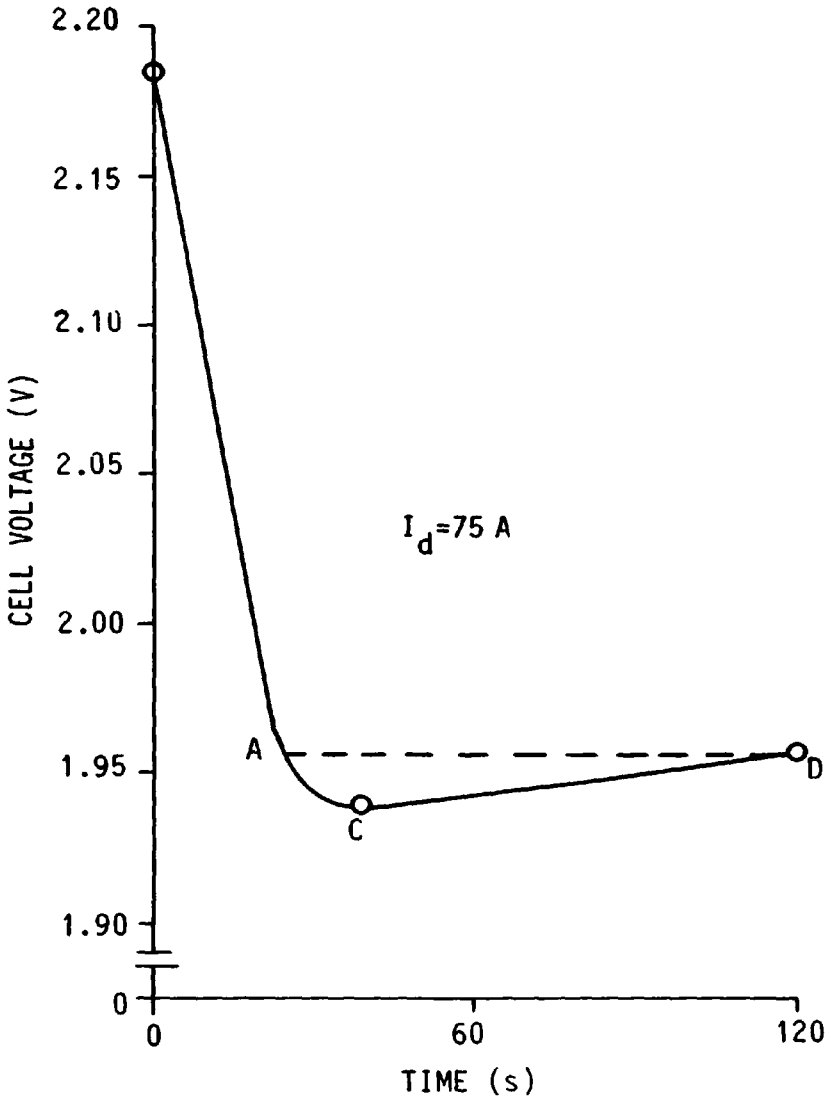

FIG. 35 THE "COUP DE FOUET" CHARACTERISTIC

50 Hz respectively, is illustrated in Fig. 34. It can be seen that for a mark/space ratio of 1/1 there is an apparent increase in resistance of 0.38×10^{-3} ohms throughout the period of discharge, whereas for a mark/space ratio of 1/4 there is an increase in resistance of approximately 0.91×10^{-3} ohms.

From the results it is evident that for the tubular armoured or flat-plate cells, pulsed discharging can produce an increase in the available capacity of the cell when compared to equivalent continuous current discharging. It may be seen from the results that the percentage increase in available capacity was greater for the tubular armoured than for the flat-plate cells. For example, when pulsed discharging the flat-plate cells at a frequency, mark/space ratio, and peak current of 50 Hz, 1/1, and 75 A ($0.5C_5$ A) respectively, there was an increase in available capacity of 9.5% (cf. Figs. 31 and 32), whereas, for the tubular armoured cells, pulsed discharging at a frequency, mark/space ratio, and peak current of 50 Hz, 1/1, and 55 A ($0.5C_5$ A) respectively, produced an increase in available capacity of approximately 24.50% (Fig. 23). For tubular armoured and flat-plate cells having positive plates of similar peripheral dimensions, it is probable that the greater increase in available capacity experienced by the tubular armoured cell is due to a difference in the surface area of the two types of plate. The surface area of the tubular positive plate is greater than that of the flat-positive plate, and hence, during periods of recuperation, the diffusing electrolyte will contact a greater amount of active material, which will result in a greater recuperation effect.

4.8.2 General Comments

In practice it is found that the theoretical amounts of active

material required to produce a given amount of electricity is very much less than the actual amounts. This is because not all the active material of the plates participates in the reactions. The ratio of the amount of active material participating in the reaction to the total amount of active material is termed the 'coefficient of utilisation'. Therefore, when compared to continuous current discharging, the increase in available capacity of the cell under pulsed discharge conditions may be attributed to an increase in the 'coefficient of utilisation' of the active plate material. For example, for the pulsed discharge test on the tubular armoured cell, where the peak current, frequency, and mark/space ratio were 40 A, 50 Hz, and 1/1 respectively, the output was 127.74 ampere-hours, whereas, for the equivalent continuous discharge test the output was 108 ampere-hours (Fig. 23). Therefore, pulsed discharging has produced a relative increase of 16% in the coefficient.

From the results of the present investigations, the author agrees with the general findings of Jayne [11] but questions the findings of other authors [12 - 14]. However, it should be noted that for particular values of peak discharge current, frequency, and mark/space ratio of the pulsed waveform, the present investigations show that no relative increase in available capacity was obtained. The results are, therefore, more conservative than those obtained by Jayne, who showed that pulsed discharge virtually always produced an increase in available capacity when compared to equivalent continuous discharge, irrespective of the mark/space ratio, frequency, and peak current of the discharge waveform.

4.9 Interim Conclusions

From the results presented in this chapter, the following

interim conclusions may be drawn:

(1) Pulsed discharge can produce a considerable increase in available capacity provided the peak value of the current is taken as the discharge rate and the minimum value of cell voltage is taken as the termination of discharge voltage. However, when the mean value of the pulsed current is taken as the discharge rate and the mean value of cell voltage is taken as the termination of discharge voltage, the increase in available capacity is considerably less.

(2) The available capacity under pulsed discharge conditions of operation is inversely proportional to mark/space ratio and to a lesser extent frequency. This relationship is probably attributable to a reduction in cell recovery time with decrease in the space-time of the waveform, and to an increase in the rms value of current (see Appendix 2) resulting in increased i^2r losses within the cell.

(3) Under pulsed discharge conditions of operation the effective internal resistance of a lead-acid cell increases with time of discharge, mark/space ratio, peak value of current, and frequency. This variation in the value of the effective internal resistance may also contribute to the increased i^2r losses mentioned above.

5. AN INVESTIGATION INTO FAST CHARGING TECHNIQUES FOR LEAD-ACID BATTERIES

5.1 Introduction

One of the major problems with any battery powered EV is the time taken to replace the stored energy used by the vehicle. At present, the quickest method is to replace the discharged battery by a charged one. However, this technique incurs the penalty of having to purchase two battery systems. Therefore, over the past decade or so, considerable effort has been devoted to the investigation of charging techniques which will safely recharge the battery in less than approximately one hour. The significance of one hour is that in many industries and local services where EVs are used, such vehicles are not utilised during lunch breaks and change of working shifts. It should also be stressed that should city or town charging stations be sited, then a charging period of one hour would probably be considered a maximum.

The main aim of the present charging investigation was to find a safe means by which lead-acid traction batteries could be recharged in as short a period of time as possible. For reasons which will now be discussed it was originally thought that this aim might be realised by some form of pulsed charging.

5.2 Theoretical Considerations

As discussed in Section 2.4, only those charging techniques which do not cause excessive gassing or heating can be regarded as suitable, since an excess of either or both of these charging effects has a detrimental effect on the life and charging performance of the cell. There is, however, another aspect of gas evolution that must be considered in relation to the charging performance of the cell:

During charging, the oxygen at the positive plate and the hydrogen at the negative plate both play an unwanted role. The oxygen ions after depositing their electrons on the positive plate, form neutral oxygen. It is possible that this oxygen forms a thin insulating layer on the surfaces of the positive plate, similar to the layer which the hydrogen ions are known to form on the negative plate. Because of their insulating characteristics, the layers may act so as to inhibit the chemical reactions of the charge. Additionally, the process of electrochemical polarisation produces heat, which causes an increase in the internal temperature of the cell.

If the charging waveform is of a pulsed form then possibly the 'space' periods of the waveform would have a 'relaxation' effect on the cell, which would allow the gases to naturally disassociate themselves from the surfaces of the plates, causing depolarisation. Depolarisation would effectively increase the charge acceptance of the cell plates, causing a reduction in the rate of gas evolution and of heat generation. Furthermore, it is also possible that during these 'space' periods the higher concentration of H_2SO_4 occuring within the pores and in the immediate vicinity of the plates would diffuse towards the main body of the electrolyte, thereby assisting the charging chemical reaction process. Similarly, if the charging waveform was composed of alternate pulsed charge and pulsed discharge currents (asymmetric charging) then it is thought that the relaxation effect would still be evident, but the discharge pulses would act so as to forcibly remove the gas bubbles from the surfaces of the plates. Additionally, the discharge pulses would act so as to reduce the concentration of H_2SO_4 within the pores of the plates, further assisting the charging chemical reaction process.

5.3 A Review of Previous Investigations

The results of recent investigations (mainly in the U.S.A.) into fast charging techniques have been remarkable, but rather contradictory:

It has been stated [62] that three fundamental laws of charging have been discovered, which allow a 200 ampere-hour lead-acid traction battery to be charged in 6 minutes. It is claimed that these laws govern the charging behaviour of all secondary cells. The laws are based on an exponential charge acceptance curve which is similar in form to equation(3). However, in a recent study [63] into the charge acceptance of lead-acid batteries as a function of: past history of discharge rates; past history of charging and charge rate as a function of the ratio of time to constant gassing rate; it was concluded that 'the exponential law which states that charge acceptance is proportional to charge deficiency is, in general, an inadequate description of cell behaviour'. The validity of the three laws must be further questioned as a result of another investigation into the cell charge acceptance [64], which demonstrated that the charge acceptance curve is not of an exponential form.

It has been observed [18] that charging nickel-cadmium batteries with a continuous direct current (d.c.) or pulsed d.c. at high rates is efficient, but causes gassing and heating after the battery is approximately 60% charged. Further, it was observed that the continuous charge/discharge cycling of the batteries using these techniques, caused the battery voltage characteristic to rise prematurely, resulting in the termination of charge prior to full capacity recharge. Examination of the cells revealed abnormal plate crystalline structures. It was subsequently discovered that periodic discharging during charging, prevented the abnormal crystalline

structure from forming, and reduced the gassing and heating problems associated with fast charging until the battery was at least 90 - 95% recharged. From other tests performed on nickel-cadmium batteries [20], it has been stated that in terms of reducing charging time, increasing charge acceptance, minimising battery memory effects, and increasing battery life, charging using depolarisation discharge current pulses is much superior to conventional charging techniques. Additionally, it is claimed that the application of such a technique to a 24 ampere-hour nickel-cadmium battery allowed it to be charged in 6 minutes [19], and that where the positive to negative charge energy varied as a function of battery capacity, a 200 ampere-hour nickel-cadmium battery could be charged in no more than 1 hour [20]. Similarly, from tests performed on lead-acid batteries, it has been stated [18] that the use of depolarisation discharge pulses throughout the charging period allowed a battery with a 5-hour discharge rate capacity of 190 ampere-hours to be charged in 5 - 10 minutes.

The results of more recent investigations [65, 66] into fast charging techniques suggest that pulsed charging of lead-acid batteries offers no significant advantages over continuous current charging. In fact, where the results have been compared for the two techniques, it was found that the pulsed technique caused a decrease in the charge ampere-hour and energy efficiencies, and an increase in cell electrolyte temperature [66].

In order to evaluate the validity of these claims, investigations into the pulsed and asymmetric charging of lead-acid traction cells were performed by the author.

5.4 Test Apparatus

The cells subjected to experimentation were tubular armoured

lead-acid traction cells, whose specifications are detailed in Section 4.3.

The test facility is shown in Fig. 36, where it may be seen that a variable transformer supplies a fixed ratio transformer which feeds a single-phase bridge rectifier with output smoothing capacitors. The specifications of the variable single-phase transformer were: input: 250 V, 50-60 Hz; output: 0-270 V, 15 A; and for the fixed ratio transformer: input: 0-240 V, 5 A; output: 0-12 V, 100 A; 1.2 kVA. The bridge circuit diodes had a mean forward current rating of 60 A, and the smoothing circuit was composed of 68,000 uF-16 V capacitors. The charge/discharge currents for the test cells were controlled by means of bi-polar transistor converters which could operate in both the continuous and pulsed modes. From Fig. 36 it is apparent that the facility for pulsed and asymmetric charging is essentially the same except that for the asymmetric mode a second bi-polar transistor converter is introduced into the circuit as shown by the broken line. Practical cell voltage and cell current waveforms for pulsed and asymmetric charging are shown in Fig. 37. The ampere-hours supplied to, or removed from the cells were monitored by means of a bi-polar ampere-hour meter which had a measuring accuracy of 0.1%.

5.5 Design of Experimentation

The pulsed charging investigations were performed using single-stage, two-stage and three-stage charging techniques, and were intended to fully evaluate the relative merits of pulsed and continuous current charging techniques up to and beyond the gassing level of the battery. The asymmetric charging tests were designed such that the battery charging performance could be compared with that obtained from the pulsed and continuous current charging tests. Throughout the

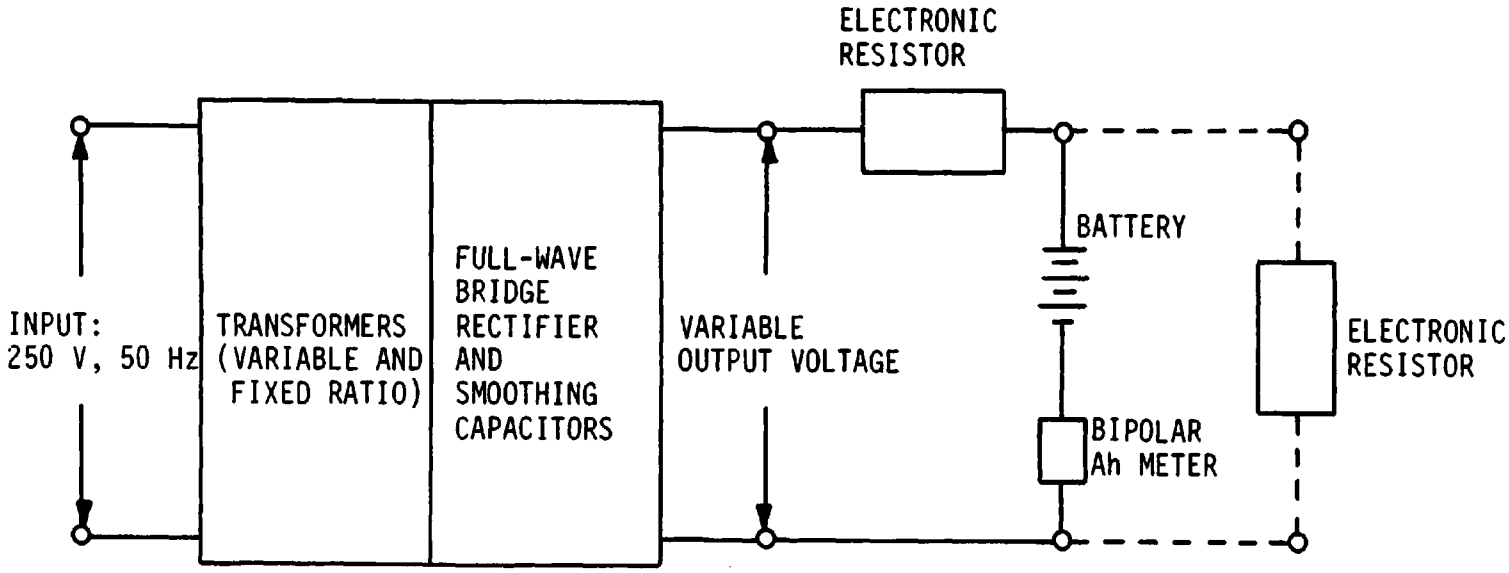

FIG. 36 CHARGING FACILITY

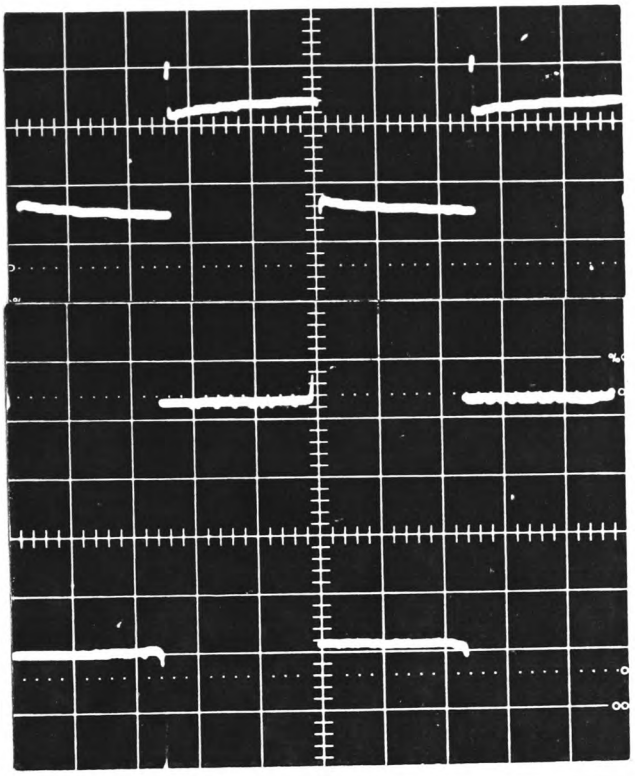

VOLTAGE WAVEFORM

FIG. 37(a) PULSED WAVEFORMS

CURRENT WAVEFORM

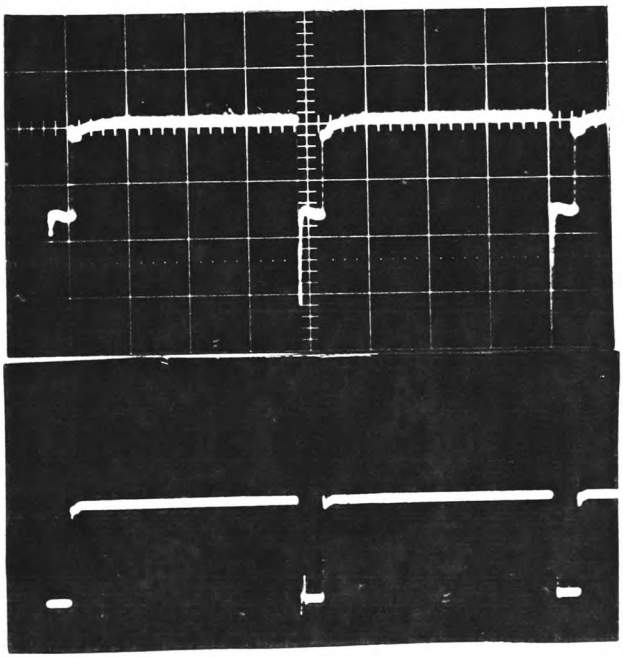

VOLTAGE WAVEFORM

FIG. 37(b) ASYMMETRIC WAVEFORMS

CURRENT WAVEFORM

FIG. 37 TYPICAL VOLTAGE AND CURRENT WAVEFORMS OF THE CELL FOR PULSED CHARGING AND ASYMMETRIC CHARGING

experimentation the mean value of the complex current waveform (pulsed or asymmetric waveform) was made equal to the continuous current charging rate.

The cells were discharged by a constant current method, with the magnitude of the current held constant throughout the experimentation at $C_5/10$ for the single-stage tests, $3/35 \cdot C_5$ for the three-stage tests and $C_5/5$ for the two-stage and asymmetric tests. The fully discharged condition was established when the cell terminal voltage dropped to 1.7 V.

The effects of history of discharge of the cells was suppressed by subjecting the cells to a steady 5-hour rate discharge before and after each specific test. The mean capacity of these two tests was taken as the reference capacity of the cells. For reference purposes and to overcome the effects of history of charge, the test cells were subjected to a two-stage continuous current charge routine between each specific charge test. The charging rates used for the first and second stages were $C_5/5$ and $C_5/15$ respectively, with a change over value of voltage of 2.4 V/cell.

The single-stage tests were terminated when the capacity supplied to the cells reached 134 ampere-hours, whereas, the two-stage, three-stage, and asymmetric tests were terminated when the cell voltage and specific gravity reached values which remained constant over 3 hours, readings being taken at 1-hour intervals.

Prior to all discharge tests the cells were allowed to rest on open-circuit for approximately 1 hour to allow the bulk of the occluded gases to escape. Prior to all charge tests the cells were allowed to rest on open-circuit for a period of 1 hour.

The ambient temperature of the test cells was maintained within 1°C of 30°C by immersing the cells in a temperature controlled tank.

5.6 Measurement Technique

Ideal waveforms of cell voltage and cell current associated with the two complex current charging techniques are illustrated in Fig. 38.

The peak and minimum values of cell voltage (V_{pk} and V_{mn} respectively) were measured by means of a calibrated C.R.O. connected directly across the cell terminals, whereas, the peak charge and discharge values of current (I_{pk} and I_{dp} respectively) were measured using a non-inductive shunt. The frequency, mark/space ratio, and duration of the charge and discharge times (t_c and t_d respectively) of the complex waveforms were also measured by means of a calibrated C.R.O. The mean value of cell voltage, V_{av}, was measured by means of a precision moving coil voltmeter, and the mean value of the pulsed current, I_{av}, was measured by means of a precision moving coil ammeter; the accuracy of these measurements were verified by means of the precision digital bi-polar ampere-hour meter. The volume and rate of gas evolved were measured by means of a water displacement technique using a calibrated gas jar. The specific gravity of the electrolyte was measured by a hydrometer and temperature corrected to 15°C by means of a scale correcting thermometer. The cell internal resistance under pulsed charging conditions was determined by means of equation (14).

The relationships between the values of current, voltage, frequency, mark/space ratio, and capacity for a pulsed charging waveform are defined by equations (10) - (13). For an asymmetric waveform, equations (12) and (13) may be similarly used, but the mean and rms values of current are given by:

$$I_{av} = \frac{1}{1 + N} (I_{pk} N - I_{dp}) \qquad (15)$$

$$I_{rms} = \frac{1}{T} (I_{pk}^2 \cdot t_c + I_{dp}^2 \cdot t_d)^{1/2} \qquad (16)$$

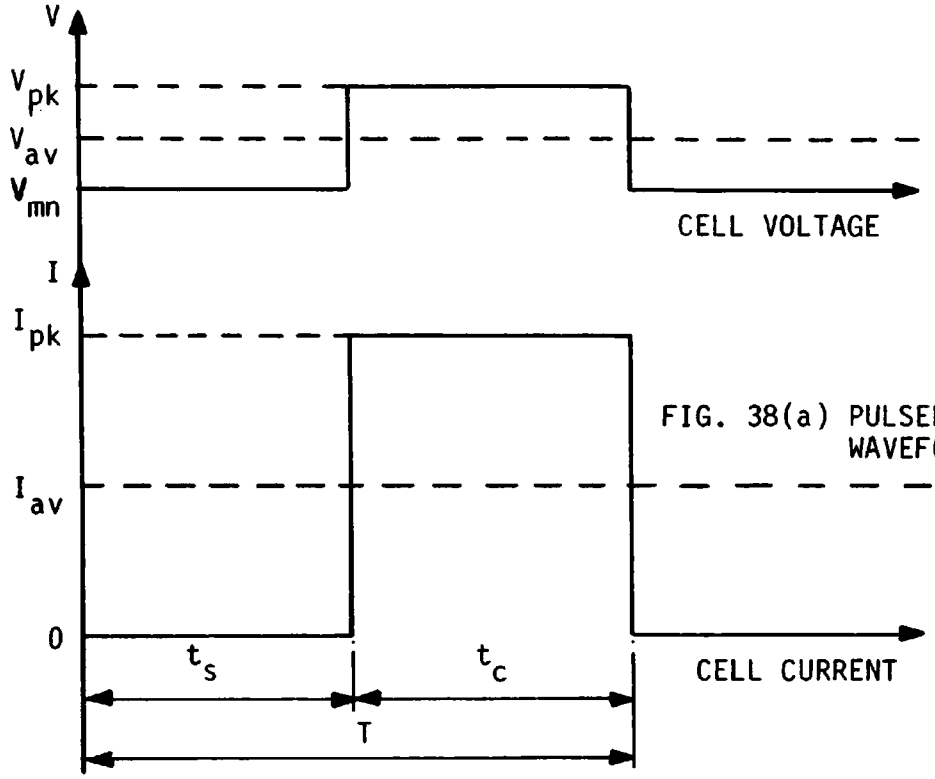

FIG. 38(a) PULSED WAVEFORMS

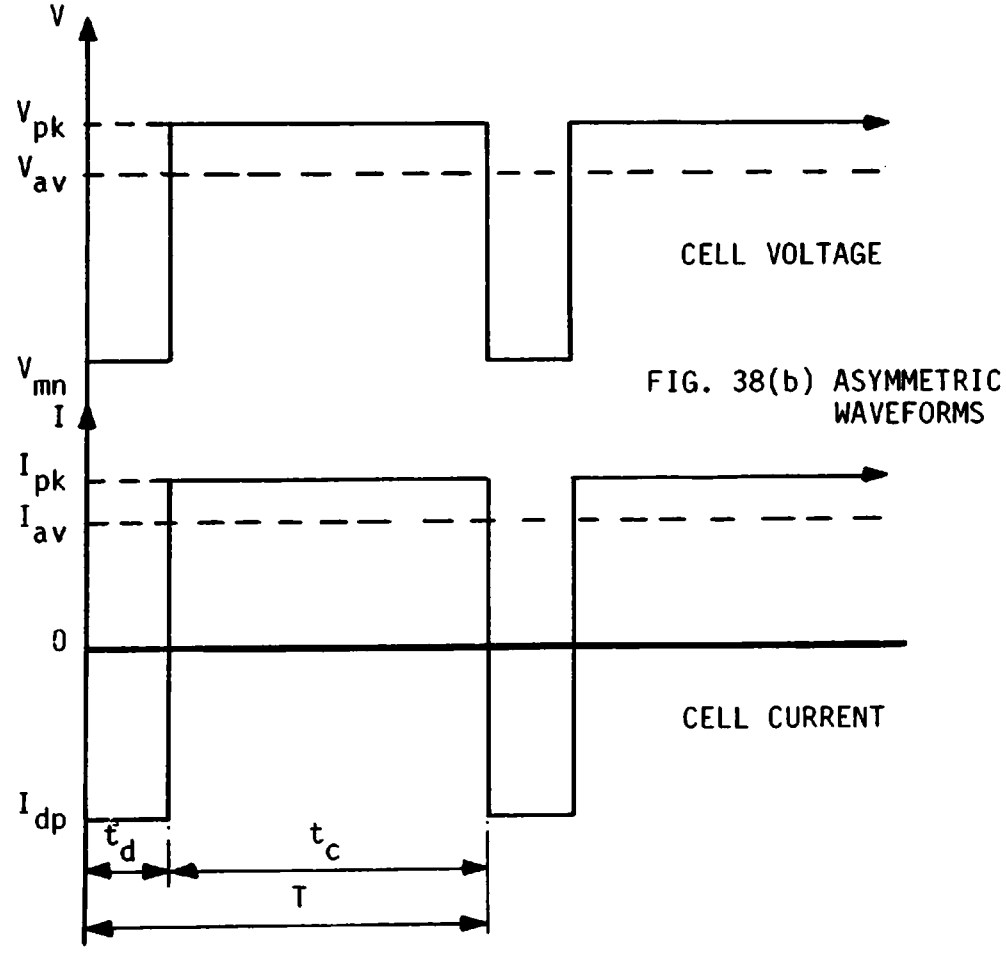

FIG. 38(b) ASYMMETRIC WAVEFORMS

FIG. 38 IDEAL VOLTAGE AND CURRENT WAVEFORMS FOR PULSED AND ASYMMETRIC CHARGING

where: $N = t_c/t_d$.

The relationships between the measured quantities for complex current and continuous current charging were expressed in terms of the following ratios:

$$\text{Gas Volume Ratio (GVR)} = \frac{\text{Volume of gas evolved for complex current charging}}{\text{Volume of gas evolved for continuous current charging}}$$

$$\text{Ampere-hour Efficiency} = \frac{\text{Ampere-hours out}}{\text{Ampere-hours in}}$$

$$\text{Temperature Ratio} = \frac{\text{Electrolyte temp. rise for complex current charging}}{\text{Electrolyte temp. rise for continuous current charging}}$$

$$\text{Ampere-hour Efficiency Ratio (AHER)} = \frac{\text{Ampere-hour eff. for complex current charging}}{\text{Ampere-hour eff. for continuous current charging}}$$

$$\text{Charging Time Ratio (CTR)} = \frac{\text{Charging time for complex current charging}}{\text{Charging time for continuous current charging}}$$

5.7 Experimental Tests

5.7.1 Pulsed Tests

(1) Three-stage Charging

For both pulsed and continuous current charging tests, the

cells were charged using a three-stage procedure, where the mean value of current for each stage and change-over value of voltage were:

Stage	Mean Value of Current	Change-over Voltage
1	$\frac{90}{55} I_{C_5}$	2.4 V/cell
2	$\frac{42}{55} I_{C_5}$	2.6 V/cell
3	$\frac{20}{55} I_{C_5}$	-

The values of frequency and mark/space ratio used were:

$$f = 50, 250, 500 \text{ and } 1000 \text{ Hz}$$

and M = 4/1 and 1/1.

(2) Single-stage Charging

For both pulsed and continuous current charging tests, the amount of charge supplied to the cells remained constant at 121.8% of the C_5 nominal capacity. In both types of test the mean value of the charging current was maintained constant at $18/11 \cdot I_{C_5}$.

The values of frequency and mark/space ratio used were:

$$f = 100 \text{ and } 500 \text{ Hz}$$

and M = 4/1, 2/1, 1/1 and 1/2.

(3) Two-stage Charging

For both pulsed and continuous current charging tests, the cells were charged by a two-stage procedure, where the mean value of current for each stage and the change-over value of voltage were:

Stage	Mean Value of Current	Change-over Voltage
1	$n.I_{C_5}$; where n = 1,2 an 3	2.4 V/cell
2	$I_{C_5}/3$	-

The values of frequency and mark/space ratio were maintained constant at:

$$f = 100 \text{ Hz and } M = 2/1$$

5.7.2 Asymmetric Tests

For the asymmetric current charging tests, the cells were charged by a two-stage procedure, where the mean value of current for each stage and the change-over value of voltage were:

Stage	Mean Value of Current	Change-over Voltage
1	$2.I_{C_5}$	2.4 V/cell
2	$I_{C_5}/3$	-

The values used for the frequency, the discharge depolarisation pulse (I_{dp}) and the ratio of charge to discharge energy (CD_r) were:

f = 12 and 100 Hz ;

$I_{dp} = m.I_{C_5}$, where m = 2,4 and 8 ;

$CD_r = n$, where $CD_r = I_{pk}.t_c/I_{dp}.t_d$ (see Fig. 38), and n = 3.5, 6, 9.5

5.8 Results

For the pulsed charging tests, the results of the three-stage, single-stage, and two-stage investigations are shown in Figs. 39 - 41, Figs. 42 - 46, and Figs. 47 - 56 respectively. The results of the asymmetric investigations are shown in Figs. 57 - 68.

5.9 Comments on Results

5.9.1 Comments on Pulsed Charging Results

Fig. 39 shows the variation of total gas evolved with frequency

when fully charging a lead-acid cell in three stages, for mark/space ratios of 4/1 and 1/1. For the frequencies and mark/space ratios considered, pulsed charging increases the total volume of gas evolved when compared to the equivalent continuous current charging routine. It can be seen that at a fixed frequency value, pulsed charging with a mark/space ratio of 4/1 results in a greater volume of gas evolved than pulsed charging with a mark/space ratio of 1/1, and that for both mark/space ratios the total volume of gas evolved increases with increase in frequency. At a frequency of 1000 Hz and mark/space ratios of 4/1 and 1/1, the increase in total gas evolved when compared to the equivalent continuous current charge is 32% and 24% respectively.

The variation in ampere-hour efficiency of charge with frequency for various mark/space ratios is shown in Fig. 40. For the frequencies and mark/space ratios considered, pulsed charging reduces the ampere-hour efficiency of charge when compared to continuous current charging. The results show that increasing the frequency of the pulsed charging currents while maintaining a constant mark/space ratio results in a reduction of the ampere-hour efficiency of charge, whereas, reducing the mark/space ratio from 4/1 to 1/1 at a fixed value of frequency, results in an increase in the ampere-hour efficiency of charge. At a frequency of 1000 Hz and mark/space ratios of 1/1 and 4/1, the ampere-hour efficiency of charge is decreased by 2.1% and 2.4% respectively, when compared to equivalent continuous current charging of the lead-acid cell.

Fig. 41 shows the variation of temperature ratio with frequency for various values of mark/space ratio. It can be seen, that pulsed current charging increases the temperature ratio, when compared to continuous current charging. Increasing the frequency of the pulsed charging currents while maintaining a constant mark/space ratio

produces an increase in the temperature ratio, whereas, increasing the mark/space ratio from 1/1 to 4/1 at a fixed value of frequency, results in a reduction of the temperature ratio, for the frequency values considered.

Fig. 42 illustrates the variation of ampere-hour efficiency with mark/space ratio for frequencies of 100 Hz and 500 Hz when partially charging the cell. At a frequency of 100 Hz, increasing the mark/space ratio from 1/2 to 4/1 results in an increase in ampere-hour efficiency. At a frequency of 500 Hz, a similar increase in mark/space ratio produces an increase and then a decrease in ampere-hour efficiency, indicating that for the values considered optimum values of mark/space ratio exist, however, for the results shown, it can be seen that when compared to continuous current charging, pulsed current charging does not increase the ampere-hour efficiency of charge. Fig. 43 shows that for fixed pulsed current charging frequencies of 100 Hz and 500 Hz, increasing the mark/space ratio of the pulsed currents from 1/2 to 4/1 results in a decrease of the temperature ratio. The variation of GVR with mark/space ratio at frequencies of 100 Hz and 500 Hz is illustrated in Fig. 44. At the mark/space ratio values considered, increasing the mark/space ratio of the pulsed charging currents at a constant value of frequency, results in an overall decrease of the GVR, this decrease being much smaller for the 500 Hz than for the 100 Hz frequency charge. For a constant value of mark/space ratio the GVR is greater for the 100 Hz than for the 500 Hz pulsed current charge.

The variation of cell internal resistance with ampere-hour input for various charging frequencies and mark/space ratios is illustrated in Fig. 45. When both the frequency and mark/space ratio are maintained constant throughout the charging period, it may be seen

that the internal resistance decreases with increasing ampere-hour input. It may also be seen that maintaining the frequency of the pulsed currents constant while increasing the mark/space ratio, results in a decrease of the cell internal resistance, especially for lower values of ampere-hour input. Maintaining the mark/space ratio of the charging current constant while increasing the frequency of operation produces a decrease in internal resistance throughout the charging period, again, especially for lower values of ampere-hour input.

From Fig. 46 it may be seen that there is a non-linear increase in the gas evolution rate with increasing ampere-hour input, for the frequencies and mark/space ratios specified.

Fig. 47 shows the variation of AhER with initial charging current, when fully charging a lead-acid cell in two-stages. It may be seen that for constant current charging, increasing the initial charging current reduces the AhER. Using pulsed charging currents of 100 Hz with a mark/space ratio of 2/1 shows that at certain values of charging current, an increase in the AhER over the equivalent continuous current charge is experienced.

Fig. 48 shows that increasing the initial constant current charging rate produces an increase in the GVR. The results show that for pulsed current charging at a frequency of 100 Hz and mark/space ratio of 2/1, a lowering of the GVR is obtained for certain pulsed values of initial charging current.

Fig. 49 illustrates the variation of CTR with initial charging current for both continuous and pulsed charging conditions at a frequency of 100 Hz and mark/space ratio of 2/1. It can be seen that using certain charging rates produces a drop in the CTR. Little benefit is achieved by using pulsed current as opposed to continuous current charging.

The variation of the volume of gas evolved per cell with ampere-hour input during the first stage of charging, for continuous and pulsed charging currents, is shown in Figs. 50 and 51. For continuous current charging, increasing the initial charging rate produces an increase in the volume of gas evolved at corresponding values of ampere-hour input; as is also true for the pulsed charging mode. For both charging modes, the total volume of gas evolved for the first stage of charge, is proportionately related to the charging rate.

An example of the variation of the volume of gas evolved per cell with ampere-hour input for the second stage of charging is shown in Fig. 52, for an initial continuous charging current of 44 A. The characteristic is representative for all the tests performed for pulsed and continuous charging modes. The result shows that at a particular charge level, there is a considerable increase in the gas evolution rate, which remains virtually constant until termination of charge.

Fig. 53 illustrates the variation of cell voltage with ampere-hour input for various continuous charging rates. For the rates considered, there was, at the commencement of the charge, a rapid increase in cell voltage followed by a slight decrease in the voltage level. Dolazalek [67] proposed that this effect was due to the insulating $PbSO_4$ layer covering the surfaces of the active plate material. This proposal was supported by Berndt and Voss [61] who suggested that the effect is based on resistance polarisation, caused by a $PbSO_4$ layer on the active plate material. Vinal [48], however, proposed that the rise in terminal voltage is probably due to the sudden increase in concentration of the electrolyte as sulphuric acid is liberated in the pores of both the positive and negative plates; the voltage rise is then restricted by the diffusion process. As the ampere-hour input value increases, there is a gradual, almost linear

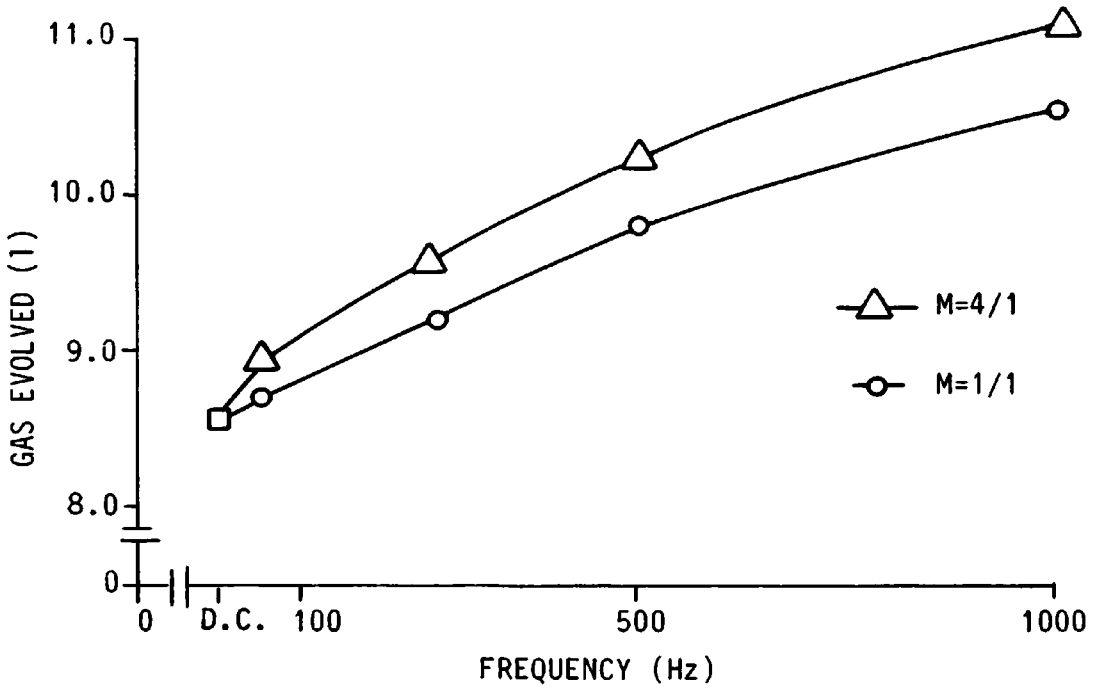

FIG. 39 VARIATION OF VOLUME OF GAS EVOLVED WITH FREQUENCY FOR VARIOUS VALUES OF MARK/SPACE RATIO

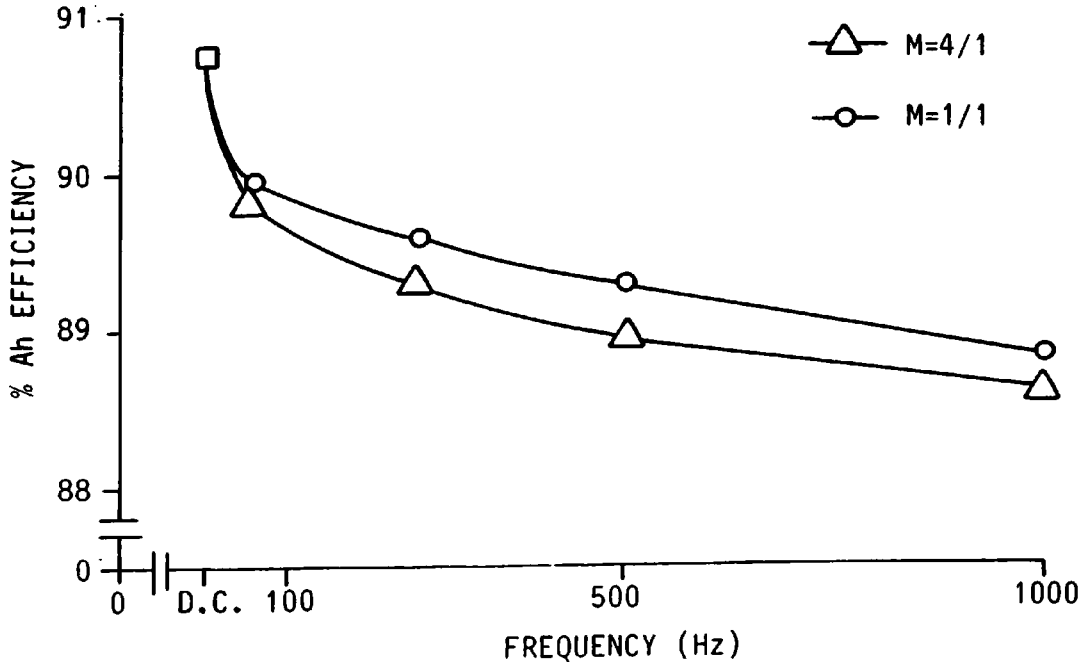

FIG. 40 VARIATION OF CELL EFFICIENCY WITH FREQUENCY FOR VARIOUS VALUES OF MARK/SPACE RATIO

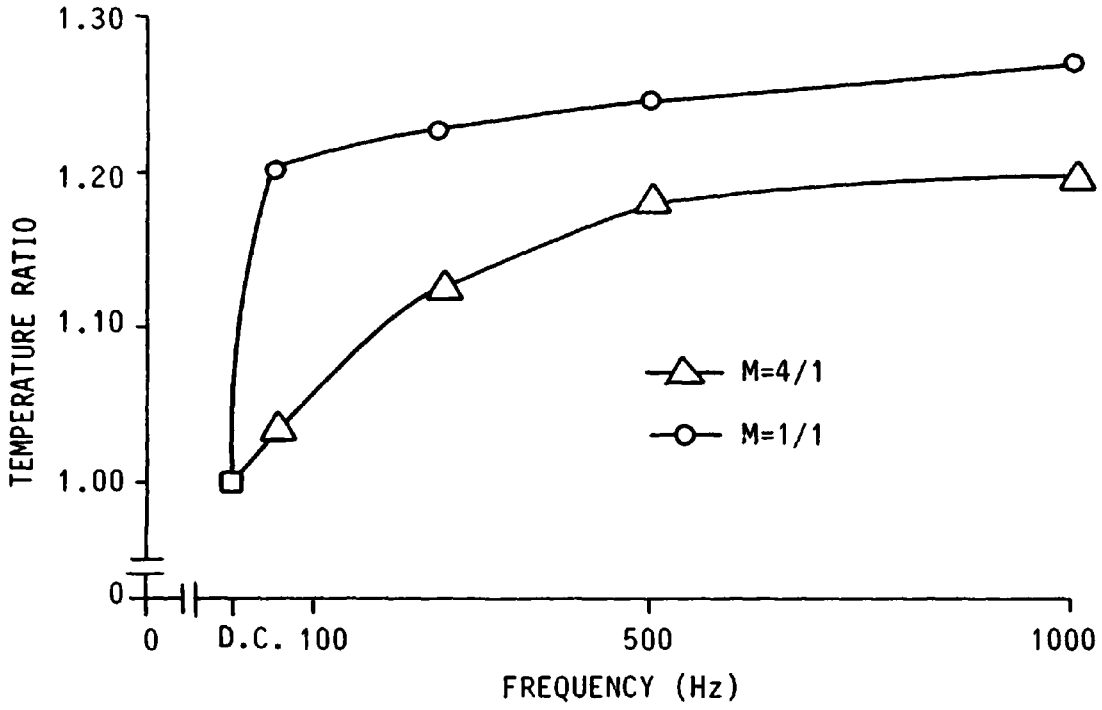

FIG. 41 VARIATION OF TEMPERATURE RATIO WITH FREQUENCY FOR VARIOUS VALUES OF MARK/SPACE RATIO

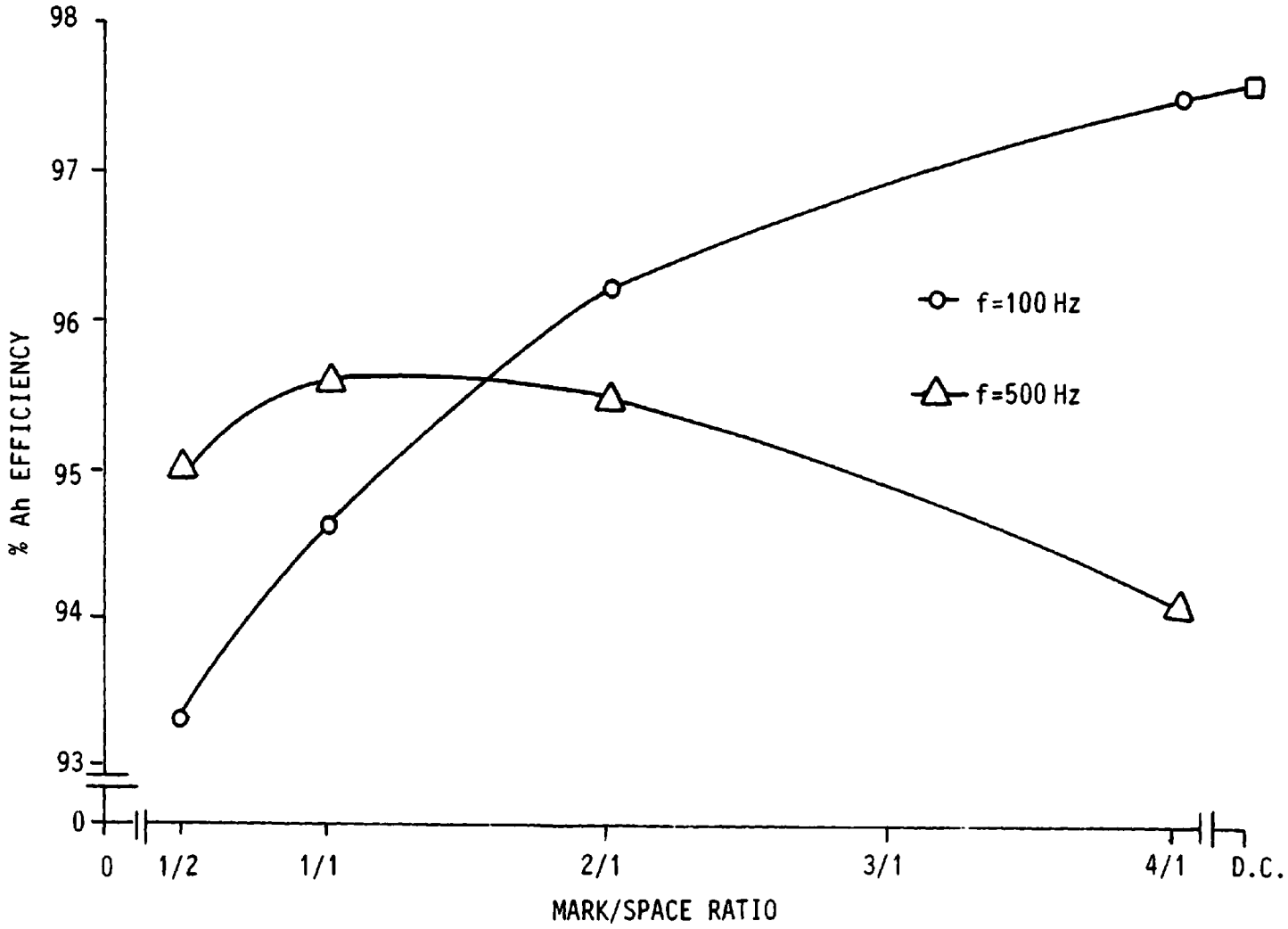

FIG. 42 VARIATION OF Ah EFFICIENCY WITH MARK/SPACE RATIO FOR VARIOUS VALUES OF FREQUENCY

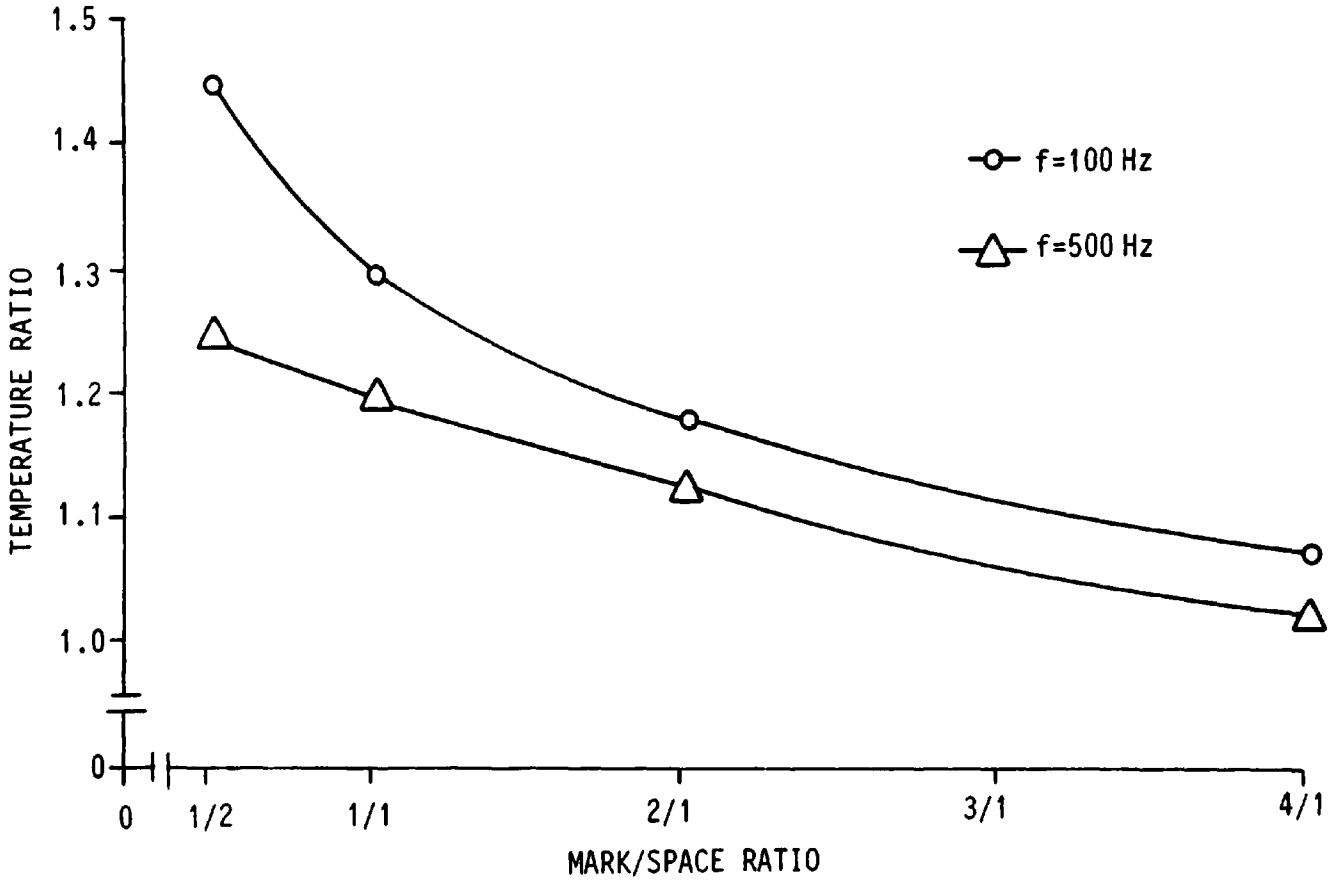

FIG. 43 VARIATION OF TEMPERATURE RATIO WITH MARK/SPACE RATIO FOR VARIOUS VALUES OF FREQUENCY

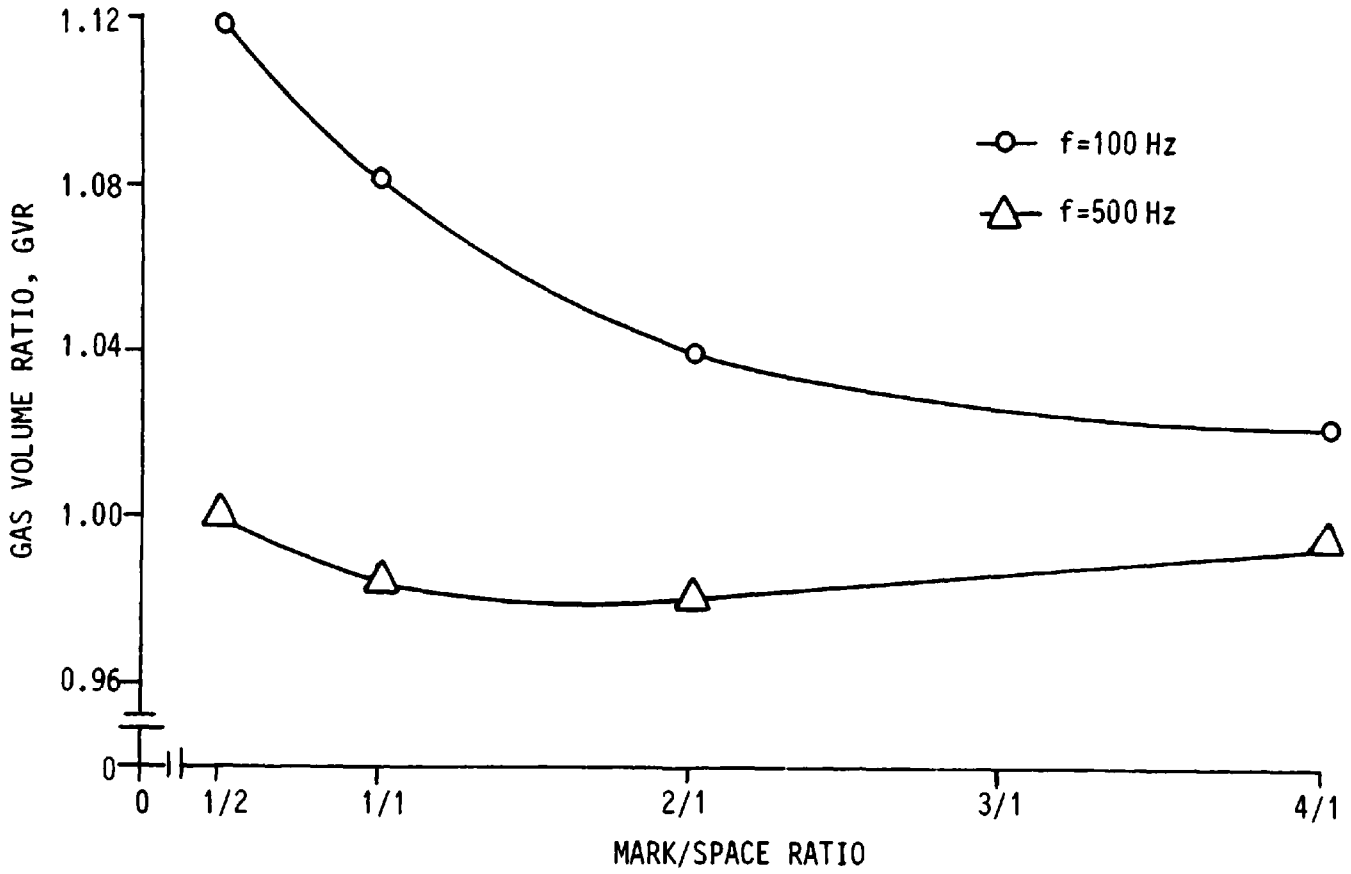

FIG. 44 VARIATION OF GAS VOLUME RATIO WITH MARK/SPACE RATIO FOR VARIOUS VALUES OF FREQUENCY

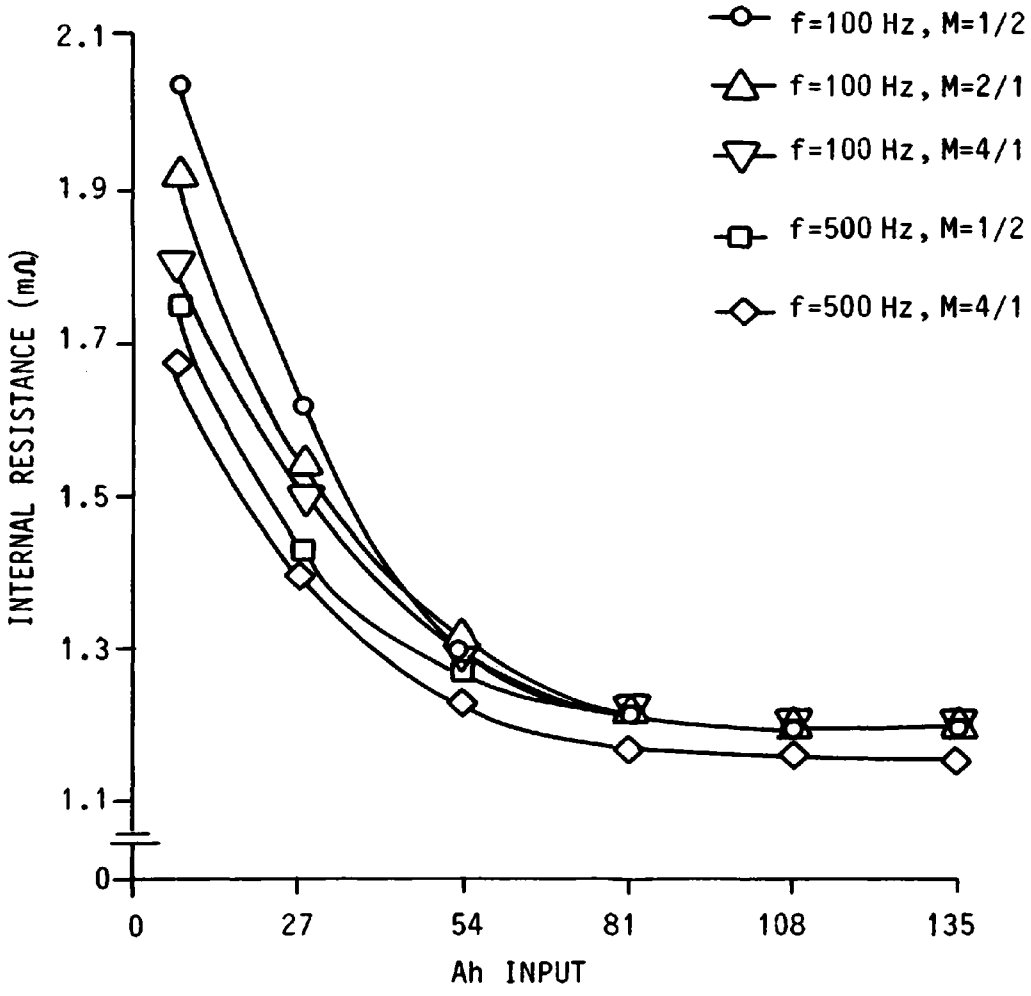

FIG. 45 VARIATION OF CELL INTERNAL RESISTANCE WITH Ah INPUT FOR VARIOUS VALUES OF FREQUENCY AND MARK/SPACE RATIO

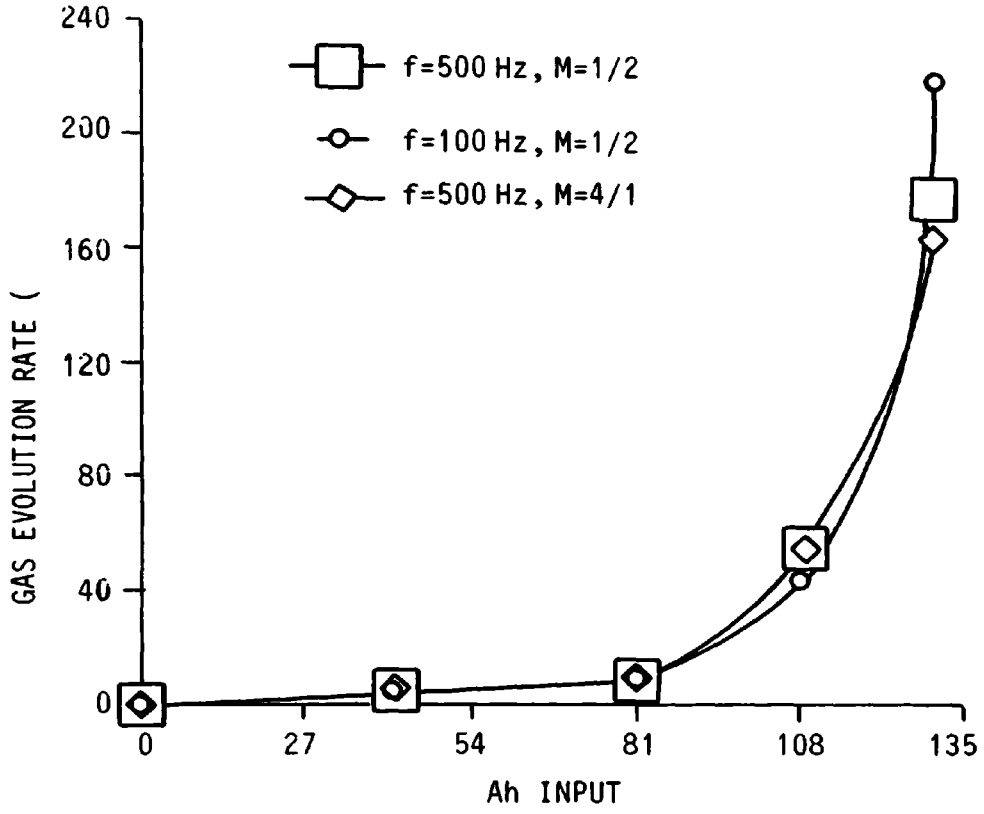

FIG. 46 VARIATION OF CELL GAS EVOLUTION RATE WITH Ah INPUT FOR VARIOUS VALUES OF FREQUENCY AND MARK/SPACE RATIO

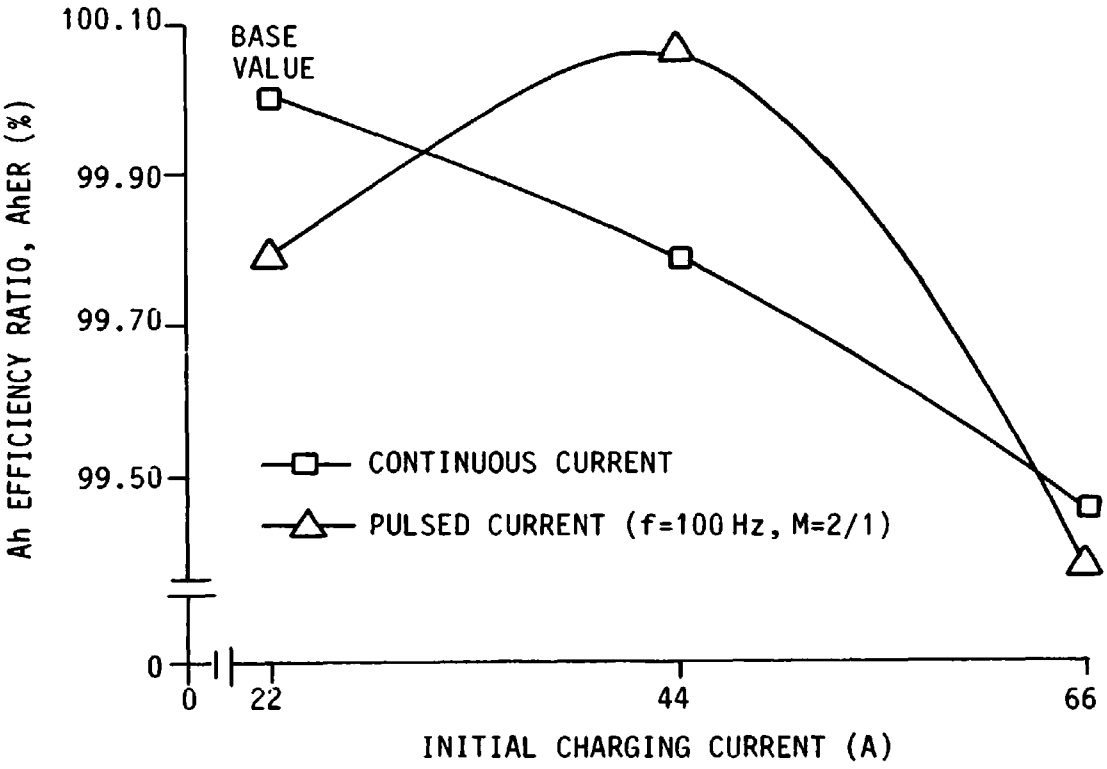

FIG. 47 VARIATION OF Ah EFFICIENCY RATIO WITH VARIOUS VALUES OF CHARGING CURRENT FOR CONTINUOUS AND PULSED CHARGING

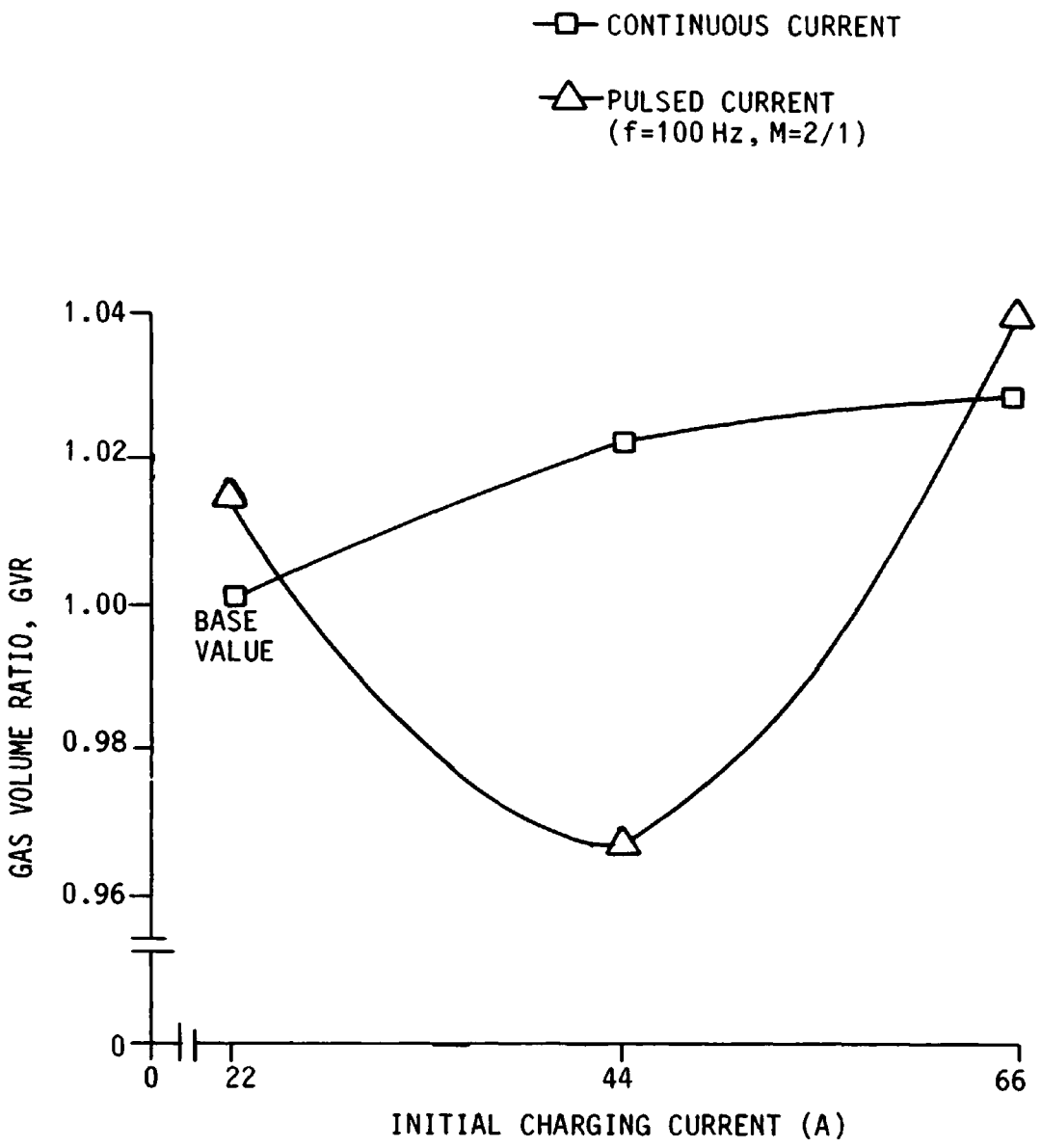

FIG. 48 VARIATION OF GAS VOLUME RATIO WITH VARIOUS VALUES OF CHARGING CURRENT FOR CONTINUOUS AND PULSED CHARGING

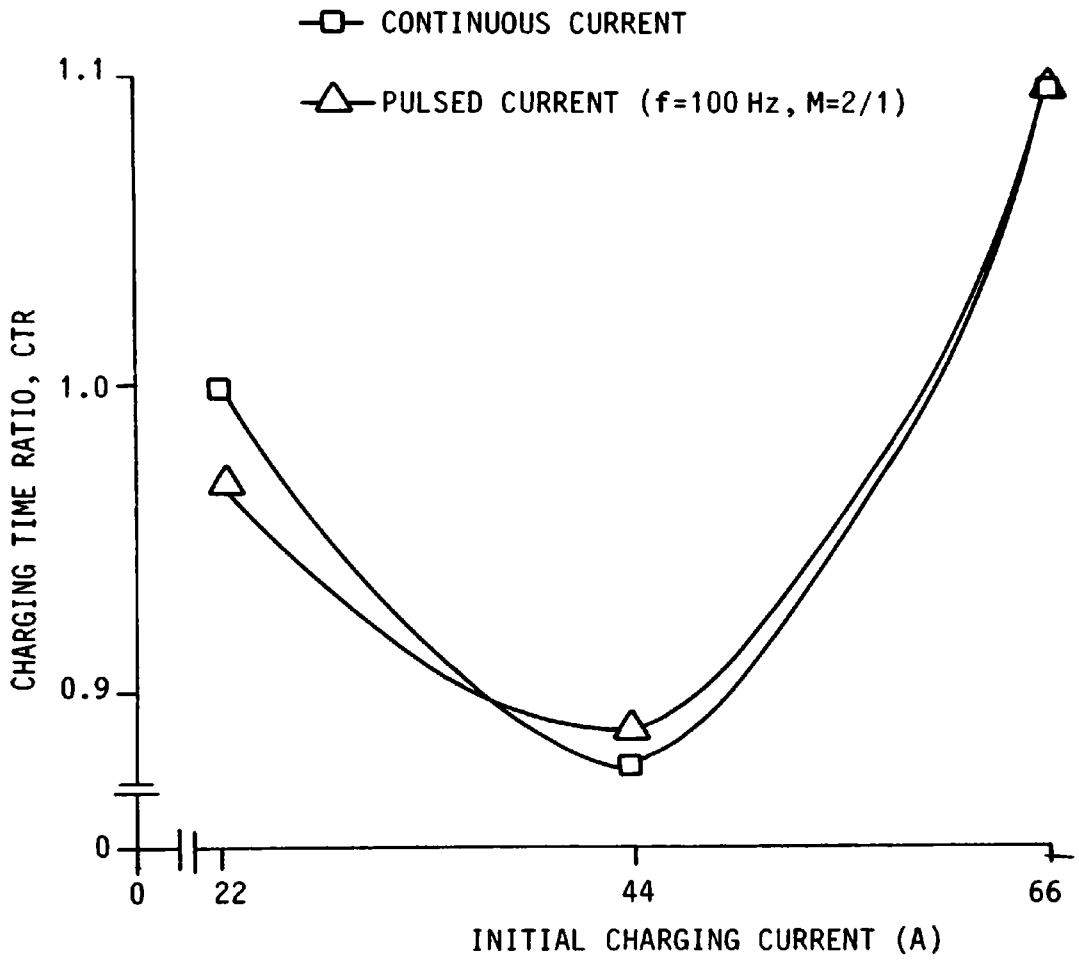

FIG. 49 VARIATION OF CHARGING TIME RATIO WITH VARIOUS VALUES OF CHARGING CURRENT FOR CONTINUOUS AND PULSED CHARGING

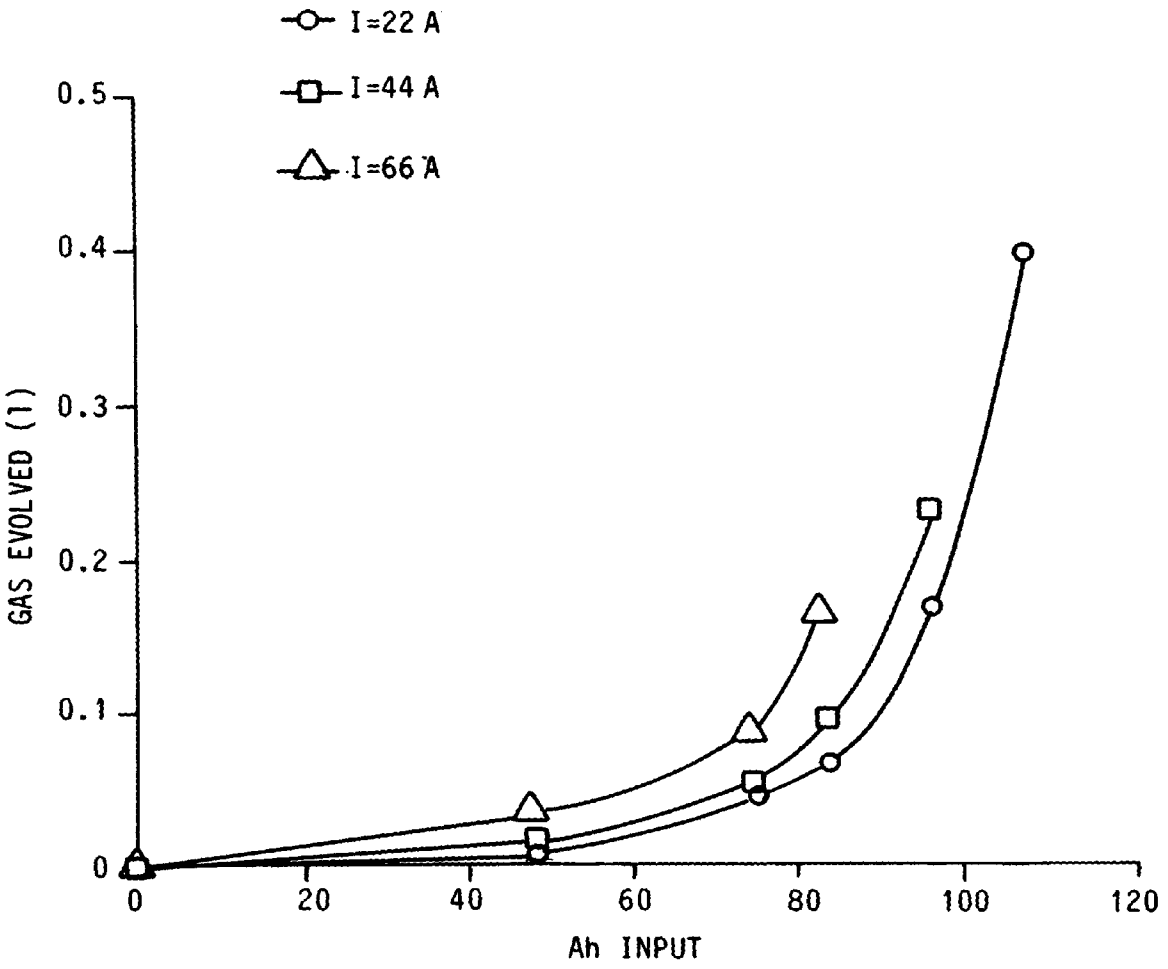

FIG. 50 VARIATION OF VOLUME OF GAS EVOLVED/CELL WITH Ah INPUT FOR VARIOUS VALUES OF FIRST STAGE CONTINUOUS CHARGING CURRENT

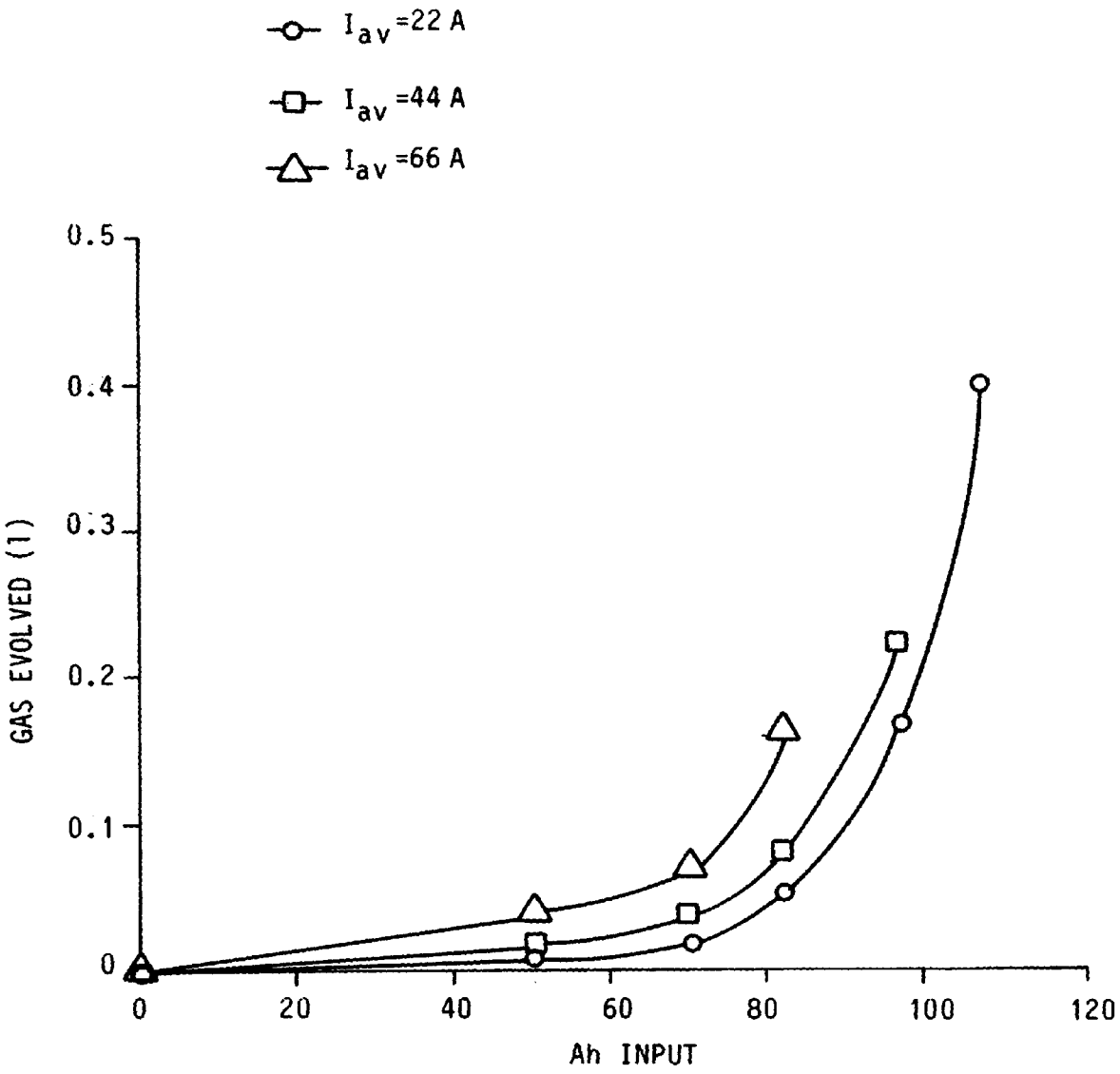

FIG. 51 VARIATION OF VOLUME OF GAS EVOLVED/CELL WITH Ah INPUT FOR VARIOUS VALUES OF FIRST STAGE PULSED CHARGING CURRENT

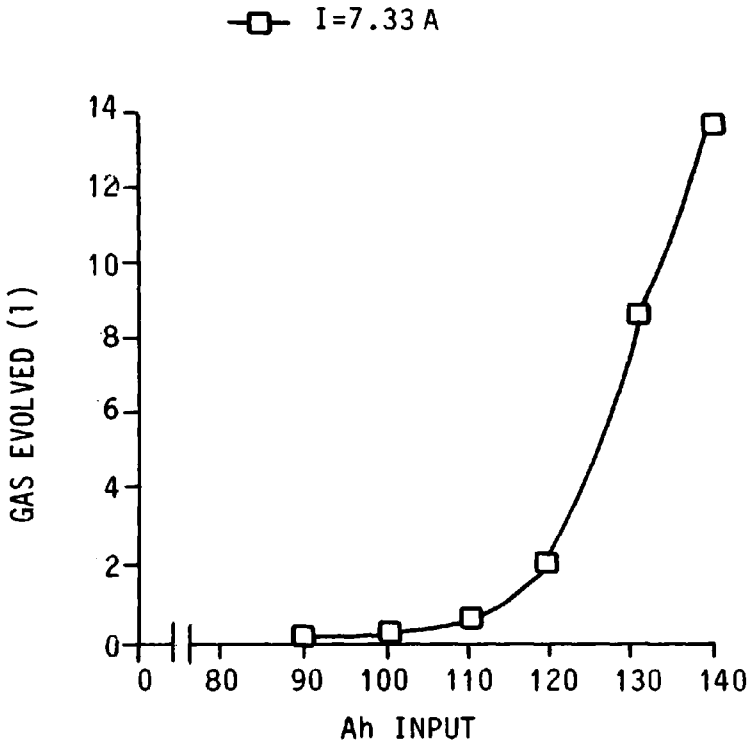

FIG. 52 VARIATION OF VOLUME OF GAS EVOLVED/CELL WITH Ah INPUT FOR THE SECOND STAGE OF CHARGING

increase in terminal voltage until just prior to 2.40 V, where the rate-of-change of voltage increases. At this stage some of the charge is now being used in dissociating the water of the sulphuric acid solution into hydrogen and oxygen, and so there is a marked increase in the gas evolution rate (Fig. 50).

During the second stage of charging (Fig. 53) an abrupt rise in terminal voltage is observed. This is partly due to the increasing concentration of the acid within the pores of the plate. The increase cannot be accounted for by an increase in the internal resistance of the cell, since it has been established (Fig. 45) that the internal resistance decreases with increasing state-of-charge. At this time of voltage increase however, most of the sulphate ions that are readily available for reaction have been utilised, and the concentration of lead ions in the electrolyte has diminished. The relationship between the potentials of the plates and the ionic concentrations in the electrolyte is defined by the Nernst equation [68] which may be expressed as:

$$E = E_+ - E_- = 1.87 + 0.029 . \log \frac{Pb^{4+}}{Pb^{2+}} \qquad (17)$$

where: E_+ and E_- = the potentials of the positive and negative plates respectively.

The equation shows that as the number of divalent lead ions diminishes, the voltage of the cell increases. Therefore, when the $PbSO_4$ on the plates becomes exhausted and the $PbSO_4$ ions in the electrolyte are diminished, the potential of the plate rises. By comparing Figs. 52 and 53 it may be seen that during this period of sharply rising potential, the rate of cell gas evolution increases considerably. As in the first stage of charging, this increase in gas evolution rate occurs within a voltage range of 2.30 - 2.40 V. Consideration of Fig.

55 shows that the rise in cell voltage and increase in gas evolution rate is accompanied by an increase in the temperature of the cell electrolyte.

The variation of cell voltage and cell electrolyte temperature during pulsed charging are shown in Figs. 54 and 56 respectively. Comparing the corresponding results in Figs. 55 and 56 for continuous and pulsed charging respectively, it may be seen that at any instant in time during the charging period, the increase in electrolyte temperature is greater for the pulsed than for the continuous current mode of charging. The relative increase may be attributed to an increase in the rms value of the current under pulsed conditions (Appendix 2), resulting in increased i^2r losses within the cell. As the charging rate is reduced for the second stage of charging, the temperature of the electrolyte gradually drops until, when the cell begins to gas more freely, the temperature of the electrolyte increases. By considering the mean value of the pulsed voltage waveform, Figs. 53 and 54 show that for pulsed and continuous current charging the corresponding cell voltage v ampere-hour characteristics are virtually identical. Therefore, the above comments concerning the interdependence of cell voltage, electrolyte temperature, and gas evolution for continuous current charging are equally applicable for the pulsed charging mode.

From the foregoing observations it may also be deduced for a cell on charge, that the point at which gassing commences is primarily dependent on the value of cell voltage. Further, by comparing Fig. 53 with Figs. 50 and 52 it may also be deduced that the rate of gas evolution is dependent on both the state-of-charge and voltage of the cell.

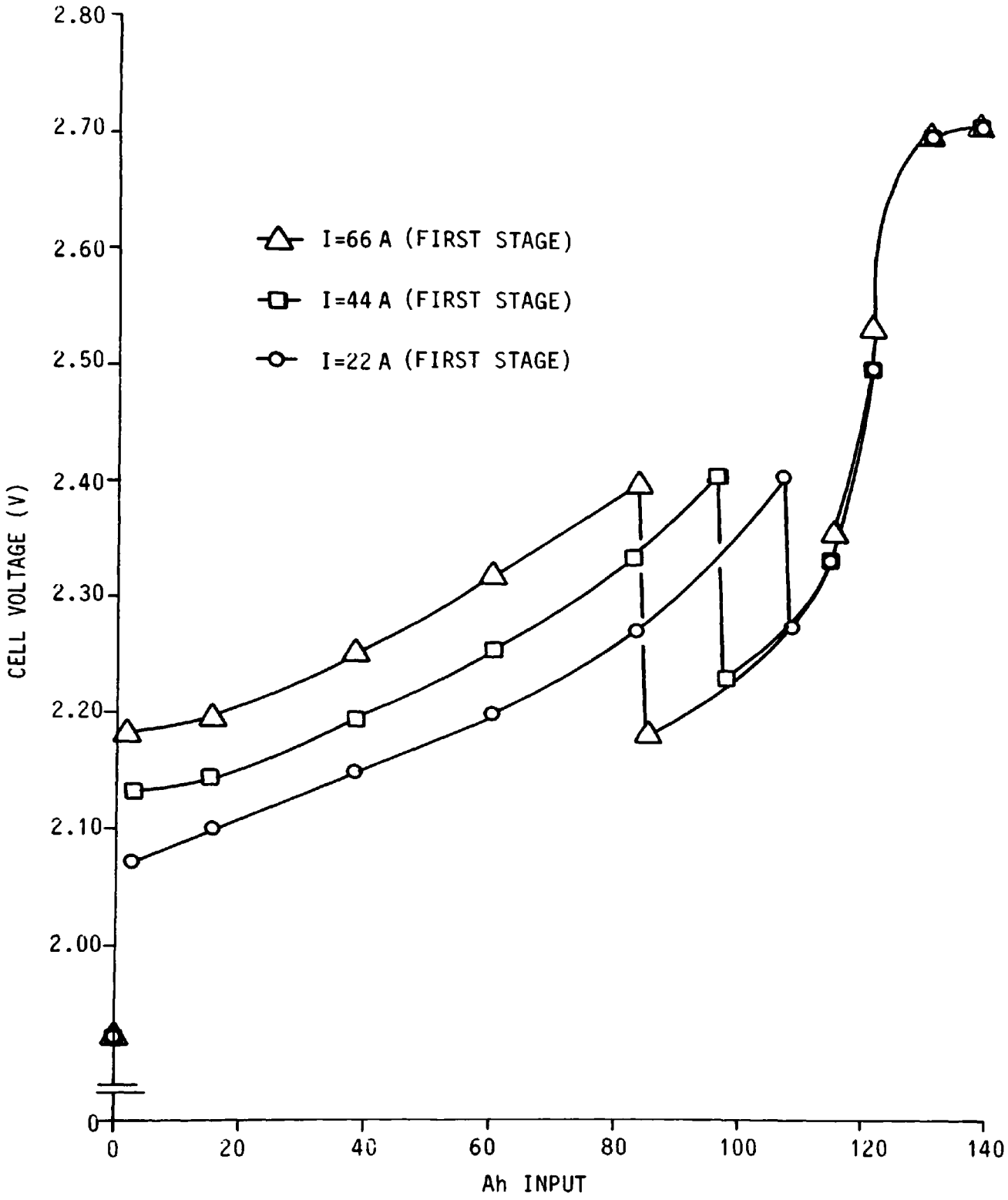

FIG. 53 VARIATION OF CELL VOLTAGE WITH Ah INPUT FOR VARIOUS VALUES OF CONTINUOUS CHARGING CURRENT

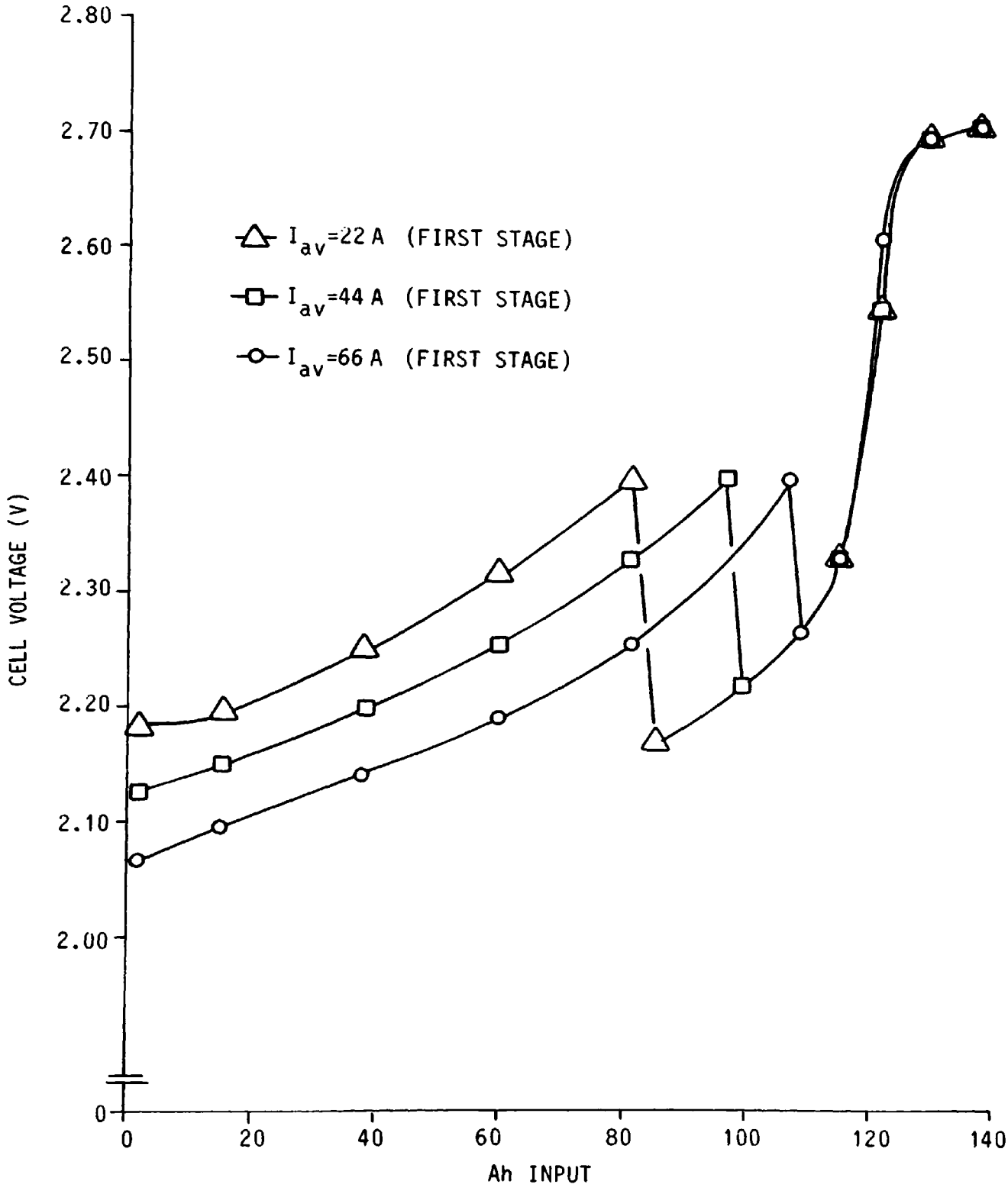

FIG. 54 VARIATION OF CELL VOLTAGE WITH Ah INPUT FOR VARIOUS VALUES OF PULSED CHARGING CURRENT

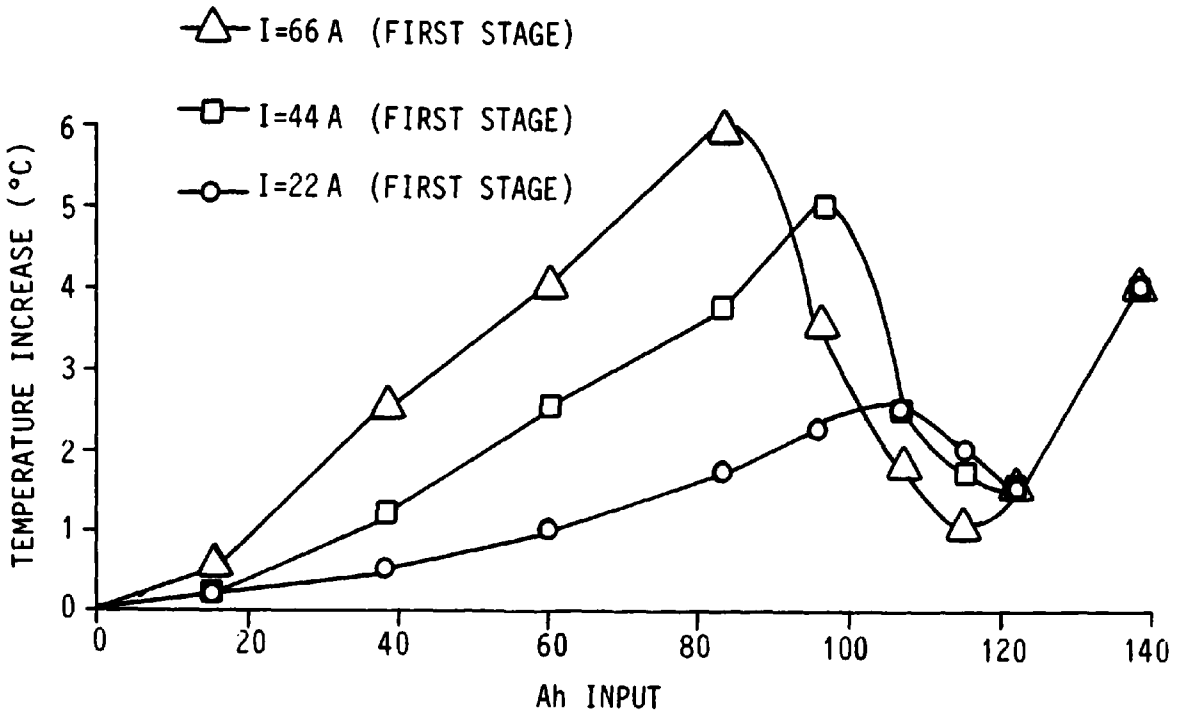

FIG. 55 VARIATION OF TEMPERATURE INCREASE WITH Ah INPUT FOR VARIOUS VALUES OF CONTINUOUS CHARGING CURRENT

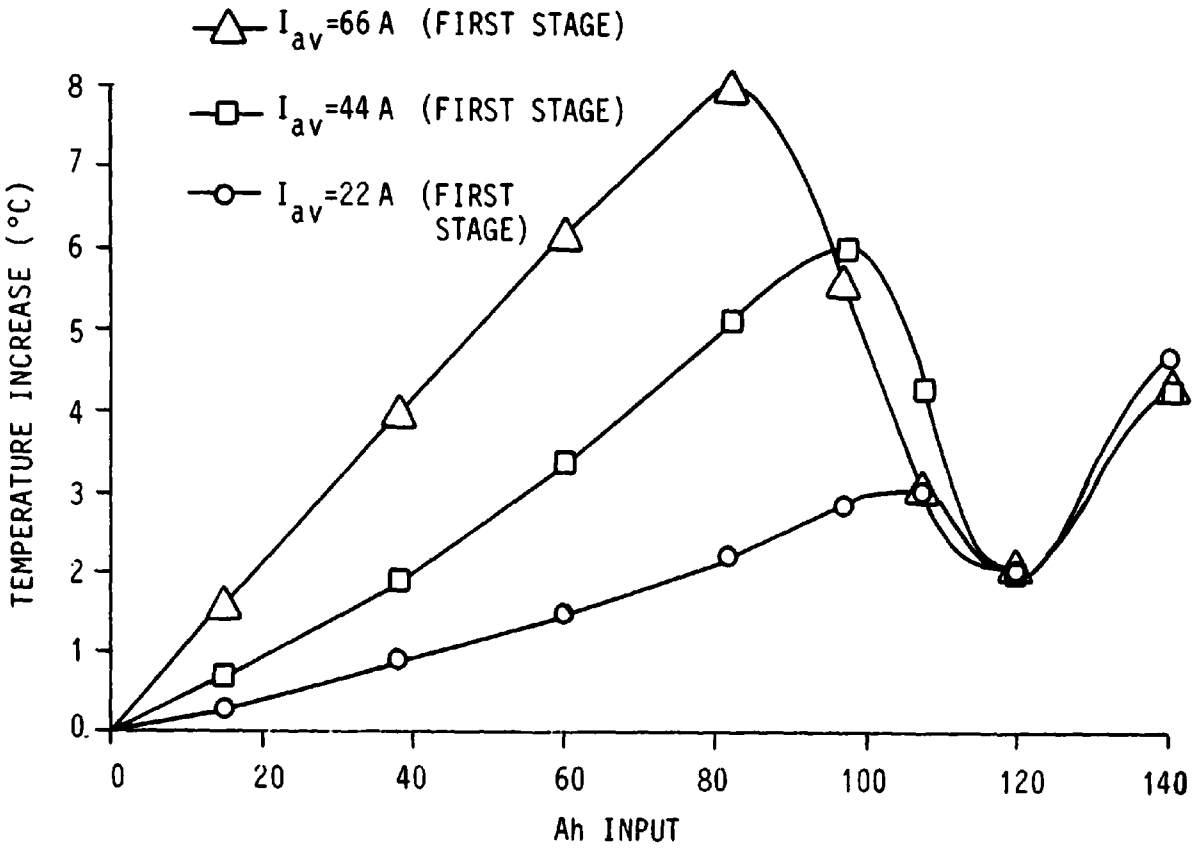

FIG. 56 VARIATION OF TEMPERATURE INCREASE WITH Ah INPUT FOR VARIOUS VALUES OF PULSED CHARGING CURRENT

5.9.2 Comments on Asymmetric Charging Results

Figs. 57 and 58 show the variation of the volume of gas evolved with ampere-hour input for the first stage of charging, for various values of CD_r, at an average charging current of 44 A and at frequencies of 12 Hz and 100 Hz respectively. From the graphs it may be seen that for the various charging conditions considered, the general characteristic of the two sets of graphs is the same, and may be considered to be of an exponential form. It may be seen that for any value of ampere-hour input, the volume of gas evolved is less for the asymmetric than for the continuous current charging mode. The asymmetric charging results indicate that for charging frequencies of 12 Hz and 100 Hz, an optimum value of CD_r exists between the values of 3.5/1 and 9.5/1.

The variation of the volume of gas evolved with ampere-hour input for the second stage of charging is shown in Figs. 59 and 60. It may be seen that the general form of the two sets of graphs is the same, as for the first stage of charging. For the particular tests considered, the results show that for a given ampere-hour input, asymmetric charging produces a reduction in the volume of gas evolved when compared to equivalent continuous current charging; the comparative reduction is more pronounced at the 100 Hz than at the 12 Hz frequency charge. For an asymmetric charging frequency of 12 Hz, a variation in CD_r produces no significant change in the gas volume v ampere-hour characteristic, however, at a frequency of 100 Hz, an increase in CD_r results in a decrease in the volume of gas evolved. It may be seen that when the values of average charging current and CD_r were maintained constant, an increase in the frequency of the charging waveform produced a decrease in the volume of gas evolved. In Figs. 59 and 60 it may be seen that at an input of approximately 110

ampere-hours, the rate of gas evolution increased considerably, after which, the evolution rate remained virtually constant until the end of charge. This characteristic is similar to that obtained when pulsed charging the cell, and is discussed in Section 5.9.1.

Figs. 61 and 62 show the results obtained for the total volume of gas evolved from the cell when asymmetrically charging with various values of I_{dp}, at mean current, frequency, and CD_r values of 44 A, 100 Hz, and 6/1 respectively. Fig. 61 shows the volume of gas evolved v ampere-hour input characteristic for the first stage of charging, whereas Fig. 62 shows the characteristic for the second stage of the charge. The figures show that for a given ampere-hour input, increasing the value of I_{dp} results in a reduction in the volume of gas evolved.

From Figs. 63 and 64 which show the variation of the AhER and the GVR respectively for various asymmetric charging values of CD_r, I_{dp}, and frequency, it may be seen that for a constant charging frequency of 12 Hz or 100 Hz, the AhER was increased, as a result of an increase in the value of CD_r; also, as the frequency of the charging waveform was increased with CD_r constant, the AhER increased. From Fig. 64 it may be seen that when CD_r and I_{dp} are maintained constant, the GVR was reduced as the charging frequency was increased from 12 Hz to 100 Hz. At a constant charging frequency of 100 Hz, a reduction in the GVR was observed as CD_r was increased, whereas for a frequency of 12 Hz, the GVR remained unchanged as CD_r increased. Fig. 63 shows that when the frequency and CD_r were maintained constant at 100 Hz and 6/1 respectively, an increase in I_{dp} produced an increase in the AhER; the increase in I_{dp} was also accompanied by a decrease in the GVR (Fig. 64).

Figs. 65-68 show a strong similarity with the results obtained

from the equivalent pulsed charging tests. The comments concerning the interdependence of cell voltage, electrolyte temperature, and gassing for the pulsed charge tests, and their comparison with those obtained from continuous current charging, are therefore equally applicable for the corresponding tests in the asymmetric charging mode.

The variation of electrolyte temperature increase with ampere-hour input for various asymmetric charging conditions is shown in Figs. 65 and 66. The graphs show that at any value of ampere-hour input, asymmetric charging produced a larger increase in electrolyte temperature than continuous current charging. For a charging waveform having a constant value of I_{dp} (88 A) and a constant frequency of 12 Hz or 100 Hz, the graphs show that when CD_r was reduced from 9.5/1 to 3.5/1, the temperature of the electrolyte was increased throughout the charging period. At a constant CD_r value and charging frequency of 6/1 and 100 Hz respectively, the electrolyte temperature throughout the charging period increased when I_{dp} increased.

Figs. 67 and 68 show the variation of the cell terminal voltage with ampere-hour input for various values of CD_r, with a constant I_{dp} value of 88 A, at charging frequencies of 100 Hz and 12 Hz respectively. It is evident from both figures that at any value of ampere-hour input, the mean value of cell terminal voltage is less for asymmetric than for equivalent continuous current charging. This reduction in terminal voltage may be partly attributed to the comparative reduction in the volume of gas evolved by the cell under asymmetric charging conditions.

The proposed [18 - 20] advantage to be gained by the use of asymmetric charging as opposed to using conventional charging techniques is the increase in the charge acceptance of the cell plates, causing a reduction in gas evolution, heat generation, and charging

time. Figs. 57 - 62 confirm that for the particular tests performed, asymmetric charging does produce a reduction in the volume of gas evolved when compared to equivalent continuous current charging, however, it should be noted that the reduction is not significant. An appreciation of how the charge acceptance characteristic of the cell varies for asymmetric and continuous current charging may be obtained by determining the gradients of the gas volume v ampere-hour input curves of Figs 57 - 62. It may be seen that whether the cell is experiencing a constant current or asymmetric charge, there is no significant variation in the gradient of these curves for the two modes of charging. This observation is supported by Fig. 63 which shows that for the asymmetric tests performed, there is an approximate increase in the AhER of only 2.5% when compared to the equivalent continuous current charging result.

For the tests performed, the results of Figs. 65 and 66 clearly show that when compared to continuous current charging, asymmetric charging does not produce a decrease in cell electrolyte temperature. In fact, for certain asymmetric charging conditions, the cell temperature increase can be up to 100% greater than the temperature increase produced by the equivalent continuous current charge. For a cell on charge, one possible source of heat production is electrochemical polarisation [45]. However, since the total volume of gas evolved at any ampere-hour input value is less for asymmetric than for the equivalent continuous current charge then it may be deduced that electrochemical polarisation is not a contributory factor to the considerable increase in electrolyte temperature experienced under asymmetric charging conditions. Probably, the main factor is an increase in the rms value of current under asymmetric charging conditions (see equation (16)) resulting in increased i^2r losses within

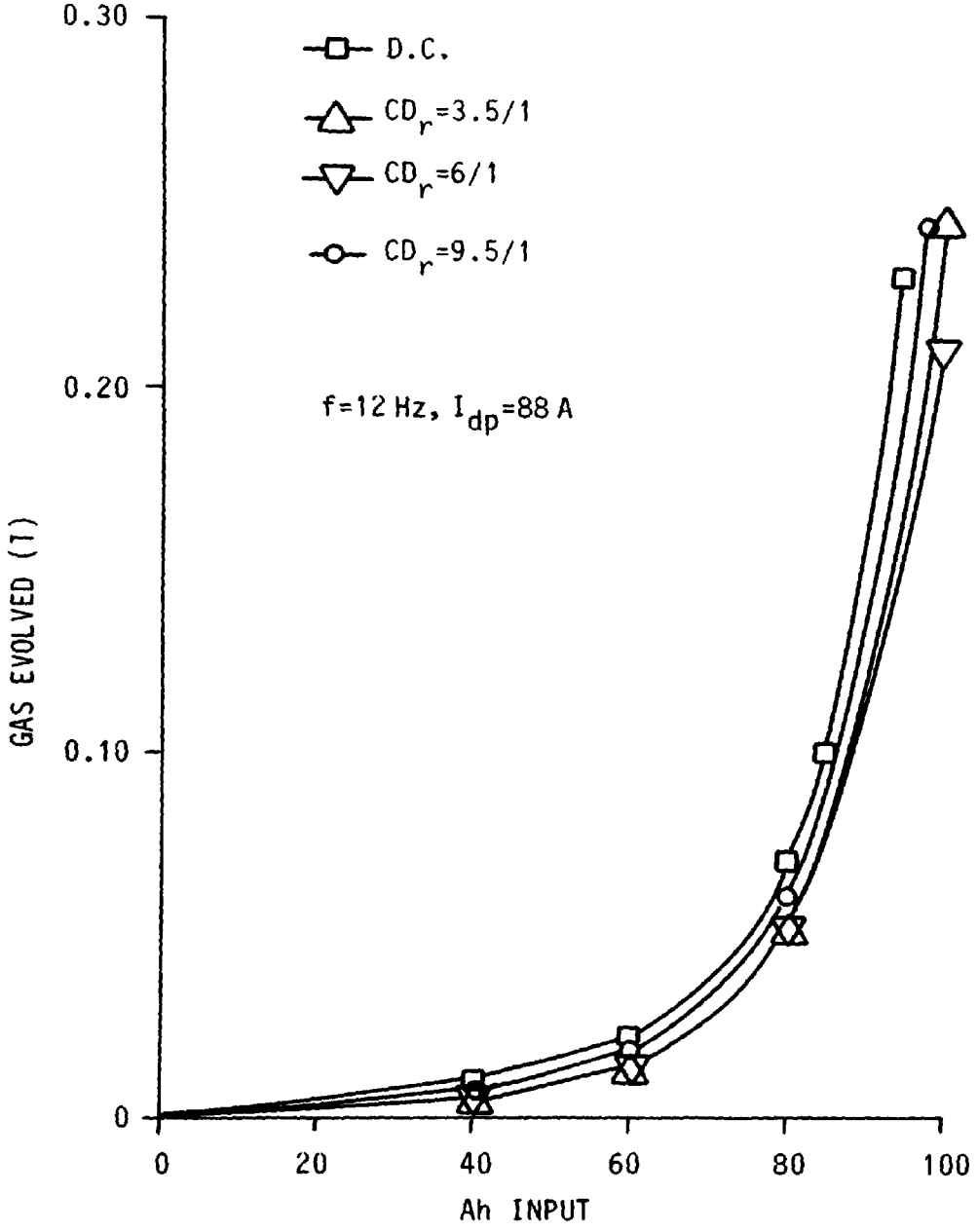

FIG. 57 VARIATION OF VOLUME OF GAS EVOLVED/CELL WITH Ah INPUT FOR VARIOUS VALUES OF CHARGE-DISCHARGE RATIO FOR THE FIRST STAGE OF CHARGING

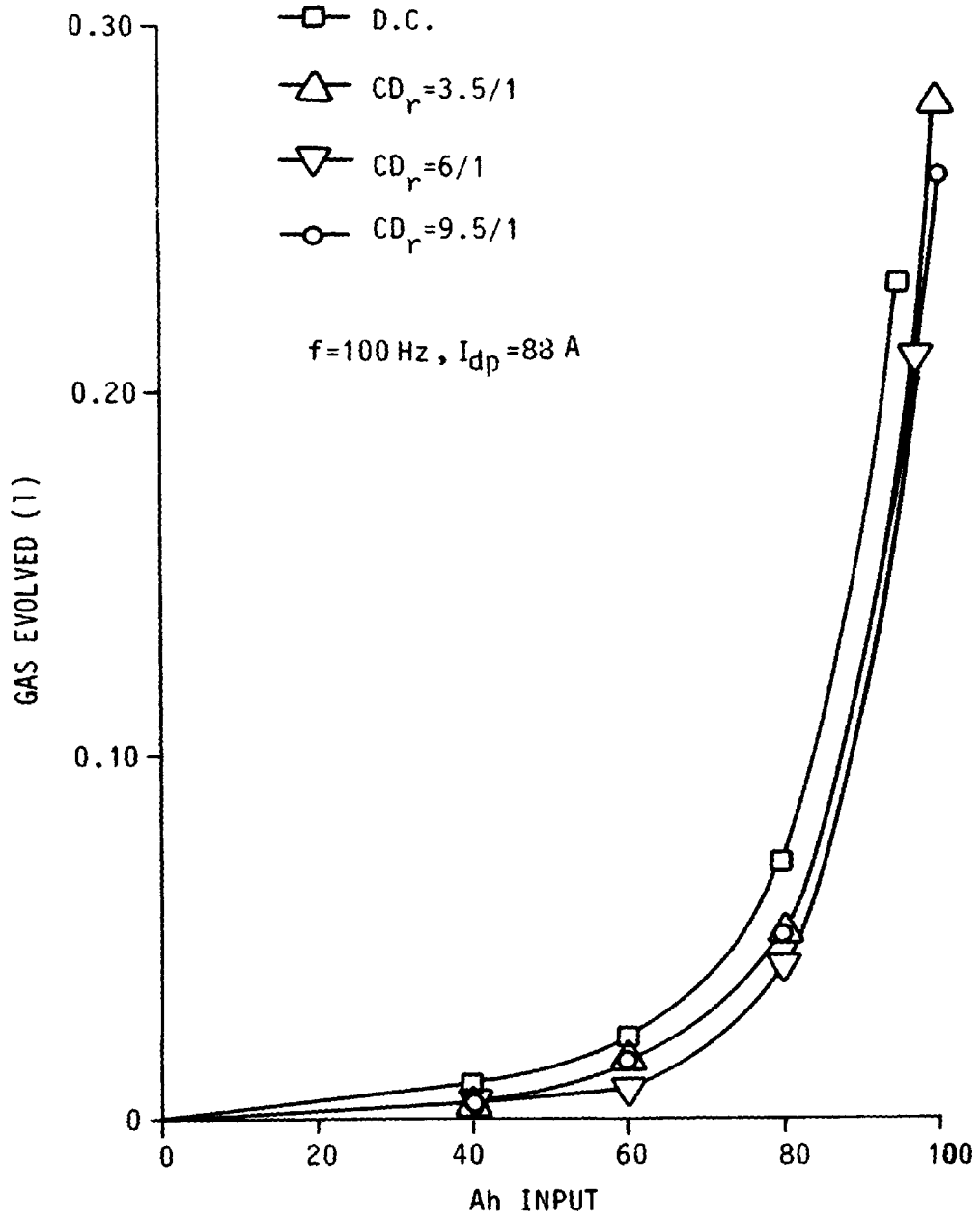

FIG. 58 VARIATION OF VOLUME OF GAS EVOLVED/CELL WITH Ah INPUT FOR VARIOUS VALUES OF CHARGE-DISCHARGE RATIO FOR THE FIRST STAGE OF CHARGING

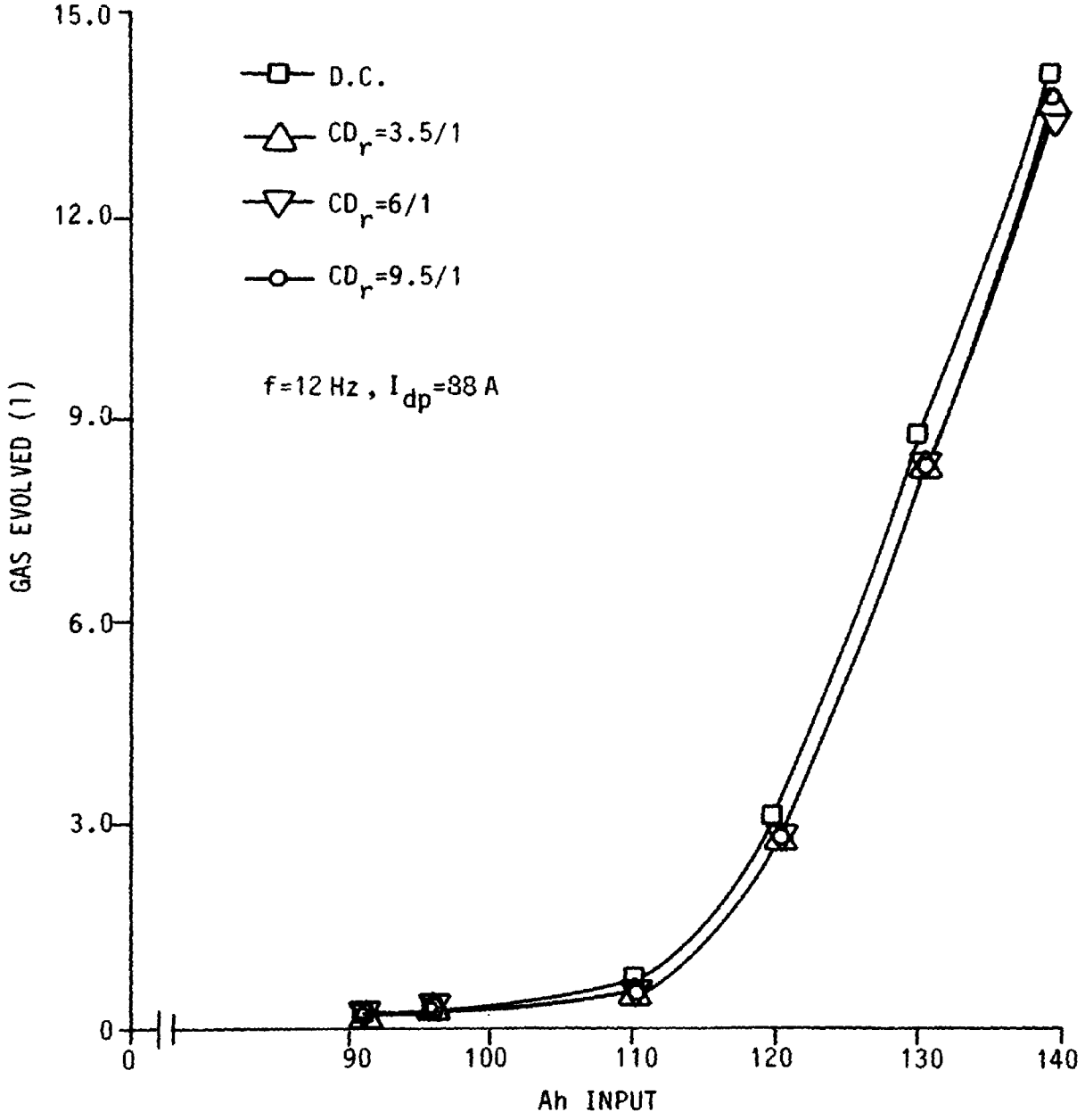

FIG. 59 VARIATION OF VOLUME OF GAS EVOLVED/CELL WITH Ah INPUT FOR VARIOUS VALUES OF CHARGE-DISCHARGE RATIO FOR THE SECOND STAGE OF CHARGING

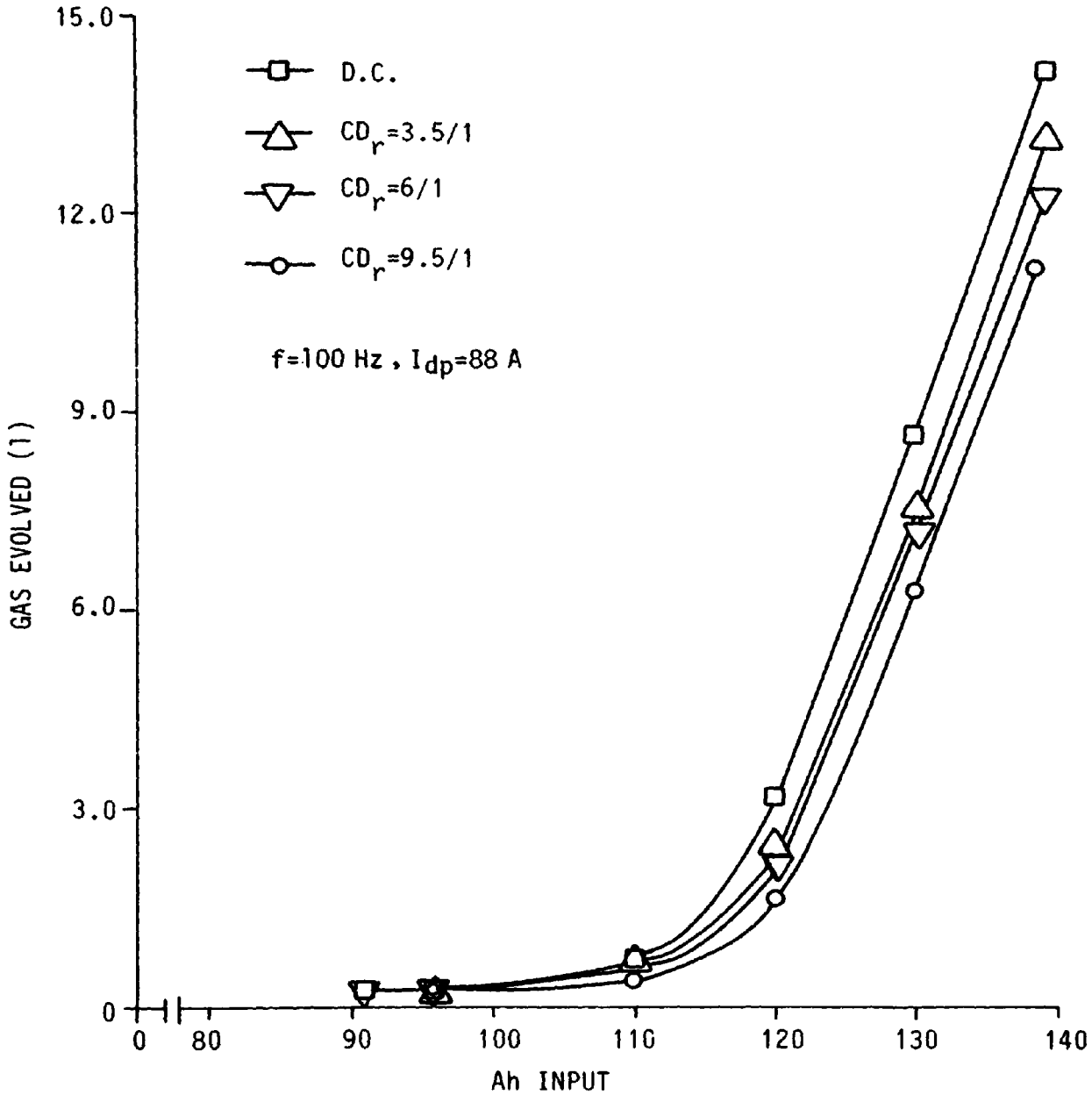

FIG. 60 VARIATION OF VOLUME OF GAS EVOLVED/CELL WITH Ah INPUT FOR VARIOUS VALUES OF CHARGE-DISCHARGE RATIO FOR THE SECOND STAGE OF CHARGING

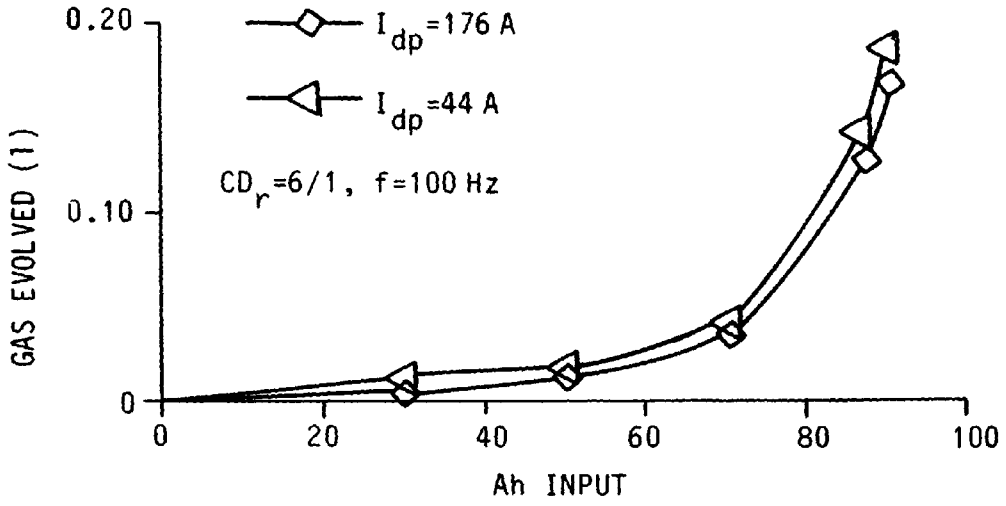

FIG. 61 VARIATION OF VOLUME OF GAS EVOLVED/CELL WITH Ah INPUT FOR VARIOUS VALUES OF DE-POLARISATION CURRENT FOR THE FIRST STAGE OF CHARGING

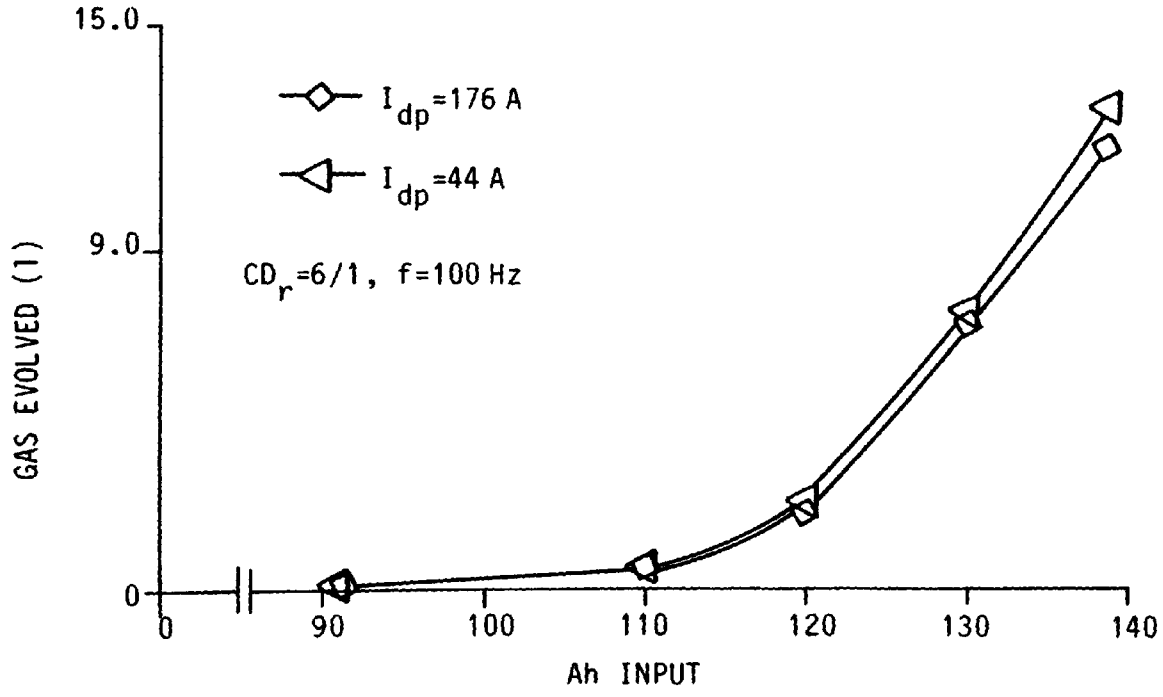

FIG. 62 VARIATION OF VOLUME OF GAS EVOLVED/CELL WITH Ah INPUT FOR VARIOUS VALUES OF DEPOLARISATION CURRENT FOR THE SECOND STAGE OF CHARGING

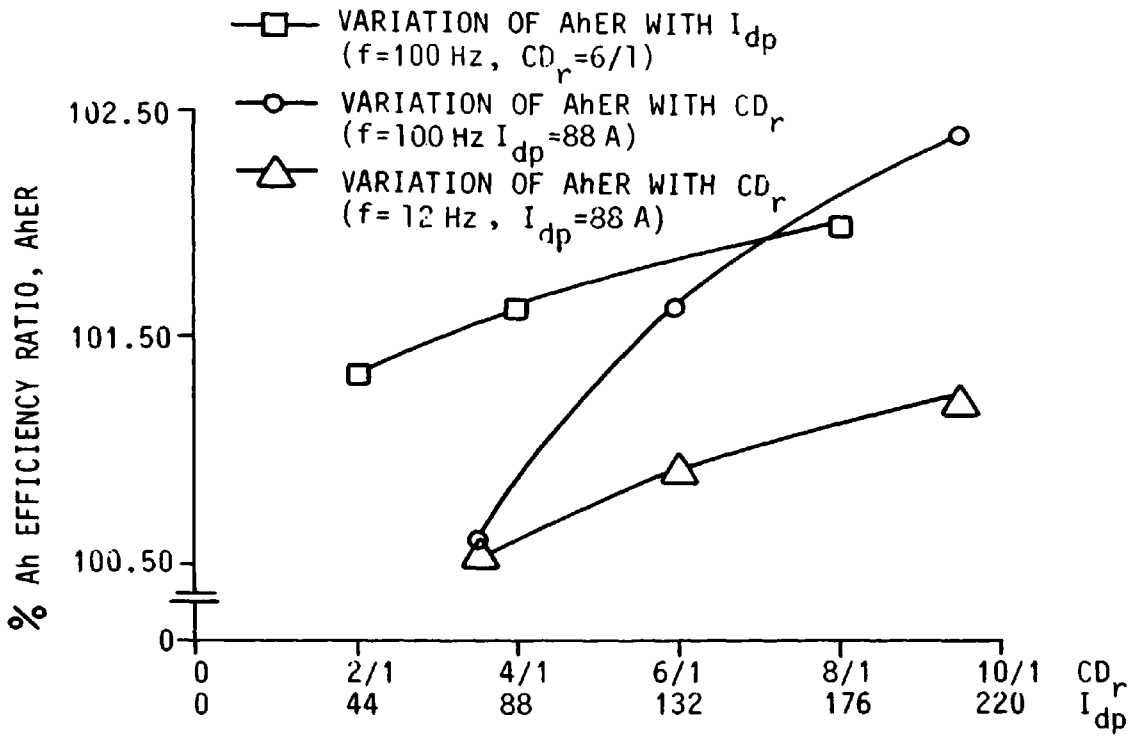

FIG. 63 VARIATION OF AhER WITH VARIOUS VALUES OF CHARGE-DISCHARGE RATIO AND DEPOLARISATION DISCHARGE CURRENT

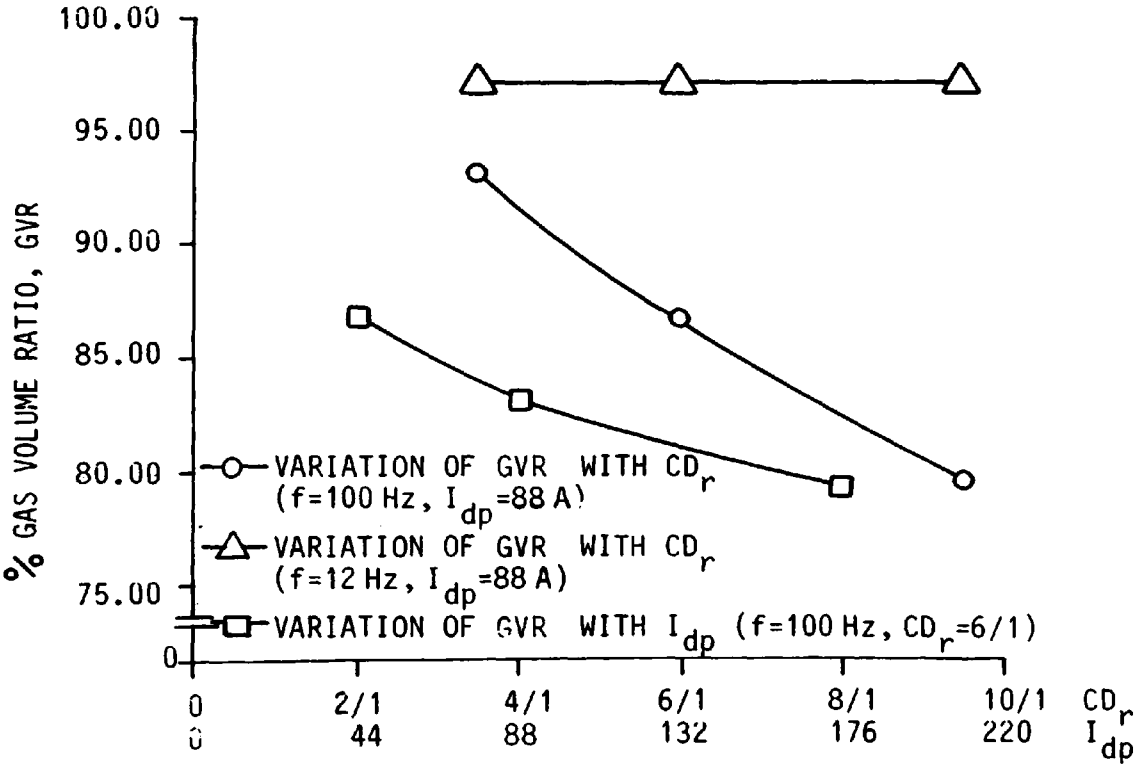

FIG. 64 VARIATION OF GAS VOLUME RATIO WITH VARIOUS VALUES OF CHARGE-DISCHARGE RATIO AND DEPOLARISATION CURRENT

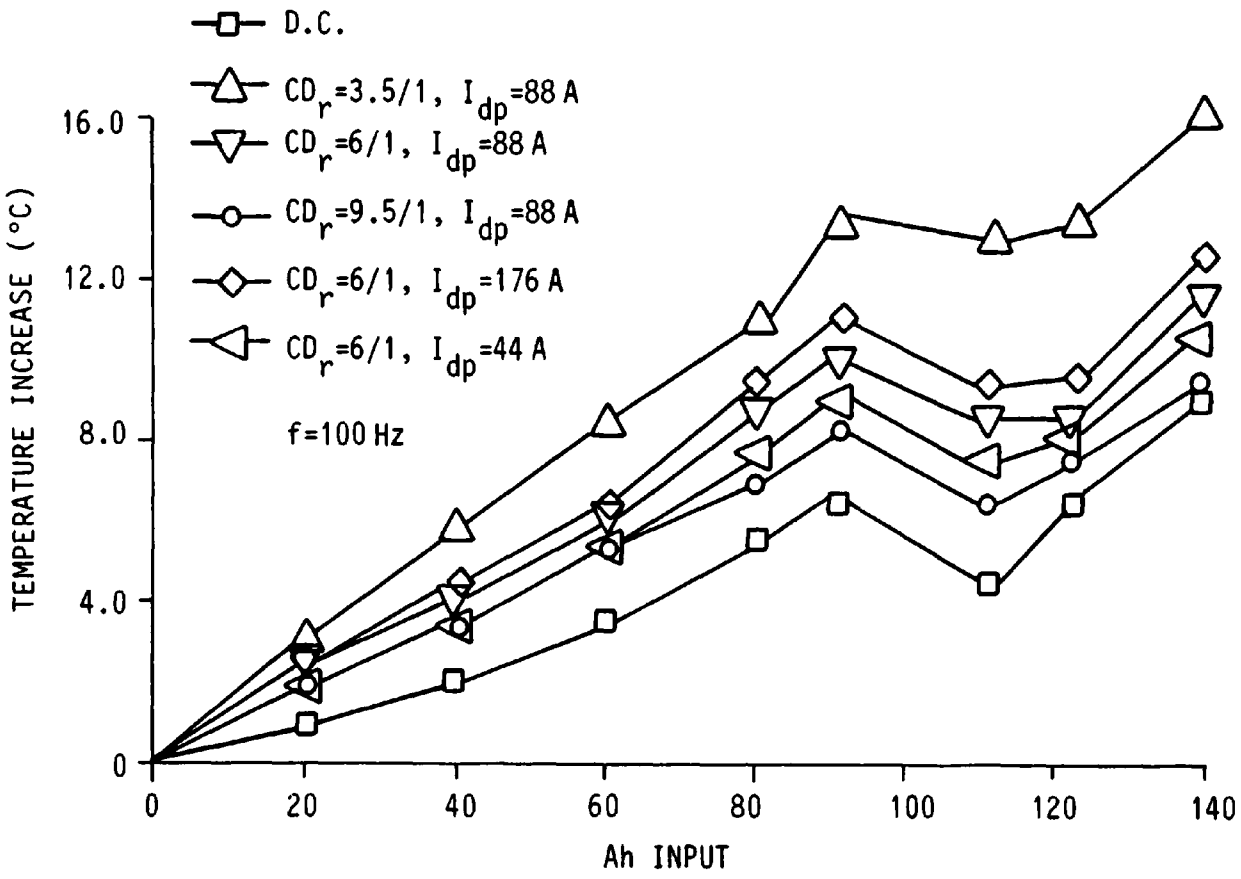

FIG. 65 VARIATION OF TEMPERATURE INCREASE WITH Ah INPUT FOR VARIOUS VALUES OF CHARGE-DISCHARGE RATIO AND DEPOLARISATION CURRENT

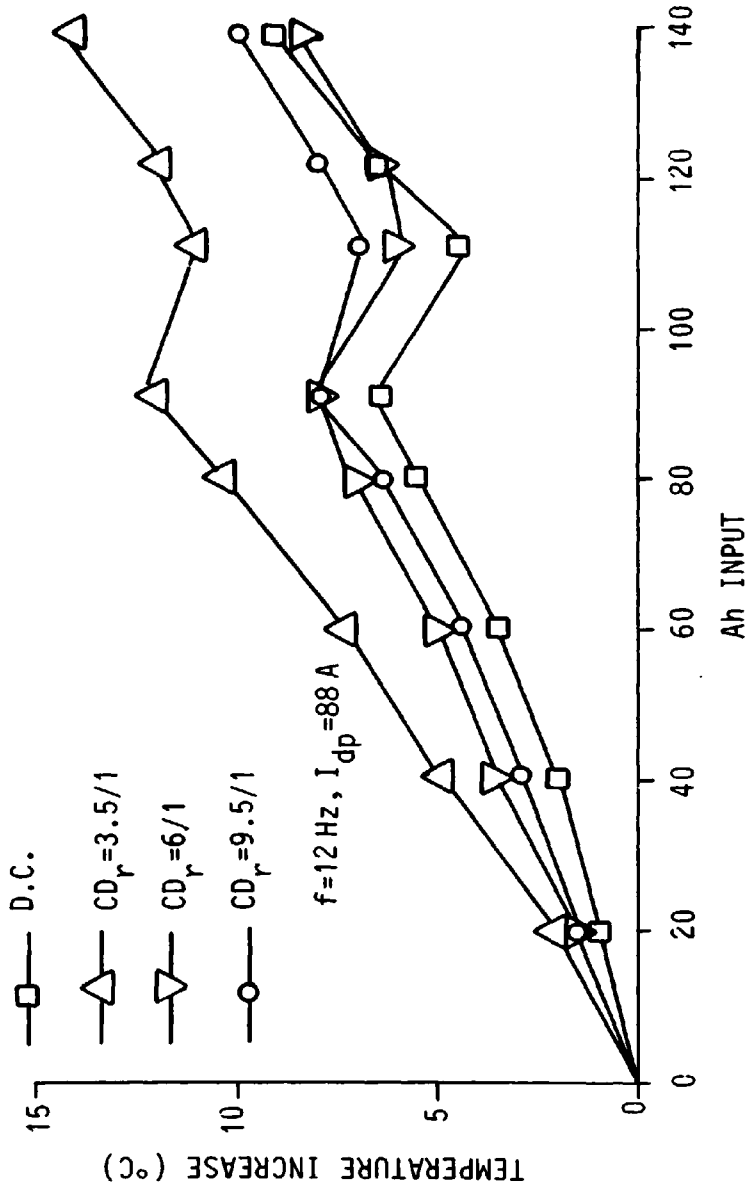

FIG. 66 VARIATION OF TEMPERATURE INCREASE WITH Ah INPUT FOR VARIOUS VALUES OF CHARGE-DISCHARGE RATIO

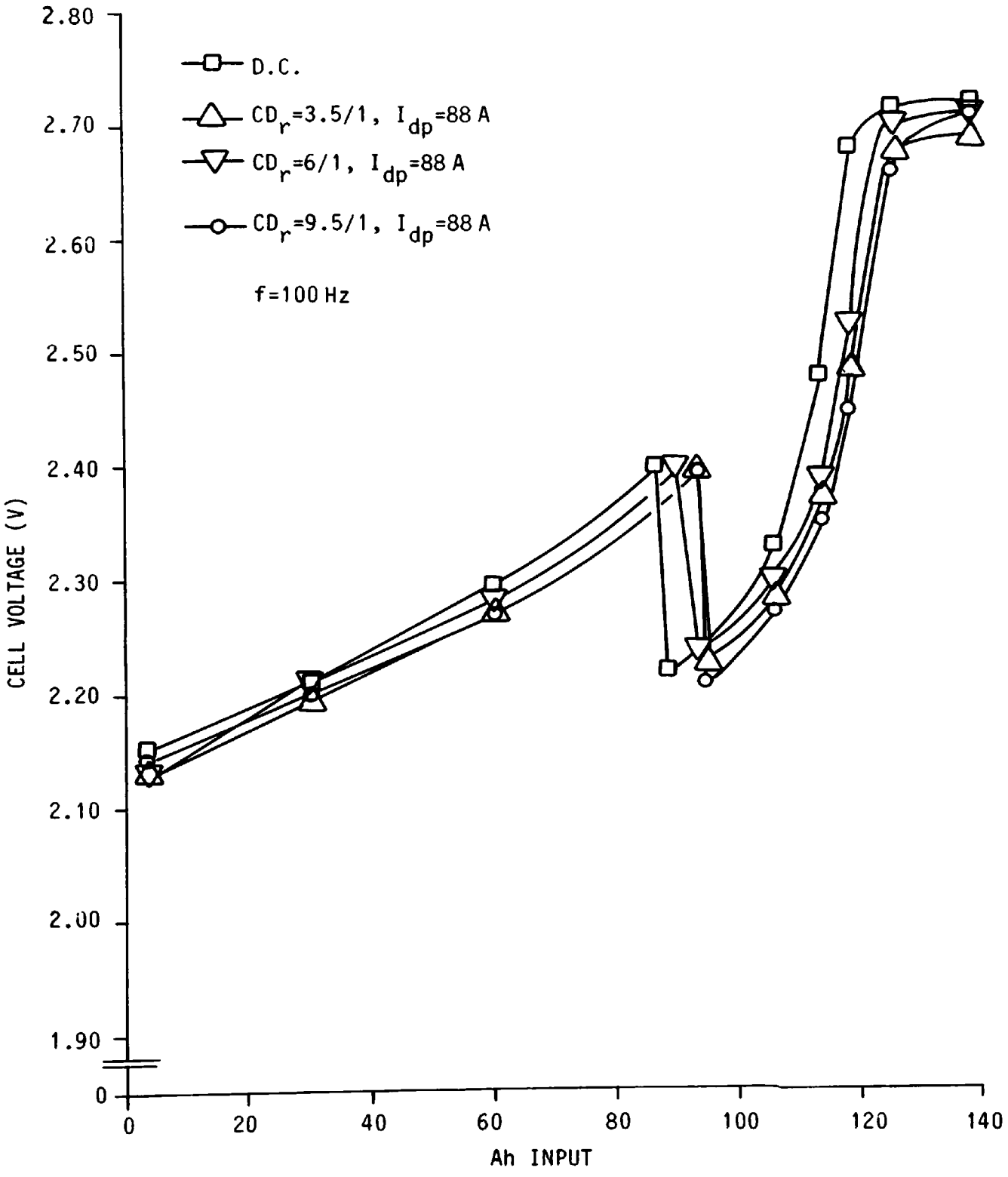

FIG. 67 VARIATION OF CELL VOLTAGE WITH Ah INPUT FOR VARIOUS VALUES OF CHARGE-DISCHARGE RATIO

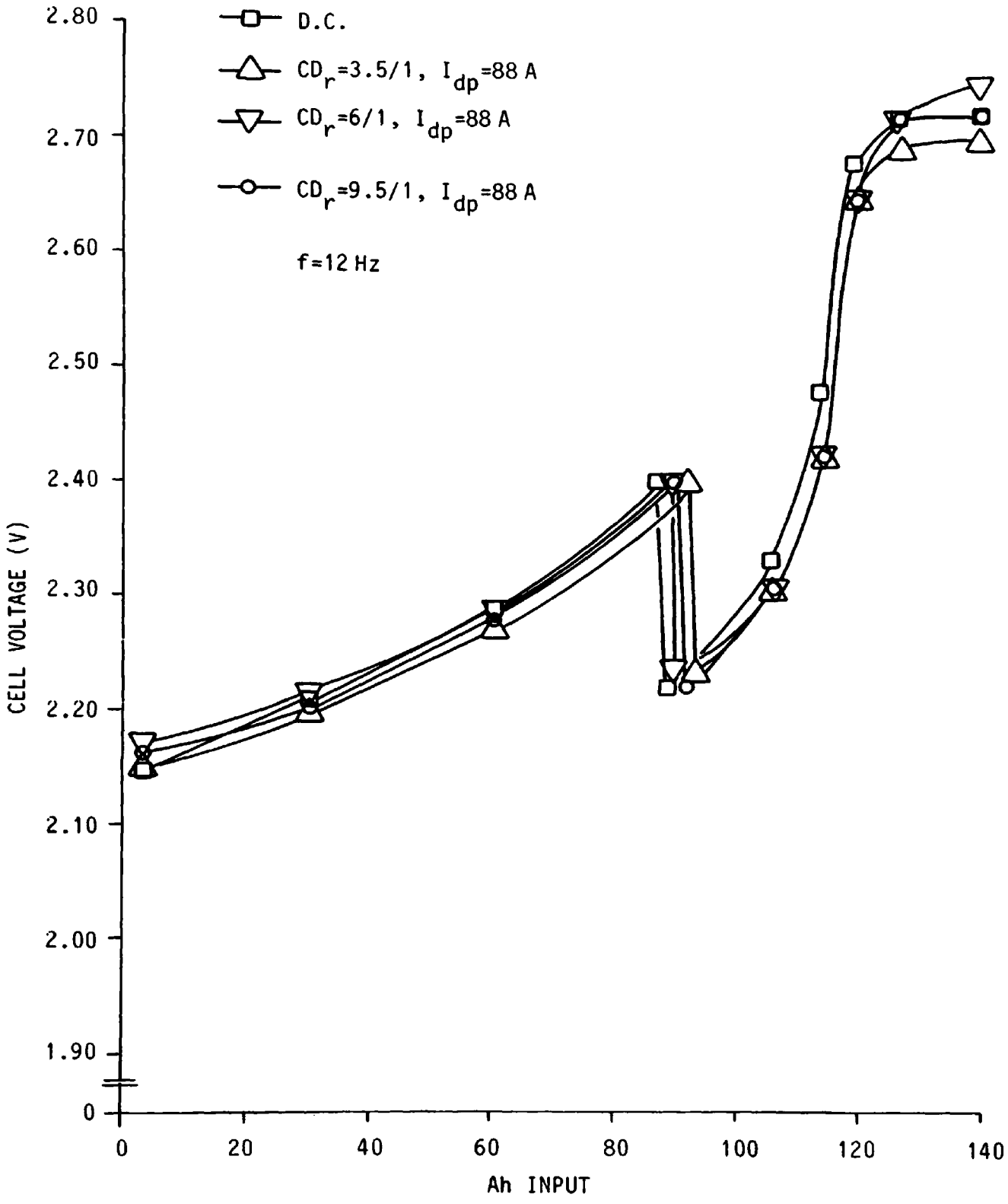

FIG. 68 VARIATION OF CELL VOLTAGE WITH Ah INPUT FOR VARIOUS VALUES OF CHARGE-DISCHARGE RATIO

the cell. Any variations in the electrolyte temperature between the various asymmetric charging results may likewise be attributed to variations in the rms value of the charging waveforms. For example, in Figs. 65 and 66, when the values of charging frequency, I_{dp}, and mean current (44 A) are maintained constant, the increase in electrolyte temperature as CD_r is successively reduced from 9.5/1 to 6/1 to 3.5/1 may be attributed to an increase in the rms value of the charging waveform, resulting in increased i^2r losses.

Since the volume of gas evolved v ampere-hour input characteristics for the equivalent asymmetric and continuous current tests are not significantly different, then the cell mean terminal voltage v ampere-hour input characteristics for the equivalent charging tests should demonstrate good correlation. However, as may be seen from Figs. 67 and 68, considerable differences in terminal voltage exist especially during the second stage of charging. These differences are probably due to the considerable differences in cell temperature as is evident from Figs. 65 and 66.

Comparing the relative effects of asymmetric and pulsed charging on the charging behaviour of the cells, the general observations are that asymmetric charging produces: (1) a greater increase in electrolyte temperature; (2) a small reduction in the total volume of gas evolved; and (3) no significant reduction in charging time or increase in charge ampere-hour efficiency.

5.10 Interim Conclusions

(1) From the frequency and mark/space ratio values considered in the three-stage pulsed charging tests, it may be concluded that pulsed current charging offers no advantages over continuous current charging. In fact, when compared to continuous current charging,

pulsed charging has the disadvantage of increasing both the volume of gas evolved and the cell electrolyte temperature, and of reducing the ampere-hour efficiency of charge.

(2) For single-stage charging of a lead-acid cell, pulsed current charging offers no advantages over continuous current charging, even though certain optimum values of mark/space ratio and frequency exist for the specified pulsed charging results.

(3) For two-stage charging of a lead-acid cell, pulsed current charging can offer slight advantages over continuous current charging for the particular test values considered.

(4) Asymmetric charging of a lead-acid cell offers no significant advantages over continuous current or pulsed current charging. In fact, when compared to continuous or pulsed charging, asymmetric charging has the disadvantage of considerably increasing the electrolyte temperature.

6. A MODEL FOR PREDICTING THE PERFORMANCE OF LEAD-ACID TRACTION CELLS

6.1 Introduction

Even though the lead-acid traction battery is one of the oldest devices used in electrical power systems, there are no universal techniques available for accurately describing its performance characteristics. This is partly due to the diversity in the types of lead-acid batteries, and the differences that exist even among the generic group of lead-acid traction batteries. It may also be due to the fact that there was little need to analytically describe battery performance until the recent renewed interest in EVs.

The fundamental problem in predicting battery state (state-of-charge and terminal voltage) is the dependence of the performance of the battery on a variety of factors: discharge rate, temperature, aging and history, etc. The effects of aging and history can only be accurately determined by performing an exhaustive series of tests. Other effects are virtually impossible to accurately quantify, for example, those due to: vibration resulting in shedding of active plate material; internal leakage; and the spread of performance between individual cells in a battery pack, and between batteries of similar age and duty. The determination of such effects is, therefore, beyond the scope of the author's investigation, however, the effects of discharge rates and temperature on the available capacity and terminal voltage will be considered in detail.

The basic desirable simulation qualities of a battery discharge model is that it:

(1) is accurate under dynamic load applications;

(2) compensates for variations in cell electrolyte temperature;

(3) considers recuperation and regeneration effects;

(4) directly determines the battery state;

(5) determines battery voltage, energy and power characteristics;

(6) accounts for continuous direct current and pulsed direct current discharge;

(7) has a non-iterative solution;

(8) is easily implemented for onboard indication; and

(9) considers the battery state as continuous for discrete current changes.

A discussion of these qualities in relation to existing lead-acid traction battery models will now be given .

6.2 Existing Lead-Acid Traction Battery Models

An early effort to model battery terminal voltage conditions was made by Shepherd [69], who represented battery terminal voltage per cell by an equation which may be expressed as:

$$E = E_o - Li - Ki \frac{1}{1 - f} \tag{18}$$

where: E = terminal voltage per cell

E_o = open circuit terminal voltage per cell

i = current, A

f = $i.t/Q_o$ = battery state-of-discharge

Q_o = battery charge capacity, ampere-hours

L and K = constants related to internal resistance

Shepherd tried to relate the constants in the above equation to internal electrochemical phenomena of lead-acid batteries, but this has proved to be a very difficult process and generally valid for only one specific battery. Therefore, the equation should be considered as useful for describing general battery terminal characteristics only. The constants must be found by curve-fitting techniques using specific

measured terminal voltage characteristics. The equation attempts to describe the cut-off point, i.e. the state-of-charge at which the terminal voltage decreases very rapidly, and so is more often used as a maximum capacity predictor than as a state-of-charge prediction method. Most of Shepherd's analysis in developing equation (18) was based upon constant current discharge tests at low current magnitudes which are not typical of the loading experienced in EV applications. Consequently, the constants in the equation are seldom adequate for conditions of large or widely varying current loading, and so the accuracy of the equation suffers considerably under dynamic conditions.

Hoxie developed a model for predicting battery state-of-charge, the original form of which is to be found in the literature [70]. As a result of other investigations [71] the model has been subject to modifications, which have resulted in the following, more easily implemented algorithm:

$$1 = \frac{I_1}{N \frac{K}{t_c - t_1}} + \frac{I_2 - I_1}{N \frac{K}{t_c - t_2}} + \frac{I_3 - I_2}{N \frac{K}{t_c - t_3}} + \ldots\ldots + \frac{I_n - I_{n-1}}{N \frac{K}{t_c - t_n}} \qquad (19)$$

where: $I_1, I_2, I_3 \ldots I_n$ = discharge current for periods 1, 2, 3 .... n, A

$t_1, t_2, t_3 \ldots t_n$ = time span of discharge segments corresponding to currents $I_1, I_2, I_3 \ldots I_n$ respectively, hours

t_c = time to end of discharge, hours

K = Peukert capacity coefficient

N = Peukert current exponent.

The model iteratively determines the time to end of discharge as a function of battery characteristics and load profile. For a desired

discharge cycle, the end of discharge is determined by iteration (guess t_c and determine value of right side of equation; revise guess until value equals one). However, the Hoxie model's iterative solution technique makes it difficult to implement (requiring much computer memory and time) and renders it unsatisfactory for onboard applications. Additionally, the iterative technique makes direct determination of battery state-of-charge difficult. The model indirectly estimates battery recuperation effects by the time-weighing of the discharge currents.

In the AiResearch approach [72], the battery capacity varies as a function of both time averaged and instantaneous discharge rates. In this approach, the state-of-charge, S_c, is expressed as:

$$S_c = 1 - \frac{(C_u \cdot R_a + C_u \cdot (1 - R_a))}{C_i \qquad\qquad C_a} \tag{20}$$

where: C_u = capacity used, ampere-hour

C_i = capacity based on instantaneous current, ampere-hour

C_a = capacity based on average current, ampere-hour

R_a = ratio of average to instantaneous current or inverse (whichever is < 1).

This method estimates recuperation through the time averaging effects. Under dynamic loading conditions, however, the state-of-charge can be discontinuous, because of the discrete change in the ratio of average to instantaneous discharge currents ($R_a < 1$) for discrete current changes.

Heldt and Canders [73] developed a model for predicting battery state-of-charge and terminal voltage. The model is based upon a fractional utilisation approach, the basic algorithm of which may be expressed as:

$$\frac{\Delta m}{m} = \frac{t_j}{t_c} \tag{21}$$

where: m = battery active mass, kg

t_j = time span of j^{th} discharge segment, hours

t_c = time to end of discharge, hours

The fractional utilisation approach treats each time span of current production (t_j) as if it were the consumption of a mass fraction of the available battery material. This method does not inherently account for battery recuperation effects, but has the advantage of being easily implemented. The voltage model derived by Heldt and Canders is a function of cell internal resistance, discharge rate and no-load voltage (emf). The internal resistance and emf are themselves dependent upon the discharge rate and state-of-charge respectively. However, it will be shown* that under continuous discharge conditions of operation, the cell internal resistance is a function of both discharge rate and state-of-charge. Further, it will be shown in subsequent sections of this chapter, that the emf is also a function of both the discharge rate and state-of-charge. Therefore, the voltage model developed by Heldt and Canders can only be used as a method of approximately predicting the cell terminal voltage. Visscher [74] also used the fractional utilisation approach for determining battery state-of-charge, with the Peukert [55] curve serving as the battery information (t_c) for the model. However, the state-of-charge model does not account for battery recuperation effects. Further, the voltage model, which is a function of discharge rate, cell internal resistance, state-of-charge, and emf, does not recognise the dependence of cell internal resistance and emf on the discharge rate.

* The value of internal resistance during discharge is evaluated in Section 6.4

A model developed by Bozek [75] attempts to account for the time-varying discharge rates encountered in EVs by averaging these discharge rates over the discharge time in question. The average discharge rate is then used to determine battery state-of-charge by means of the equation:

$$S_c = 1 - \frac{i.dt}{K} \tag{22}$$

where: i = instantaneous discharge current, A

K = Peukert capacity coefficient, corresponding to the average discharge current.

Battery recuperation effects are estimated by the time averaging process. The usefulness of the model is limited, since Bozek makes no attempt at developing a voltage model of the battery.

In an attempt to account for dynamic load conditions, Martin and Goodson [76] developed a state-of-charge model which was based on the mass transfer processes occuring within the electrolyte of the cell. Fundamental to the development of the model is the assumption that a constant concentration of electrolyte exists at the plate/electrolyte boundary. The validity of the model is questionable since it will be shown* that the electrolyte concentration at the plate/electrolyte boundary is among other things, a function of both the discharge rate and the duration of discharge. The capacity determining equation developed by Martin and Goodson may be expressed as:

$$C_p + t_m \frac{dC_p}{dt} = \frac{K}{I^{(N-1)}} \tag{23}$$

where: C_p = predicted capacity, ampere-hours

t_m = mass transfer time constant, hours

I = discharge current, A

* See equation (87), derived by the author in Appendix 3

The quantities K and N are obtained from Peukert's capacity equation, and have been defined previously. The value of t_m was determined by Martin and Goodson to be a function of the diffusion rate of the electrolyte, which was assumed to be a constant. However, it is well known that the diffusion rate is, among other things, dependent upon discharge rate and temperature and, under such variable discharge conditions is very difficult to quantify. No attempt was made by Martin and Goodson to develop a voltage model for the battery.

None of the models discussed above consider the effects of temperature or pulsed discharge currents on the state-of-charge and terminal voltage of the cell. This is surprising, since lead-acid traction batteries used in modern EVs are subjected to considerable variations in temperature, and may be required to operate under both pulsed or continuous current discharge conditions. Therefore, for batteries used under such conditions, the usefulness of existing models in predicting battery performance is severely limited. To overcome these limitations, the author developed a model for predicting battery state for use under the realistic operating conditions found in EVs.

6.3 Determining Battery State-of-Charge for Continuous Direct Current Discharge

6.3.1 The Effects of Discharge Rate and Temperature on the Available Capacity of the Battery

Batteries used for EV propulsion have varying discharge current duties: typically, a high discharge current during vehicle starting, a relatively low discharge current when full speed is reached, and no current when the vehicle is stationary. Similarly, because of variations in climatic conditions and energy losses within the cell during its operation, the electrolyte temperature may vary considerably.

A series of continuous direct current discharge tests were performed to quantify the effects of variations in discharge rate and temperature on the available capacity of the battery. The tests were designed to supplement those performed in Chapter 4. Tests were performed at discharge rates (I_d) and temperatures (T) of:

I_d = 10 A and 220 A; at T = 30°C

I_d = 10,25,75,150 and 220 A; at T = 5°C and 55°C

The results, together with the relevant results of Chapter 4, are presented in Fig. 69.

From Fig. 69, with reference to the nominal 5-hour discharge rate capacity (C_5), the variation of available capacity, v, with discharge rate and temperature may be expressed by:

$$v = P.\left(e^{-1.55.K^D} + \frac{E.K}{K^2 + 1}\right) \qquad (24)$$

where: $P = 1.58.T^{0.141}$

$D = 0.722.T^{-0.144}$

$E = T/(618.627.T + 7796.865)$

$K = I_d.10^{-2}$

If the duration of battery operation is composed of m loading periods, with each discharge period consisting of p time intervals of equal duration, Δt, then the effective capacity removed, C_{er}, from the battery during discharge periods is given by:

$$C_{er} = \sum_{a=1}^{m} \left[\sum_{n=1}^{p} \frac{I_{d(n)}}{v_n} \cdot \Delta t \right]_a \qquad (25)$$

6.3.2 The Effects of Regeneration on the Available Capacity

In view of the low energy density of currently available lead-acid traction batteries, the reduction of vehicle energy requirements and the conservation of battery energy have always been design objectives for EVs. Of the many proposed methods for achieving these

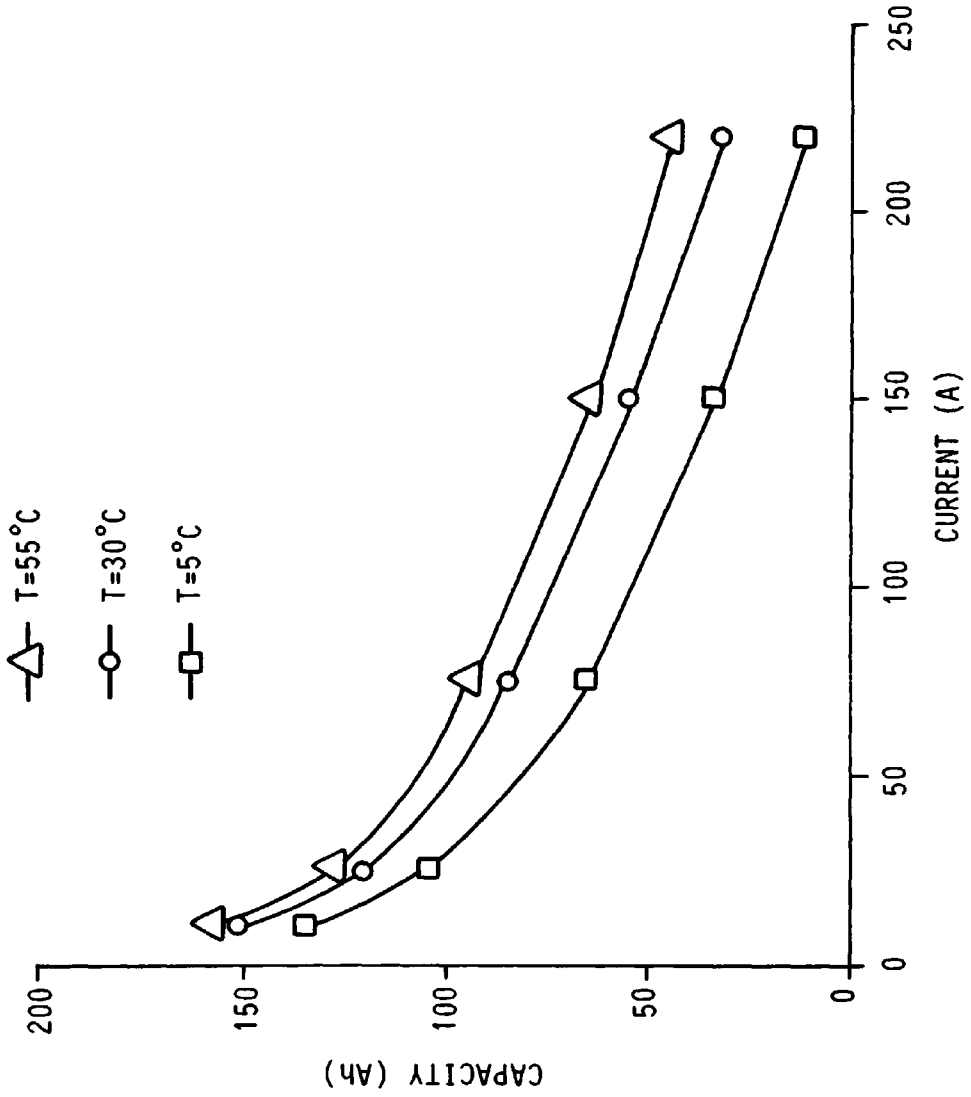

FIG. 69 VARIATION OF CAPACITY WITH DISCHARGE CURRENT FOR VARIOUS VALUES OF CELL TEMPERATURE

objectives, energy regeneration during periods of vehicle speed reduction has always been attractive. It has been shown [77], that for a conventional electric delivery vehicle on a selected route, approximately 28% of the battery energy was dissipated in the vehicles mechanical brakes during speed regulation and stopping.

In practice, only a limited proportion of the total energy available for regeneration can be actually recovered and stored, a proportion of the energy will be dissipated in the vehicle transmission system and the motor, for example. The amount of charge stored in the battery, will depend on the ability of the battery to convert the regenerated energy into recoverable electrochemical energy, that is, the charge acceptance of the battery. Irrespective of such sources of energy loss, it has been shown [78] that regeneration can increase the operational range of the vehicle. Therefore, to accurately predict battery performance, the effects of regeneration must be considered.

Usually, the time of a regeneration is only seconds in duration. Under such conditions, it is possible that the battery does not experience high gassing voltages, even when high charging currents are employed. Fig. 70 shows the results of tests which were performed to determine the validity of this. In the tests, the cell was discharged at a rate of I_{C_5} A to a specified value of state-of-charge. Immediately after removing the load current, a charging current of $3.I_{C_5}$ was applied to the cell, and the cell terminal voltage was recorded at intervals of 5, 20 and 50 seconds after the commencement of charge. The procedure was repeated for various values of state-of-charge. From Fig. 70 it may be seen that even when the battery is near the fully charged condition and the charging time is 50 seconds (a time far in excess of that normally encountered), the generally accepted gassing voltage of 2.40 V is not attained. Therefore, under these

conditions, the charge acceptance of the cell may be taken as unity.

A unity value for the charge acceptance may be shown to be realistic by analysing the charging results obtained by the author in Chapter 5. Detailed investigations [63] into the charge acceptance of lead-acid cells have shown that the gas evolution rate is virtually independent of the state-of-charge and is primarily dependent on the cell terminal voltage value. The problem of determining the amount of energy stored in the cell during regeneration, is, therefore, confined to establishing the relationship between cell charge acceptance and terminal voltage. The per unit charge acceptance, C_a, of the cell may be obtained from a knowledge of the volume of gas evolved over a given period of ampere-hour input by means of the equation:

$$C_a = 1 - \frac{V_o \cdot E_o}{I_c \cdot t} \qquad (26)$$

where: V_o = the volume of oxygen evolved at standard temperature and pressure, cm^3

t = the charging time, seconds.

I_c = the charging current, A

E_o = the volume electrochemical equivalent of oxygen, A seconds.

The value of E_o can be calculated by using Faraday's Law of Electrolysis as follows:

96,500 Coulombs of charge (1 Faraday) = 1/4 mole of oxygen = 5.5 litres of oxygen

and 1 ampere-hour = 3600 Coulombs

Therefore 5.5 litres of oxygen = 26.806 ampere-hour

Therefore 1 cm^3 of oxygen = 0.00479 ampere-hour = 17.244 A seconds = E_o

Equation (26) was applied to the results shown in Fig. 50. A consideration of Fig. 53 enabled the results shown in Fig. 71 of the average charge acceptance up to a specified charging voltage to be determined. The gas volume results of Fig. 50 were obtained at

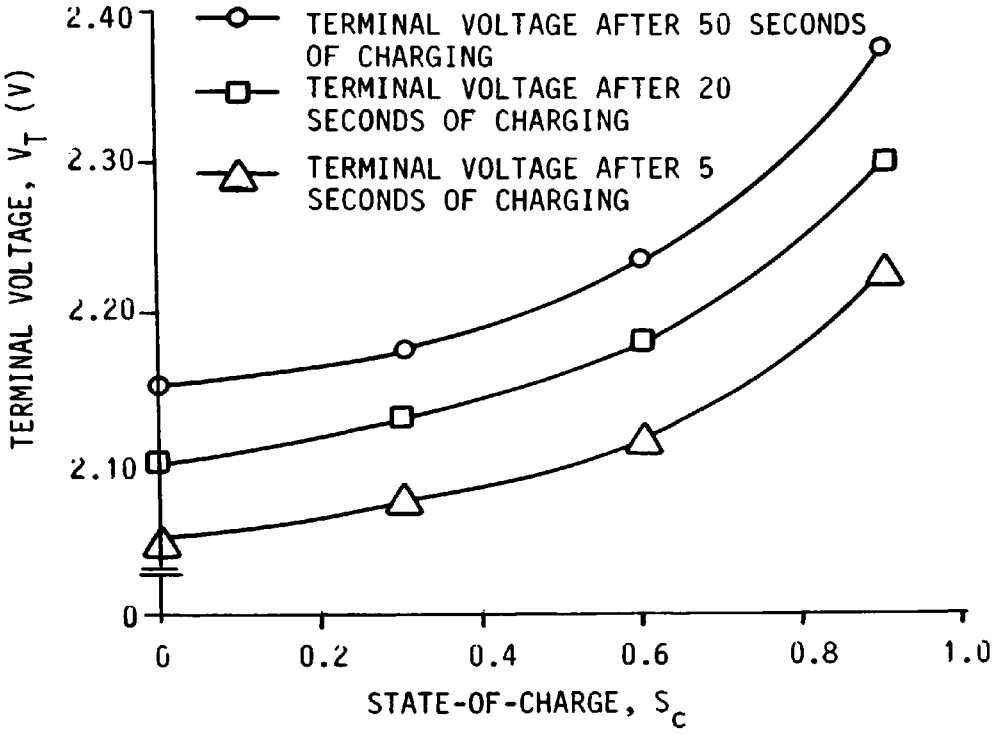

FIG. 70 VARIATION OF CELL TERMINAL VOLTAGE WITH STATE-OF-CHARGE FOR VARIOUS DURATIONS OF REGENERATION

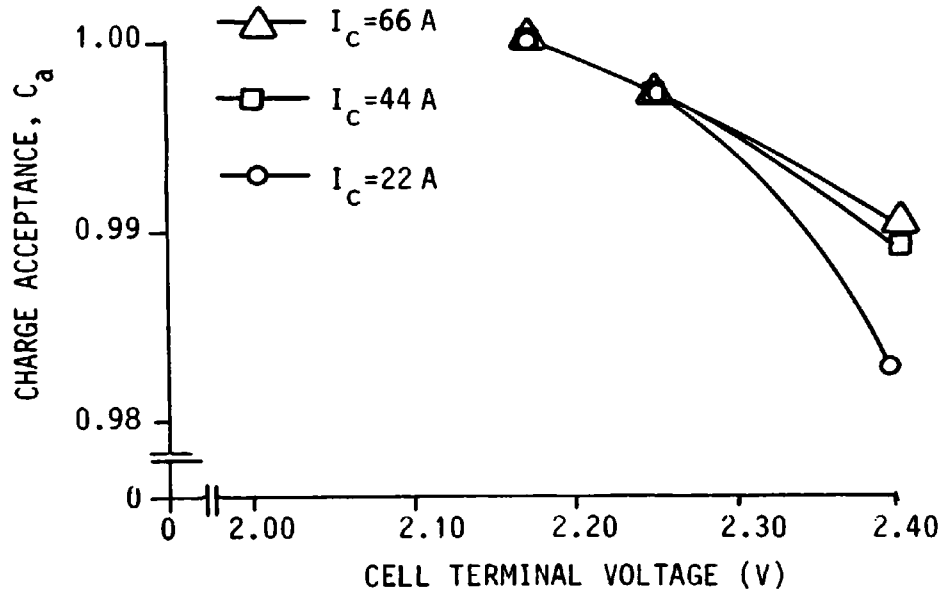

FIG. 71 VARIATION OF CHARGE ACCEPTANCE WITH TERMINAL VOLTAGE FOR THE CELL FOR VARIOUS VALUES OF CHARGING CURRENT

standard pressure and at room temperature. By using the Universal Gas Law, the volume of gas evolved at standard temperature and pressure is given by:

$$V_o = \frac{V_l \cdot T_0}{T_l} \tag{27}$$

where: V_l = volume of gas evolved at room temperature, cm^3

T_0 = standard temperature (25°C)

T_l = room temperature, °C

Fig. 71 shows that without incurring any significant error, the charge acceptance of the cell during periods of regeneration may be taken as unity, and hence, all the regenerated energy is converted into usable electrochemical energy.

Using a similar method to that described above for oxygen, the volume electrochemical equivalent of hydrogen (E_h) may be shown to be 8.622 A seconds. Therefore, in assuming that the gas evolved from the cell is composed entirely of oxygen (as is the case in equation (26)), Fig. 71 gives the minimum values of cell charge acceptance, and hence, a unity value for the charge acceptance is realistic.

Investigations have shown [64, 79] that within the temperature range normally encountered by lead-acid batteries in EVs, the gas evolution rates of the positive and negative plates of a lead-acid cell are virtually independent of temperature. The results of Fig. 71 are, therefore, valid under such conditions of varying temperature.

Accounting for periods of regeneration, the effective capacity removed from the battery is, therefore, given by:

$$C_{er} = \sum_{a=1}^{m} \left[\sum_{n=1}^{p} \frac{I_{d(n)} \cdot \Delta t}{v_n} \right]_a - \sum_{a=1}^{q} \left[\sum_{n=1}^{z} I_{c(n)} \cdot \Delta t \right]_a \tag{28}$$

where q = the number of regeneration periods

6.3.3 The Effects of Recuperation on the Available Capacity of the Battery

It is evident from the pulsed discharging investigations of Chapter 4, that battery recuperation which occurs between periods of battery loading, can have a significant effect upon the discharge performance of the battery, especially for a conventional EV.

Battery recuperation may occur during periods when the vehicle is coasting or stationary. Coasting the vehicle is an obvious method for reducing vehicle energy requirements. In practice, however, most attempts to conserve energy which rely upon the discretion of the vehicle driver have failed [77], as one of the driver's main objectives is to complete the journey in the minimum time. However, the energy saving could be attained by means of a completely automatic coasting device, or by encouraging the vehicle drivers to coast such vehicles to a halt. In terms of vehicle operating time, coasting is practical, for investigations on a conventional EV have shown [77] that very little reduction in operating time of the vehicle was achieved by eliminating coasting completely.

The recuperation phenomenon occuring between periods of battery loading, is the result of diffusion processes occuring within the electrolyte of the cell, and is primarily dependent upon (1) the discharge rates during the preceding loading period, (2) the cell electrolyte temperature, and (3) the depth of discharge.

Tests were performed to quantify the effects of recuperation on the available capacity of the cell. The cell was discharged at a constant continuous discharge rate to a specified state-of-charge. The cell was then allowed to rest on open-circuit for a specified time period, and subsequently discharged at the same rate as that used

* The mechanism of battery recuperation is discussed in Appendix 3.

initially, to a terminal voltage of 1.70 V. The total output capacity of the cell was then calculated. The procedure was repeated for different values of discharge rate, recuperation time, state-of-charge, and temperature. By making the discharge rates and temperatures of these tests the same as those used in Fig. 69, the effects of the recuperation periods on the available capacity could be determined. Recuperation periods of 1, 5 and 15 minutes were used.

The tests showed that the amount of recuperated capacity is described by the recuperation factor:

$$p = 0.157.L^{0.5}.(1 - e^{-h/k}) \tag{29}$$

where: $L = (1 - S_c)$ = the depth of discharge

h = the recuperation time, minutes

$k = 68.66.T^{-1.137}$

T = the electrolyte temperature, °C

During the no-load period, the capacity recuperated, C_p, is:

$$C_p = p.C_r \tag{30}$$

where: C_r = the capacity removed during the preceding loading period, ampere-hour

The effective capacity removed with w periods of recuperation is:

$$C_{er} = \sum_{a=1}^{m} \left[\sum_{n=1}^{p} \frac{I_{d(n)}.\Delta t}{v_n} \right]_a - \sum_{a=1}^{q} \left[\sum_{n=1}^{z} I_{c(n)}.\Delta t \right]_a - \sum_{a=1}^{w} \left[p.C_r \right]_a \tag{31}$$

6.4 A Battery Voltage Model for use with Continuous Direct Current Discharging

When discharging, the battery experiences an internal voltage drop due to its ohmic resistance. Therefore, the basic equation describing the behaviour of the terminal voltage V_T is:

$$V_T = E - I_d.r_{dc} \tag{32}$$

where: E = the no-load voltage, volts

r_{dc} = the internal resistance of the battery under continuous current discharge conditions, ohms

I_d = the discharge rate, A.

The no-load voltage and internal resistance of the cell were determined while performing the recuperation tests described in Section 6.3.3. During the recuperation periods the values of E were recorded; the true value of E was taken to be the value of terminal voltage when all the diffusion processes within the electrolyte had ceased, that is, the constant value of the voltage. The internal resistance was determined by the relationship:

$$r_{dc} = \frac{E - V_T}{I_d} \tag{33}$$

The nature of the dependence of E on the depth of discharge, the temperature of the electrolyte, and the discharge rate is shown in Fig. 72, and may be represented by the equation:

$$E = -m.L + c \tag{34}$$

where: $m = 0.207.e^{-0.01.I_d} + C_5.10^{-5}.(T - 32)$ (35)

$c = 0.0005.(38.62.C_5 - T)$ (36)

The variations of r_{dc} is shown in Fig. 73, and may be represented by the equations:

$r_{dc} = r_0 + r_1.(32 - T)$; for $T <= 32°C$ (37)

$r_{dc} = r_0 + r_2.(32 - T)$; for $T > 32°C$ (38)

where: $r_0 = (1/\sqrt{2}).L + (2.523 - 0.006.I_d)$; for $L <= 0.6$ (39)

$r_0 = 1/(0.57 + 650/C_5.I_d) - (\sqrt{3}/2.L.e^{-0.01.I_d})$; for $L > 0.6$ (40)

$r_1 = I_d/13.5.(5.46.I_d - C_5)$ (41)

$r_2 = 0.031 - 0.0067.I_d/C_5$ (42)

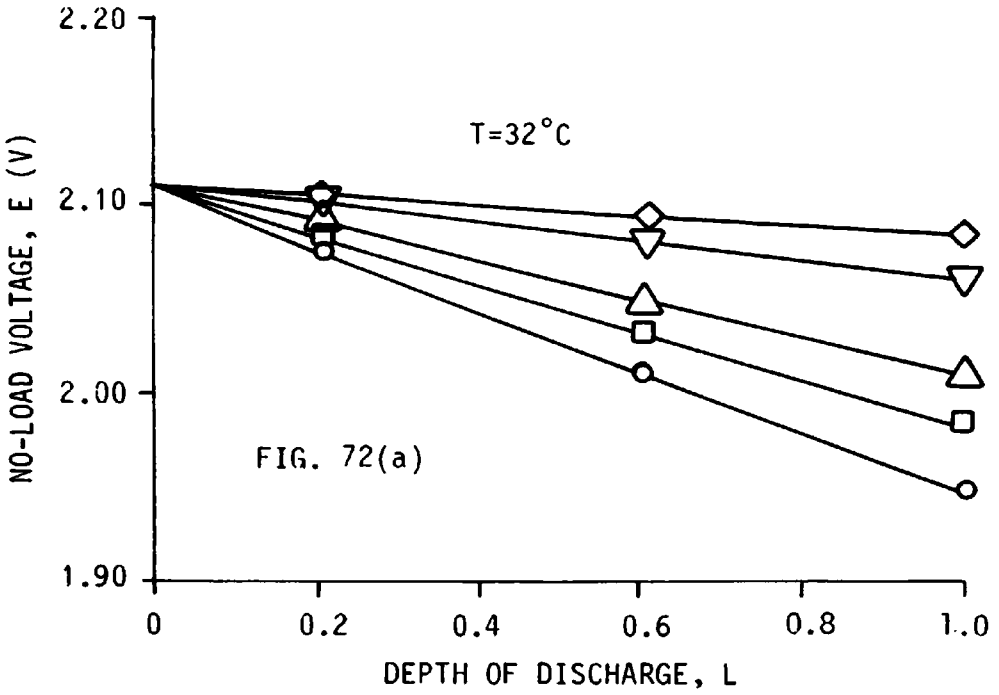

FIG. 72(a)

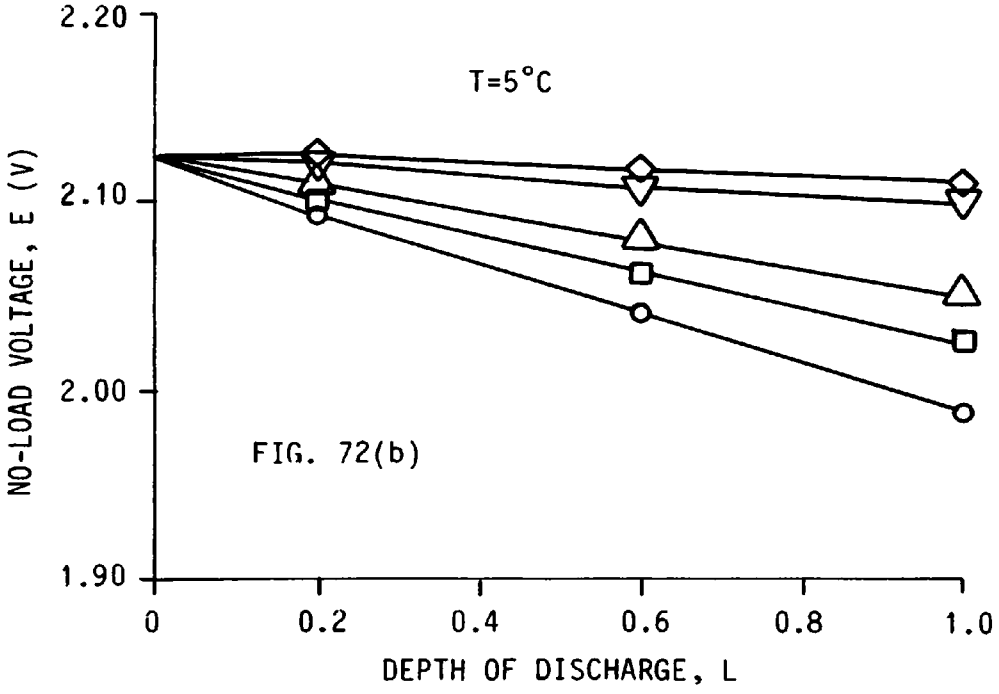

FIG. 72(b)

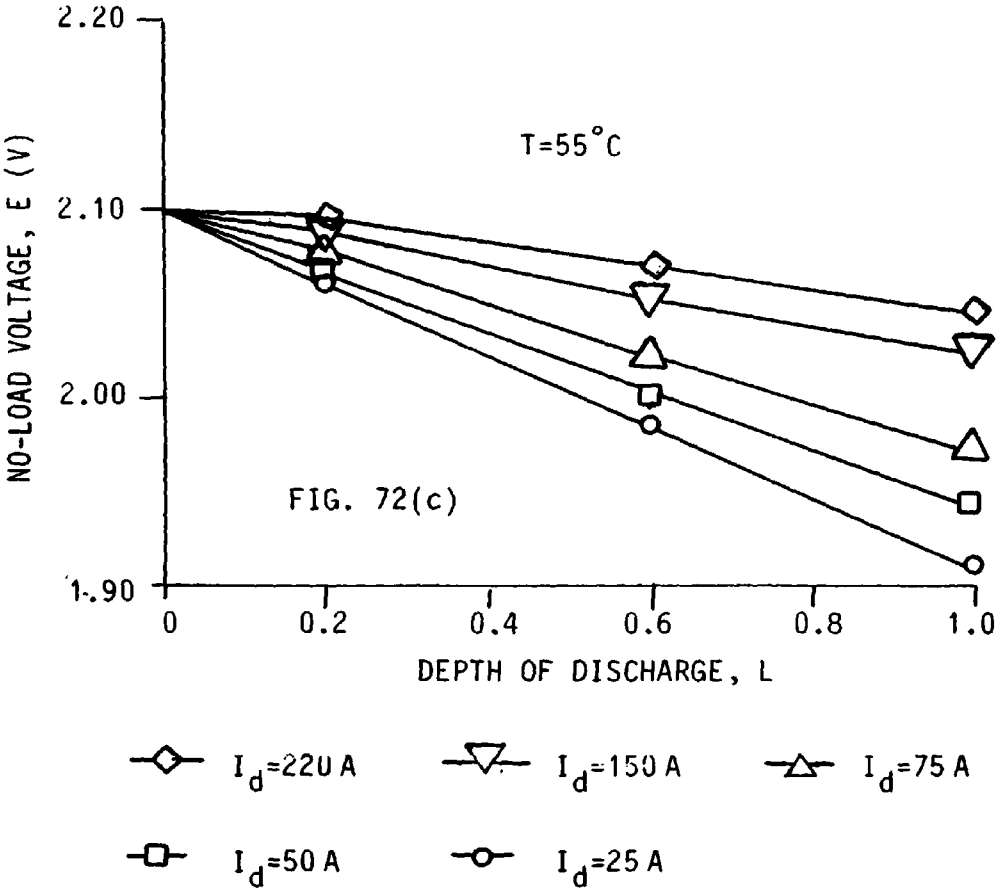

FIG. 72 VARIATION OF NO-LOAD VOLTAGE WITH DEPTH OF DISCHARGE FOR VARIOUS VALUES OF DISCHARGE RATE AND ELECTROLYTE TEMPERATURE

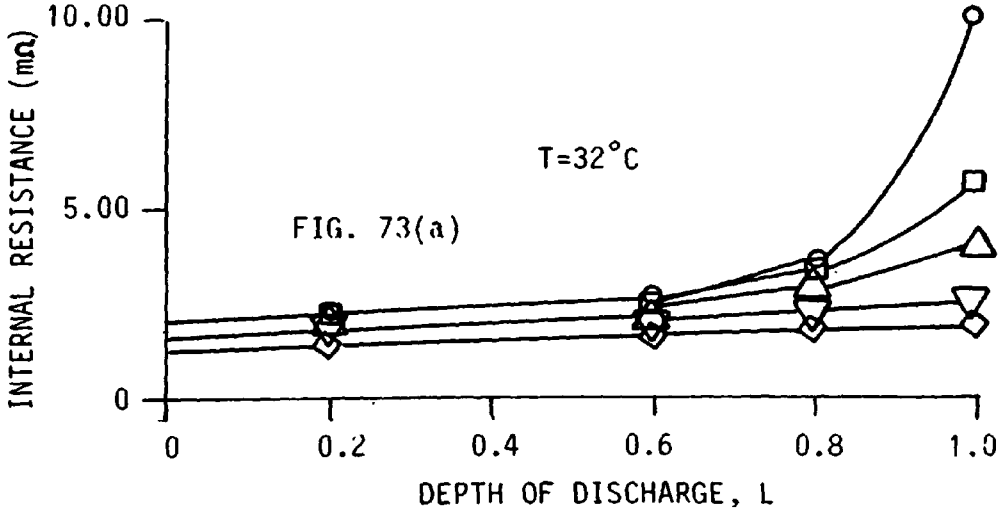

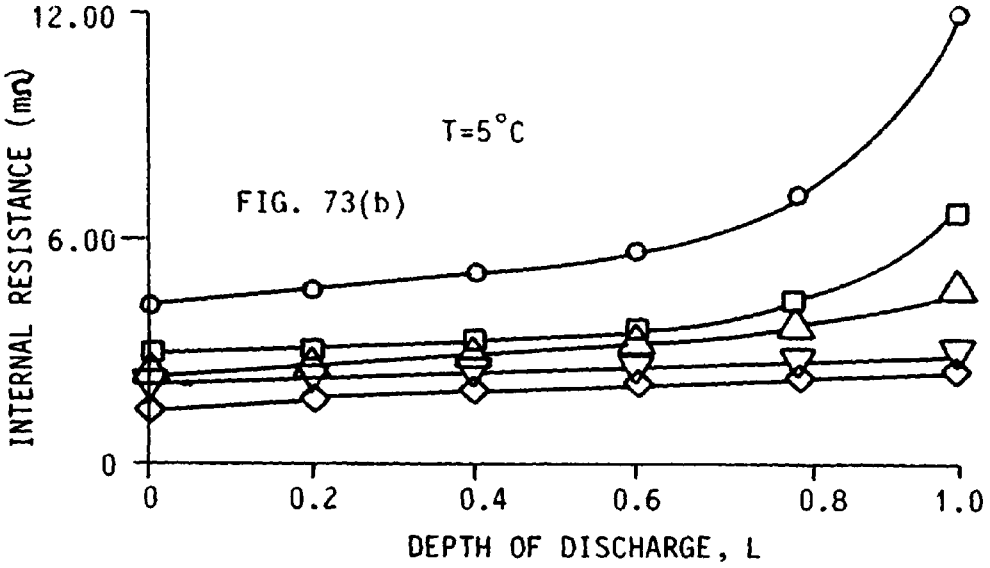

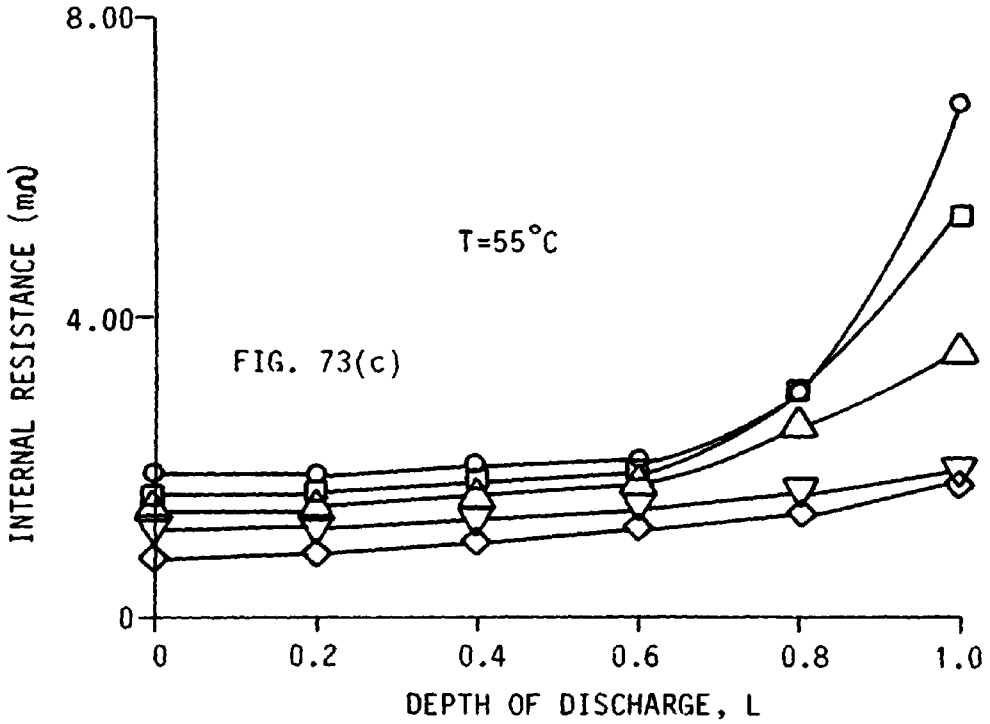

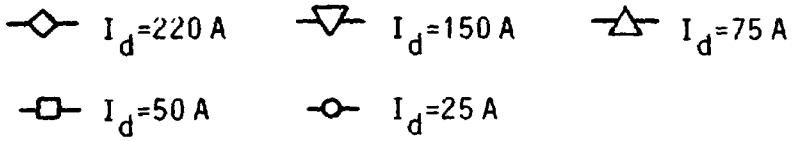

FIG. 73 VARIATION OF CELL INTERNAL RESISTANCE WITH DEPTH OF DISCHARGE FOR VARIOUS VALUES OF DISCHARGE RATE AND TEMPERATURE

The terminal voltage is, therefore, given by:

$$V_T = -(0.207.e^{-0.01.I_d} + C_5.10^{-5}.(T-32)).L + 0.0005.(38.62.C_5 - T) - I_d.(r_0 + r_1.(32 - T)) \quad \text{for } T <= 32°C \qquad (43)$$

$$V_T = -(0.207.e^{-0.01.I_d} + C_5.10^{-5}.(T-32)).L + 0.0005.(38.62.C_5 - T) - I_d.(r_0 + r_2.(32 - T)) \quad \text{for } T > 32°C \qquad (44)$$

where: r_0, r_1 and r_2 are defined by equations(39)-(42).

6.5 Determining Battery Status when using Pulsed Discharge Currents

It may be seen from Fig. 24 that provided the mean value of the pulsed current is taken as the discharge rate, and the mean value of the pulsed voltage waveform as the termination of discharge voltage, then the available discharge capacity of the cell is the same for the continuous current and pulsed current modes of discharge; similarly, the cell terminal voltage and the specific gravity during discharge as shown by the example of Fig. 74.

A number of uninterrupted pulsed current discharge tests were performed to determine the effects of variations in average discharge current and temperature on the available capacity of the battery. The tests were designed to supplement these performed in Chapter 4, and were performed at temperatures of 5°C and 55°C for the pulsed discharge conditions specified in Table 3. The results substantiated that when using equation (9), the available capacity of the cell is the same for the continuous current and pulsed current modes of discharge, and showed that under such discharge conditions, the available capacity is independent of frequency, for values between 50 Hz and 1000 Hz. The effective results of the tests are shown in Fig. 75.

From equations (12) and (14) the values V_{pk} and V_{mn} of the pulsed voltage waveform may be determined:

$$V_{pk} = V_{av} + I_{pk}.r_{dp}.\frac{M}{M+1} \qquad (45)$$

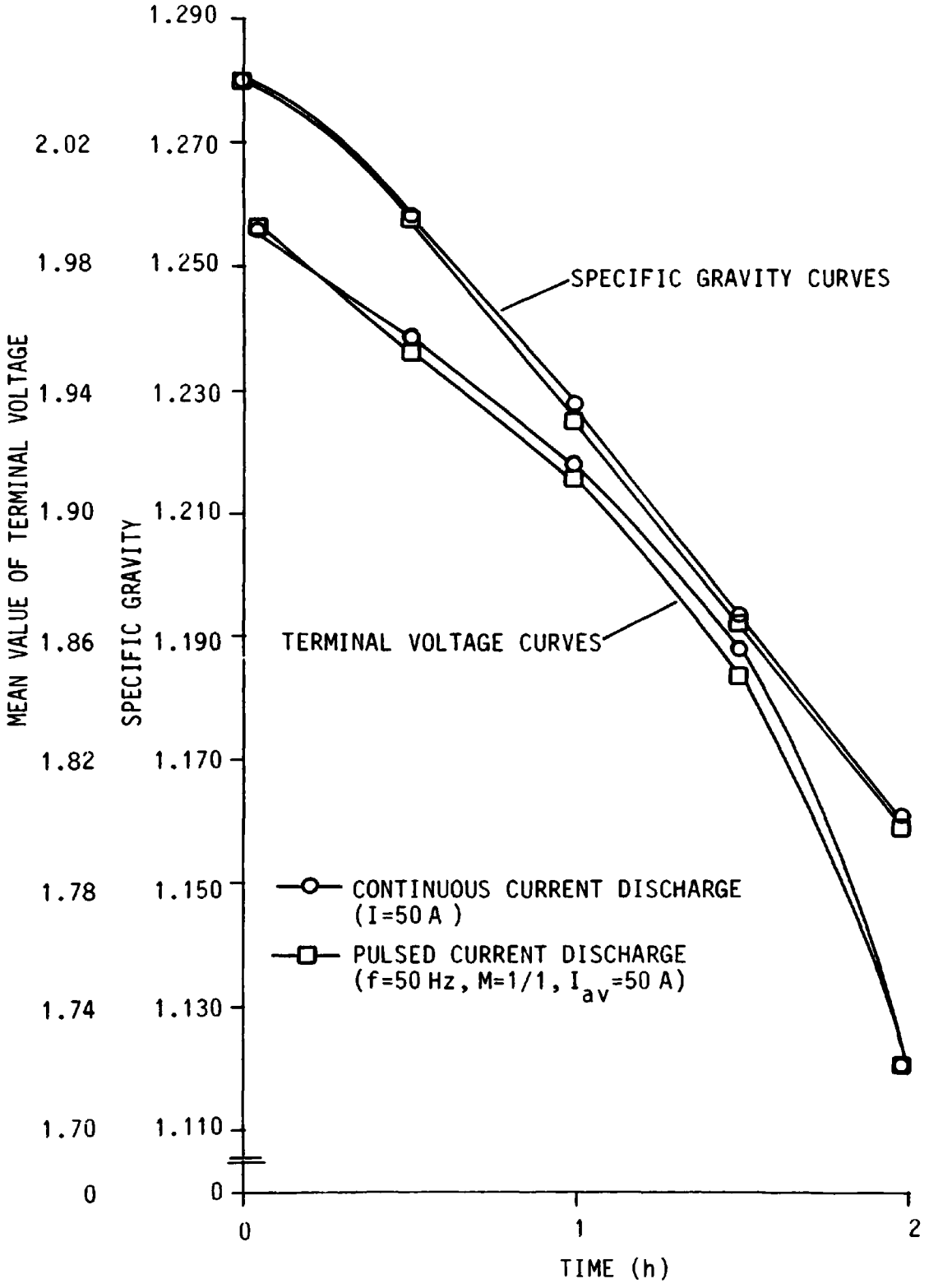

FIG. 74 VARIATION OF CELL TERMINAL VOLTAGE AND SPECIFIC GRAVITY WITH DISCHARGE TIME FOR CONTINUOUS AND PULSED CURRENT DISCHARGE

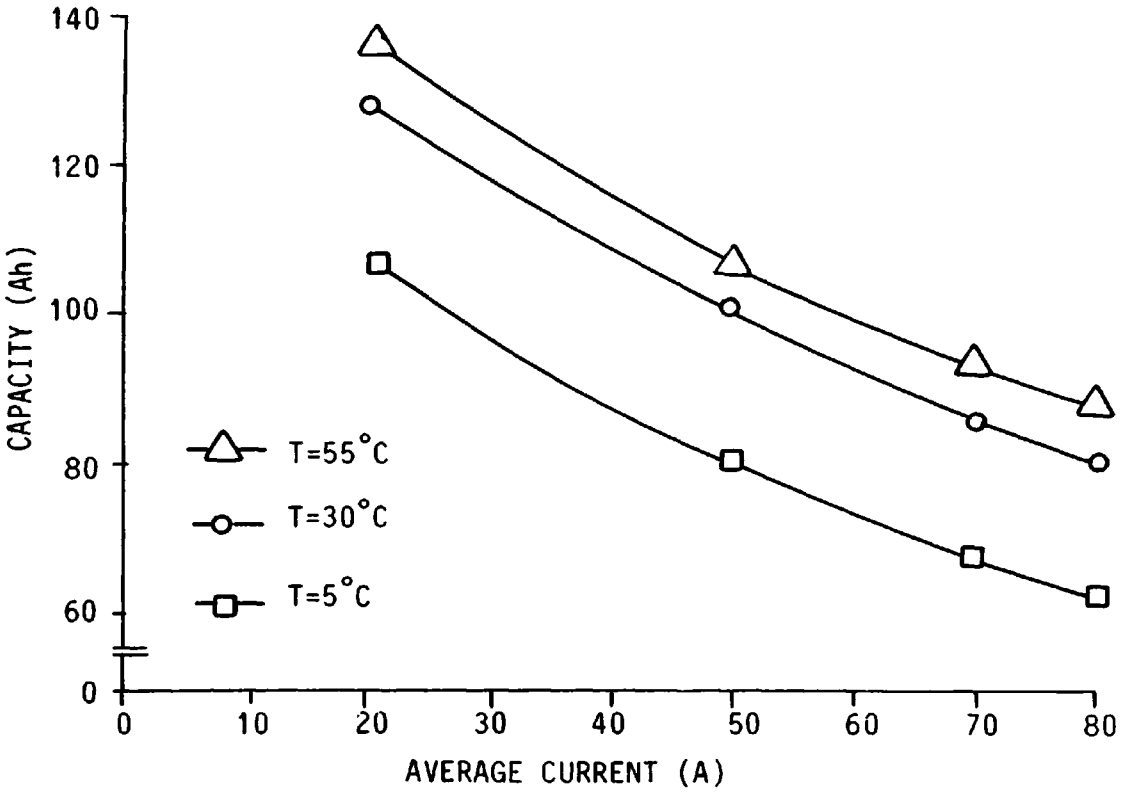

FIG. 75 VARIATION OF CAPACITY WITH AVERAGE DISCHARGE CURRENT FOR VARIOUS VALUES OF ELECTROLYTE TEMPERATURE

$$V_{mn} = V_{pk} - I_{pk} \cdot r_{dp} \quad (46)$$

where: r_{dp} = the internal resistance of the cell under pulsed discharge conditions of operation, ohms.

It was found that the value of r_{dp} could be represented by:

$$r_{dp} = r_c(r_f + 1) \quad (47)$$

The factor r_c may be determined from:

$$r_c = m.L + c \qquad \text{for } 0 <= L < 0.6 \quad (48)$$

where: $m = 0.50 - 5.06/I_d$

$c = 1/(0.85 - 0.33.I_d/C_5)$

and I_d = the average discharge current of the pulsed waveform, A.

$$r_c = (1/(b.L + a)) + d \quad \text{for } 0.60 < L <= 1.0 \quad (49)$$

where: $b = -1.257 + 1.62.I_d/C_5$

$a = 1.512 - C_5.I_d/10^4$

$d = 0.026.L^{5.18}$ = the temperature coefficient of resistance, $m\Omega/°C$

The factor r_f accounts for variations in internal resistance with frequency, and is described by:

$$r_f = 0 \qquad \text{for } f <= 500 \text{ Hz} \quad (50)$$

$$r_f = L.(f/500 - 1)/(11.0 - 9.60 .L) \quad \text{for } 500 < f <= 1000 \text{ Hz} \quad (51)$$

From Fig. 18 it may be seen that when current is taken from the battery, it initially experiences a high rate of drop in terminal voltage, which is followed by an exponential decay in the voltage level. The effective internal resistance is, therefore, composed of (1) a resistance r_d corresponding to the high rate of voltage drop, and (2) an effective internal resistance r_e corresponding to the exponential period of voltage drop and caused by the diffusion processes occuring within the electrolyte. For the range of pulsed discharge tests performed, it was found that the ratio r_d/r_e was independent of the peak current, mark/space ratio, and frequency of

the waveform, and given by:

$$r_e/r_d = 1/(7.76 - 4.65.L) \qquad (52)$$

The peak value of the pulsed voltage waveform is, therefore, given by:

$$V_{pk} = V_{av} + I_{pk} \cdot \frac{M}{M+1}(r_f + 1)\left[(0.50 - 5.06/I_d).L + 1/(0.85 - 0.33.I_d/C_5)\right]$$
$$\text{for} \quad 0 <= L < 0.6 \qquad (53)$$

$$V_{pk} = V_{av} + I_{pk} \cdot \frac{M}{M+1}(r_f + 1)\left[(1/((-1.257 + 1.62.I_d/C_5).L + 1.512 - C_5.I_d/10^4) + 0.026.L^{5.18})\right] \text{ for } 0.60 < L <= 1.0 \qquad (54)$$

and the minimum value of the voltage waveform is given by:

$$V_{mn} = V_{pk} - I_{pk}(r_f+1)\left[(0.50 - 5.06/I_d).L + 1/(0.85 - 0.33.I_d/C_5)\right] \qquad (55)$$
$$\text{for } 0 <= L < 0.6$$

$$V_{mn} = V_{pk} - I_{pk}(r_f+1)\left[(1/((-1.257 + 1.62.I_d/C_5).L + 1.512 - C_5.I_d/10^4) + 0.026.L^{5.18})\right] \quad \text{for } 0.60 < L <= 1.0 \qquad (56)$$

where r_f is defined by equations (50) - (51).

6.5.1 Terminal Voltage During Regeneration and Recuperation Periods

The electrochemical reactions occuring within the cell are reversible. Since EV regeneration periods are only seconds in duration, it may be assumed that during such periods no polarisation and equalistion of the acid concentration curve at the surfaces of the plates is experienced by the cell. Therefore, under such conditions, the terminal voltage is given by:

$$V_T = E + I_c \cdot r_d \qquad (57)$$

where r_d is defined by equation (52).

The terminal voltage during a recuperation period was found to be given by equations (34) - (36), where I_d is the discharge rate immediately preceding the recuperation period.

6.5.2 Considerations when using Pulsed Discharge Currents

Fig. 23 shows that under certain pulsed discharge conditions the battery does not experience an increase in available capacity when compared to that obtained from using continuous uninterrupted discharge currents. In fact, Fig. 23 indicates that a decrease in capacity could be experienced under certain conditions. Therefore, when pulsed discharging lead-acid batteries, certain constraints should be placed upon the values of frequency, mark/space ratio, and peak current of the pulsed waveform if the battery is to be efficiently discharged. Figs. 23 and 25 indicate that if energy efficiency under pulsed discharge conditions is to be observed then, for the frequency and mark/space ratio values considered in the tests, the peak value of the current waveform should, in general, not exceed a value equal to the nominal 5-hour capacity rating of the battery for mark/space ratio values greater than 4/1.

By taking the mean value of the pulsed voltage waveform as the termination of discharge voltage, the value of the on-load terminal voltage (V_{mn}) will be less than 1.70 V for a mean termination of discharge voltage having this value. Since battery manufacturers are uncertain whether deep voltage discharges are detrimental to the stability of the active material of the plates, the value of V_{mn} at termination of discharge should be evaluated. If the value of V_{mn} is thought to be too low, then it would be unacceptable to use V_{av} as the termination of discharge voltage. Examples of values of V_{mn} at termination of discharge for various pulsed discharging conditions are shown in Table 5, where it may be seen that the minimum value of the pulsed voltage waveform (V_{mn}) does not differ considerably from the mean value of 1.70 V at termination of discharge.

	AVERAGE VALUE OF PULSED CURRENT (A)		
	20	50	70
M	1/1	1/1	1/1
f (Hz)	50	50	50
V_{mn} (V)	1.63	1.59	1.55

TABLE 5 MINIMUM CELL VOLTAGE VALUES AT THE END OF DISCHARGE FOR VARIOUS PULSED DISCHARGE CONDITIONS

6.6 The Power and Energy Output of the Cell

The tendency in EV development is to disregard power requirements and to build vehicles with performance characteristics far inferior to conventional ICEVs. As a result, many existing EVs are prohibited from using certain routes. If EVs having performance characteristics for safe travel on modern highways are to be designed, the battery model must be capable of accurately determining battery power and energy characteristics.

The battery voltage characteristic is significant in EV analysis since it is the principal factor in determining battery power which, in turn, determines vehicle performance. For example, a typical EV may have a maximum speed of 55 mph at full charge, but near the end of discharge the maximum speed will be less. The reduction in speed is due to the reduced ability of the batteries to deliver power at useful voltages as the batteries become more discharged. Routine operator decisions concerning the passing of, or the merging with other vehicles becomes more difficult because the EV capabilities are not constant.

During discharge, the power delivered (P_d) by the battery which is at a state-of-charge S_c, is given by:

$$P_d = V_{S_c} \cdot I_d \tag{58}$$

where: V_{S_c} = the terminal voltage of the battery at state-of-charge S_c; for pulsed currents, V_{S_c} is the mean value of the terminal voltage

I_d = the discharge rate; for pulsed currents, I_d is the mean value of the pulsed current

At a given state-of-charge, the remaining available energy (E_a) of the battery at the reference discharge rate is:

$$E_a = S_c \cdot C_5 \cdot V_{S_c/2} \tag{59}$$

where: $V_{S_c/2}$ = the terminal voltage corresponding to a state-of-

charge of $S_c/2$.

The total available energy (E_t) at the reference discharge rate is:

$$E_t = C_5 \cdot V_{S_c=0.5} \tag{60}$$

The per-unit value of energy available (E_u) is, therefore, given by:

$$E_u = E_a/E_t = \frac{S_c \cdot V_{S_c/2}}{V_{S_c/0.5}} \tag{61}$$

6.7 The Implementation and Testing of the Models

The computer used to implement the models was the CBM Pet [80]. The linking of the computer to the battery was performed using standard interface equipment [81] as shown in Fig. 76; and a details of the interface equipment is given in Appendix 4. The exchange of data between the computer and the interface unit takes place over the IEEE data bus at time intervals known as the sampling rate, which is set under software control. The printer, which is shown in the system of Fig. 76, was incorporated to provide a tabulated output of the test results for subsequent analysis.

The temperature of the cell electrolyte and the discharge rate were monitored by the computer via the interface unit. The temperature of the electrolyte was measured by means of a thermocouple, which was submerged deep into the electrolyte; the thermocouple temperature sensing circuit is described in Appendix 5.1. The discharge rate was determined by monitoring a shunt voltage. The measured values of discharge rate and temperature were then introduced into the model program , and the cell voltage and state-of-charge was calculated and recorded.

When using pulsed discharge currents, it is possible that when

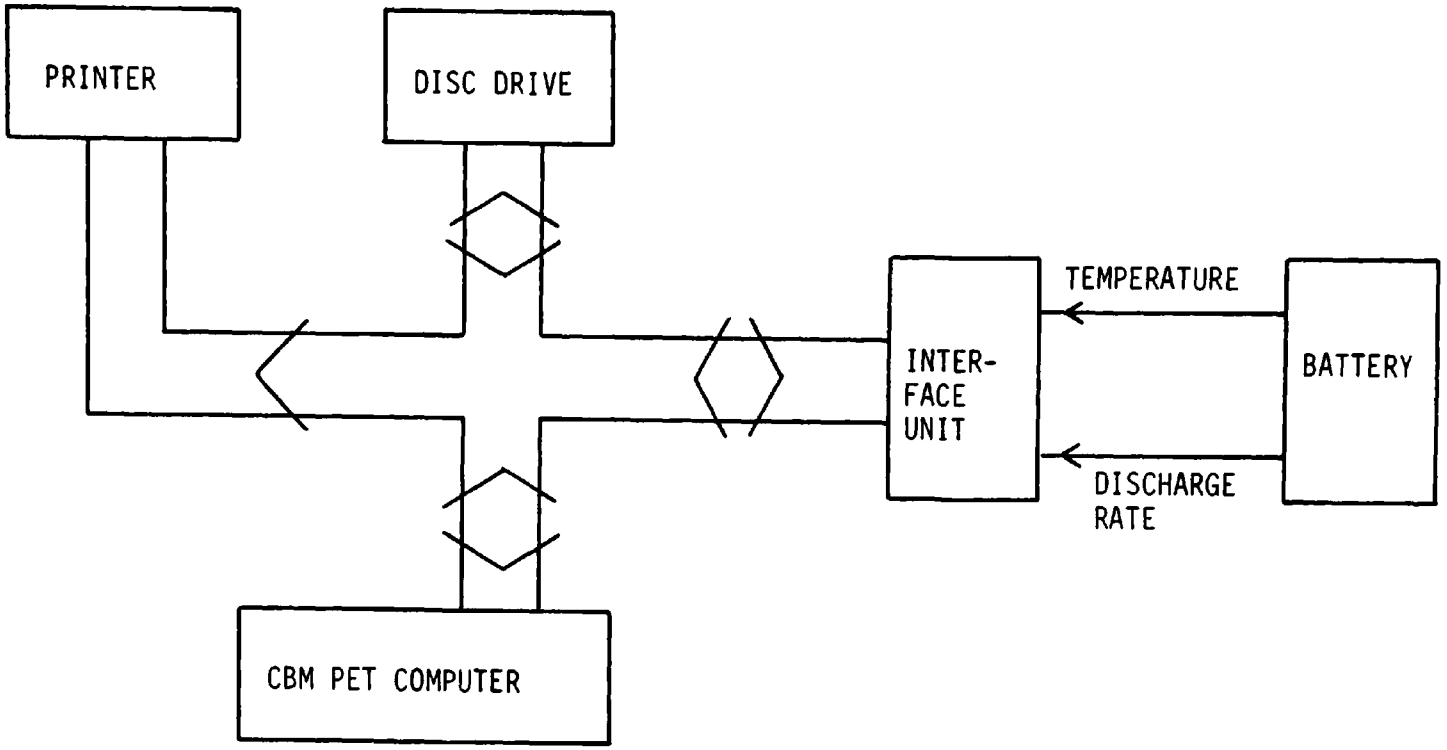

FIG. 76 SYSTEM CONFIGURATION FOR IMPLEMENTATION OF THE MODEL

sampling the shunt voltage, the sampling may occur during the space-time of the pulsed waveform. To ensure that the peak value of the waveform is sampled, a basic sample-and-hold circuit was constructed which recorded the peak value of the shunt voltage occuring between sampling. (see Appendix 5.2.)

To test the models, the battery was repeatedly subjected to the test cycles shown in Fig. 77 until it was fully discharged. The value of the charging current, I_c, was made equal to $2.I_{C5}$, and the value of I_d was made equal to $5.I_{C5}$ and $7.I_{C5}$ in test cycles 1 and 2 respectively. At the instants in time t_1, t_2 and t_3 as specified in test cycles 1 and 2, measurements of the terminal voltage, electrolyte temperature and specific gravity, and state-of-charge were recorded. Tests were performed using continuous currents and pulsed currents. For the pulsed current tests, a frequency and mark/space ratio of 50 Hz and 1/1 respectively was used, and the mean value of the waveform was made equal to I_d and I_c for the discharge and charge portions respectively of the test cycles. The results of the tests are shown graphically in Fig. 78.

6.8 Normalising the Battery Models

The usefulness of any battery model is severely limited unless it can be used on all batteries within the same generic class. Therefore, there is a need to normalise the models developed by the author.

The state-of-charge model was derived with reference to the C_5 nominal capacity of the battery and hence may be applied to all batteries within the same generic class. If it is assumed that the reference and vehicle batteries have the same power density per cell, and that the ampere-hour capacity per cell (nominal C_5) is an accurate

measure of cell weight, then the relationship between the power delivered by the reference battery (P_r) and that delivered by the vehicle battery (P_v) is given by:

$$P_v = \frac{P_r \cdot C_{5(v)}}{C_{5(r)}} \qquad (62)$$

where: P_r is obtained from equation (58).

For a given discharge rate, the terminal voltage of the vehicle battery is, therefore, given by:

$$V_T = \frac{P_v}{I_d} \qquad (63)$$

6.9 Comments on the Modelling Results

From Fig. 78 it may be seen that the models accurately predict the state of the battery. The results of the continuous current tests shown in Fig. 78(a) and (b) show that throughout the period of battery operation, the maximum deviation in terminal voltage is 2.00%, 2.32% and 1.86% during discharge, recuperation, and regeneration respectively, whereas, for the pulsed current tests shown in Fig. 78(c) and(d)the maximum deviation is 1.84%, 2.56% and 1.87% respectively. At termination of discharge there is a maximum deviation in state-of-charge of 5% and 6% for the continuous current and pulsed current tests respectively.

The requirements of a comprehensive battery discharge model as specified in Section 6.1 have been satisfied by the author's terminal voltage and state-of-charge models. Previously developed models, which were discussed in Section 6.2, do not satisfy these requirements, resulting in models which are wholly unsatisfactory for determining the battery status in EV applications where the battery is subjected to considerable variations in loading and temperature. Of particular interest in the author's models is the consideration of cell electrolyte temperature and the effects of pulsed direct current

discharges on the battery status. Additionally, other status affecting factors such as recuperation and regeneration have been accurately determined from experimental tests performed by the author.

It is interesting to note that of the models discussed in Section 6.2, only some of these [69, 70, 73, 74] have been experimentally tested and the results published. Furthermore, not all of these models determine both the terminal voltage and state-of-charge. Even allowing for the limitations of these models, the author's models are accurate and demonstrate significant advantages.

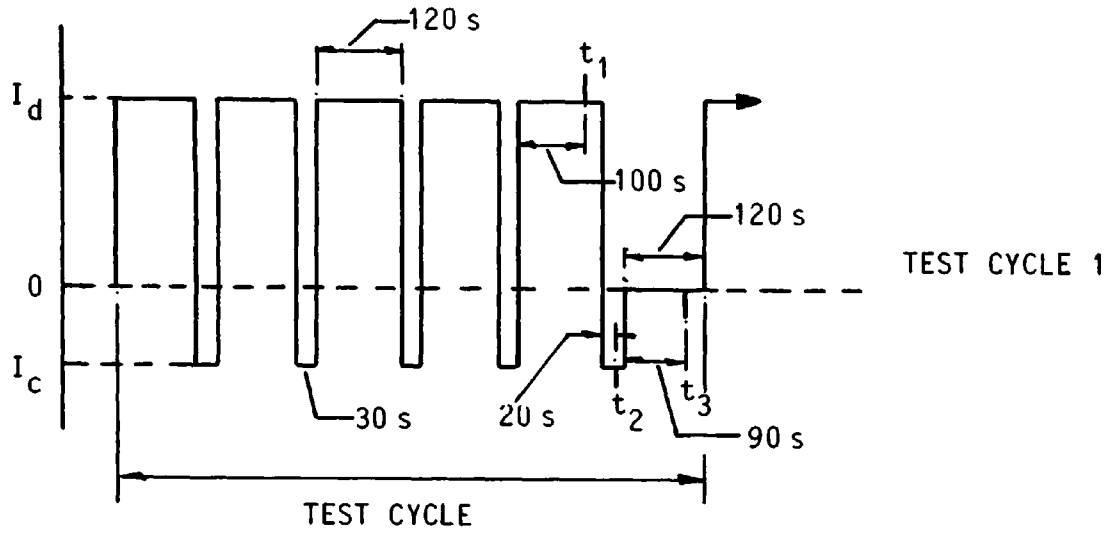

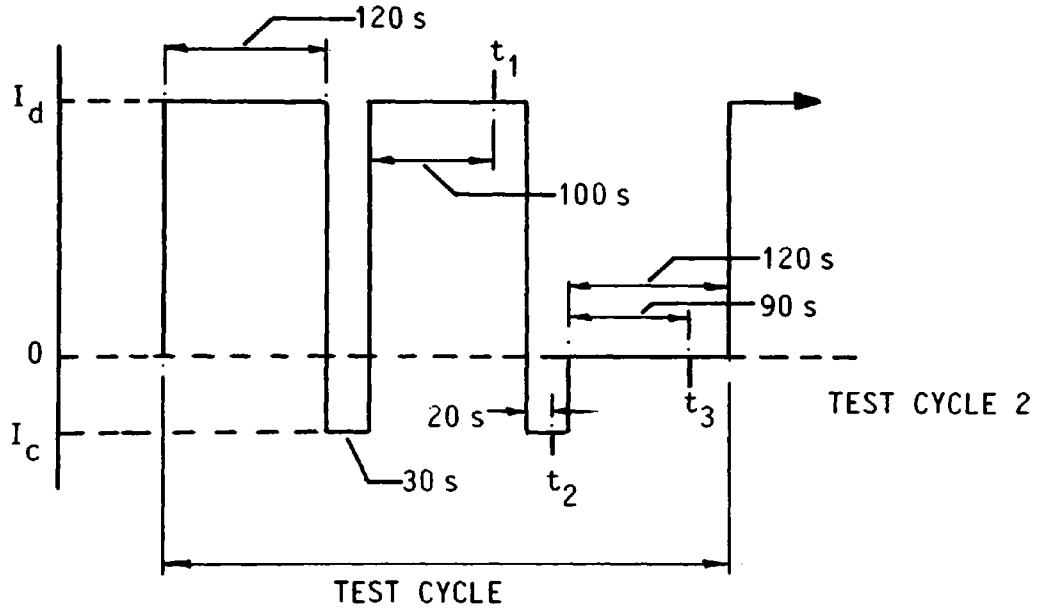

FIG. 77 TEST CYCLES

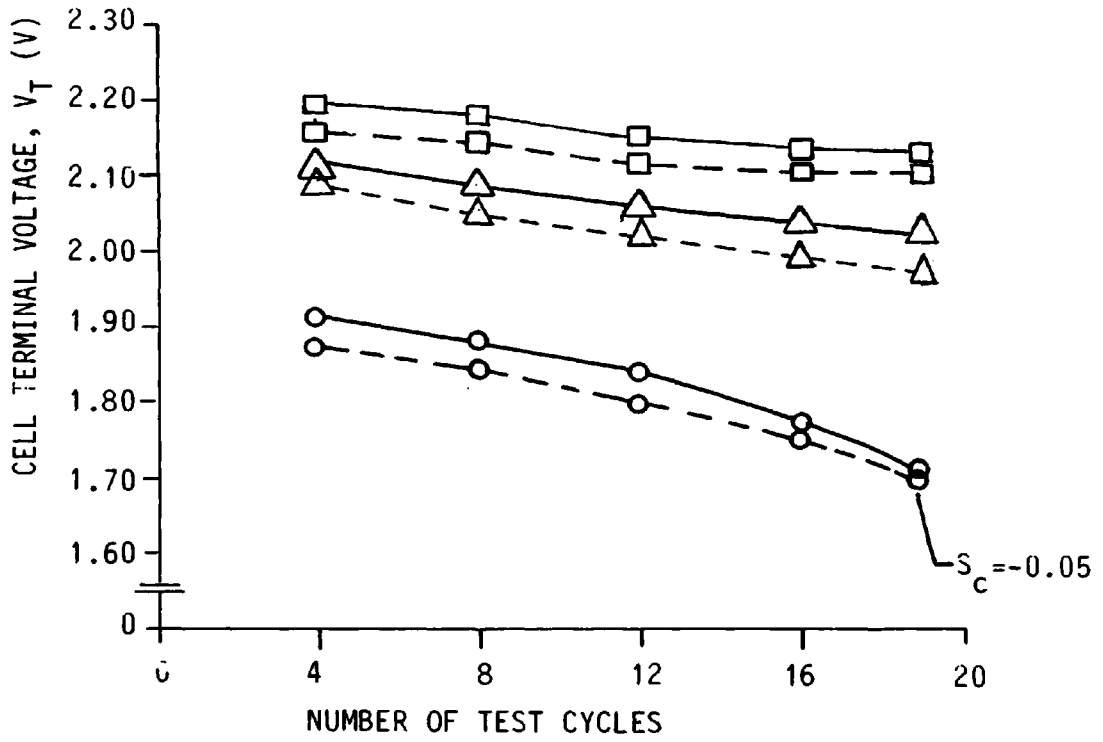

FIG. 78(a) CONTINUOUS CURRENT TEST (TEST CYCLE 1)

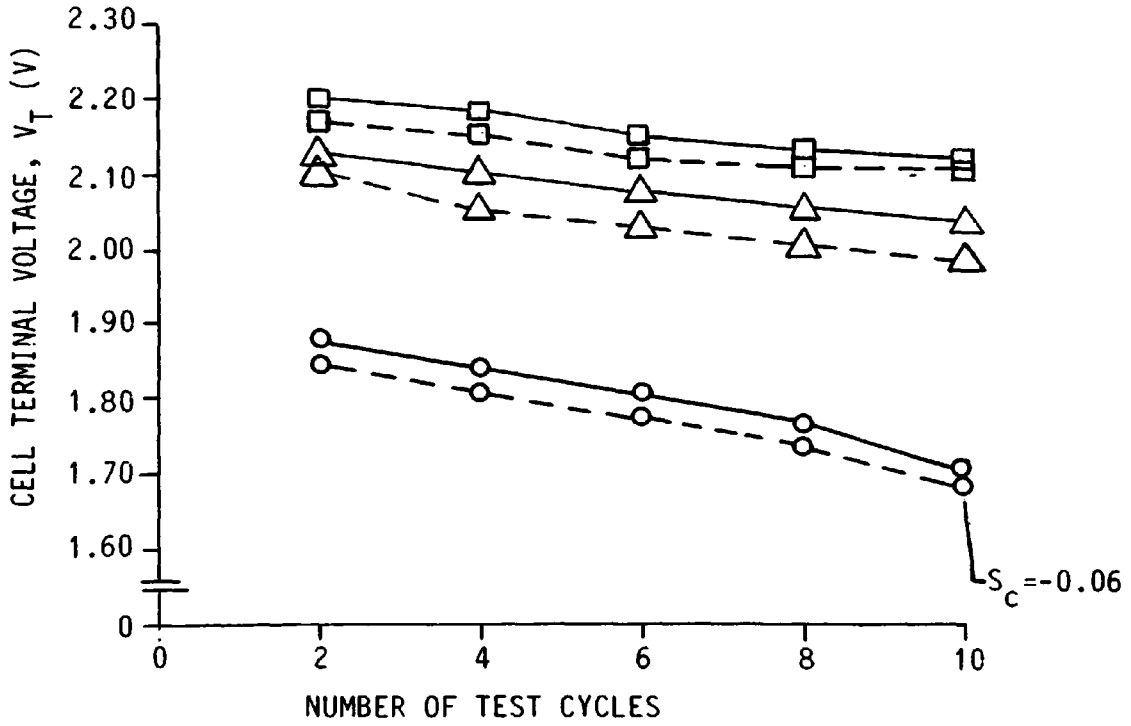

FIG. 78(b) CONTINUOUS CURRENT TEST (TEST CYCLE 2)

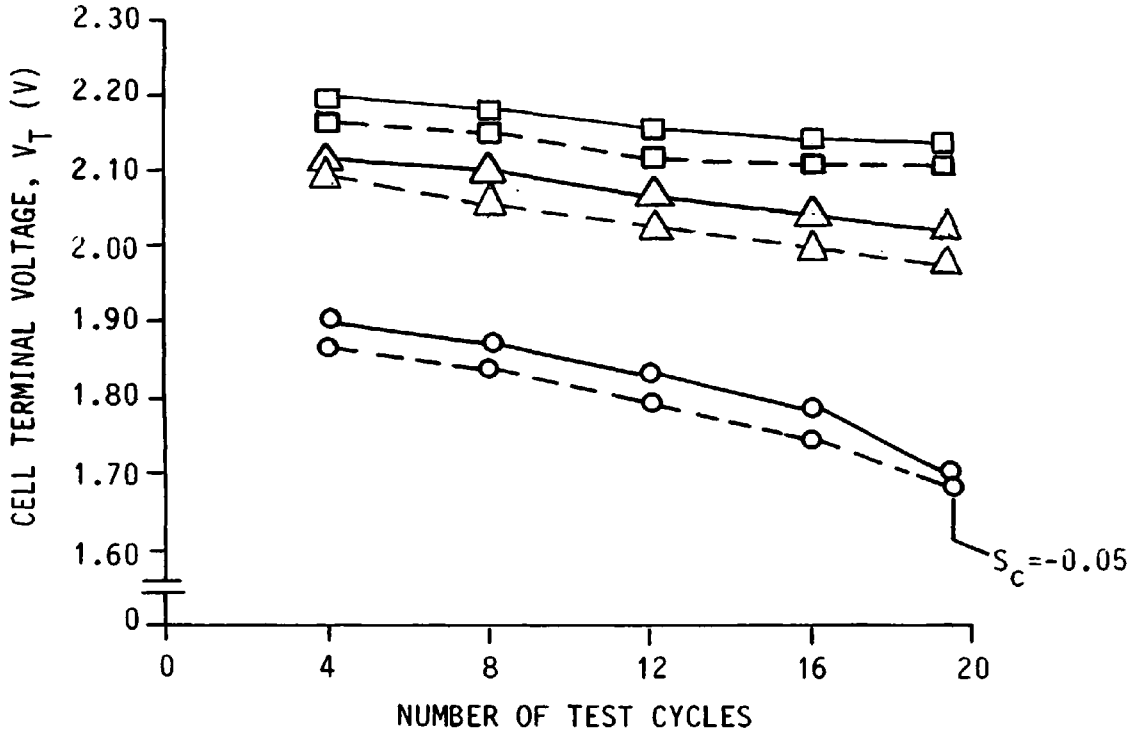

FIG. 78(c) PULSED CURRENT TEST (TEST CYCLE 1)

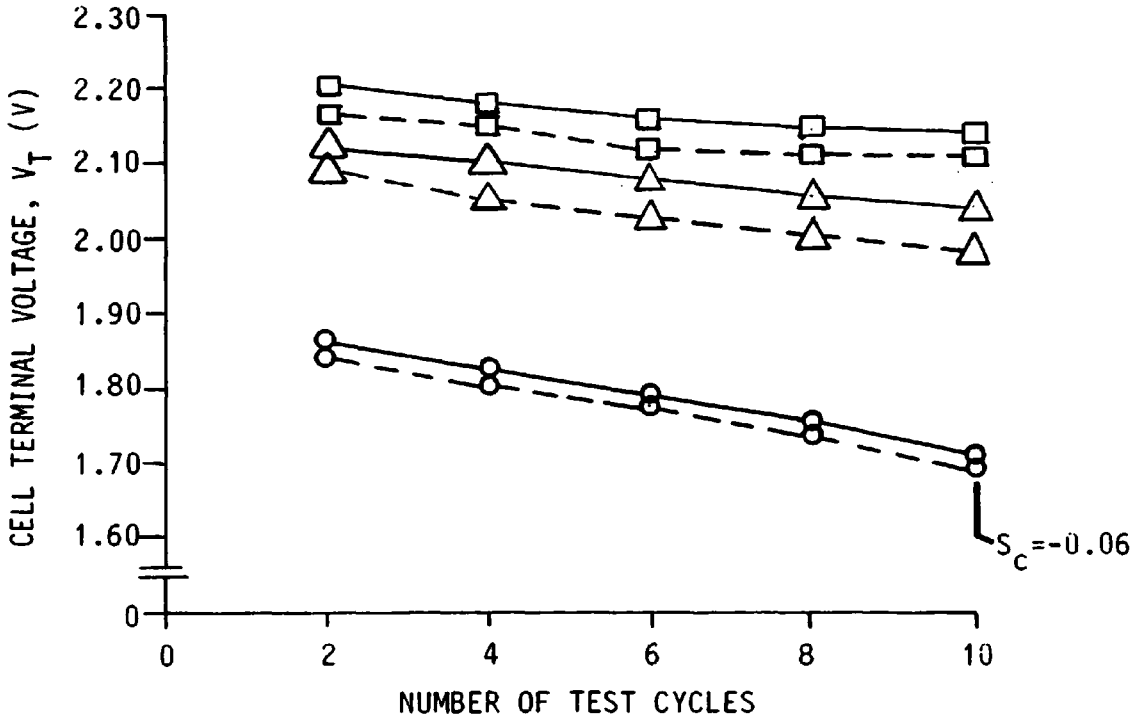

FIG. 78(d) PULSED CURRENT TEST (TEST CYCLE 2)

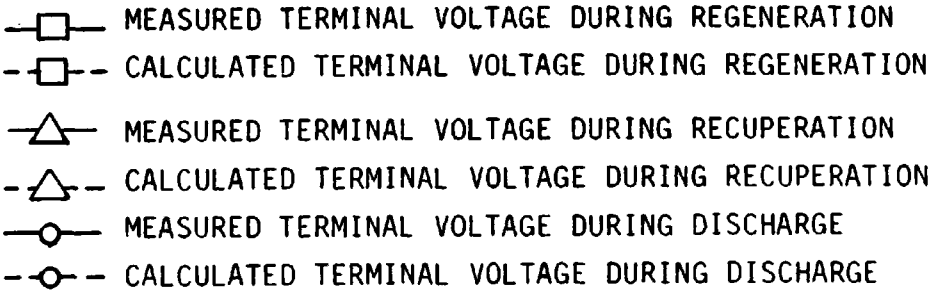

FIG. 78 RESULTS WHEN APPLYING TEST CYCLES FOR CONTINUOUS AND PULSED CURRENTS

7. CONCLUSIONS

To realise practical EV transportation, significant improvements in the efficient use of lead-acid traction batteries must be made coupled with the development of an accurate battery state indicator. To date, such developments have not been forthcoming.

There has been considerable controversy over the effects of pulsed discharge currents on the available capacity of lead-acid traction batteries. Investigations have shown that when compared to conventional continuous current discharging, pulsed current discharging can provide a considerable increase [11] in available capacity, no alteration [12, 13] in available capacity, or even a decrease [14] in available capacity. However, from the wide range of pulsed discharge tests performed by the author, it was found, as shown in Figs. 24 and 26, that for certain values of frequency, mark/space ratio and peak current of the pulsed waveform, pulsed discharge can provide up to a 27% increase in available capacity when compared to that obtained from using conventional continuous current discharging, provided the peak value of the pulsed current waveform is taken as the discharge rate and the minimum value of the pulsed voltage waveform as the termination of discharge voltage. Also, it is shown by Fig. 26 that the available capacity for pulsed discharge is inversely proportional to mark/space ratio and to a lesser extent frequency. This is likely due to a reduction in cell recovery time with decrease in the space-time of the waveform and to an increase in the rms value of current, resulting in increased i^2r losses within the cell. The variation of the effective internal resistance with time of discharge, mark/space ratio, peak value of current and frequency may also contribute to the variation in i^2r losses mentioned above. It is also interesting to note from

Fig. 24 that for certain pulsed discharge conditions no relative increase in available capacity is obtained. The results of the author's investigations, therefore, agree with the general findings of Jayne [11]. However, the results were more conservative than those obtained by Jayne, who obtained a maximum relative increase in available capacity of 68%. Additionally, Jayne's results differed from the author's in that they always showed an increase in available capacity when compared to that obtained from equivalent continuous current discharging.

Compared to using conventional continuous current charging techniques it has been said [20] that the use of depolarisation discharge pulses interspersed throughout the charging period provides a number of advantages, with the main ones being a significant reduction in charge time and an increase in charge efficiency. For example, it has been said [18] that a 190 ampere-hour lead-acid traction battery may be charged in 5-10 minutes. A previous pulsed charging investigation [66] has stated that no advantages are to be gained by using a pulsed current charging technique compared to using a continuous current charging technique. Rather, the investigation claimed that pulsed current charging causes a relative decrease in the charge ampere-hour and energy efficiencies, and an increase in cell electrolyte temperature. The results obtained by the author show that no benefits are obtained from using depolarisation discharge current charging techniques. In fact, for the tests performed this charging technique reduced the efficiency of the charge and caused an increase in cell electrolyte temperature of up to 300% when compared to using a conventional continuous current charging technique. It was shown from the pulsed charging results obtained by the author that for a three-stage charging technique, pulsed current charging offers no advantages

over continuous current charging. In fact, for the tests performed, three-stage pulsed charging has the disadvantage of increasing the total volume of gas evolved, and causing a maximum relative increase in cell electrolyte temperature of up to 16%, and reducing the ampere-hour efficiency of the charge. Single-stage pulsed current charging of a lead-acid cell offered no advantages over conventional continuous current charging. For two-stage charging, pulsed current charging offered slight advantages over continuous current charging in terms of increasing the ampere-hour efficiency of the charge, of reducing the total volume of gas evolved, and of reducing the charge time.

EV lead-acid traction batteries experience considerable variations in their operating conditions. For example, they are subjected to regenerative charging currents, and discharge currents of up to a few hundred amperes and cell electrolyte temperatures ranging from 0°C to 40°C are not unusual. Existing lead-acid battery state indicators and models either do not adequately account, or do not account at all for such variations, and also are impractical to implement, as may be appreciated from Section 6.2. Additionally, existing state indicators and models do not account for variations in cell electrolyte temperature or for the effects of pulsed discharge currents on the battery state. The voltage and state-of-charge models developed by the author, however, satisfy the requirements for a battery state indicator and model as detailed in Section 6.1. Significantly, the models accurately account for the effects of recuperation and regeneration on the battery state, and for the effects of wide variations in discharge rate and cell electrolyte temperature normally encountered by the battery in EV operation. Furthermore, an accurate pulsed discharge battery state indicator and model was derived by the author for use under the same variable operating conditions as

in the continuous current discharge case. The models were tested under dynamic conditions of operation, with realtime measurements of battery discharge parameters being made by means of a microcomputer. The models were found to be accurate.

The method used by the author for determining battery status is particularly adaptable for use onboard the EV. Microprocessor based systems for the control of the EV operation are increasingly being used, and it would be a simple task to use the microprocessor system to monitor the battery state, since the author's models only require the realtime measurement of two battery discharge parameters, these being discharge rate and cell electrolyte temperature, and the use of only a small amount of memory space. Alternatively, a cost effective dedicated microprocessor based system may be used to determine the battery state. Here again the microprocessor would require only a limited memory space, and only an interface circuit employing two input/output ports.

REFERENCES

1. Bayliss, D. : Electric Vehicles - Can They Be Fitted Into Urban Britain? Electric Vehicle Development, PPL Conference Publication Number 14.

2. Bockris, J. O'M; Drazic, D.M. : Electrochemical Science, Taylor and Francis Ltd., London, 1972.

3. Dell, R.M. and Jensen, J. : Implications of Future Large-Scale Use of Electric Vehicles in Europe, Drive Electric 80 Conference Proceedings, 14-17 October 1980.

4. Muller, H.G. and Wonk, V. : Efficiency of Coal Use, Electricity for EVs Versus Synfuels for ICEs, SAE Technical Paper Series 800109, 1980.

5. Purcell, J.O., Finlay, H. : Electric Vehicles in Fleet Service and Prospects for Volume Production, EVC Symposium V1, Baltimore Convention Center, Baltimore, Maryland, October 21-23, 1981.

6. Barak, M. : Electrochemical Power Sources, Primary and Secondary Batteries, IEE Energy Series 1. Peter Peregrinus Ltd.

7. Cook, A.R. : A Review of Battery Research and Development, Proc. of the American Power Conference, 1974, pp. 1047 - 1054.

8. Barak, M. : Batteries and fuel cells, IEE Review, Vol. 117, 1970, pp 1561 - 1583.

9. Isaac, A., Pitt, V. : Physics. Ham Lyne Publishing Group Ltd., London, 1972.

10. Rand, D.A.J. : Lead-Acid Traction Batteries for Electric Road Vehicle Propulsion - Directions for Research and Development. Jrnl. Power Services, Vol. 5, pp. 221 - 234, 1980.

11. Jayne, M.G. : An investigation into the pulsed and steady discharge of lead-acid batteries, using a thyristor chopper circuit. M.Sc. Thesis, 1973.

12. Cataldo, R.L. : Response of Lead-Acid Batteries to Chopper-Controlled Discharge : Preliminary Results. National Aeronautics and Space Administration, Lewis Research Center, Cleveland, Ohio 44135. February 1978.

13. Ahamed, T.U. : Operation of Lead/Acid Battery With Thyristor Chopper Burden. M.Sc. Thesis, 1980.

14. Kamada, K. et al : New Lead-Acid Batteries for Electric Vehicles and Approach to their Evaluation Method.

15. Jayne, M.G. : Power Sources, 6, Academic Press, London, 1977, p. 35.

16. Taylor, D.F. and Siwek, E.G. : SAE Paper 730252, Int. Autom. Eng. Cong., Detroit, U.S.A. 1973.

17. Smithrick, J.J. : Pulsed Charging of Lead-Acid Traction Cells. NASA TM - 81513, May 1980.

18. Sparks, R.H. : Rapid Charging Batteries for Electric Propulsion Systems. Paper 720109 pres. at SAE Automative Engineering Congress, Detroit, Michigan. 1972, pp. 1-13.

19. Burkett, W.B. : The Rapid Charging of Batteries. Battery Council International, April, 1971, Pheonix, Arizona.

20. Benjamin, F. : The Reflex Principle of Charging Nickel-Cadmium and Other Batteries. I.E.E.E. Power Processing and Electronics Specialists Conference. May 22, 1972, pp. 111 - 119.

21. Hayward, B.R. : Operational Experience with the Silent Carrier Delivery Van and A Review of Marketing Prospects Related to Total Costs. Electric Vehicle Development Group, Second International Conference, 23rd - 24th May 1978

22. Bevan, J., Heinburger, D.A., Metalf, M.A. : A survey of electric and hybrid simulation programs. Report No. NASA-CR-162457, Nov. 1978.

23. Nix, G.F. : Assessment of Hybrid Electric Vehicle Literature Survey. Electrical Engineering Department, University of Manchester, February 1972.

24. Langdon, E. : Interim view of London electric goods vehicle trials, Electric Vehicle Developments, November 1979.

25. Micham, A.J., Bumby, J.R. : Survey of hybrid electric vehicles, Vol. I Technical Assessment and Recommendations IRD 77/12 Research Report 1977.

26. Roan, V.P. : Diesel-Electric Hybrid Bus, SAE Paper 780294, Meeting Detroit, Feb. 27 - Mar. 3 1978.

27. Unnewehr, L., Aniler, J.E., Foote, L.R., Moyer, D.F., Stadler, H.L. : Hybrid vehicle for fuel economy. SAE Paper 760121, Detroit USA 23-27 Feb. 1976.

28. Burrows, C.R., Price, G., Perry, F.G. : An assessment of flywheel energy storage in electric vehicles. SAE Paper 800885. (See also - Automative Engineering. Vol. 88. No. 8 pp 73 - 77. Aug. 1980).

29. Lynn, D.K., McCormick, J.B., Bobbett, R.E., Deronin, C., Kerwin, W.J. : Fuel Cell Systems for Vehicular Applications. SAE Paper 800059. (See also - Automative Engineering. Vol. 88. No. 4 pp 78 - 84. April 1980).

30. Brown, D.H. : Hybrid Battery System. SAE Paper 710236. Jan. 11-15, 1971.

31. Helling, J., Schrenk, H., Giera, B. : Hybrid drive with flywheel component for economic and dynamic operation. Proc. International Electric Vehicle Symposium and Exposition Washington D.C. 19-21 Feb. 1974.

32. Bradford, M., Knights, D.E. : An outline investigation of a hybrid (COMBAT) trolley bus. Int. Conference on Economic Use of Electric Road Vehicles in a changing environment. Sheffield, England. pp 58-64 (Peter Peregrinus) 23-24 May 1978.

33. Hellewell, D.S. : An Operators Requirements and Operational Experience with Battery Electric Buses and a Consideration of Future Developments. Electric Vehicle Development Group, Second International Conference.

34. Pollack, J.J. : Some Guidelines for the Application of Adjustable Speed A.C. Drives, IEEE Trans. Ind. Appl., IA-9, 6 : pp 704 - 710, 1973.

35. Bedford, B.D. and Hoft, R.G. : Principles of Inverter Circuits, Wiley and Sons, New York, U.S.A., 1964.

36. Plunkett, A.B., Kliman, G.B. : Electric vehicle A.C. drive development. SAE Paper 800061.

37. Lawrenson, P.J., Stephenson, J.M., Blenkinsop, P.T., Corda, J., Fulton, N.N. : Variable-speed switch reluctance motors. IEE Proc. Vol. 127, Pt.B. No. 4 Mar. 1980.

38. Lee, G.A., Corbett, A.E. : Development of a hybrid electric vehicle using high efficiency disc motors. EVDG 3rd International Conference. Resources for EVs and their infrastructure. London, England. pp 79 - 87. Nov. 1979.

39. Ikeura, K., Hosaka, A., Yano, T. : Microprocessor control brings about better fuel economy with good driveability. SAE Trans. 1980 No. 800056.

40. Colliver, F.W., Wesson, W.D., Grigsby, L.L. : Microprocessor Control of an electric vehicle. 28th IEEE Vehicular Technology Conf. 1978.

41. Martinetto, F., Testa, D. : Electronic control of a hybrid propulsion system based on a Fiat 127 Engine. IEE Conference on Automotive Electronics No. 181 p 117. Nov. 1979.

42. S.A.E. Handbook. SAE Recommended Practice J227a. pp 27.07 - 27.12 1979.

43. Christian, J.M. : World guide to battery-powered road transportation, McGraw Hill, New York, 1980.

44. Cook, A.R. : Proceedings of the Symposium on Batteries for Traction and Propulsion, sponsored by Columbus Sect. of Electrochem. Soc., (1972), Fig. 24, p 101.

45. Gross, S. : Rapid charging of lead acid batteries. Conf. Record of 8th Annual Meeting of IEEE, Ind. Soc. Oct. 1973.

46. Smith, G. : Storage Batteries, Pitman.

47. Crompton traction batteries sales information brochure

48. Vinal, G.W. : Storage batteries. 4th Edition. Wiley.

49. Gladstone, J.H., Tribe, A. : Chemistry of the Planté and Faure accumulators, Nature, 25, 221 and 461, 26, 251, 342, and 602; 27, 583 (1882 - 1883).

50. Moore, W.J. : Physical Chemistry, Fifth Edition, Longman.

51. Davtyan, O.K. : The Capacity of Acid Storage Batteries, Bull. acad. sci. U.S.S.R., Classe sci. teck., 737 (1946).

52. Fick, A. : Uber Diffusion, Pogg. Annalen, 94, 59 (1855).

53. Schroeder, L. : Berecknung von Akkumulatoren fur Elektricitatsinerke, Elektrotech, S. 12, 585 (1891).

54. Leibenow, C. : Uber die Berechnung der Kapazitateines Bleiakkumulators fer variabeler stromstarke, S. Elecktrochem, 4, 63 (1897).

55. Peukert, W. : Uber die Abhangigkeit der Kapacitat von der Entladestromatarke bei Bleiakkumulatoren, Elektroteck, S. 18, 287 (1897).

56. Rabl, M. : Berecknung der Kapazitat von Bleiakkumulaturen bei Teilweiserent - ladung bis zu beliebigen Spannungsgrezen Anderung de Kapazitatsjurven mit der Temperature, S. Elektrochem., 42, 114 (1936).

57. Jumau, J. : Sur Le Role De La Diffusion Dans Le Fonctionnements Des Plaques Positines De L'Accumulateur Au Plomb, Revue D'Electricite, 3 September, 1898.

58. General Electric : Silicon Controlled Rectifier Manual, Sixth Edition.

59. Willihnganz, E., Rohher, P. : Battery Impedance. Electrical Engineering, Vol. 922, pp 922 - 925, 1959.

60. Mandil, J. : Main experiments carried out to date, Fourth International Electric Vehicle Symposium, Dusseldorf, 31st August - 2nd September 1976.

61. Berndt, D., and Voss, E. : The voltage characteristics of a lead-acid cell during charge and discharge. In Collins, D.H. (Ed.) Batteries 2 (Pergamon Press Ltd., Oxford, 1965), pp 17 - 27.

62. Mas, J. : The Charging Process. Proc. 2nd Int. Elect. Vehicle Symp. Atlantic City, N.J., U.S.A. pp 228 - 246, 1971.

63. Rippel, W.E. : Charge Acceptance Characteristics of the Lead-Acid Cell. Proc. 2nd Int. Elect. Vehicle Symp., Atlantic City, N.J., U.S.A. pp 247 - 274, 1971.

64. Peters, K., Harrison, A.I., and Durant, W.H. : Charge Acceptance of the Lead Cell at Various Charging Rates and Temperatures. Collins, D.H., Power Sources 2 1963, pp 1 - 16.

65. Smithrick, J.J. : Rapid, Efficient Charging of Lead-Acid and Nickel Zinc Traction Cells, Proc. 13th Intersociety Energy Conversion, Engng, Conf., 1978.

66. Smithrick, J.J. : Pulsed Charging of Lead Acid Traction Cells, NASA TM - 81513, May 1980.

67. Dolezalek, F. : Theory of the Lead Accumulator, p 80, tr. by von Ende, John Wiley and Sons, New York, 1904.

68. Ref. 48, p. 181.

69. Shepherd, C.M. : Design of Primary and Secondary Cells. II. An Equation Describing Battery Discharge. Jnl. of Electrochem. Soc., Vol. 112, pp 657 - 664, 1965.

70. Hoxie, E.A. : Some Discharge Characteristics of Lead Acid Batteries, A.I.E.E. Trans., Vol. 73, Part 2, pp 17-22, 1954.

71. Taylor, D.F. and Siwek, E.G. : The Dynamic Characterisation of Lead-Acid Batteries for Vehicle Applications, International Automative Engineering Congress, Detroit, Mich., January 8 - 12, 1973.

72. Chang, Ming-Cheng : Computer Simulation of an Advanced Hybrid Electric-Powered Vehicle, Society of Automative Engineers. Paper 780217, March 1978.

73. Heldt, J. and Canders, W.R. : Experimentally Supported Simulation of a Lead Battery Used as an Energy Store for Electric Cars, Elektrotechnische Zeitung, 1978, 99 (6), 342-347

74. Visscher, W. : Battery State of Charge Model for Driving Cycle Operation, Drive Electric, 25-28 October 1982, Amsterdam.

75. Bozek, J.M. : An Averaging Battery Model for a Lead-Acid Battery Operating in an Electric Car, National Aeronautics and Space Administration, Lewis Research Center, December 1979.

76. Martin, H.L. and Goodson, R.E. : New Concepts in Battery Performance Simulation and Monitoring, EV Expo 80, Cervantes Convention Center, St. Louis, Missouri, May 20 - 22, 1980.

77. Hind, M. : Ph.D. Thesis, University of Bristol.

78. Richardson et al : System design implications of electric and hybrid vehicles, Intersociety Energy Conversion Conference, Binlder Colarado. Paper No. 689109, Aug. 1968, pp 789 - 796.

79. Bode, H. : Lead-Acid Batteries.

80. West, R. : Programming the PET/CBM.

81. CIL Microsystems, multipurpose computer interface, Model PC 1 6100

ACKNOWLEDGEMENTS

The author gratefully acknowledges the advice and encouragement of Dr. M.G. Jayne, Principal Lecturer of the Electrical and Electronic Engineering Department, The Polytechnic of Wales, who supervised the research to which this thesis relates.

Great appreciation and thanks are expressed to Mr.G.H. Thompson former Head of the Electrical and Electronic Engineering Department, for his substantial support of the research, and also to Mr.P.A.Witting the present head of the department for his co-operation in preparing this thesis.

The author also wishes to express his gratitude to the Director, Deputy Directors and the Governing Body of The Polytechnic of Wales for supporting his application for registration with the C.N.A.A., and provision of the examination facilities.

The author also wishes to thank The Polytechnic of Wales for the services provided, and the technical staff of the Electrical and Electronic Engineering Department for the construction of experimental equipment.

Great appreciation is expressed to the Science and Engineering Research Council (S.E.R.C.), without who's financial support the project could not have been undertaken.

Finally, gratitude is expressed to all those authors of the many texts which have been utilised in support of this research.

APPENDIX I: CHOPPER CIRCUITS

1.1 The Bi-Polar Transistor Chopper

The chopper circuit is shown in Fig. 79. The pre-amplifiers TrA and TrB set the current levels for transistors Tr1 to Tr19, and hence the operating current level of the chopper. The base currents of TrA and TrB are adjusted by means of the current regulator, the circuit diagram of which is shown in Fig. 80. In Fig. 80, T1 acts as an emitter follower, which together with ZG_1 produces a regulated positive voltage for OP-07; a regulated negative voltage is supplied to OP-07 by means of ZG_2. The voltage input to OP-07 is adjusted by means of R_c, which, therefore, varies the output of the amplifier and hence the operating current of the chopper unit. Short circuit protection of the amplifier is provided by the 300 ohm resistor at the output of pin 6 of the amplifier, and the 20 K resistor at pin 1 is used as the offset voltage adjust.

Pins 1 and 3 of the remote contact (Fig. 79) may be used to control the operation of the chopper unit; with the arrangement shown the unit is enabled, however, by shorting the two pins the unit may be disabled. Using the remote contact, it is possible to operate the unit in the pulsed or continuous current mode. To achieve pulsed current operation, a reed relay was connected across the remote contact pins, and the relay operated by means of a pulse generator unit.

1.2 The Thyristor Chopper

1.2.1 Analysis of the Chopper Circuit

In the following analysis the static and switching characteristics of the rectifiers and thyristors are assumed ideal, except for the turn-off time required by the thyristors. Forward voltage drop, inverse leakage currents, inverse recovery current, and

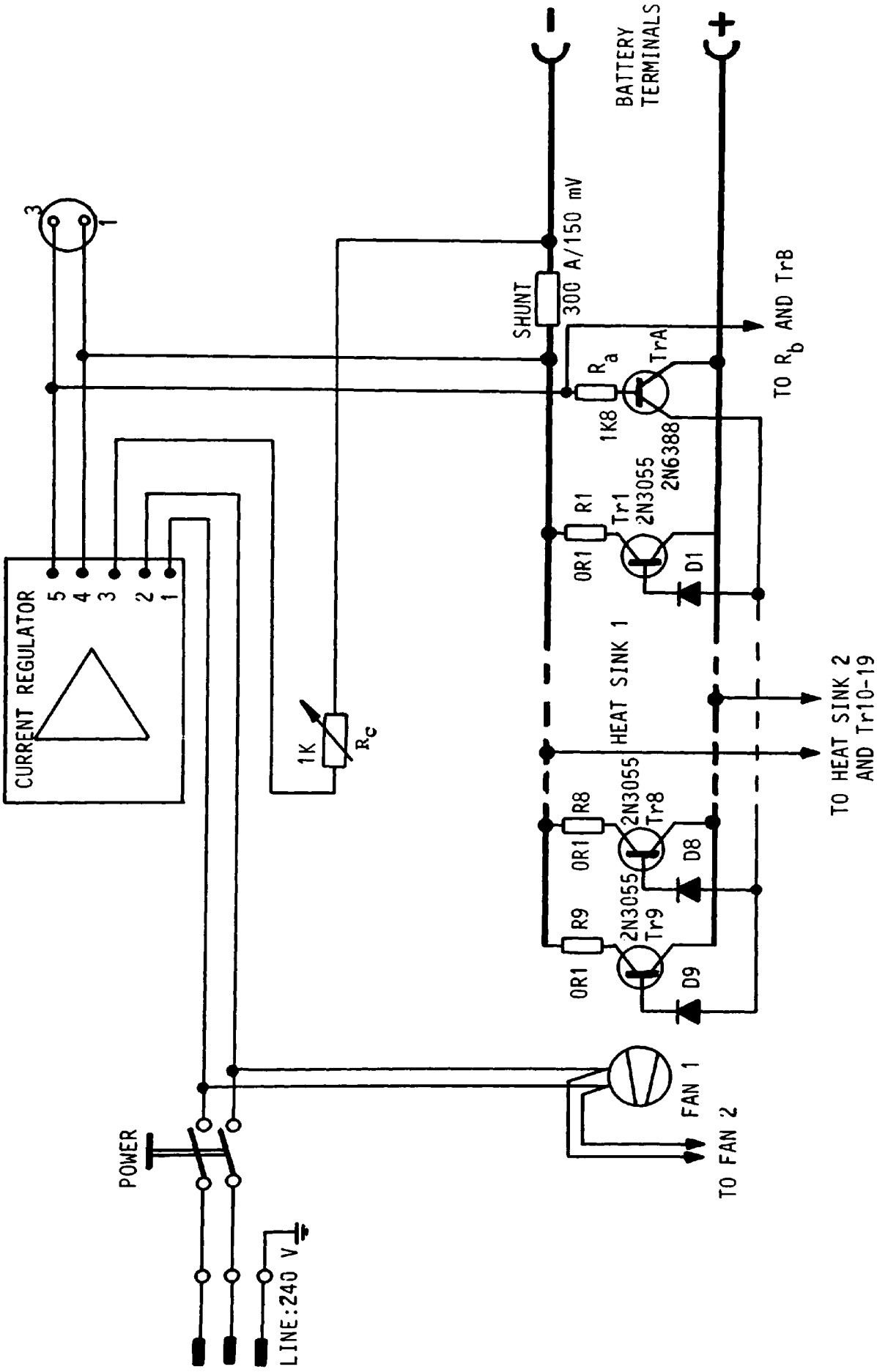

FIG. /9 DISCHARGE FACILITY

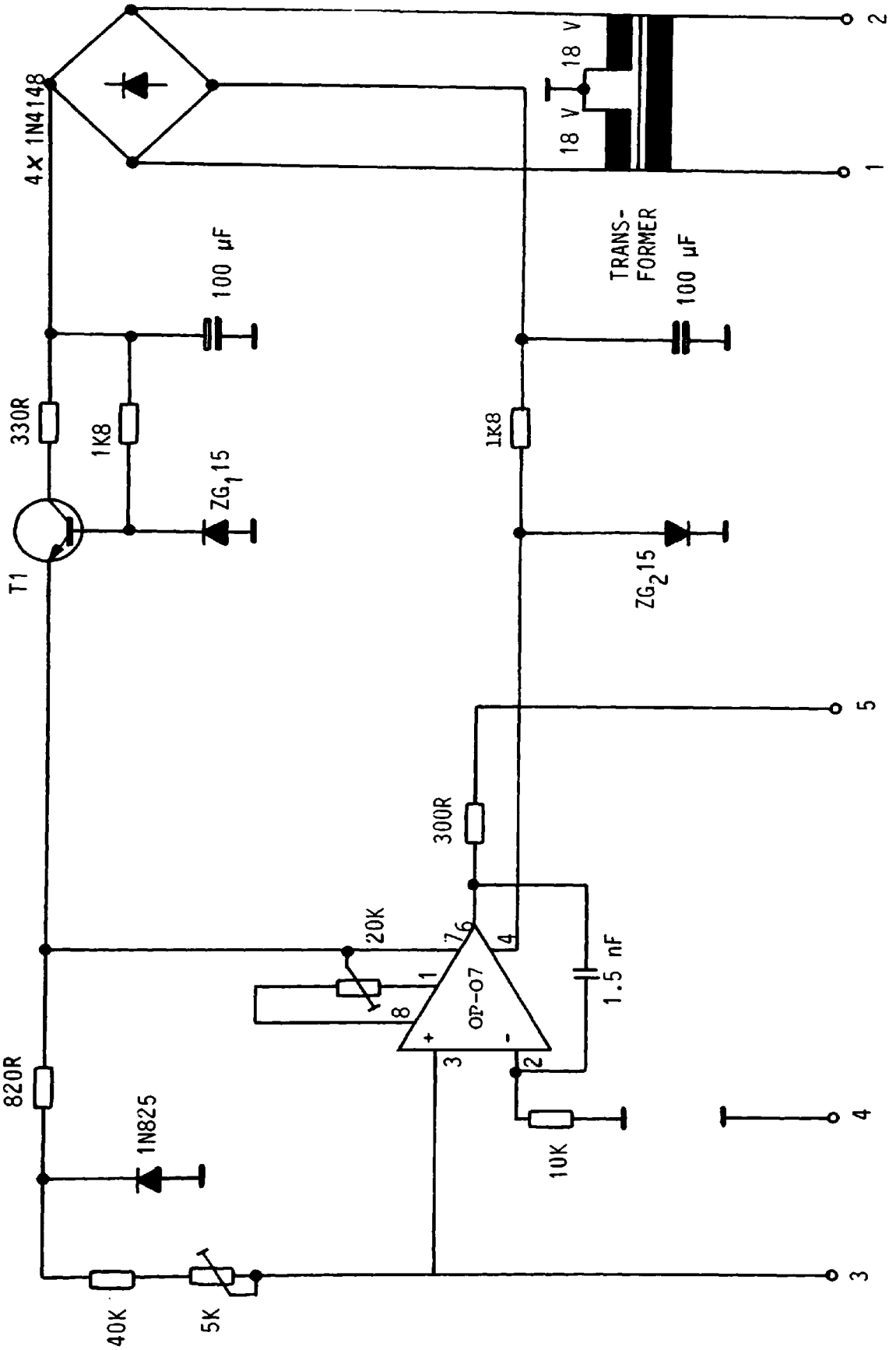

FIG. 80 CURRENT REGULATOR CIRCUIT

turn on time are negligible. The inductance of the battery is also neglected.

The chopper circuit is shown in Fig. 81. Chopper operation is initiated by turning thyristor T_2 'on', which allows capacitor C to charge according to the circuit of Fig. 82(a).

Let $R_b + R_L + r_{T2} = R_2$

At time $t = 0(+)$, $i_{C2} = \frac{V_b}{R_2}$ and $V_{C2} = 0$

$V_b = i_{C2}R_2 + V_c$

Therefore $V_b = i_{C2}R_2 + \frac{1}{C}\int i_{C2}dt$

The Laplace transform of the above equation becomes:

$$\frac{V_b}{s} = i_{C2}(s).R_2 + \frac{i_{C2}(s)}{C.s}$$

$$\text{Therefore } i_{C2}(s) = \frac{V_b}{s(R_2 + \frac{1}{C.s})} = \frac{V_b/R_2}{(s + \frac{1}{CR_2})}$$

The inverse Laplace transform of this equation gives:

$$i_{C2} = \frac{V_b}{R_2} e^{-t.C.R_2}$$

$V_C = \frac{1}{C}\int i_{C2}dt$, which gives

$$V_C = V_b\,(1 - e^{-t/C.R_2}) \qquad (64)$$

The turn 'on' of thyristor T1 and T3 provides a circuit for the load current and the discharge of capacitor C. The equivalent circuit for this mode is Fig. 82(b).

Let $R_1 = r_{D1} + R_{T3.T1} + r_L$

At time $t = 0(+)$, $V_{C1} = -V_b$, and $i_{C1} = 0$.

$$0 = V_{C1} + L\frac{di_{C1}}{dt} + i_{C1}R_1$$

Therefore $0 = \frac{1}{C}\int i_{C1}\,dt - V_b + L\,\frac{di_{C1}}{dt} + i_{C1}R_1$

The Laplace transform of this equation is:

$$0 = \frac{i_{C1}(s)}{s.C.} + s.L.\ i_{C1}(s) - \frac{V_b}{s} + R_1\ i_{C1}(s)$$

$$\text{Therefore } i_{C1}(s) = \frac{\frac{V_b}{L}}{s^2 + \frac{R_1}{L}s + \frac{1}{L.C}}$$

Let $\frac{1}{L.C} = W_o^2$, $\alpha = \frac{R_1}{2L}$ and $W^2 = W_o^2 - \alpha^2$

$$\text{then } i_{C1}(s) = \frac{\frac{V_b}{L}}{(s+\alpha)^2 + W^2}$$

the inverse Laplace transform of this equation gives:

$$i_{C1} = \frac{V_b}{L.W}\ e^{-\alpha t}\ \text{Sin}\ W.t$$

$$\text{or } i_{C1} = \frac{V_b}{L.W}\ e^{-\alpha t}\ \text{Cos}\ (W.t - \frac{\pi}{2}) \qquad (65)$$

If R_1 is small, $W_o^2 \gg \alpha^2$

$W \approx W_o$

$$\text{Therefore } L.W \approx L.W_o = \sqrt{\frac{L}{C}} = \frac{1}{W_o C}$$

$$\text{Also } \frac{\alpha}{W_o} = \frac{R_1}{2W_oL} = \frac{1}{2Q}\ \text{, where } Q = \frac{X}{R_1}$$

$$\text{Therefore } i_{C1} \approx \frac{V_b}{X}\ e^{-\frac{W_o t}{2Q}}\ \text{Cos}\ (W.t - \frac{\pi}{2}) \qquad (66)$$

The voltage across the capacitor, C is given by:

$$V_{C1} = \frac{1}{C}\int i_{C1}\,dt - V_b$$

The Laplace transform of this equation is:

$$V_{C1}(s) = \frac{i_{C1}(s)}{s.C.} - \frac{V_b}{s}$$

Substituting for $i_{C1}(S)$ from previous equation gives:

$$V_{C1}(s) = \frac{\dfrac{V_b}{s.L.C.}}{s^2 + \dfrac{R_1}{L}\, s + \dfrac{1}{L.C}} - \frac{V_b}{s}$$

$$\text{Therefore } V_{C1}(s) = s\left[\frac{\dfrac{V_b}{C.L}}{(s + \dfrac{R_1}{2L})^2 + (\dfrac{1}{L.C} - \dfrac{R_1^2}{4L^2})}\right] - \frac{V_b}{s}$$

$$V_{C1}(s) = \frac{\dfrac{V_b}{C.L}}{s\left[(s+\alpha)^2 + W^2\right]} - \frac{V_b}{s}$$

By partial fraction,

$$V_{C1}(s) = \frac{V_b}{C.L\ (\alpha^2 + W^2)}\left[\frac{1}{s} - \frac{s+2}{(s+\alpha)^2 + W^2}\right] - \frac{V_b}{s}$$

The inverse Laplace transform of this equation is:

$$V_{C1} = -V_b + \frac{V_b}{C.L\ (\alpha^2 + W^2)}\left[1 - \frac{K}{W} e^{-\alpha t} \operatorname{Sin}(W.t + \Psi)\right]$$

where $\Psi = \tan^{-1}\dfrac{W}{2\alpha - \alpha} = \tan^{-1}\dfrac{W}{\alpha}$

and $K = \left[(2\alpha - \alpha)^2 + W^2\right]^{1/2} = \sqrt{\alpha^2 + W^2} = \dfrac{1}{\sqrt{L.C}} = W_o$

Therefore $V_{C1} = -V_b \cdot \dfrac{W_o}{W} e^{-\alpha} \operatorname{Sin}(W.t + \Psi)$

$$V_{C1} = V_b \cdot \frac{W_o}{W} e^{-\alpha t} \operatorname{Cos}\left[(W.t + \Psi) - \frac{\pi}{2}\right]$$

If the same assumption is made as was made earlier, mainly

$W \approx W_o$ and $W_o \gg \alpha$

then $\frac{W_o}{W} \approx 1$ and $\Upsilon = \tan^{-1} \frac{W}{\alpha} \approx \frac{\pi}{2}$

Therefore $V_{C1} \approx V_b \, e^{-\frac{W.t}{2Q}} \quad \text{Cos } W.t$ (67)

During the commutation period of thyristors T1 and T3, the equivalent circuit of the chopper is given by Fig. 82(c). After T1 and T3 have turned 'off' $R_{T1.T3}$, and the equivalent circuit may be modified as shown in Fig. 82(d).

Let $r_b + R_L + R_{T2} = R_2$

At time $t = 0(+)$, $V_C = -V_b$

Therefore $V_b = i.R_2 + V_C$

$$V_b = i.R_2 + \frac{1}{C} \int idt - V_b$$

Laplace transform of this equation is:

$$\frac{2V_b}{s} = i(s).R_2 + \frac{i(s)}{C.s}$$

$$\text{Therefore } i(s) = \frac{2V_b}{R_2} \; \frac{1}{\left(s + \frac{1}{CR_2}\right)}$$

The inverse Laplace transform of this equation is:

$$i = \frac{2V_b}{R_2} \; e^{-\frac{t}{C.R_2}} \qquad (68)$$

The voltage V_C across capacitor C, is given by:

$$V_C = \frac{1}{C} \int i \, dt - V_b$$

Laplace transform of this equation is:

$$V_C(s) = \frac{i(s)}{C.s} - \frac{V_b}{s}$$

substituting for i(S) gives:

$$V_C(s) = \frac{2V_b}{C.R_2\, s\,(s + \frac{1}{C.R_2})} - \frac{V_b}{s}$$

By partial fractions,

$$V_C(s) = 2V_b \left[\frac{1}{s} - \frac{1}{s + \frac{1}{C.R_2}} \right] - \frac{V_b}{s}$$

The inverse Laplace transform of this equation gives:

$$V_C = V_b\,(1 - 2e^{-t/C.R_2}) \qquad (69)$$

The turn 'off' time for thyristor T2 is the interval between t = 0 and the instant when $V_C = 0$, therefore

$$0 = V_b\,(1 - 2e^{-t/C.R_2})$$

and $t = 0.69R_2.C$ (70)

The only current which flows through diode D1 and choke L, is current i_{C1}. The peak and mean values of i_{C1} can be calculated using equation (65) as follows:

$$i_{C1}\,(\text{peak}) = \frac{V_b}{L.W} = \frac{V_b}{L/\sqrt{L.C}}$$

Therefore $i_{C1}\,(\text{peak}) = V_b\sqrt{C/L}$ (71)

It must be remembered that the oscillatory current i_{C1}, only flows for one half-cycle, during one cycle of operation of the 'chopper'.

Therefore, half periodic time = $\pi\sqrt{L.C} = \frac{\pi}{W_o} \approx \frac{\pi}{W}$

Let time for one cycle of 'chopper' operation = T.

Therefore $i_{C1}\,(\text{mean}) = \frac{1}{T}\int_0^{\pi/W} \frac{V_b}{L.W}\, e^{-\alpha t}\, \text{Cos}\,(W.t - \frac{\pi}{2}).\, dt.$

Using integration by parts, the above equation may be reduced to the following:

$$i_{C1(mean)} = \frac{V_b}{L.T.W^2} \frac{1}{(1 + \frac{\alpha}{W})} \left[e^{-\alpha t} \left(\text{Sin}\ (W.t - \frac{\pi}{2}) - \text{Cos}\ (W.t - \frac{\pi}{2}) \right) \right]_0^{\pi/W}$$

$$i_{C1(mean)} = \frac{V_b.C}{T} + \frac{V_b.C}{T} \; e^{-\frac{\alpha.\pi}{\sqrt{L.C}}}$$

$$\text{Therefore } i_{C1(mean)} = \frac{V_b.C}{T} \left[1 + e^{-\frac{\alpha.\pi}{\sqrt{L.C}}} \right] \qquad (72)$$

The peak and mean values of the current through the thyristor T2, can be calculated as follows:

$$i_{T2}\ (peak) = \frac{2V_b}{R_2}\ , \text{ from equation (68)} \qquad (73)$$

The period over which T2 conducts, is given by:

$t = 0.69R_2.C$, from equation (70)

If the period over which the thyristor chopper operates is given by T, then :

$$\text{mean value of } i_{T2} = \frac{1}{T} \int_0^{0.69R_2.C} \frac{2V_b}{R_2} e^{-\frac{t}{CR_2}}\, dt.$$

$$\text{mean value of } i_{T2} = \frac{2V_b}{T.R_2} (-C.R_2) \left[e^{-\frac{t}{C.R_2}} \right]_0^{0.69R_2.C}$$

$$\text{Therefore } i_{T2(mean)} = \frac{2V_b.C}{T} \left[1 - e^{-0.69} \right] \qquad (74)$$

The peak and mean current which flows through thyristors T1 and T3 can be calculated using equation (65) and the steady state relationship:

$$I_{T1.T3} = \frac{V_b}{R_2}$$

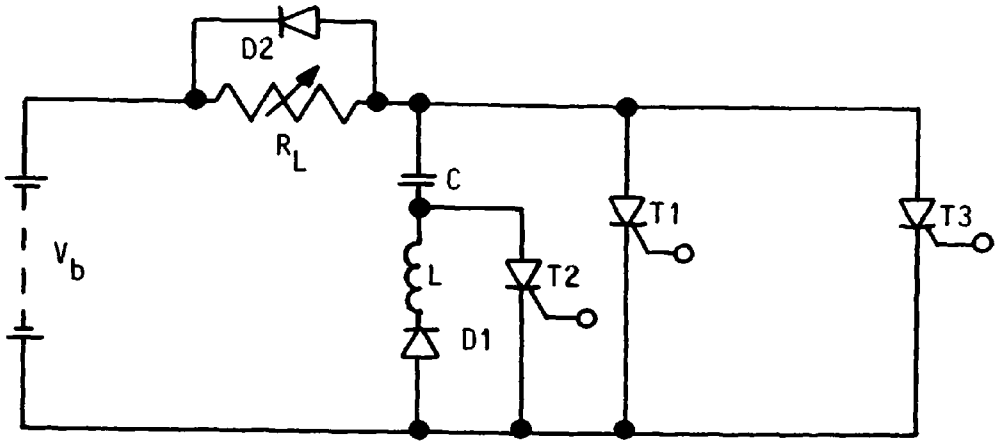

FIG. 81 CHOPPER CIRCUIT

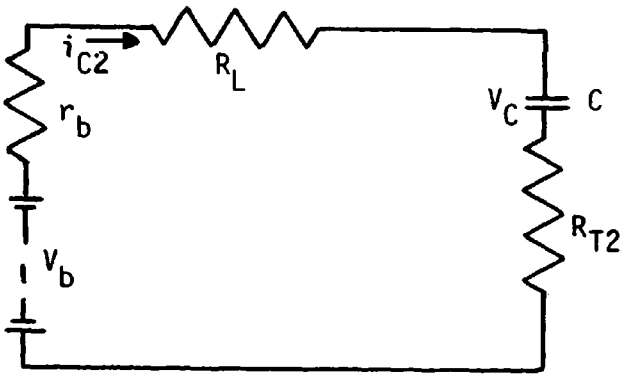

FIG. 82(a)

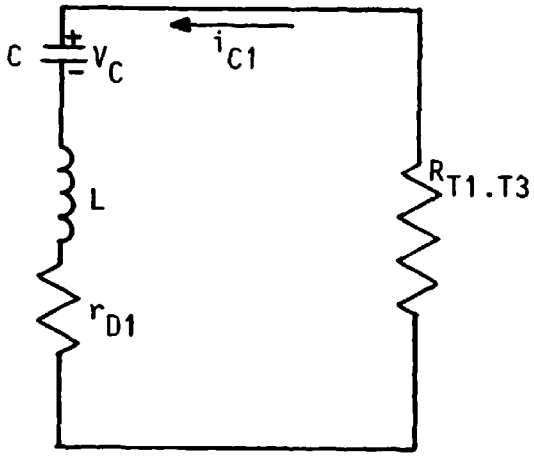

FIG. 82(b)

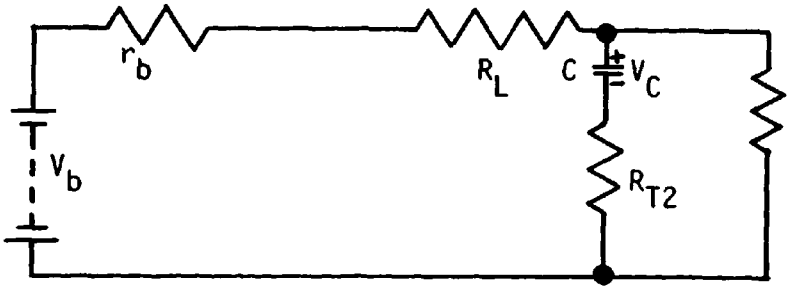

FIG. 82(c)

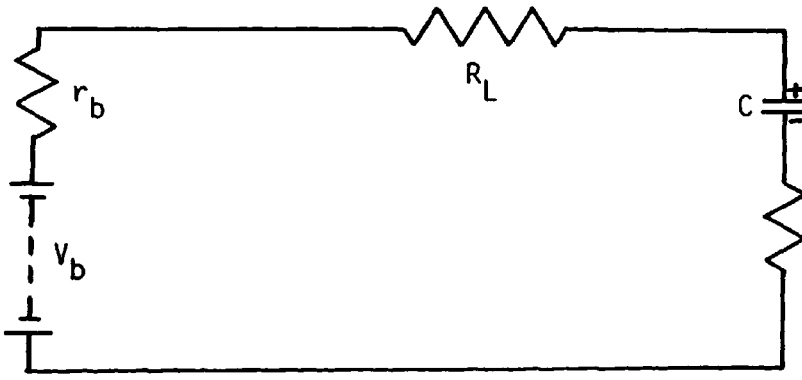

FIG. 82(d)

FIG. 82 INTERMEDIATE EQUIVALENT CIRCUITS

Therefore $i_{T1.T3}$ (peak) $= \frac{V_b}{R_2} + \frac{V_b}{L.W} = V_b\left(\frac{1}{R_2} + \sqrt{\frac{C}{L}}\right)$

$$i_{T1.T3} \text{ (peak)} = V_b\left(\frac{1}{R_2} + \sqrt{\frac{C}{L}}\right) \qquad (75)$$

The mean value of $i_{T1.T3}$ can be calculated as follows:

$$i_{T1.T3} \text{ (mean)} = \frac{1}{T}\left[\int_0^{T1\ ON} \frac{V_b}{R_2}\,dt + \int_0^{\pi/W} \frac{V_b}{L.W}\, e^{-\alpha t}\, \text{Cos}\,(W.t - \frac{\pi}{2})\,dt\right]$$

The 'on' time of thyristors T1 and T3 can be related to M and the periodic time T, as follows:

$$T_1 \text{ on} = \frac{T \times M}{M + 1} = \frac{T}{(1 + \frac{1}{M})}$$

$$\text{Therefore } i_{T1.T3} \text{ (mean)} = \frac{V_b}{R_2\,(1 + \frac{1}{M})} + \frac{V_b.C}{T}\left[1 + e^{-\frac{\alpha.\pi}{\sqrt{L.C}}}\right] \qquad (76)$$

1.2.2 Design Criteria for Chopper Circuit

The chopper was required to work from a voltage source of 72 V, since this is the usual voltage limit for an EV battery. The maximum value of the mean load current was 70 amperes.

The specifications for the chopper are as follows:

Maximum working voltage = 80 V

Minimum working voltage = 30 V

Maximum mean value of current pulse = 70 A

Maximum operating frequency = 500 Hz

(governed by control circuit)

Mark/space ratio (M) limits: $1/9 < M < 9/1$

Therefore, at 500 Hz:

Minimum t_{on} = minimum t_{off} = 0.2 milliseconds.

Maximum t_{on} = maximum t_{off} = 1.8 milliseconds.

Recommended 'turn-off' time for the thyristors was 25 μ seconds. Using equation (70) of Appendix 1.2.1,

$$t_2 = 0.69 R_2 C$$

where $R_2 = V_{mn}/I_{av}$ = 30/70 = 0.43 ohm, and t_2 = 25 μseconds.

Therefore $C > \dfrac{25 \times 10^{-6}}{0.69 \times 0.43}$ = 84.26 μF

A 250 μF capacitance was used.

The time required to build-up a commutating charge on C is equal to 1/2 of the periodic time of the oscillatory current in the commutating circuit. This value of time must be less than the shortest 'on-time' of the main thyristor, therefore from the analysis of Appendix 1.2.1

$$\pi \sqrt{L.C} < 0.2 \text{ milliseconds}$$

Therefore $L < \dfrac{(0.2 \times 10^{-3})^2}{250 \times 10^{-6} \times \pi^2}$ = 16.21 μH

A 100 μH air cored inductor was used.

The peak value of current which the inductance and catching diode D1 have to withstand can be calculated using equation (71) of Appendix 1.2.1

i_{C1} (peak) = $V_b \sqrt{C/L}$

Therefore i_{C1} (peak) = V_b (peak) $\sqrt{C/L}$ = $80 \times \sqrt{\dfrac{250 \times 10^{-6}}{100 \times 10^{-6}}}$

= 127 A maximum

The mean value of the current i_{C1} may be calculated using equation (72) of Appendix 1.2.1. If it is assumed that the term in

$$i_{C1}\ (\text{mean}) = \frac{V_b.C\ (1 + e^{-\alpha\pi\sqrt{LC}})}{T}$$

brackets, $e^{-\alpha\pi\sqrt{LC}}$, is very small then,

$$i_{C1}\ (\text{mean}) = \frac{V_b.C}{T}$$

$$= \frac{V_b(\text{peak})}{T(\text{mn})} = \frac{80 \times 250 \times 10^{-6}}{2 \times 10^{-3}}$$

$$= 10 \text{ A maximum}$$

A diode with a peak current rating of 200 A, a mean current rating of 13 A and a peak-inverse voltage rating of 400 V was used.

The peak value of current which flows in the auxiliarly thyristor is given by equation (68) of Appendix 1.2.1.

$$i(\text{peak}) = \frac{2.V_b}{R_2(\text{mn})} = \frac{2x80}{30/70} = 373 \text{ A}$$

The mean current in the auxiliarly thyristor can be calculated using equation (74) of Appendix 1.2.1. An available thyristor was used

$$i(\text{mean}) = \frac{2\times80\times250 \times 10^{-6}\ (1 - e^{-0.69})}{2\times10^{-3}}$$

$$= 10 \text{ A maximum}$$

whose ratings were well in excess of these requirements.

The peak current of the main thyristor can be calculated using equation (75) of Appendix 1.2.1.

$$i_{T1.T3} = V_b(\text{peak}) \left[\frac{1}{R_2} + \sqrt{\frac{C}{L}}\right]$$

$$= 80 \left[\frac{1}{0.43} + \sqrt{\frac{250x10^{-6}}{100x10^{-6}}}\right]$$

$$= 313 \text{ A maximum.}$$

The mean current rating of the main thyristor can be calculated using equation (76) of Appendix 1.2.1.

$$i_{T1.T3} = \frac{V_b(peak)}{R_2\ (1 + 1/M)} + \frac{V_b.C}{T}$$

where $e^{-\alpha\pi/\sqrt{LC}}$ is assumed zero.

Therefore $i_{T1.T3} = \frac{80}{0.43\ (1 + 1/9)} + \frac{80 \times 250 \times 10^{-6}}{2 \times 10^{-3}}$

$= 178$ A maximum.

1.2.3 The Main and Auxiliary Thyristor Triggering Circuits

A schematic diagram of the thyristor chopper triggering module is shown in Fig. 83.

The 8038CC waveform generator provides the basis for the triggering module. This integrated circuit is capable of producing sine, square, triangular, sawtooth, ramp and pulse waveforms. The 741 operational amplifier provided output buffering, and was also used to adjust the mark/space ratio of the output waveform. This involved comparing the triangular output waveform (pin 3 of 8033CC chip), which is symmetrical about zero, with a variable d.c. voltage level. The frequency of the outputs of the waveform generator are dependent on the value of resistance connected to pins 4 and 5 of the waveform generator and the value of capacitance connected to pin 10.

The rectangular output waveform of the 741 operational amplifier was passed through NOR (MM74C02N) and NAND (MM74C00N) gates, to produce two separate pulse trains. In this way, the thyristor gates were fired by a burst of pulses rather than one pulse, to ensure their operation. The 741S operational amplifiers buffer the C-MOS oscillator outputs.

The main voltage supply associated with the thyristor circuit is isolated from the control module by means of a pulse transformer. In order that the 741S operational amplifier was not distorted in an effort to drive, a Darlington pair configuration was used.

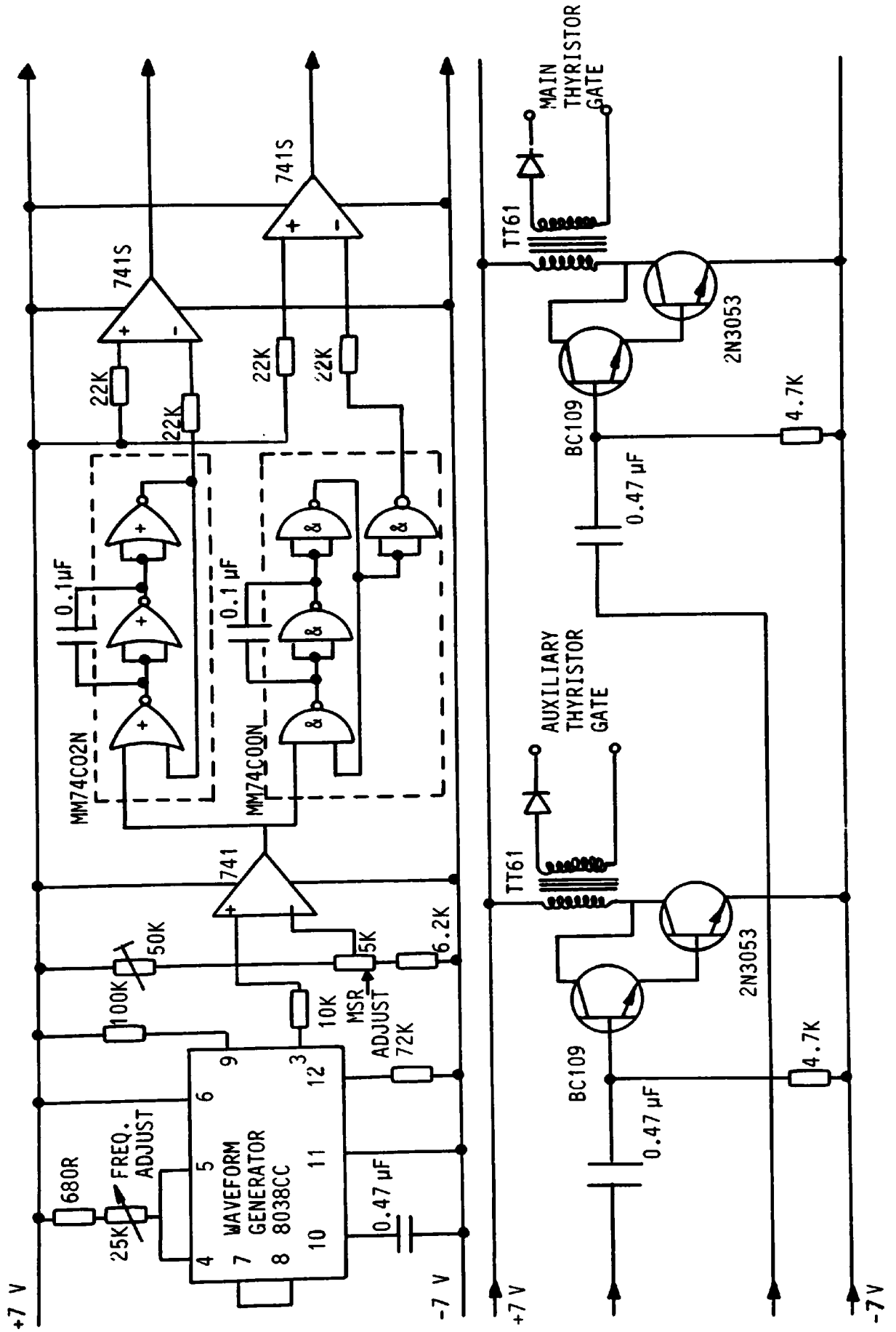

FIG. 83 THE THYRISTOR CHOPPER TRIGGERING CIRCUIT

APPENDIX 2: THE RMS VALUE OF A PULSED CURRENT WAVEFORM

The rms value of a function f(t) is:

$$\text{rms} = \left[\frac{1}{b-a} \int_a^b f(t)^2 \, dt \right]^{1/2} \tag{77}$$

Referring to the current waveform of Fig. 84, and letting $b - a = T$; and $t_m = \tau$.

$$\text{rms} = \left[\frac{1}{T} \int_t^{t+\tau} I^2_{pk} \cdot dt \right]^{1/2}$$

$$\text{rms} = \left[\frac{1}{T} \left(I^2_{pk} \cdot t \right)_t^{t+\tau} \right]^{1/2}$$

$$\text{rms} = \left[\frac{1}{T} I^2_{pk} \cdot \tau \right]^{1/2}$$

$$\text{rms} = I_{pk} \left[\frac{\tau}{T} \right]^{1/2} \tag{78}$$

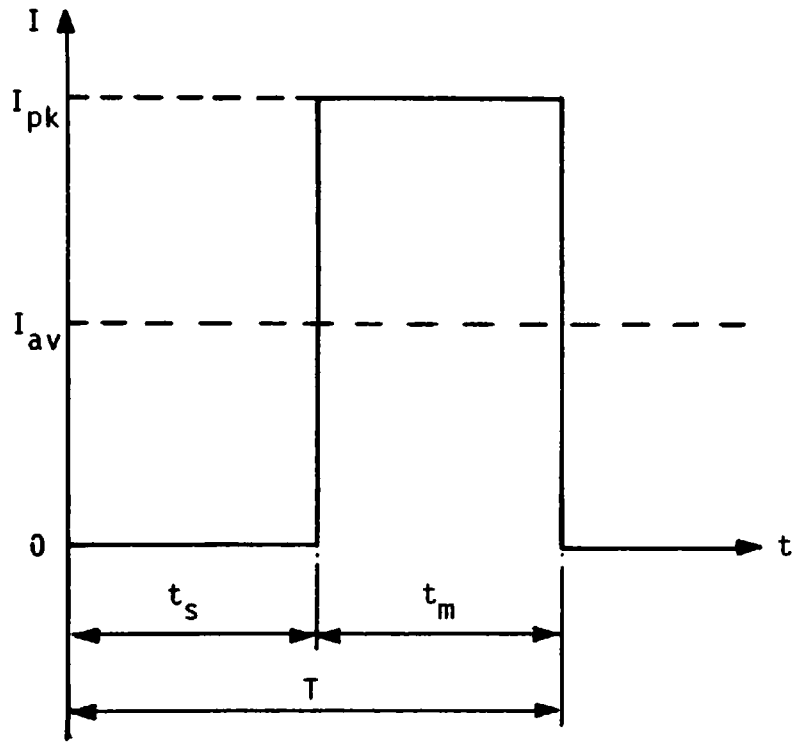

FIG. 84 PULSED CURRENT WAVEFORM

APPENDIX 3: THE ACID CONCENTRATION CURVE AND RECUPERATION

The variation of electrolyte acid concentration with reference to the cell electrode, is a function of time and distance from the electrode. Under these conditions, the diffusion process occuring within the electrolyte is defined by Fick's Second Law of Diffusion which may be expressed as:

$$\frac{dc}{dt} = D.\frac{\partial^2 c}{\partial x^2} \qquad (79)$$

where: c = the acid concentration, gram ions/cm^3

t = time, second.

x = distance in direction of transfer, cm

D = the diffusion coefficient, cm^2/second.

It is assumed that for the above equation, the boundary conditions at the electrode are:

$$\text{at } x = 0, \quad \partial c/\partial x = Nd/c \qquad (80)$$

$$\text{at } t = 0, \quad c = c_b \qquad (81)$$

where: Nd = the rate of removal of ions at the electrode, and

c_b = original uniform concentration.

Applying Laplace Transform techniques on equations (79) and (80),

equation (79) becomes : $sF - c_b = D\frac{\partial^2 F}{\partial x^2}$ (82)

where: $F = \mathcal{L}(c)$, and $\mathcal{L}$ = Laplace transform

and equation (80) becomes : $\frac{\partial F}{\partial x} \quad \frac{1}{s} \cdot \frac{Nd}{D}$ (83)

From equation (82) we may obtain the linear differential equation:

$$\frac{\partial^2 F}{\partial x^2} - \frac{s}{D} \cdot F = -\frac{c_b}{D} \qquad (84)$$

Equation (84) can be solved to give:

$$F = Ae^{\sqrt{(s/D)}x} + Be^{-\sqrt{(s/D)}x} + \frac{1}{s} \cdot c_b$$

If we assume that F and c must be finite for all x, then the positive exponential term must be removed, that is, A = 0.

$$\text{Therefore } F = Be^{-\sqrt{(s/D)}x} + \frac{1}{s} \cdot c_b \qquad (85)$$

Differentiating equation (85) and equating the result to equation (83) gives:

$$\frac{\partial F}{\partial x} = -\sqrt{\frac{s}{D}} \cdot Be^{-\sqrt{(s/D)}x} = \frac{1}{s} \cdot \frac{Nd}{D} \quad \text{at } x = 0$$

$$\text{Therefore } B = -\frac{Nd}{\sqrt{D}} \cdot \frac{1}{\sqrt{s^3}} \qquad (86)$$

Substituting equation (86) into equation (85) gives:

$$F = -\frac{Nd}{D} \frac{1}{s^{3/2}} .e^{-\sqrt{(s/D)}x} + \frac{1}{s} \cdot c_b$$

From standard Laplace tables:

$$\frac{1}{\sqrt{s}} .e^{-x\sqrt{(s/D)}} \Rightarrow \frac{1}{\sqrt{\pi t}} .e^{-x^2/4Dt}$$

Therefore $\frac{1}{s^{3/2}} \cdot e^{-x\sqrt{(s/D)}} = \frac{1}{\sqrt{\pi}} \int_0^t \frac{1}{t^{1/2}} e^{-x^2/4Dt} \cdot dt$

Therefore $c(x,t) = \mathcal{L}^{-1}(F) = c_b - \frac{Nd}{D} \cdot \frac{1}{\sqrt{\pi}} \int_0^t \frac{1}{t^{1/2}} e^{-x^2/4Dt} \cdot dt$ (87)

The rate of removal of ions at the electrode, Nd, may be defined by:

$$Nd = \frac{I(1 - T)}{nF} \quad (88)$$

where: I = discharge rate, A

T = transference number (the fraction of current carried by a given ion in solution)

n = the valence charge of the ion

F = the Faraday, A-second/gram equivalent

Equations (87) and (88) clearly show that the concentration of acid with reference to the electrode is dependent on the discharge rate. It is well known that the diffusion coefficient, D, is dependent on temperature, hence the acid concentration curve is also a function of temperature. Inspection of equation (87) reveals that at a given discharge time, t, the variation of acid concentration with distance from the electrode is of an asymptotic form. During periods of no-load, the battery experiences recuperation effects due to the 'levelling out' of the acid concentration curve, as diffusion occurs towards the cell electrodes. That the diffusion process occurs is apparent by observing the increase in cell terminal voltage during these no-load periods between loading.

APPENDIX 4: THE INTERFACE SYSTEM

A PCI 6100 unit produced by CIL Microsystems Ltd. was used as the interface system [81]. The unit has 8 analogue inputs and 4 analogue outputs, with 4 change-over relays. The system is provided with 8 bit inputs and outputs.

The analogue inputs are differential, and after multiplexing are fed to a programmable gain amplifier. Gain ranges are settable in software in the ranges 100 mV, 1 V and 10 V. The analogue to digital conversion times are of the order of 1 mS.

The analogue outputs are provided for by a single microprocessor (6502) controlled D-A converter, which is scanned around 4 Sample and Hold amplifiers, which maintain the output level. The output voltage values are held in RAM and converted as necessary. Output voltage is in the range ± 10 V and is 8 bit resolution.

The output relays are change-over relays, whose operation is under Bus control. They are rated as 240 V and 1 A.

The specification of the Interface Unit is given in Table 6, for a temperature of 20°C and an Input Range setting of ± 10 V unless otherwise specified.

GENERAL	
Resolution (input and output)	8 bits
Calibrated Accuracy (20°C)	±1%
Span Vs Temperature	±100 ppm
Zero Vs Temperature	±50 ppm
Hysteresis	1 bit
Power Supply	220 to 240 V ± 10%
Operating temperature	0 - 50°C
INPUT SECTION	
Number of inputs	8
Operating time per Channel	< 0.5 mS
Input Ranges	Programmable ± 100 mV, ± 1V, ± 10 V
Input Impedance	1 Megohm
Input Common Mode Range (Common Mode and Signal)	± 10 V
Common Mode Rejection (d.c.)	110 dB
Input Noise	1 bit
OUTPUT SECTION	
Number of outputs	4
Output Voltage (referred to instrument OV)	± 10 V
Output Current	± 5mA
Output Impedance	.1 ohm
Output Update Frequency	< 1 mS
Output Ripple	< 1 bit
RELAY SECTION	
Number of Relays	4
Contact Type	Single Pole Change-Over Silver Contacts
Contact Rating	1A 240 VAC

TABLE 6 SPECIFICATION OF INTERFACE UNIT

APPENDIX 5: MONITORING THE BATTERY ELECTROLYTE TEMPERATURE AND THE PULSED DISCHARGE CURRENT

5.1 The Thermocouple Temperature Sensing Circuit

The thermocouple temperature sensing circuit is shown in Fig. 85. R3 and R4 divide down the 10 mV/ K output of the LM 335 zener diode to match the Seebeck coefficient of the thermocouple (40.80 uV/ $^{\circ}$C). The BZY 88 zener diode and it's associated voltage divider provide a voltage to counteract the 0° C output of the LM 335. Circuit 1 of Fig. 85 was calibrated by adjusting R1 so that V1 = α T, where α is the Seebeck coefficient and T is the ambient temperature in degree Kelvin; R2 was then adjusted so that V1 - V2 was equal to the thermocouple output voltage at the known ambient temperature.

The output voltage (E1 - E2) of Circuit 1 is of the order of micro-volts; this voltage level is too low to be sampled via the Interface System, and so to make the voltage level more acceptable for sampling, Circuit 2 was constructed for the purpose of increasing the output voltage of the temperature sensing circuit to the order of milli-volts. To ensure that the gain of the circuit remained constant for the range of electrolyte temperature considered in the investigation, an instrumentation amplifier arrangement consisting of three 741 operational amplifiers was used. The arrangement basically consists of two buffering amplifiers (OP1 and OP2) and a third amplifier OP3, together with it's associated resistors form a differential amplifier having a gain of unity; only the resistors of OP3 need to be matched. The primed resistor R8 is used to balance out any common mode voltage. Using R9 the gain of Circuit 2 was set to 40, in accordance with the relationship:

$$\frac{V_o}{E1 - E2} = 1 + \frac{2}{a} \qquad (89)$$

where: $a = R9\ (K\Omega)/10^2$

For the temperature range of 0°C to 50°C, the output characteristic of the sensor was given by:

$$V_o = 1.81\ T_c - 84.21 \qquad (90)$$

where: V_o = output voltage, mV

T_c = temperature of electrolyte, °C

To optimise between the performance and cost of the sensor the specifications of the resistors were carefully chosen. The specifications were:

Circuit 1

R1 and R2: tolerance = ±10%

R3 to R7: tolerance = ±1%; temperature coefficient = ±50 ppm/°C; 0.25 W @ 70°C. (Metal Film Resistors).

and $R4 = \dfrac{\alpha}{10mV/°C} \cdot R3 = 0.816K$

$R6 = \dfrac{-T_o \cdot \alpha}{V_z} (0.9R5) = 0.3K$

$R7 = 5.R5 = 1M$

where: T_o = absolute zero (-273.16°C)

V_z = reference voltage (6.8 V for BZY 88)

Circuit 2

All fixed resistors : tolerance = ±5%

All potentionmeters : tolerance = ±10%

5.2 Pulsed Discharge Current Sampling

The peak value (I_{pk}) of the pulsed current was sampled at regular time intervals by means of the circuit of Fig. 86. The voltage across a non-inductive shunt (V_i) produced by the current waveform is inputed to OP1. The two op-amps. are housed in a single I.C. which has the commercial designation LM 324. When it is required to store the peak value of V_i, a series of pulses are applied to the quad bilateral switch (4016) and the low loss capacitor assumes the voltage V_i. The output voltage (V_o) is sampled using the Interface System and the value transferred into the modelling program contained within the PET software. After sampling, the network was reset by 'shorting' the capacitor using Relay 1 of the Interface System, and the next sampling sequence was initiated.

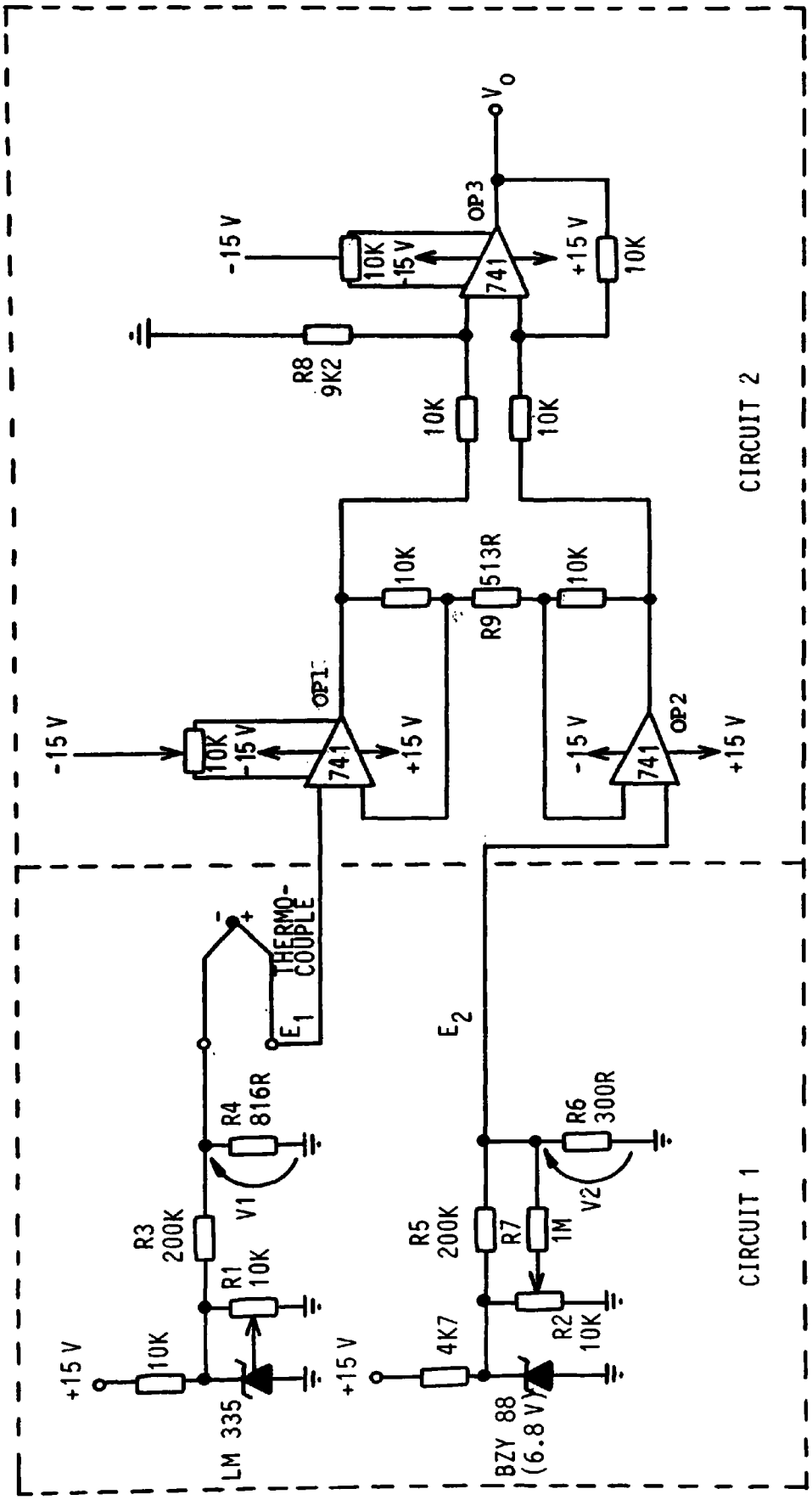

FIG. 85 TEMPERATURE SENSOR CIRCUIT

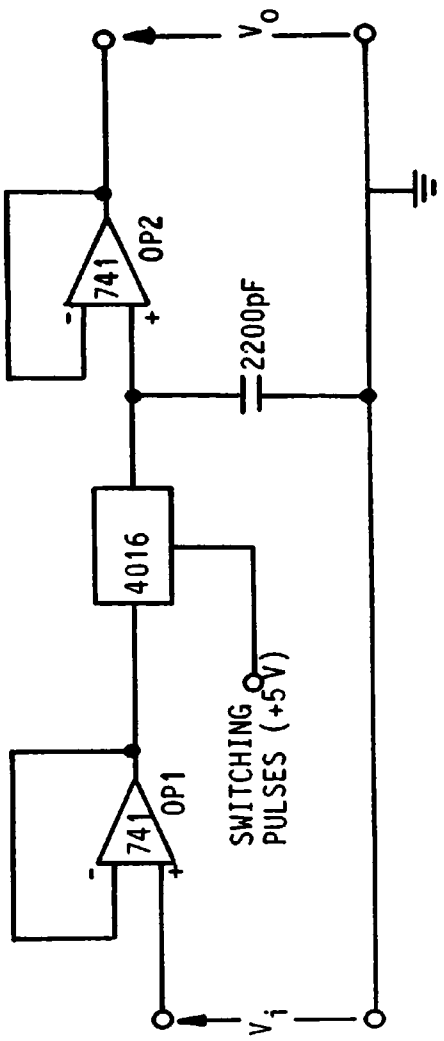

FIG. 86 PULSE SAMPLING CIRCUIT